IMPACT OF 0.7 INCH DIAMETER STRANDS ON

NU I-GIRDERS

Nebraska Department of Roads (NDOR)

Project Number: SPR-1(08) P311

June 2011

IMPACT OF 0.7 INCH DIAMETER STRANDS ON

NU I-GIRDERS

Nebraska Department of Roads (NDOR)

Project Number: SPR-1(08) P311

<u>FINAL REPORT</u>

<u>PRINCIPAL INVESTIGATORS</u>

Maher K. Tadros and George Morcous

<u>SPONSORED BY</u>

Nebraska Department of Roads

University of Nebraska - Lincoln

June 2011

Report No.	Government Accession No.	Recipient's Catalog No.
Title and Subtitle IMPACT OF 0.7 INCH DIAMETER STRANDS ON NU I-GIRDERS		1. Report Date June 2011
		2. Performing Organization Code
3. Author(s) George Morcous, Kromel Hanna, and Maher K. Tadros		4. Performing Organization Report No.
5. Performing Organization Name and Address College of Engineering University of Nebraska-Lincoln Omaha, Nebraska 68182-0178		6. Work Unit No.
		7. Contract or Grant No.
8. Sponsoring Agency Name and Address Nebraska Department of Roads Bridge Division P. O. Box 94759 Lincoln, NE 68509-4759		9. Type of Report and Period Covered Final Report
		10. Sponsoring Agency Code
11. Supplementary Notes		

12. Abstract

Since the Federal Highway Administration (FHWA) allowed the use of 0.6 in. (15.2 mm) diameter strands at 2 in. (51 mm) minimum spacing in 1996, they have been increasingly used in the production of pretensioned concrete bridge girders. For several years, 0.7 in. (17.8 mm) diameter strands have been successfully used in cable bridges and for mining applications. Using these large diameter strands in pretensioned concrete girders at 2 in. (51 mm) spacing will result in approximately 35% increase in the prestressing force compared to the same number of 0.6 in. (15.2 mm) diameter strands, which will, consequently, allow for longer spans, shallower structural depth, and/or wider girder spacing. For the same prestressing force, using 0.7 in. (17.8 mm) diameter strands results in fewer strands to jack and release, fewer chucks, and higher flexural capacity due to lowering the center of gravity of the strands. In this report, the design and production challenges of using 0.7 in. (17.8 mm) diameter strands in pretensioned concrete bridge girders are discussed. Several experimental investigations were carried out to determine the mechanical properties of 0.7 in. (17.8 mm) diameter strands, address production concerns, and evaluate transfer length, development length, and end zone cracking associated with using such large diameter strands in pretensioned members. Specimens included pretensioned rectangular prisms, 24 in. deep T-girders, NU900, and NU1100 girders. Positive production experience and predictable test results indicated that 0.7 in. (17.8 mm) diameter strands can be used with no major changes to the current production practices and/or design criteria according to the current AASHTO LRFD specifications.

13. Keywords: AASHTO specifications, bridge design, prestressed I-girders, transfer length, development length, shear capacity,		14. Distribution Statement	
15. Security Classification (of this report) Unclassified	16. Security Classification (of this page) Unclassified	17. No. of Pages:	22. Price

Form DOT F1700.7 (8-72)

DISCLAIMER

The contents of this report reflect the views of the authors who are responsible for the facts and the accuracy of the data presented herein. The contents do not necessarily reflect the official views or policies of the Nebraska Department of Roads, nor of the University of Nebraska-Lincoln. This report does not constitute a standard, specification, or regulation. Trade or manufacturers' names, which may appear in this report, are cited only because they are considered essential to the objectives of the report. The United States (U.S.) government and the State of Nebraska do not endorse products or manufacturers.

ACKNOWLEDGEMENTS

ABSTRACT

Since the Federal Highway Administration (FHWA) allowed the use of 0.6 in. (15.2 mm) diameter strands at 2 in. (51 mm) minimum spacing in 1996, they have been increasingly used in the production of pretensioned concrete bridge girders. For several years, 0.7 in. (17.8 mm) diameter strands have been successfully used in cable bridges and for mining applications. Using these large diameter strands in pretensioned concrete girders at 2 in. (51 mm) spacing will result in approximately 35% increase in the prestressing force compared to the same number of 0.6 in. (15.2 mm) diameter strands, which will, consequently, allow for longer spans, shallower structural depth, and/or wider girder spacing. For the same prestressing force, using 0.7 in. (17.8 mm) diameter strands results in fewer strands to jack and release, fewer chucks, and higher flexural capacity due to lowering the center of gravity of the strands.

In this report, the design and production challenges of using 0.7 in. (17.8 mm) diameter strands in pretensioned concrete bridge girders are discussed. Several experimental investigations were carried out to determine the mechanical properties of 0.7 in. (17.8 mm) diameter strands, address production concerns, and evaluate transfer length, development length, and end zone cracking associated with using such large diameter strands in pretensioned members. Specimens included pretensioned rectangular prisms, 24 in. deep T-girders, NU900, and NU1100 girders. Positive production experience and predictable test results indicated that 0.7 in. (17.8 mm) diameter strands can be used with no major changes to the current production practices and/or design criteria according to the current AASHTO LRFD specifications.

ACRONYMS

AASHTO	American Association of State Highway and Transportation Officials
ACI	American Concrete Institute
AMS	Average Maximum Strain
BOPP	Bridge Operations, Policy, and Procedure
CAD	Computer Aided Drawing
DEMEC	Detachable Mechanical (gauges)
DOT	Department of Transportation
FDOT	Florida Department of Transportation
FHWA	Federal Highway Administration
LRFD	Load and Resistance Factor Design
LVDT	Linear Voltage Differential Transducers
NCHRP	National Cooperative Highway Research Program
NDOR	Nebraska Department of Roads
NU	Nebraska University
PCA	Portland Cement Association
PKI	Peter Kiewit Institute
UNL	University of Nebraska - Lincoln
WWR	Welded Wire Reinforcement

TABLE OF CONTENTS

1 INTRODUCTION

1.1 Background

In 1988, U.S. strand manufactures proposed increasing the diameter of prestressing strands used in pretensioned concrete bridge girders from 0.5 in. to 0.6 in., while maintaining the minimum spacing between strands at 2 in. The objective of this proposal was to increase the total prestressing force transferred to the concrete by 42%, which significantly improves the structural capacity and durability of bridge girders. At that time, the development length equation developed in the early 1960s – based on research conducted by Hansen and Kaar – stated that the minimum spacing between strands required to ensure adequate bond with the surrounding concrete must be equal to four times the strand diameter (Hansen and Kaar, 1959). This means that 0.6-in.-diameter strands cannot be used at a spacing less than 2.4 in. This large spacing hinders the advantages of having larger diameter strands because it results in a prestressing force per unit area of concrete less than that of 0.5 in.-diameter strands at 2 in. spacing. In addition, most manufacturers refused to accommodate the new spacing requirements because of the high expenses associated with retooling their prestressing beds and equipment. Therefore, the Federal Highway Administration (FHWA) issued a memorandum that forbade the use of 0.6 in. diameter strands at 2 in. spacing on public structures until further studies could be carried out to ensure their safety (Lane and Rekenthaler, 1998).

After several years of research conducted by Buckner at the Virginia Military Institute and the corresponding introduction of the development length magnification factor k, the FHWA announced in 1996 that the minimum spacing for 0.6 in. diameter strands is 2 in., and the minimum spacing for 0.5 in. diameter strands is 1.75 in. (Buckner, 1995). Shortly after that announcement, the American Association of State Highway and Transportation Officials (AASHTO) adopted the FHWA new spacing requirements in its bridge design specifications.

Large 0.7 in. diameter strands were first used in external prestressing cables of the Narrows Bridge over the Swan River in Perth, Western Australia, which opened to traffic in November 1959 (James, 2001). Since then, several bridges were built around the world using 0.7 in. diameter strands for unbonded/external post-tensioning. In the United States, there are currently

only two manufacturers producing 0.7 in. diameter strands, Ivy Steel & Wire and InSteel Industries Inc.; however, these strands are used primarily in mining applications.

ASTM A416–06 is the first standard that introduces 0.7 in. diameter Grade 270 low-relaxation strand for prestressed concrete applications (ASTM, 2006). AASHTO M203-07 specifications followed exactly the same requirements as ASTM A416-06 for 0.7 in. diameter strands (AASHTO, 2007). These requirements are similar to those of smaller size strands with regard to minimum breaking strength (270 ksi), yield strength (243 ksi), and elongation (3.5%). The 0.7 in. diameter strands have a cross-sectional area of 0.294 in.^{2} and a density of 1 lb/ft. Prestressing one 0.7 in. diameter strand up to 75% its ultimate strength results in a prestressing force of 59.5 kips, which is 35% higher than that of 0.6 in. diameter strand and 92% higher than that of 0.5 in. diameter strand.

A detailed study on optimized sections for high-strength concrete bridge girders was carried out by Russell et al. In this study, the effect of strand size and spacing on the capacity and cost of different concrete bridge girders was evaluated at various concrete strengths. Despite the unavailability of 0.7 in. diameter strand in the U.S. market at the time of the study, its cost-effectiveness compared to other strand sizes was evaluated. This comparison has indicated that using 0.7 in. diameter strands at 2 in. with a 10,000 psi bulb-tee girder (BT-72) results in the longest girder span and most cost-effective superstructure compared to 0.5 in. diameter and 0.6 in. diameter strands (Russell, et al. 1997). Another analytical study conducted by Vadivelu and Ma has shown that the span capacity of a BT-72 with 0.6 in. diameter strands can be achieved by using a BT-54 with 0.7 in. diameter strands (Vadivelu and Ma, 2008).

Figure 1.1 shows the percentage of increase in prestressing forces when 0.7 in. diameter strands are used in pretensioned concrete girders at different horizontal and vertical spacing compared to that of 0.6 in. diameter and 0.5 in. diameter strands at 2 in. spacing. This figure demonstrates the significant increase in prestressing force that can be applied to the bottom flange of a concrete girder when 0.7 in. diameter strands are used at a smaller spacing.
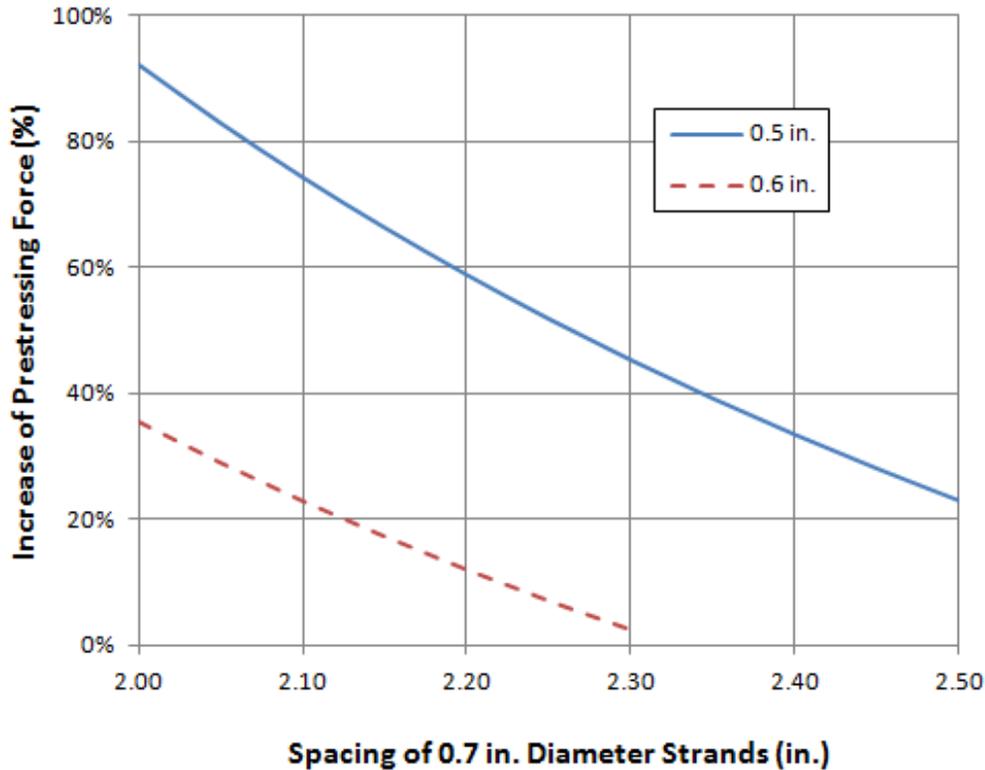
Figure 1.1: Effect of strand spacing on the increase in prestressing force.

For example, a NU900 I-girder, the smallest girder of the NU series, can span up to 89 ft using sixty 0.5 in. diameter strands, and up to 109 ft using sixty 0.6 in. diameter strands (note: 60 is the maximum number of strands at 2 in. spacing in NU girders). However, the same girder can span up to 130 ft when sixty 0.7 in. diameter strands are used (NDOR P322, 2010). This example was calculated using the *AASHTO LRFD Bridge Design Specifications* service III limit state for a two-span bridge continuous for live load (AASHTO, 2007). The bridge has 12 ft spacing between girder lines; a final concrete strength of 12 ksi; a 7.5 in. thick, 4 ksi, cast-in-place concrete deck; and a 1 in. haunch. Figure 1.2 shows the cross section dimensions of a NU900 I-girder, design assumptions, and the span comparison when the three different strand diameters are used. It should be noted that the minimum required girder concrete strength at release increases as the prestressing force increases, which indicates the need for higher strength concrete when 0.7 in. diameter strands are used.
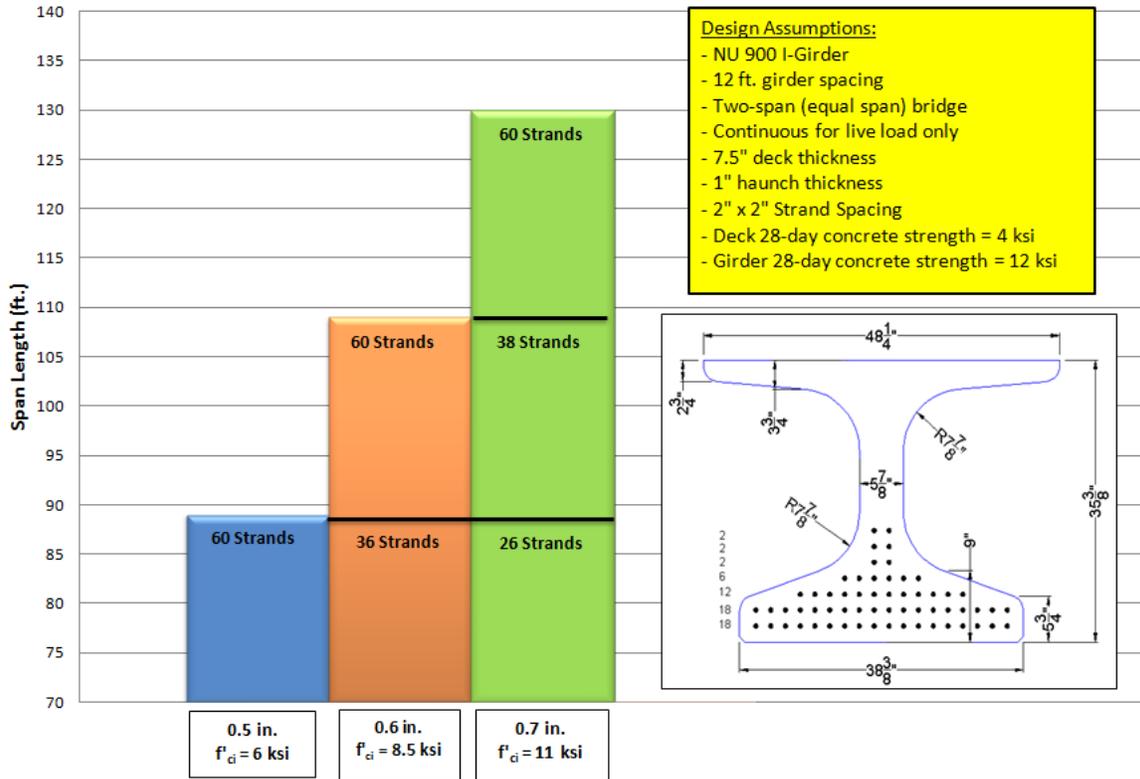
Figure 1.2: Maximum span length when different strand sizes are used.

Another advantage of 0.7 in. diameter strands is using fewer strands and chucks to obtain the same amount of prestressing force of 0.6 in. diameter strands. This results in significant labor savings during the jacking and release operations, in addition to higher flexural capacity due to lowering the center of gravity of the strands. Figure 1.2 also shows that a NU900 I-girder can span 109 ft using only thirty-eight 0.7 in. diameter strands compared to sixty 0.6 in. diameter strands, which is 22 (37%) less strands to jack and release per girder. The same girder can span 89 ft using only twenty-six 0.7 in. diameter strands compared to sixty 0.5 in. diameter strands, which is 34 (57%) less strands to jack and release per girder.

Figure 1.3 shows the number of prestressing strands required for a NU900 I-girder at various span lengths and girder spacing when 0.6 in. diameter and 0.7 in. diameter strands are used. This design chart clearly demonstrates the effect of using larger diameter strands on increasing girder span and reducing girder spacing, which could result in significant savings in the total bridge construction cost.
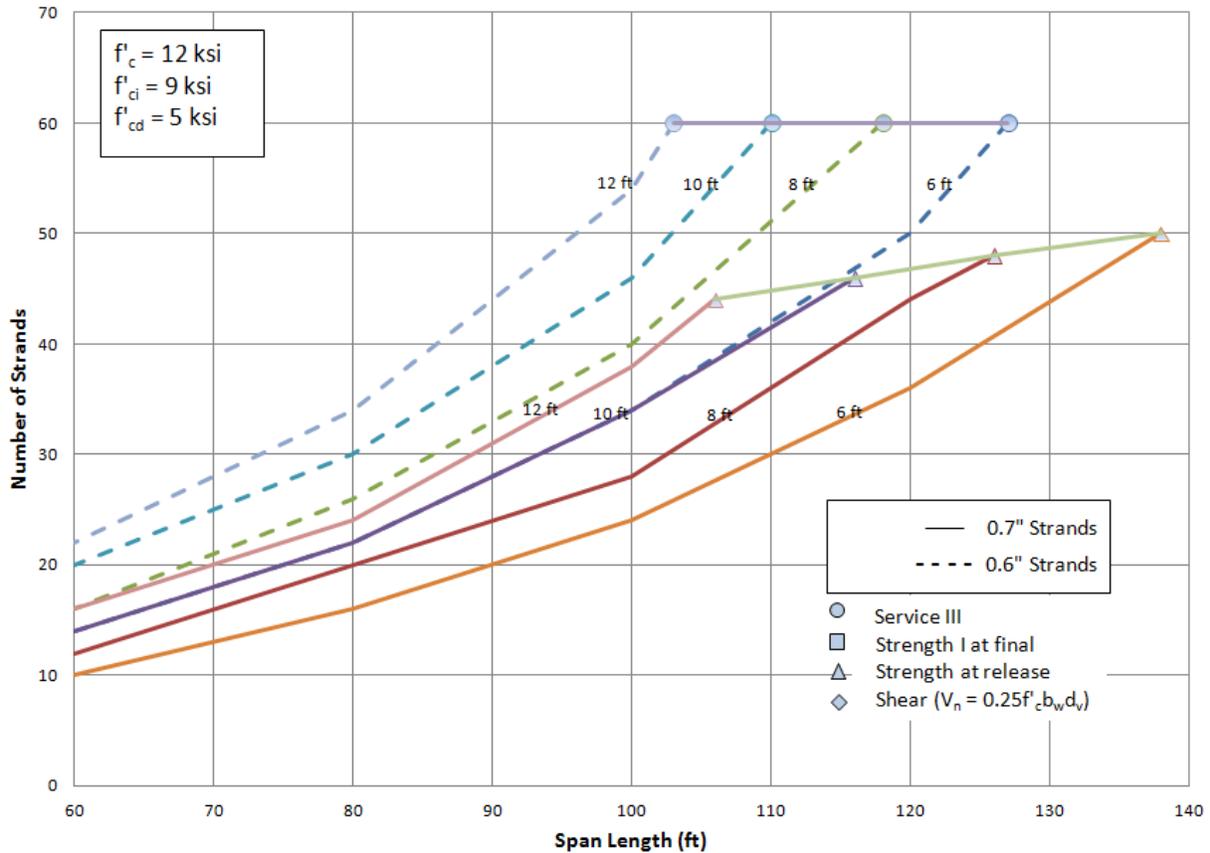
4

Figure 1.3: Comparing the number of required strands (0.6 in. and 0.7 in.) at different span length and girder spacing.

In the last few years, the use of high strength concrete (more than or equal to 10 ksi) in precast/prestressed bridge girders has became a common industry practice. For this development to be beneficial in making high-strength girders, a parallel development in prestressing strands is needed to enhance the flexural capacity of the girder. Combining the use of 0.7 in. diameter strands with high-strength concrete will significantly improve the flexural capacity of bridge girders allowing for longer spans, shallower depths, and/or wider girder spacing. Figure 1.4a shows the steady increase in the positive moment capacity of a NU900 I-girder with concrete strength when using 0.7 in. diameter strands, which is not the case with 0.5 in. diameter and 0.6 in. diameter strands. This is because the higher tensile force of the larger strand diameter results in a deeper compression block that benefits from the higher concrete strength of the top flange. Figure 1.4b demonstrates that the higher compressive strength of the girder concrete is essential for the strand to be fully utilized, which means the strands ultimate stress is higher than its yield

5

strength of 243 ksi. This confirms the conclusions made by Russell et al. (1997) regarding optimized girder design that combines 0.7 in. diameter strands and 10 ksi concrete.
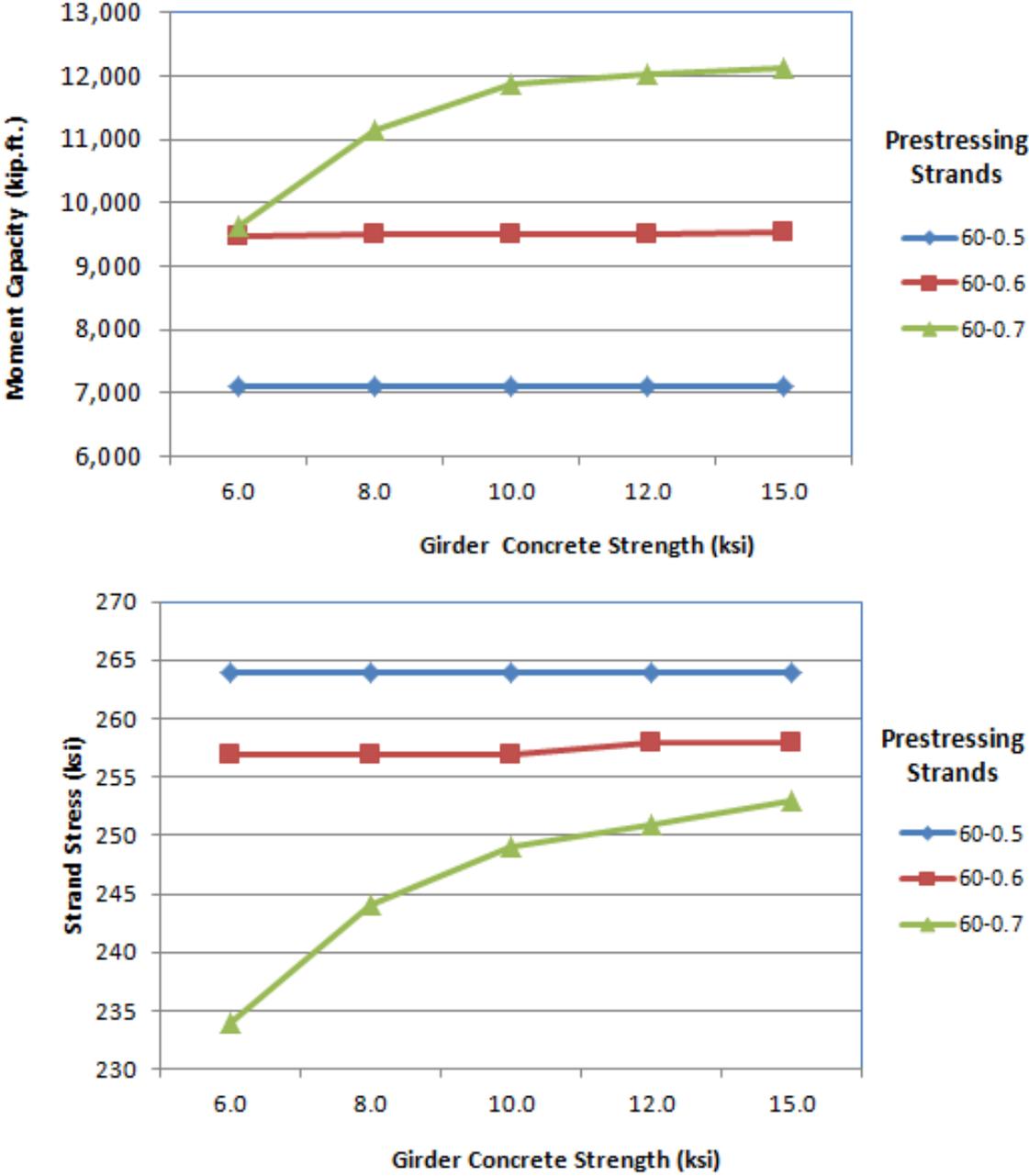

Figure 1.4: Effect of girder concrete strength on: a) moment capacity (top); and b) strand stress (bottom).

In spite of the advantages of using 0.7 in. diameter strands in pretensioned concrete bridge girders, extensive investigation is needed to evaluate the impact of larger strand diameter on the girder design, as well as the production challenges associated with handling heavier and stiffer strands. Also, current AASHTO LRFD specifications provide requirements for the transfer length, development length, end zone reinforcement, and minimum spacing of prestressing strands for diameters equal to 0.5 in. and 0.6 in., but not 0.7 in. The applicability of these requirements to 0.7 in. diameter strands needs to be experimentally evaluated.

1.2 Research Objectives

The main objective of this research is to develop the quality control and design criteria required to introduce 0.7 in. diameter strands at 2 in. spacing in pretensioned concrete I-girders for bridge construction. The focus of this article is to investigate the challenges associated with the design and production of I-girders using 0.7 in. diameter strands. These challenges include: transfer length, development length, end-zone reinforcement, concrete strength, level of confinement, flexural capacity, shear capacity, strand testing, debonding strands, depressing strands, etc.

1.3 Report Organization

This report is organized as follows:

- Chapter 2 presents the first bridge constructed using 0.7 in. diameter strands in North America. It also presents the relevant research on modeling the stress-strain relationship of prestressing strands as well as their transfer and development length equations.
- Chapter 3 summarizes the experimental investigation conducted to evaluate the mechanical properties of 0.7 in. diameter strands. This includes the tension testing of 102 stand specimens and NASP pullout testing of 58 strand specimens.
- Chapter 4 presents the experimental investigation conducted on girders made of ultra-high performance concrete (UHPC) and pretensioned with 0.7 in. diameter strands at 2 in. by 2 in. spacing. This includes two full-scale girders: NU900 and BDT. Two-point depressing of 0.7 in. diameter strands was also investigated.
- Chapter 5 summarizes the experimental investigation conducted on 43 rectangular prisms made of high performance concrete (HPC). Four prisms were used to evaluate the transfer

length, while the remaining 39 prisms were used to evaluate the pullout of pretensioned 0.7 in. diameter strands at different concrete strengths and levels of confinement.

- Chapter 6 presents the design, fabrication, and testing of eight T-girders made of HPC and pretensioned using six 0.7 in. diameter strands. The flexural and shear capacities of these girders were evaluated at different concrete strengths and levels of confinement.

- Chapter 7 presents the design, fabrication, and testing of three NU1100 specimens. Each specimen was tested in flexure and shear to evaluate the impact of the development length of 0.7 in. diameter strands on the flexural and shear capacities of NU I-girders.

- Chapter 8 summarizes research findings, conclusions, and recommendations. It also highlights the issues that need to be addressed in future research.

2 LITERARURE REVIEW

2.1 Prestressed Concrete Girders with 0.7 in. Diameter Strands

The Pacific Street bridge over 1-680 in Omaha, Nebraska, opened to traffic in August 2008 as shown in Figure 2.1, is the first bridge in the United States that used 0.7 in. diameter strands in the fabrication of precast/prestressed bridge girders. The bridge consists of two identical spans, 98 ft long each with 17 degrees skew angle. The bridge has six traffic lanes with a total width of 105 ft 8 in. The bridge superstructure consists of twenty NU900 I-girders (i.e., ten for each span) that are spaced at 10 ft 8 in. Figure 2.2 shows the cross section of the NU900 girder used in this bridge. Each girder had a specified 28-day compressive strength of 10 ksi and was pre-tensioned using 30-0.7 in. diameter strands spaced at 2 in. horizontally and 2.5 in. vertically. The girders were made continuous for deck weight and live load using threaded rod continuity system (NDOR P587, 2010). The 8 in. thick cast-in-place concrete deck had a specified 28-day compressive strength of 5 ksi and was post-tensioned using 36-0.6 in. diameter mono strands in the longitudinal direction. The twenty NU900 girders were fabricated at Coreslab Structures, Omaha. Production challenges in girder fabrication were minimal as they were limited to strand handling due to the significantly high stiffness of 0.7 in. diameter strands during the pullout from coils. This could be remedied by simply using larger diameter coils for 0.7 in. diameter strands than those used for 0.5 and 0.6 in. diameter strands. The tensioning process was very smooth except that new jaws for strand jacks and new chucks need to be ordered in advance and bulkhead holes need to be enlarged to fit 0.7 in. diameter strands. Strand debonding and release operations were performed similar to those with smaller diameter strands (Schuler, 2009).

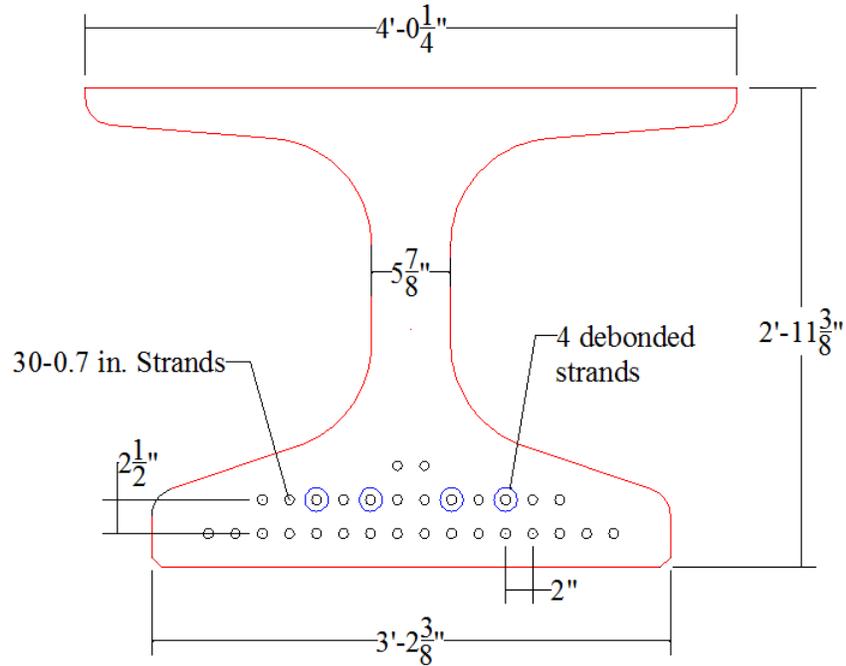Figure 2.1: Pacific Street Bridge over I-680, Omaha, NE.

Figure 2.2: Cross section of NU900 used in the Pacific Street Bridge

The experimental investigation for the Pacific Street Bridge project was conducted at the PKI Structural Laboratory of the University of Nebraska-Lincoln in 2007. In this investigation, a 40 ft long NU900 was pretensioned using 24 - 0.7 in. diameter strands at 2.2 in. horizontal and 2.25 in. vertical spacing as shown in Figure 2.3. Concrete strength at release was 6.7 ksi and at final it was 8.0 ksi. The transfer length of the 0.7 in. diameter strands was measured using surface strain measurements and was found to be 35 in., which is less than the value predicted using AASHTO LRFD specifications. The development length was evaluated by applying a load at the AASHTO LRFD predicted development length (14 ft). The specimen failed in shear, after exceeding its ultimate flexural capacity without any significant slippage of strands. For more details on this experiment, refer to Reiser (2007).
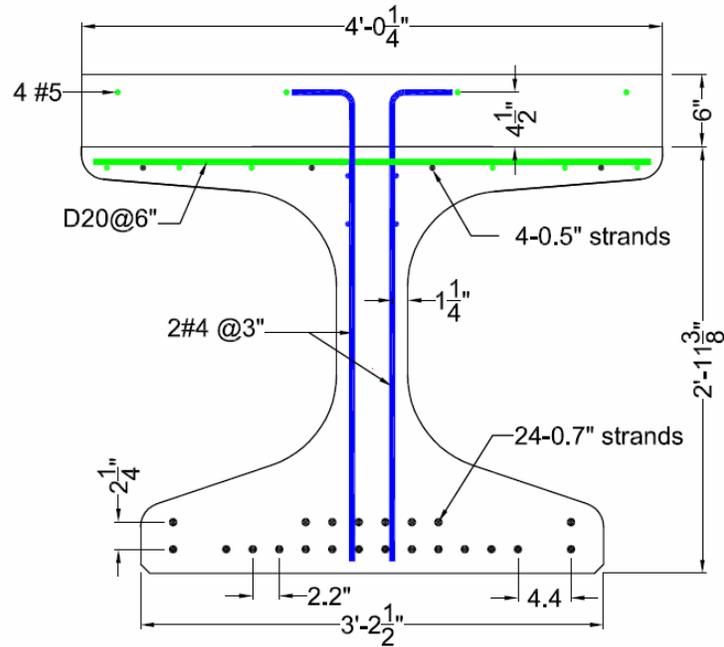
Figure 2.3: Cross section of the tested NU900 specimen

2.2 Modeling the Behavior of Prestressing Steel

The stress-strain relationship for prestressing steel is very important for the strength design of prestressed concrete girders. The PCI Design Handbook gives the following Equations for this relationship, which can be plotted as shown in Figure 2.4 (PCI, 2006)

$$\varepsilon_{ps} \leq 0.0086: \quad f_{ps} = 28{,}500\varepsilon_{ps} \ (ksi)$$

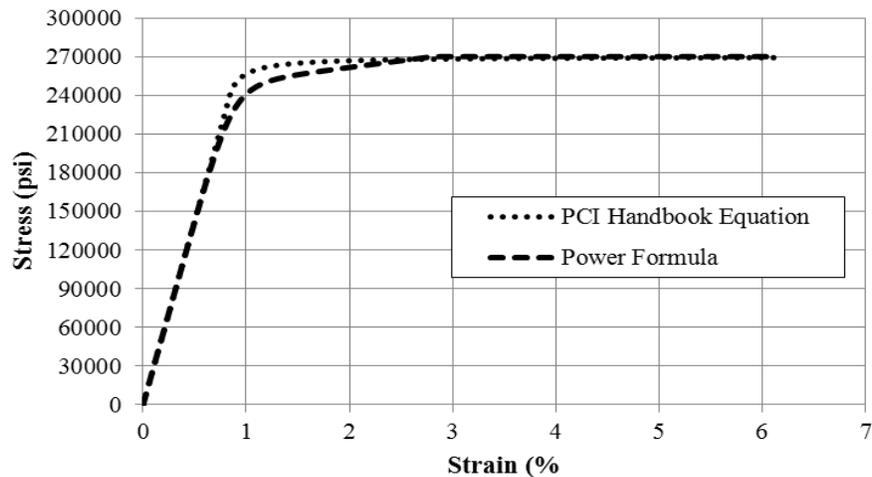$$\varepsilon_{ps} < 0.0086: \quad f_{ps} = 270 - \frac{0.04}{\varepsilon_{ps} - 0.007} \ (ksi)$$

Figure 2.4: Stress vs. Strain Prediction Methods for Prestressing Steel

Another formula, known by Power Formula, was proposed by Mattock (1979) to describe the stress-strain relationship of prestressing strands. The Power Formula is also plotted in Figure 2.4 and presented below:

$$f_{ps} = \varepsilon_{ps} E_{ps} \left[Q + \frac{1-Q}{\left\{ 1 + \left(\frac{E_{ps}\varepsilon_{ps}}{K f_{py}} \right)^R \right\}^{1/R}} \right]$$

The constants Q and K as well as f_{py} are determined through material testing, or more often ASTM minimum standards. Devalapura and Tadros (1992) performed several tests from five independent strand manufacturers to determine these constants. From this data, as well as from manufacturer's statistical data, it was possible to derive constants for the Power Formula such that the prediction curve would be as close of fit as possible to the experimental lower bound and predict the yield to the ASTM minimum of 243 ksi. The following simplified equation was proposed with recommended constants in Table 2.1.

$$f_{ps} = \varepsilon_{ps} \left[A + \frac{B}{\left\{ 1 + (C\varepsilon_{ps})^D \right\}^{1/D}} \right] \le f_{pu}$$

Table 2.1: Constants Recommended for the Simplified Power Formula

	A	B	C	D
Skogman et a. (1988)	423	27,577	110.8	8.449
Devalapura and Tadros (1992)	887	27,613	112.4	7.360
Loflin (2008)	421	30,048	121.5	6.114

The constants found in Deva1apura and Tadros (1992) were compared to constants presented four years earlier by Skogman et al. (1988). More recent constants, based on Grade 270 prestressing strand, were presented by Loflin (2008) using multiple strand diameters. Statistical fitting of the Simplified Power Formula was used to determine the average constants listed in Table 2.1. A wide range of values for the constants of the Power Formula were presented in Loflin (2008), but there was again significant difference between all three sets of values presented in Table 2.1 and plotted with the Simplified Power Formula in Figure 2.5.
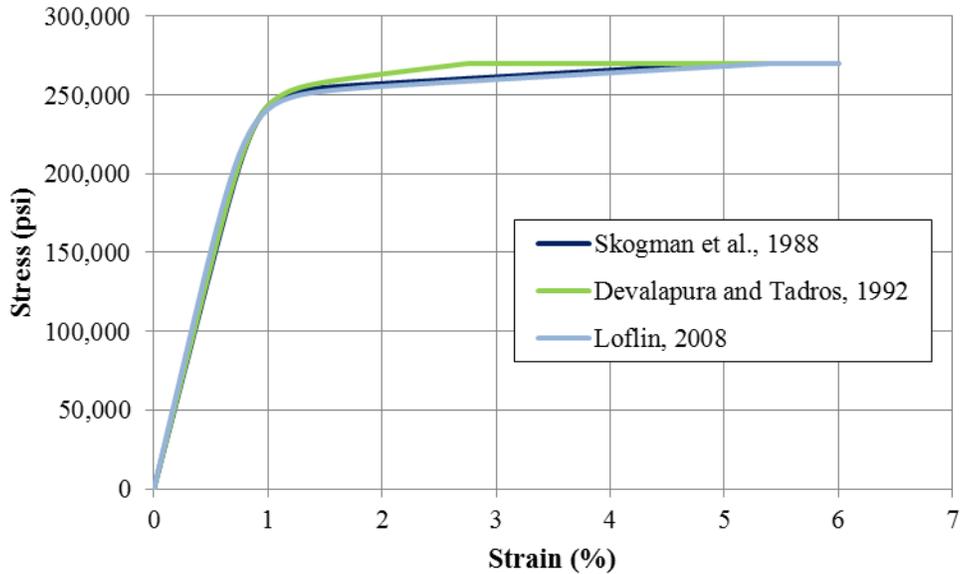
Figure 2.5: Simplified Power Formula Plotted with Various Constants

The constants in Table 2.1 and Figure 2.5 were not determined based on data from 0.7 in. diameter prestressing strands. Rather, data were gathered on a wide variety of smaller diameter strands which tend to have higher values for yield and ultimate strength. For this reason and for the purpose of industry survey, the research contained in this project will attempt to determine the effectiveness of the above equations at predicting stress vs. strain behavior for 0.7 in. diameter strands, as well as the ability of the industry to attain ASTM minimum standards. A number of other curves have been recommended by various researchers for the prediction of steel stress in prestressed member strength calculations (Loov, 1988; and Harajli and Naaman 1985), but the Power Formula as well as the PCI Design Handbook Formula are the two most commonly used and recommended by designers and researchers.

2.3 Transfer and Development Length of Prestressing Strands

The main obstacle for the introduction of 0.7 in. diameter prestressing strands to the precast industry is the quantification of bond characteristics. The bond characteristics include the transfer and development lengths for a given strand spacing, concrete strength, and level of confinement. According to the 2007 AASHTO LRFD specifications with 2008 interim revisions, the transfer length and development length for fully bonded prestressing strands are calculated as follows:

13

$$l_t = 60d_b$$

(Section 5.11.4.1)

l_t= transfer length (in.)

d_b= nominal strand diameter (in.)

$$l_d \geq k\left[f_{ps} - \frac{2}{3}f_{pe}\right]d_b$$

(Section 5.11.4.2)

l_d= development length (in.)

f_{ps}= average stress in prestressing steel (ksi)

f_{pe}= effective stress in prestressing steel (ksi)

k = factor equal to 1.0 for pretensioned panels, piling, and other pretensioned members with a depth of less than or equal to 24.0 in., and equal to 1.6 otherwise. For partially bounded prestressing strands, the development length should be determined using section 5.11.4.2 with k factor equal to 2.0.

These equations for transfer and development lengths of prestressing strands are applicable for bridge girders with a minimum concrete strength of 4.0 ksi (section 5.4.2.1) and a bottom flange reinforcement of at least no. 3 deformed bars with spacing not exceeding 6 in. enclosing the strands (section 5.10.10.2). These equations were developed based on the results of experimental investigations carried out on prestressing strand diameters up to 0.5 in. The k factor was added later to accommodate the use of 0.6 in. diameter strands as well as the new spacing requirements (section 5.11.3.3.1). These requirements stipulate that the distance between pretensioning strands at member ends within the transfer length shall not be less than a clear distance taken as 1.33 times the maximum size of the aggregate nor less than the center-to-center distances specified as 2 in. for 0.6-in.-diameter strands, and 1.75 in. for 0.5-in.-diameter strands. The requirements also allow bundling up to four strands at locations other than member ends so that the minimum clear distance between groups of bundled strands shall not be less than 1.33 times the maximum size of the aggregate or 1.0 in. By considering the 0.7-in.-diameter strand as a bundle of two 0.5-in.-diameter strands, the 2 in. center-to-center spacing can be considered acceptable by the current specifications except for the member ends, which will be experimentally investigated in this study.

Also, according to the 2007 AASHTO LRFD specifications section 5.10.10.1, total area of reinforcement located within the distance $h/4$, where h is the overall height of the girder, from the end of the girder should not be less than 4% of the total prestressing force at transfer divided by 20 ksi. This reinforcement is required for crack control and resisting the splitting force at the girder ends due to prestressing. Using larger strand diameter results in higher concentration of prestressing force per unit area of concrete and might, consequently, require different amount and/or distribution of end zone reinforcement.

The potential impact of 0.7 in. diameter strands was studied by Vadivelu and Ma (2008). The goal of the study was verification that 0.7 in. diameter strands could be effectively implemented at 2 in. center to center spacing. A three dimensional finite element model was constructed to analytically determine the effects of the increased prestressing force at transfer. It was determined that girders reinforced with 0.7 in. diameter strands had higher stresses at the transition from bottom flange to web, when compared to 0.6 in. strands. It was hypothesized that this could be compensated for by increasing confinement around the strands in the end zone as well as adding adequate vertical reinforcement.

Transfer length is the length of the strand measured from the end of the prestressed concrete member over which the effective prestress is fully transferred to the concrete. The transferred force along the transfer length is assumed to increase linearly from zero at the end of the member to the effective prestress at the end of the transfer length. Transfer length is important for shear design and concrete stresses at release at girder ends. An over-estimated transfer length might result in inefficient shear design and higher than predicted stresses at release, while an under-estimated transfer length might result in inadequate shear design and lower than predicted stresses at release.

The development length of prestressing strands is defined as the minimum strand embedment in concrete required to reach the ultimate capacity of the section without strand slippage. Thus, at the end of the development length, the ultimate stress in the strand could be reached without strand-concrete bond failure. The development length is necessary for identifying the critical sections in flexure and shear and calculating their ultimate capacities. An under-estimated

development length might result in a lower girder capacity at sections within the development length, while an over-estimated development length might result in uneconomical design that is over reinforced. If there is not enough bond stress to reach the full design prestress in the member, a strand slip relative to the concrete occurs and a bond failure is likely to occur. Some researchers (Russell and Bums, 1993; Shahawy, 2001) acknowledged that premature bond failure can be caused by propagation of cracks though the transfer length. This statement could have significant effects on debonded strands as well as very slender members susceptible to web shear cracking.

Figure 2.6 shows the AASHTO LRFD transfer and development length predictions. These predictions often represent conservative estimates of transfer and development length based on early works. They do not truly reflect the more recent research performed using current concrete strengths or tensioning practices, including HPC and UHPC. For instance, the 1.6 multiplier for larger depth (typical bridge) members was introduced in response to since disproven results (Cousins et al. 1990). However, the AASHTO transfer and development length equations are nearly unanimously conservative (Kose and Burkett, 2005), which explains their current unchanged form.
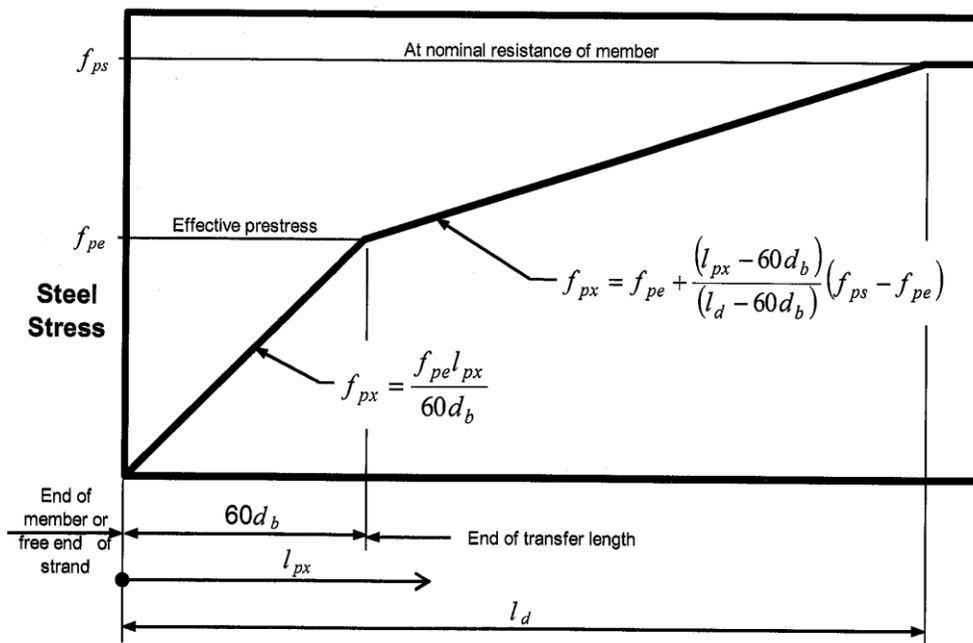

Figure 2.6: Idealized Steel Stress vs. Distance from End of Member (AASHTO LRFD 2007)

A number of mechanisms have been identified as creating the concrete to steel bond. Adhesion, friction, strand expansion and contraction due to longitudinal stresses (Poisson's Effect), and mechanical interlock all in some way contribute to the bond stress. Each of these mechanisms is briefly addressed below.

Adhesion is the bond between the concrete and the steel created when fresh concrete hardens. The bond due to adhesion is effective only until its failure, at this point it is gone, and as such it cannot be counted on. Any differential slip between the two materials effectively removes any effects from adhesion. In the transfer region, the effect of adhesion is zero, as the transfer length can be defined as a function of strand slippage (Guyon, 1960). Slip also occurs at the edges of cracks which pass across the strand as very high stresses in the steel are attained and strand diameter changes due to Poisson's effect.

Friction plays a significant role in the bond stress active during transfer and development length. Experiments by Janney (1954) with prestressed wire were able to isolate the effects of friction, as there were no deformations on the wire to enable mechanical resistance. Friction is only present when the two materials are forced, due to radial stresses, against each other. Radial stresses can be increased with the advent of concrete shrinkage, Poisson's effect, or mechanical interlock. These stresses can be reduced by any changes in strand diameter, which if large enough could remove friction entirely. Friction can also be increased through strand surface quality and the wedging action from small particles that break from the surrounding concrete.

Hoyer's effect (or Poisson's Effect) was named after E. Hoyer, who in 1939 investigated the mechanisms of bond in pretensioned concrete and recognized the mechanism (Hoyer and Friedrich, 1939). As a material is loaded in one direction, the material elongates in that direction and therefore contracts in the others, as dictated by Poisson's ratio. In this case the strand is tensioned and released into hardened concrete, at the end of the member there is zero stress in the strand and is at its normal diameter. As the strand gains stress it also contracts until the effective prestress is reached at which point the diameter remains constant. The same effect takes place along the rest of the girder as additional strand tension is applied. This difference in diameter,

specifically in the anchorage zone, creates a wedging action called Hoyer's Effect. Without Hoyer's effect the effects of friction are greatly reduced or eliminated. Janney (1954) and Hansen and Kaar (1959) noted this as the cause of a bond failure. The reduction of the strand's diameter in the transfer region would cause a successive collapse of anchorage such that a bond failure could occur. For this reason the anchorage zone is suggested to have ample reinforcement to protect the strands from catastrophic cracking.

The helical shape of the seven wire strand creates what is known as mechanical interlock, similar to the deformations on a reinforcing bar. When the concrete is cast around a strand, the strand cannot strictly pull out, it must either break the concrete which has filled the ridges and cracks between the wires or twist as can be seen in Figure 2.7.

Figure 2.7 Ridges Formed by Concrete When Cast Around 7- Wire Prestressing Strand

Mechanical interlocking is considered to be the largest contributor to flexural bond stresses (Russell and Bums, 1993), and is similar to the deformations on mild steel reinforcement. When cracking occurs, small slips are created which increases the effect of the mechanical interlock by causing the strand to react against the concrete in the strand's helical deformations.

The literature discussing the transfer and development lengths of prestressing strands is very extensive. The presented studies are only a portion of the literature available on this topic, but provide a thorough cross section of the investigations to date. Many studies have provided more extensive literature reviews on this subject, but for the sake of brevity, the following presents

numerous research efforts on prestressing transfer length and development length up to the point of the 1988 FHWA Memorandum of the use of 0.6 in. diameter strands. After 1988, many studies were initiated, and there were summarized by Lane (1998). Studies after 1998 tended to be reviews of the previous research on 0.6 in. diameter strands or investigated transfer and development in varying types of concrete.

Janney (1954)

Small scale beam and prism specimens were used to study the transfer and development length of varying reinforcement. A number of reinforcement sizes were used for the prism tests including 0.162 in. wire with clean lubricated and rusted surface conditions, along with 0.1 in., 0.197 in. and 0.276 in. wire, all of which in clean and lubricated conditions. Additionally, concrete strengths were varied. Strains were electronically gathered along the length of both beams and prisms to create strain distributions along the length of the specimens. Figure 2.8 reproduces typical graphs from Janney (1954) demonstrating the effect of both wire size and concrete strength on transfer length of wires. It was concluded that transfer bond is largely the result of friction between concrete and steel and that transfer lengths ranged between 12 and 36 in. for the types of reinforcement above, using gradual release methods. Concrete strength, wire diameter and wire surface condition were all demonstrated to affect the transfer length.
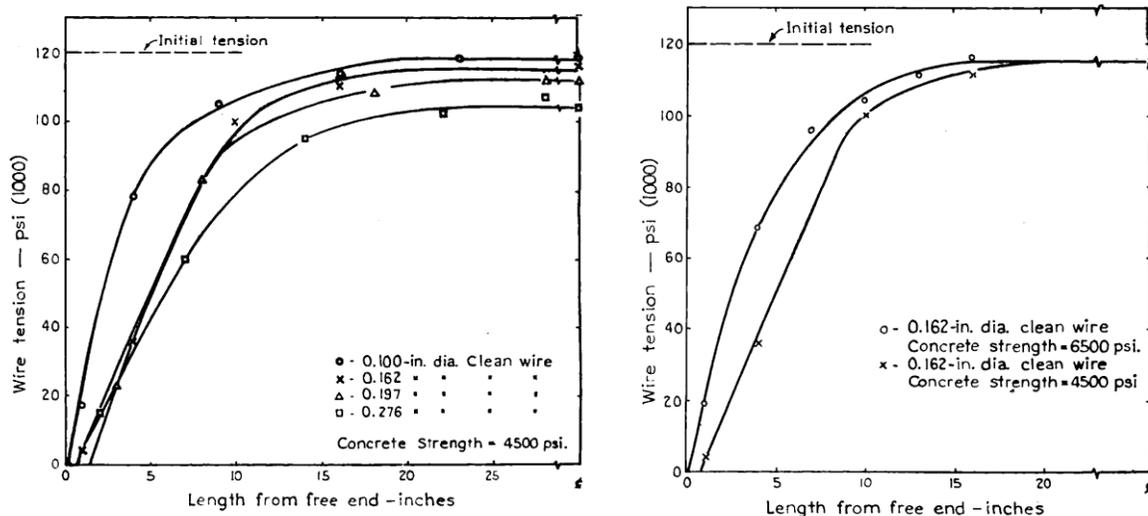

Figure 2.8: Effect of wire diameter (left) and concrete strength (right) on transfer (Janney, 1954)

Interestingly, because of the popularity of strands in bridge applications, wire transfer lengths are not directly applicable today. However, the results of this study isolate Hoyer's Effect and friction from the effects of a 7-wire strand's mechanical interlock giving insight into the mechanics of a portion of strand bond. The small scale, simple span beams were prestressed using various wires with concrete strengths near 4.5 ksi. The wires also had varying surface conditions as well as levels of prestressing. Janney noted that as the bond stress reached the ultimate bond strength, slip was initiated between the strand and the concrete. The bond stress was observed moving along the beam toward the transfer region where it initiated failure. This was termed the "Wave of Flexural Bond Stress" and theorized that as the strand stress decreased the strand diameter, it reduced the bond due to Hoyer's effect, which initiated the bond failure.

Hanson and Kaar (1959)

A total of 47 beams were tested at the Portland Cement Association (PCA) Research and Development Laboratory in the most comprehensive study of its time. Grade 250 prestressing strands with varying diameter and embedment lengths were tested to determine the effect of reinforcement percentage as well as concrete strength. Much of Janney's work was confirmed including 30% more moment resisted by rusted strands at equivalent embedment lengths, as well as Janney's "Flexural Bond Wave Theory". It was again determined that the initiation of bond failure began as the "wave" of bond stress penetrated the transfer region, however mechanical interlock was said to provide additional strength to prevent bond failure, because of the use of strands rather than wires.

Figure 2.9 presents the design recommendations of Hanson and Kaar (1959). These recommendations as well as the future review of the test data eventually led to the development length equations used by AASHTO and ACI. The curves in Figure 2.9 were limited to an initial tension of 150 ksi and concrete strength of 5.5 ksi. Values were based on average bond stress at bond slip with the following equation, which was used to equate bond force to the stress in the prestressing strand:

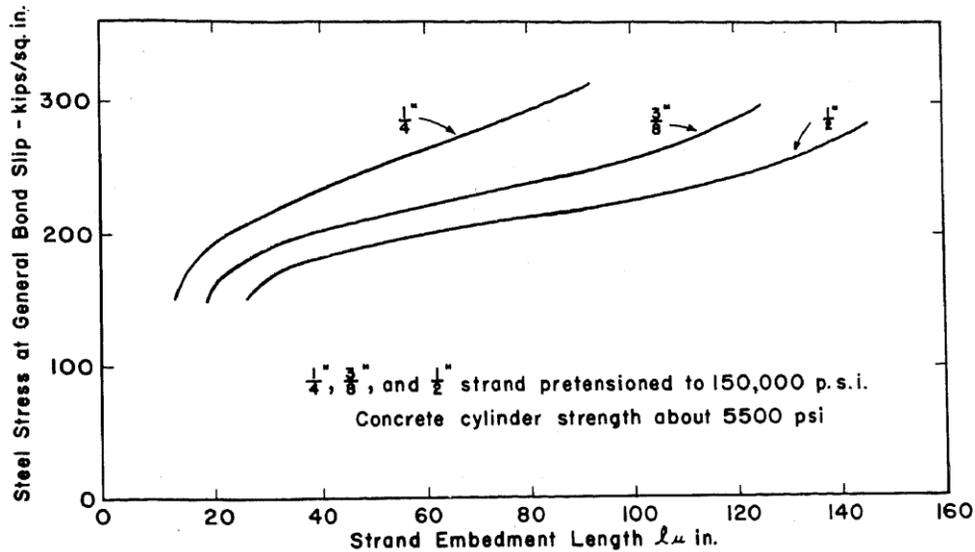$$f_{ps} = \frac{u_t \Sigma_o l_t}{A_{ps}}$$

Figure 2.9: Design Recommendations by Hansen and Kaar (1959) – Relation of Steel Stress at General Bond Slip to Strand Embedment Length (lu)

Kaar et. al. (1963)

In this broad study initiated by the PCA, 36 prestressed rectangular prisms were reinforced with prestressing strands ranging from 1/4 in. to 0.6 in. diameter with varying concrete strengths. Unlike in previous studies performed on wires by Janney (1954), no correlation was found between transfer length and concrete strength with the exception of 0.6 in. diameter strands. An inverse correlation was observed with concrete strength and transfer length for the 0.6 in. diameter strands. Also, a proportional relationship was observed for strands up to 1/2 in. diameter, but did not follow to 0.6 in. strands for which the relationship proved conservative.

Martin and Scott (1976)

In response to the failure of a shallow solid slab under construction loads, Martin and Scott (1976) tested a similar slab which resulted in a bond failure at approximately 85% of the theoretical capacity. Following the test, a re-evaluation of the current design criteria was conducted. The current design custom was based on the research presented above by Hansen and Kaar (1959) as well as Kaar et al (1963), which was performed for the PCA. Martin and Scott proposed the following equations, which specify a maximum strand stress corresponding to a given embedment length:

For $l_x < 80d_b$:

$$f_{ps} \leq \frac{l_x}{80d_b}\left(\frac{135}{d_b^{1/6}} + 31\right)$$

For $l_x > 80d_b$:

$$f_{ps} \leq \frac{135}{d_b^{1/6}} + \frac{0.39l_x}{d_b}$$

Zia and Mostafa (1977)

In response to the work performed by Kaar (1962) for the PCA and others, Zia and Mostafa (1977) conducted additional research because of concerns about the reliability of the current code equations. They believed that the use of techniques significantly different from precast practice as well as the introduction of Grade 250 prestressing strands warranted the study. The available data on transfer and development of prestressing strands was extensively reviewed by Zia and Mostafa (1977). The effect of concrete strength, as well as the style of release (sudden or gradual) was taken into account. Upon comparison of the AASHTO development length equation and the Hanson and Kaar data, it was determined that the AASHTO equation found a higher flexural bond stress than Hanson and Kaar (1959). The following transfer and development length equations were then calibrated for concrete strengths ranging from 2 to 8 ksi:

$$l_t = 1.5\frac{f_{pi}}{f_{ci}} - 4.6$$

$$l_d = \left(1.5\frac{f_{pi}}{f_{ci}} - 4.6\right) + 1.25(f_{ps} - f_{pe})$$

Cousins, Johnston and Zia (1990)

In a very important study in the history of transfer and development lengths, Cousins, Johnston and Zia (1990) tested Grade 270 epoxy coated and bare 3/8 in. to 0.6 in. diameter strands with concrete strengths near 6 ksi. Rectangular concrete prisms and beams were fabricated and tested to determine transfer and development lengths of the above strands. It was found that the AASHTO predictions were very un-conservative, with longer transfer lengths than estimated and beams initiating premature failures at embedment lengths almost 30% longer than predicted.

FHWA Memorandum (1988)

In response to the findings of Cousins, Johnston and Zia (1986), as well as differences between the current precast practice and previous research, the FHWA issued a memorandum in October, 1988 which prohibited the use of 0.6 in. diameter strands in pretensioned applications, restricted center to center strand spacing, and increased the required development length of strands by a factor of 1.6.

FHWA Memorandum (1996) and Lane (1998)

As a result of the FHWA Memorandum (1988), approximately 41 research programs were initiated between 1988 and 1998, with the goal of defining transfer and development of 0.6 in. diameter strands. A new memorandum was issued in 1996, which allowed the use of 0.6 in. diameter strands with a center to center spacing of 2 in. (0.5 in. strand spacing was reduced to 1.5 in.). However, the 1.6 multiplier was retained for fully bonded and debonded prestressing strands in the AASHTO development length equation. The FHWA then initiated a study to sift through the wide ranging reports with Lane (1998). Through the extensive review of previous studies, and further transfer and development length testing performed by Lane (1998) on full scale AASHTO Type II sections, which investigated numerous concrete and steel parameters, new equations were proposed for the development length of the strand. The following are the equations proposed by Lane (1998)

$$l_t = \frac{f_{pi}d_b}{f'_c} - 5$$

$$l_d = \left[\frac{4f_{pi}d_b}{f'_c} - 5\right] + \left[\frac{6.4(f_{ps} - f_{pe})D}{f'_c} + 15\right]$$

Barnes and Burns (1999)

A comprehensive study performed for the Texas Department of Transportation, tested 36 AASHTO Type I girders, reinforced with 0.6 in. diameter strands, and various concrete strengths, strand conditions and debonding lengths and release methods. A total of 184 transfer zones were monitored using concrete surface strain measurements as well as end slip measurements. Concrete strengths at release ranged from 4 to 9 ksi. Release methods included a "simultaneous" torch cutting method in which strands were simultaneously cut on each end of

the beams as well as standard torch cutting. Sixty flexure tests were performed on the precast members to determine their development length. Concrete strengths ranged from 5 ksi to 15 ksi. The following equations were recommended for use in design of pretensioned members with and without debonded strands, assuming cracking is prevented within or near the transfer lengths of the debonded strands:

$$l_t = \frac{5}{4}\left[\frac{f_{pt}}{\sqrt{f_{ci}}}\right]d_b \leq 10d_b$$

$$l_d = \frac{5}{4}\left[\frac{f_{pi}}{\sqrt{f_{ci}}} + (f_{ps} - f_{pe})\right]d_b$$

Kose and Burkett (2005)

Another study which summarized a collection of experimental programs from around the country was prepared by Kose and Burkett (2005). It included their testing performed at Texas Tech University (Burkett and Kose, 1999) which was a part of (Barnes and Burns, 1999). They used 313 transfer length tests and 95 development length tests in the creation of new equations. A regression model was used to combine various possible parameters, including $f'_{pu}, f_{ps}, f_{pi}, f'_c$ and f'_{ci}. The following equations were proposed for transfer and development length:

$$l_t = 95\frac{f_{pi}(1 - d_b)^2}{\sqrt{f'_{ci}}}$$

$$l_d = \left[95\frac{f_{pi}(1 - d_b)^2}{\sqrt{f'_{ci}}}\right] + \left[8 + 400\frac{(f_{pu} - f_{pi})(1 - d_b)^2}{\sqrt{f'_c}}\right]$$

Ramirez and Russell (2007)

In a comprehensive research effort conducted by Oklahoma State University and Purdue University, transfer and development lengths in HPC were investigated. Both bonded and debonded 0.5 in. and 0.6 in. diameter prestressing strands were considered. Also, a standard pullout test was developed to measure the bond strength of prestressing strands, termed the NASP Bond Test. The transfer length program included 43 rectangular shaped beams with multiple strand configurations, as well as 8 I-shaped beams. Concrete strengths at release varied 4 ksi to 10 ksi. End slip measurements as well as surface strain measurements were considered.

The development length program consisted of 50 flexure tests on rectangular specimens and 14 flexure tests on I-shaped specimens. Concrete strengths at 56 days ranged from 7 to 14.5 ksi for the rectangular specimen and 9 to 15 ksi for I-shaped specimens.

The authors concluded that both of the current transfer and development length equations were conservative for HPC. The researchers also took note that the I-shaped specimens had more well developed web shear cracking because of the thinner webs. It was therefore claimed that I-shaped beams were more susceptible to bond failures, compared to the rectangular beams. The following equations were recommended, which accounted for the concrete strength, but placed limits on the minimum transfer and development lengths:

$$l_t = \left[\frac{120 d_b}{\sqrt{f'_{ci}}} \right] \leq 40 d_b$$

$$l_d = \left[\frac{120 d_b}{\sqrt{f'_{ci}}} + \frac{225}{\sqrt{f'_c}} \right] d_b \geq 100 d_b$$

STRAND TESTING

3.1 Mechanical Properties

Over the course of nearly two years, 102 large diameter 0.7 in. diameter prestressing strands were tested to verify that the currently available strands meet the ASTM A416-06 requirements regardless of the strand producer. The two strand producers currently available in the USA have been referred to as Producer 1 and Producer 2 throughout this section. Testing was performed according to the testing specifications of ASTM A370-05. Roughly two thirds (69 samples) were tested at the PKI material testing laboratory of UNL and the remaining third (33 samples) were tested at the NDOR material testing laboratory. This was done in order for multiple agencies to independently verify the mechanical properties of 0.7 in. diameter strands. The requirements for 0.7 in. diameter strands included breaking strength, yield strength and elongation. Relaxation properties were not considered in this study, but should be independently verified. Table 3.1 lists the minimum requirements for 0.7 in. diameter prestressing strands.

Table 3.1: ASTM A416 Requirements for 0.7 in. Diameter Prestressing Strands

Steel Area	0.294 in.^{2}
Minimum Breaking Strength	79,400 lbs
Minimum Load @ 1% Extension	71,500 lbs
Minimum Extension	3.5%

All strands were received in ideal condition free of welds, rust, and any visible defects. Strands usually came in groups of three to four, where each group was from a separate heat or mill order. From the time of acquisition of the strand, until specimen rupture, care was taken with all strands to protect them from oil, excessive bending, or physical damage, which could have adulterated the test results. The testing procedure outlined in ASTM A370 – Annex A7 was followed to determine the basic mechanical properties of 0.7 in. diameter strands. University researchers observed NDOR personnel on a number of their tested samples for guidance in testing and ensuring uniformity of testing procedures. At the NDOR Materials and Research Laboratory, all strands are tensioned until they reach the minimum breaking strength and then released as per NDOR policy. This is done to reduce wear on the various apparatus, as the violent rupture of

prestressing strands could damage the sensitive instruments. None of the NDOR samples were tested to rupture, with the exception of strands that did not meet minimum breaking strengths.

Gripping devices were manufactured by the researchers to conform to section A7.3.5 of ASTM A370, similar to the "Sand Grips" outlined by Preston (1985). Grips were manufactured to fit in the jaws of the Tinius Olsen testing machine. Dimensions of the grips can be found in Figure 3.1, and a picture of the grips and assembly (grips, grit mesh and strand) can be found in Figure 3.2. The grips contain smooth semi-cylindrical grooves where the strand was placed. The radius of curvature of the grooves conforms to Note A7.2 of ASTM A370, which states that grooves must prevent the grips from clamping against each other, ensuring that all gripping force is transmitted to the strand. Disposable, abrasive grit mesh was used to aid in producing friction between the grips and the specimen to prevent slippage, also shown in Figure 3.2.
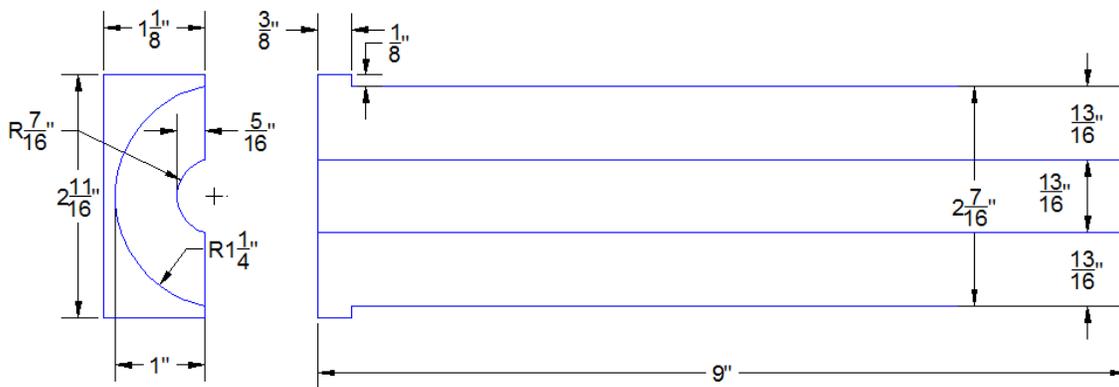
Figure 3.1: Dimensions of 0.7 in. Strand Gripping Device

Figure 3.2: Grips for 0.7 in. Diameter Strand Testing (left) – Grip Assembly (right)

The majority of the prestressing strands appropriately fractured between the jaws of the machine; and all that fractured inside the grips met the previously mentioned minimum requirements. Strands that did break within the grips tended to exhibit lower ultimate elongation values although none less than the minimum. This likely resulted from stress concentrations caused by the clamping force around the jaws. Tests such as these would likely be more extreme than the conditions of a fully bonded strand in a prestressed member (Devalapura and Tadros, 1992). Therefore if the extension would have been less than the minimum and it fractured within the jaws it would not have been discarded.

The extensometer used for the strand tension testing had a gauge length of 24 in. (ASTM A370 – A7.5.2) and an accuracy of at least 0.0001 in./in. (ASTM A416 – 6.3.1). A picture of the extensometer and strand test setup can be seen in Figure 3.3. The extensometer was attached for the first portion of loading up to approximately 1.25% to 1.5% strain, after which it was removed and the testing machine's cross head was used to monitor elongation. This required measurement of the amount of strand between the grips as a secondary gauge length. A position rate of 0.01 in./sec was used to test the specimens, conforming to section 7.4.1 of ASTM A370 for testing to determine yield properties. Masking tape was attached to the strand where the extensometer was gripping, to aid in the gripping of the extensometer's clamps.
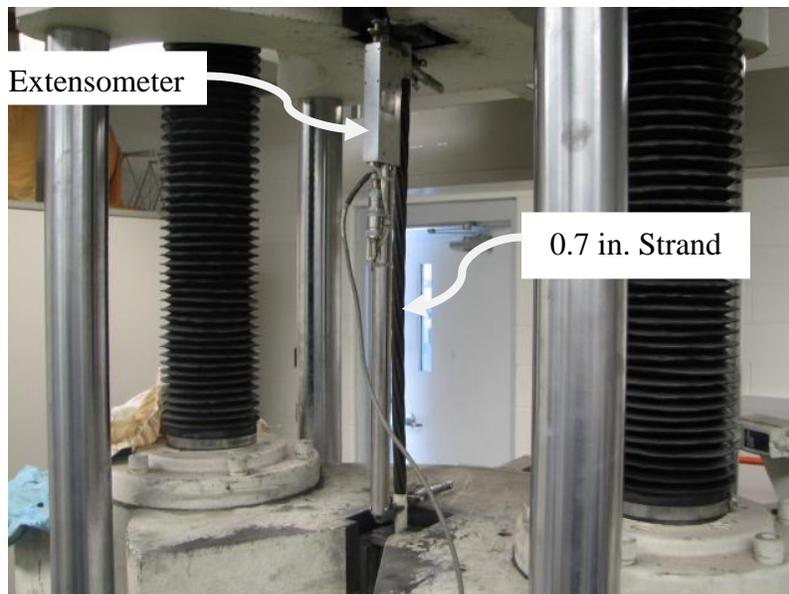

Figure 3.3: Strand Tension Testing Setup

Figure 3.4 shows the nominal diameter measurement of a 0.7 in. diameter strand using calipers that are accurate up to 0.001 in. Following specimen rupture, diameters of the individual wires of one representative strand from each order of strands was measured to determine the actual cross sectional area of each strand. A micrometer, with an accuracy of 0.0001 in., was used to measure the individual wires as demonstrated in Figure 3.4.

Figure 3.4: Strand Diameter Measurement (left) and Individual Wire Measurement (right)

A summary of the 102 strand tests, from each producer, can be found in Tables 3.2 and 3.3, while Table 3.4 combines all producer data for an overall comparison. Visual representation of the strand testing results for the load at 1% strain, ultimate load and MOE are shown in Figures 3.5 to 3.10. Individual results from the strand testing can be found in Appendix A, including tabulated results from both NDOR and PKI testing for Producer 1 and Producer 2. It should be noted that because NDOR did not load the strands until rupture, these data points are not included in the average values of Tables 3.1, 3.2, and 3.3. Though, both producers were able, on average, to meet all of the requirements shown in Table 3.1, Producer 2's average load at 1% strain was very close to the minimum. It can be seen that Producer 1 had significantly higher average values than Producer 2 for load at 1%, but slightly lower average ultimate loads. A very large variation was observed between the testing results of the two producers. This variation in quality between the two producers has also been noted for other products through material testing performed at NDOR.

Table 3.2: Statistical Summary of Producer 1 Strand Results

Producer 1	Area (in^2)	Load at 1% (lb)	f_{py} (psi)	f_{py} / 270 (%)	Peak Load (lb)	f_{pu} (psi)	Peak Position (in)	Elongation (%)	E_p (ksi)
Nominal	**0.2940**	**71,442**	**243,000**	**90.0%**	**79,380**	**270,000**	**1.167**	**3.50%**	**28,500**
Maximum	0.2961	75,060	256,177	94.9%	83,100	282,653	2.810	9.37%	29,111
Minimum	0.2930	71,250	242,537	89.8%	79,610	268,896	1.630	4.89%	26,953
Average	**0.2940**	**73,237**	**249,129**	**92.3%**	**81,896**	**278,788**	**2.130**	**7.05%**	**28,173**
Standard Deviation	0.0008	1,129	3,756	1.39%	1,029	3,256	0.401	1.42%	539
5% Percentile	0.2930	71,458	243,517	90.2%	79,610	271,766	1.638	4.91%	27,243

Table 3.3: Statistical Summary of Producer 2 Strand Results

Producer 2	Area (in^2)	Load at 1% (lb)	f_{py} (psi)	f_{py} / 270 (%)	Peak Load (lb)	f_{pu} (psi)	Peak Position (in)	Elongation (%)	E_p (ksi)
Nominal	**0.2940**	**71,442**	**243,000**	**90.0%**	**79,380**	**270,000**	**1.167**	**3.50%**	**28,500**
Maximum	0.2952	74,670	254,577	94.3%	83,400	284,106	3.010	9.03%	32,400
Minimum	0.2884	67,600	229,153	84.9%	77,300	262,034	1.607	3.11%	23,098
Average	**0.2943**	**71,802**	**243,964**	**90.4%**	**81,026**	**275,033**	**2.281**	**6.54%**	**28,165**
Standard Deviation	0.0011	1,847	6,766	2.51%	1,475	5,230	0.426	1.63%	1,219
5% Percentile	0.2927	69,100	234,118	86.7%	79,000	267,797	1.688	3.83%	26,624

Table 3.4: Statistical Summary of All Strand Results

Combined Producers	Area (in^2)	Load at 1% (lb)	f_{py} (psi)	f_{py} / 270 (%)	Peak Load (lb)	f_{pu} (psi)	Peak Position (in)	Elongation (%)	E_p (ksi)
Nominal	**0.2940**	**71,442**	**243,000**	**90.0%**	**79,380**	**270,000**	**1.167**	**3.50%**	**28,500**
Maximum	0.2961	75,060	256,177	94.9%	83,400	284,106	3.010	9.37%	32,400
Minimum	0.2884	67,600	229,153	84.9%	77,300	262,034	1.607	3.11%	23,098
Average	**0.2942**	**72,308**	**245,787**	**91.0%**	**64,913**	**237,018**	**2.228**	**6.72%**	**28,168**
Standard Deviation	0.0010	1,764	6,364	2.36%	1,393	4,850	0.422	1.57%	1,028
5% Percentile	0.2930	69,210	234,602	86.9%	79,000	267,797	1.650	4.02%	26,952

It should be noted that many strands did not pass the ASTM A416 requirements as can be seen from data points to the left of the dashed line in Figures 3.5 to 3.10. However, strands were still considered acceptable even if they did not meet the steel area requirements. If one strand did not meet ASTM requirement, but no other strand in the coil was rejected by the tester, the coil was considered acceptable, similar to the rejection requirements of ASTM A416 Section 12. Of Producer 1's strands, two out of 36 did not meet the requirements. Of Producer 2's strands, 27 out of a total of 66 did not meet the requirements. It should be noted that ten of Producer 2's strands were from the same coil as that coil was used for other experiments. More importantly, Producer 2 had seven out of eleven coils of strands that did not meet the requirements, whereas all of Producer 1's coils met them. Upon inspection of the data, it seemed that the producers had the most trouble obtaining the yield strength required, as only three strands out of the 102 had problems reaching the ultimate strength required. All three of these strands did not meet the yield strength required, and none failed the minimum extension requirement.

From Figures 3.5 and Figure 3.6, one can see that the data follows an approximate normal distribution and a large difference in variability of the Producers for load at 1% strain. A larger slope of the data points, when plotted against the standard normal probability, indicates a higher degree of variation, as the slope is inversely proportional to the standard deviation. Furthermore it can be seen that Producer 2's data is scattered on both sides of the minimum, whereas nearly all of the data is above the minimum for Producer 1. The data in Figures 3.7 and 3.8 are slightly skewed by NDOR's practice of stopping the test immediately following attainment of the minimum breaking load. Each of the data points slightly to the right of the dashed line, representing the minimum, was obtained from NDOR. Breaking strength does not follow a normal distribution, nor does it follow a straight line on the standard normal scale.

The MOE of the strand affects the precast jacking procedures and the actual effective prestress of a girder. In the precast plant the load indicated by the jack and the calculated strand elongation must agree within 5% or work must end until reconciliation of the values. This permissible value seems high but would likely be dictated by relatively inaccurate field measurements. (Preston, 1985). Also of note, is the low average MOE for all of the strands. The average of 28,168 ksi is approximately 1% off from the assumed design average. Upon inspection of Figure 3.9 and

Figure 3.10, the highly linear plots indicate normally distributed data. Again, a much steeper slope is observed from Producer 2, in spite of the very consistent average. While the ASTM does not set a limit or range in which the MOE should fall, strand areas are regulated and affect the MOE. It has been suggested that tolerance of the manufacturer's wire drawing practice can create a variation of 1.2% in MOE (Preston, 1985) which may explain the low values obtained here. These strands have slightly higher areas on average, which would indicate lower calculated stresses and MOE values.
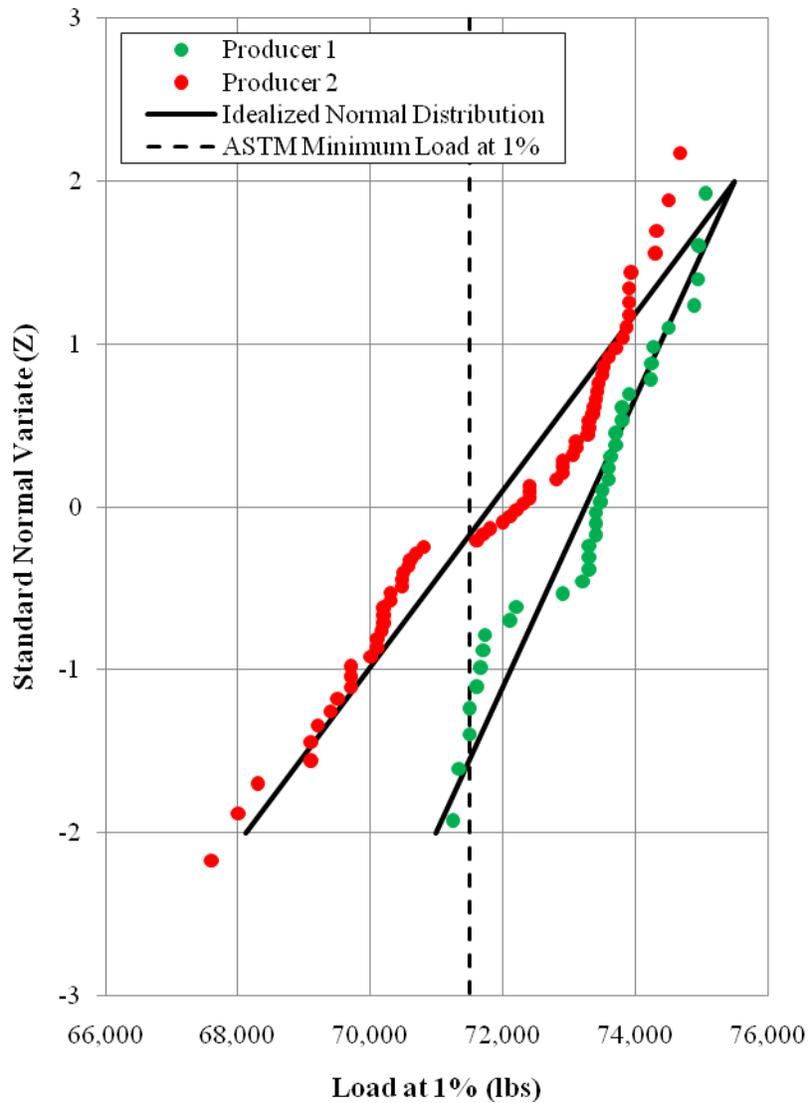
Figure 3.5: Normalized Probability vs. Load at 1% Strain for 0.7 in. Diameter Prestressing Strands from Different Producers
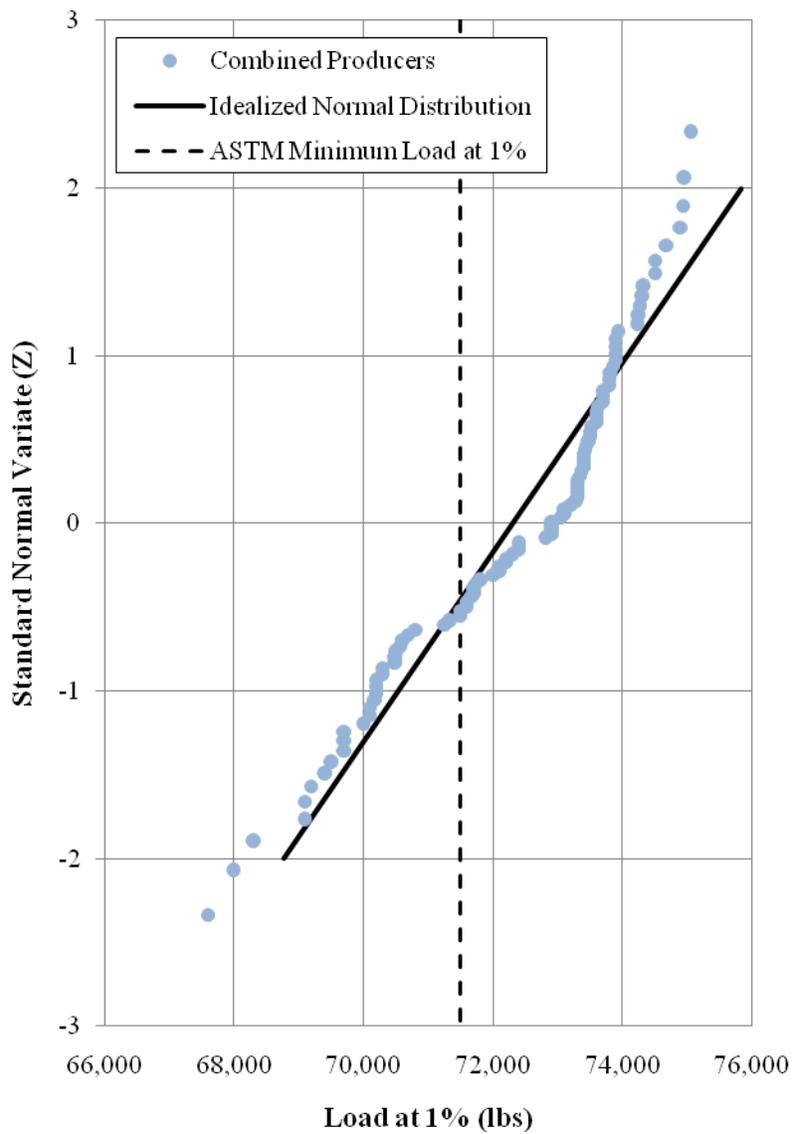
Figure 3.6: Normalized Probability vs. Load at 1% Strain for all 0.7 in. Diameter Prestressing Strands
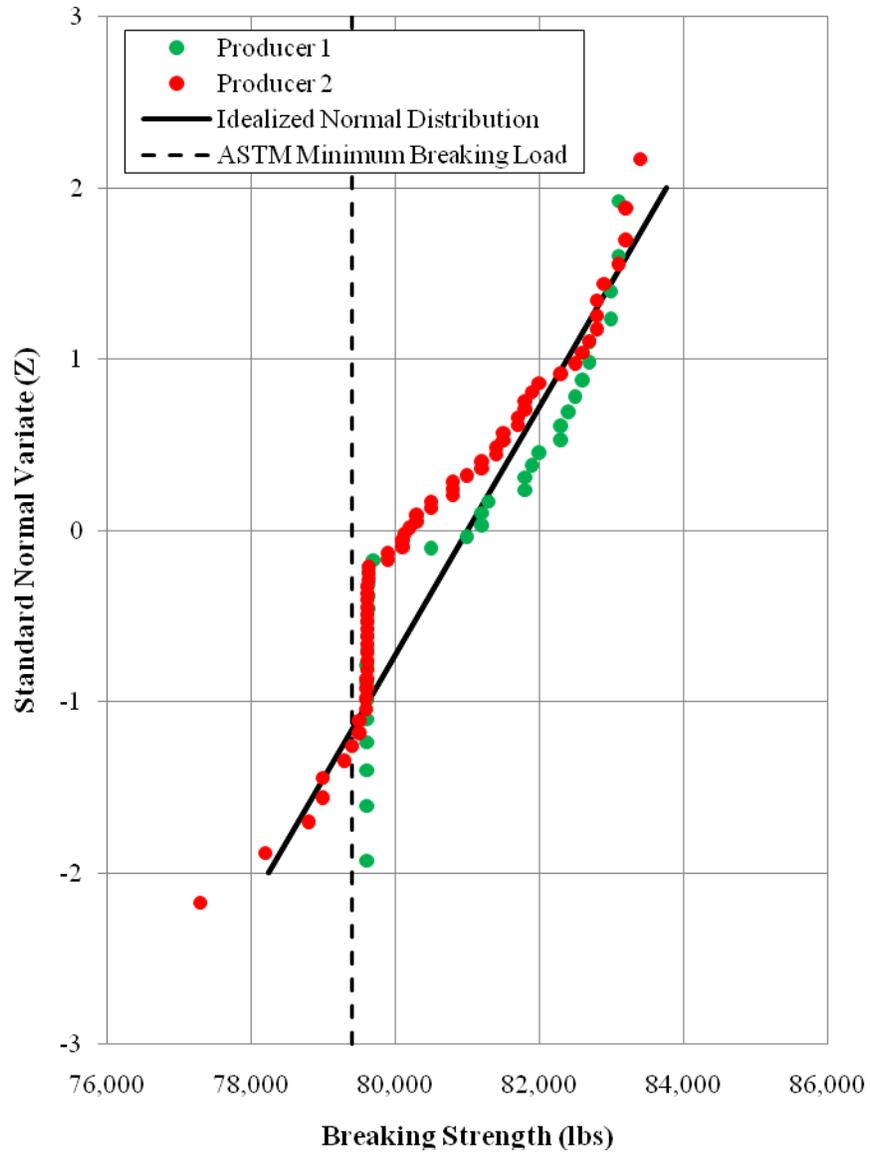
Figure 3.7: Normalized Probability vs. Ultimate Load for 0.7 in. Diameter Prestressing Strands from Different Producers
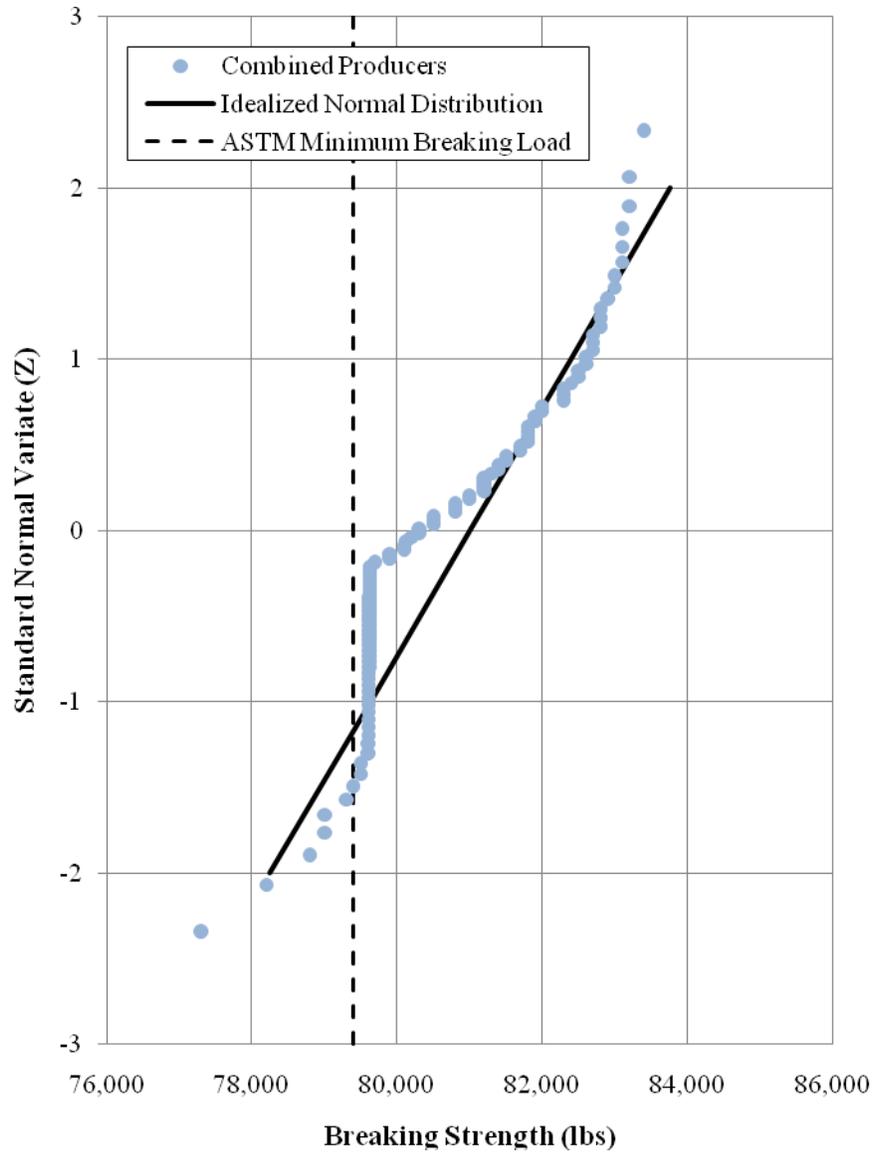
Figure 3.8: Normalized Probability vs. Ultimate Load for all 0.7 in. Diameter Prestressing Strands
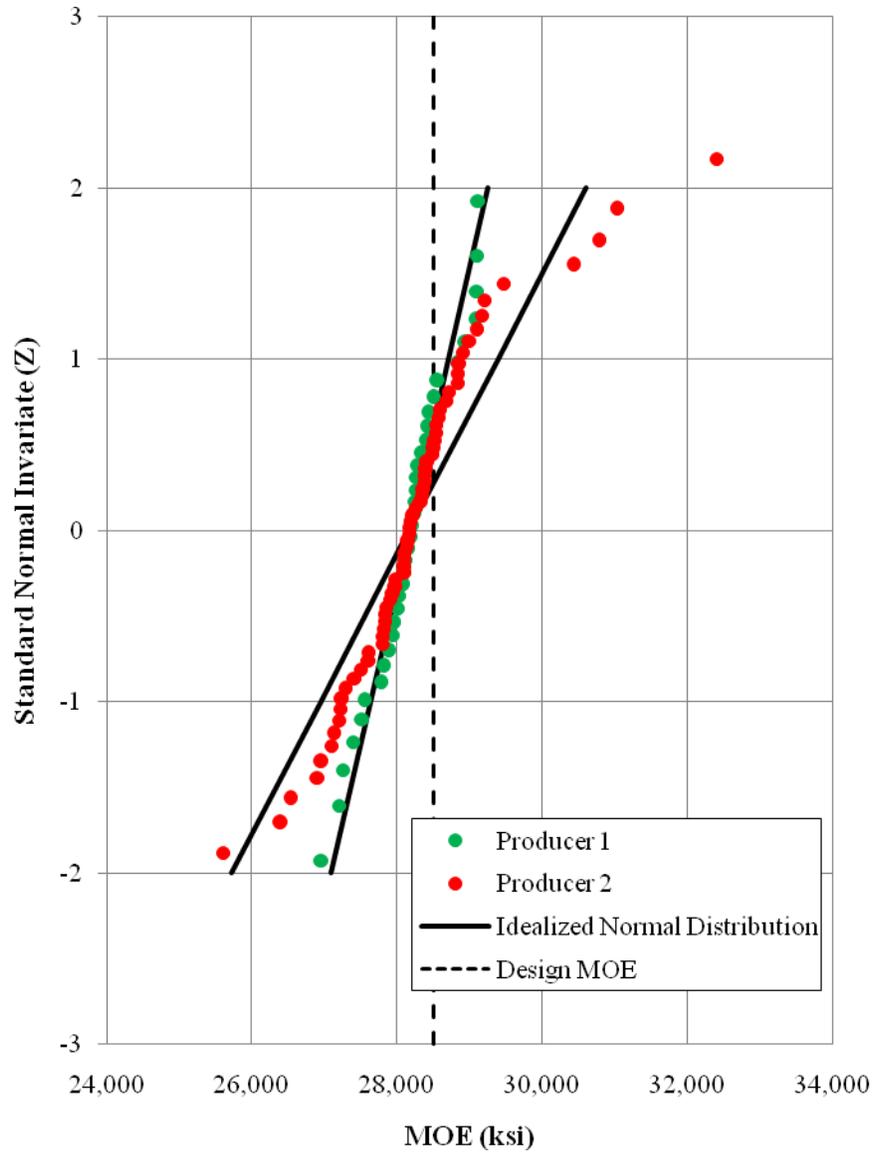
Figure 3.9: Normalized Probability vs. MOE for 0.7 in. Diameter Prestressing Strands from Different Producers
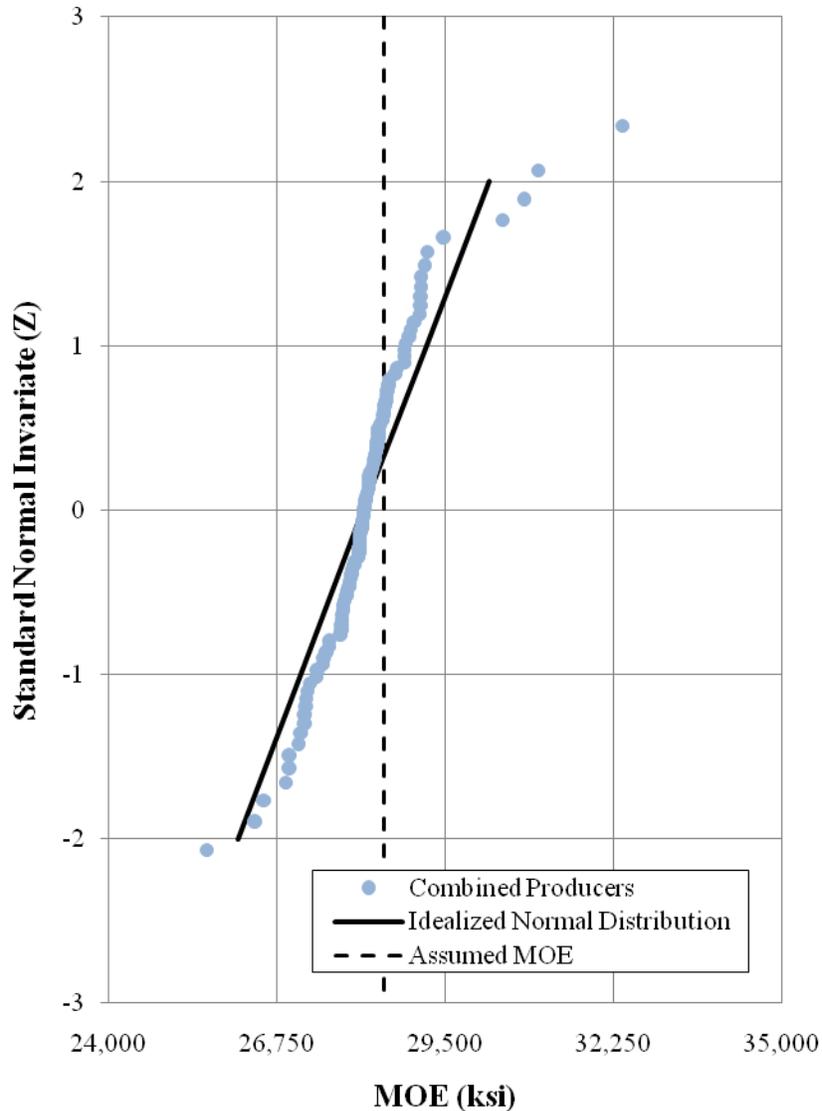
Figure 3.10 Normalized Probability vs. MOE for All 0.7 in. Diameter Prestressing Strands

Forty stress vs. strain curves were constructed for the 0.7 in. diameter strands tested above. Three to four strands from each order were used for stress vs. strain curves, with the exception of curves made for other experimentations, all of which were from Producer 2 and are elaborated upon later. The stress vs. strain curves were then compared to the PCI Design Handbook Equation and the Power Formula, discussed in the literature review. The latter used the conservative values for the constants, which are usually assumed by designers of prestressed members, recommended by Devalaupra and Tadros (1992).

Figure 3.11 shows the stress vs. strain curves plotted for both producers along with the prediction equations of the PCI Design Handbook and Power Formula. It is obvious that the stress vs. strain prediction equations do not adequately predict the behavior of the 0.7 in. diameter strands due to the lower yield stress than predicted. Both equations overestimate steel stresses around yielding behavior due to the calibration of the equations to more commonly produced diameters of strand, which tend to have higher average yield stresses. The PCI Design Handbook equation overestimates the yielding behavior more than the Power Formula does. They both underestimate the slope after yielding, which can be easily corrected through formula constants. Values in Figure 3.11, which fall well below the Power Formula represent strands that might be rejected based on low yield stress.
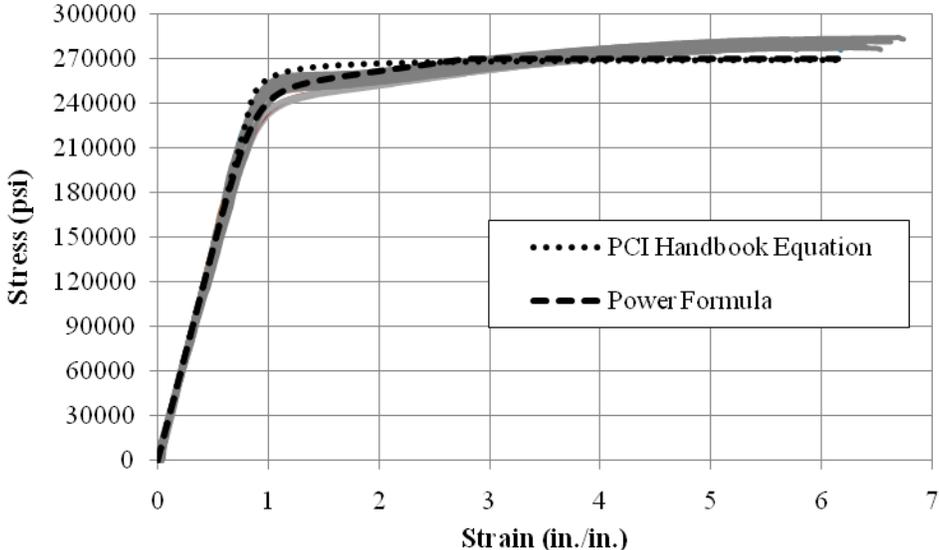
Figure 3.11: Comparing Stress-Strain Diagrams of 0.7 in. Diameter Strands vs. Existing Models

A secondary issue with the stress vs. strain behavior of the tested 0.7 in. diameter strands is the low MOE values. While there is little guidance in ASTM A416 on a minimum or maximum MOE, it is important for the designer to be confidant in design variables. An average MOE of 28,168 ksi is shown in, which is lower than assumed by designers (28,500 ksi), with a standard deviation of over 1,000 ksi.

3.2 NASP Testing

Five test methods are available for evaluating the bond of prestressing strands. Two test methods for tensioned strands: 1) ASTM A981–07 (2007) "Standard Test Method for Evaluating Bond Strength for 0.6 in. Diameter Prestressing Steel Strand, Grade 270, Uncoated, Used in Prestressed Ground Anchors"; and 2) a simple quality assurance test for strand bond (Peterman 2009). Three bond test methods are currently available for untensioned prestressing strands (Ramirez and Russell, 2008): 1) Moustafa test, where strands are pulled-out from large concrete block (Moustafa, 1974); 2) Post-tensioning Institute (PTI) test, where strands are pulled-out from neat cement mortar; and 3) North America Strand Producers (NASP) test, where strands are pulled-out from sand-cement mortar (Russell and Burns, 2008). NASP test results have proven to be the most repeatable at a testing site, reproducible among sites, and provide a reliable prediction of the performance of a pretensioned concrete product. In the NCHRP project 12-60, the NASP test was modified to evaluate the bond of 0.5 in. and 0.6 in. diameter strands in concrete and equations were developed to predict strand bond for a given concrete strength as below:

$$\text{For 0.5 in. strand diameter: } P(kips) = 14.08 \, f_c'^{\,0.37}(ksi)$$

$$\text{For 0.6 in. strand diameter: } P(kips) = 7.98 \, f_c'^{\,0.56}(ksi)$$

Where: P = NASP pull out bond value

f'_c = 1-day concrete strength

In this study, criteria for evaluating the bond of 0.7 in. diameter strands in mortar and concrete using NASP test method are presented. Fifty-eight 0.7 in. diameter strands obtained from the same manufacture but from different production cycles are tested and their results are used to develop an equation to predict the NASP pullout test value as a function of concrete strength. Moreover, NASP test results for 0.7 in. strand diameter with clean and rusted strands are measured and compared at different slip values. It should be noted that NASP test does not evaluate either the transfer or the development length of prestressing strands since it is performed on untensioned strands. It is a quality control test to determine whether the surface condition of strands is acceptable for bond with concrete (Bryan, 2008).

The NASP bond test specimen consists of an 18 in. long, 5 in. diameter and 1/8 in. thick steel pipe and a 6x6x1/4 in. steel plate as shown in Figure 3.12. The plate is attached to one pipe end with 4 bolts and nuts to seal the pipe end for concrete placement and provide a flat surface for loading. A 3/4 in. hole is made in the plate for passing the 0.7 in. diameter strand and a 2 in. bond breaker is used around the strand to reduce stress concentration at the plate location. Figure 3.12 shows a schematic diagram of NASP test setup at the University of Nebraska-Lincoln (UNL). Figure 3.13 shows the preparation of NASP specimen, and the NASP specimen mounted in the loading frame at UNL.
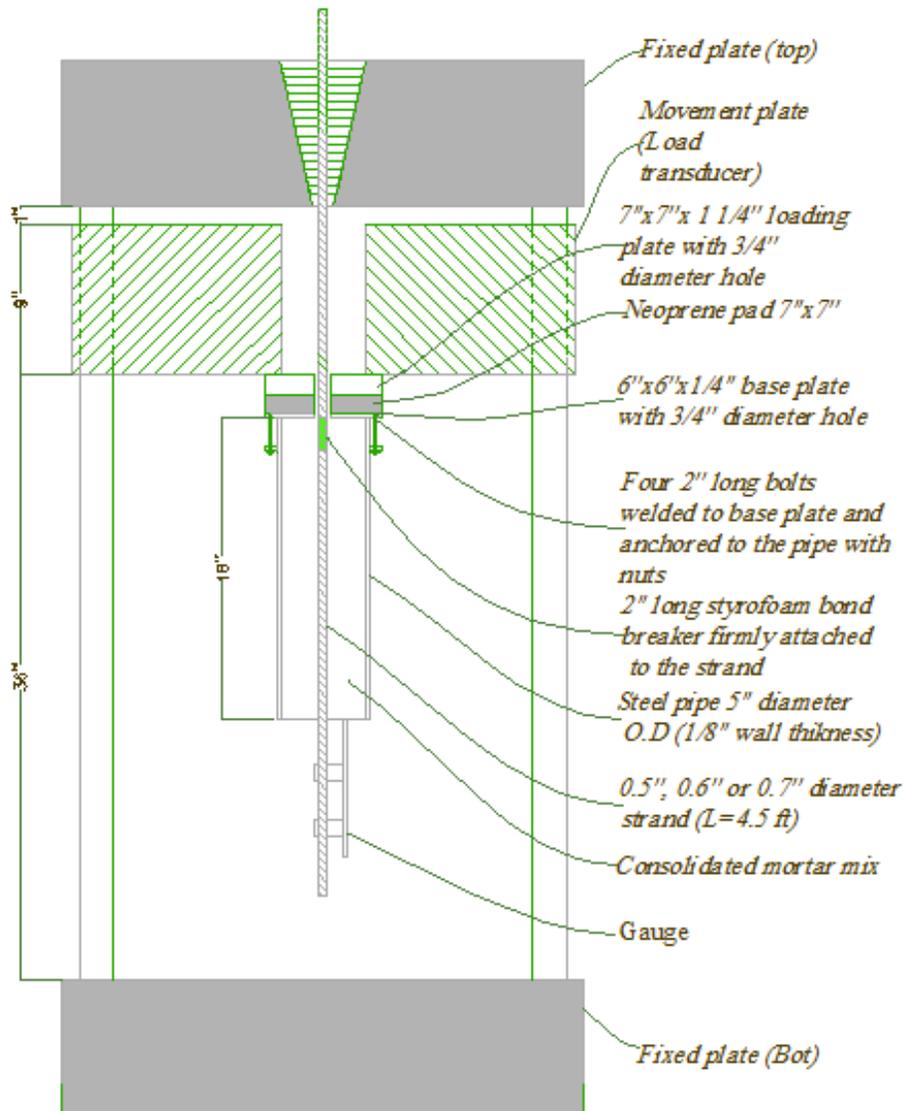
Figure 3.12: Schematic diagram of NASP test setup at UNL

Figure 3.13: Specimen and strand with 2 in. bond breaker (left), and test setup (right)

Each test specimen is prepared by casting sand-cement mortar in the steel pipe around a single prestressed strand. The sand-cement-water ratio is 2:1:0.45 and the cement used is type III cement. The sand-cement mortar is proportioned to produce strength of 4,500 to 5,000 psi at 24 hr, using standard curing, for cube specimens (ASTM C109-08). Additionally, the sand-cement mortar is required to produce a flow in the range of 100% to 125% as measured by ASTM C1437-01. The strand is pulled-out of the mortar at a displacement rate of 0.10 in. /min, 24 hr after casting. The pull-out force is measured in relation to the movement of the free end of the strand to the hardened mortar. The NASP bond test records the pull-out force that corresponds to 0.10 in. of free strand end slip. Each NASP bond test consists of six or more individual test specimens; the average value from the six specimens becomes the "NASP Bond Test Value." Values corresponding to 0.01 in. strand slip at the free end are also recorded (Russell and Brown, 2004).

The test method for the bond of prestressing strands limits the loading rate to 8,000 lb/min for 0.5 in. diameter strands and 9,600 lb/min for 0.6 in. diameter strands. Since the loading rate is

directly proportion to strand diameter, the loading rate for 0.7 in. diameter strands is estimated at 11,200 lb/min. (8000*0.7/0.5=11200 lb/min). Table 3.5 lists the acceptance criteria for 0.5 in and 0.6 in. diameter strands according to appendix H of the NCHRP report 603 (Ramirez and Russell, 2008). Since, these criteria are in proportion to the strand diameter, the acceptance criteria for 0.7 in. diameter strands are derived as shown in Table 3.5

Table 3.5: NASP acceptance criteria for different strand diameters

Strand Diameter (in)	Average value of the NASP strand bond test (kips)	Minimum value of the NASP strand bond test(kips)
0.5	≥ 10.5	≥ 9.0
0.6	≥ 12.6	≥ 10.8
0.7	≥ 14.7	≥ 12.6

NASP Bond Test results for 0.6 in. Diameter Strand:

Since the NASP test setup shown in Figure 3.12 is slightly different from the setup used in the NCHRP project 12-60, twelve 0.6 in. diameter strands were first tested. Test results were then compared against predicted values to evaluate the reliability of the modified setup. Table 3.6 lists the results of NASP tests performed at UNL on 0.6 in. diameter strands in concrete versus those predicted using NASP power regression formula. Table 3.6 also shows the number of tested specimens (N) at each concrete strength and standard deviation (S) for each set of tests. These results indicate that all specimens passed the acceptance criteria and the differences between test values and predicted values are approximately 3.5%, which confirms the agreement between the test values and predicted values.

Table 3.6: NASP bond test values for 0.6 in. diameter strands in concrete

Test	Strand diameter (in)	fc' (ksi)	N	Ave. NASP test value (kip)	S(kip)	*NASP power regression (lb)	Difference %
1	0.6	5.03	3	19.30	2.72	19.60	1.5
2	0.6	6.52	3	21.80	1.63	22.64	3.5
3	0.6	7.33	3	22.95	0.57	24.16	5.4
4	0.6	9.99	3	29.70	1.71	28.69	3.5
Average							3.5

*NASP power regression (NCHRP 12-60): $P(kips) = 7.98 f_c'^{0.56}(ksi)$

Table 3.7 lists the results of NASP tests performed at UNL on 0.6 in. diameter strands in mortar. A total of nine strands were tested and their results were compared against the values predicted using NASP power regression formula. These results indicate that all specimens passed the acceptance criteria and the differences between test values and predicted values are approximately 3.1%, which confirms the agreement between the test values and predicted values. Figure 3.14 plots the pull-out values obtained from NASP test at UNL for twenty one 0.6 in. diameter strands versus concrete/mortar strength. It also plots the NCHRP 12-60 power regression formula to illustrate that UNL test setup has adequate accuracy.

Table 3.7: NASP bond test values for 0.6 in. diameter strands in mortar

Test	Strand diameter (in)	fc' (ksi)	N	Ave. NASP test result (kip)	S(kip)	*NASP power regression (lb)	Difference %
1	0.6	4.77	3	19.30	1.12	19.03	1.4
2	0.6	4.78	3	20.32	1.24	19.06	6.2
3	0.6	4.88	3	18.90	1.34	19.24	1.8
Average							3.1

*NASP power regression (NCHRP 12-60): $P(kips) = 7.98 \, f_c'^{0.56}(ksi)$
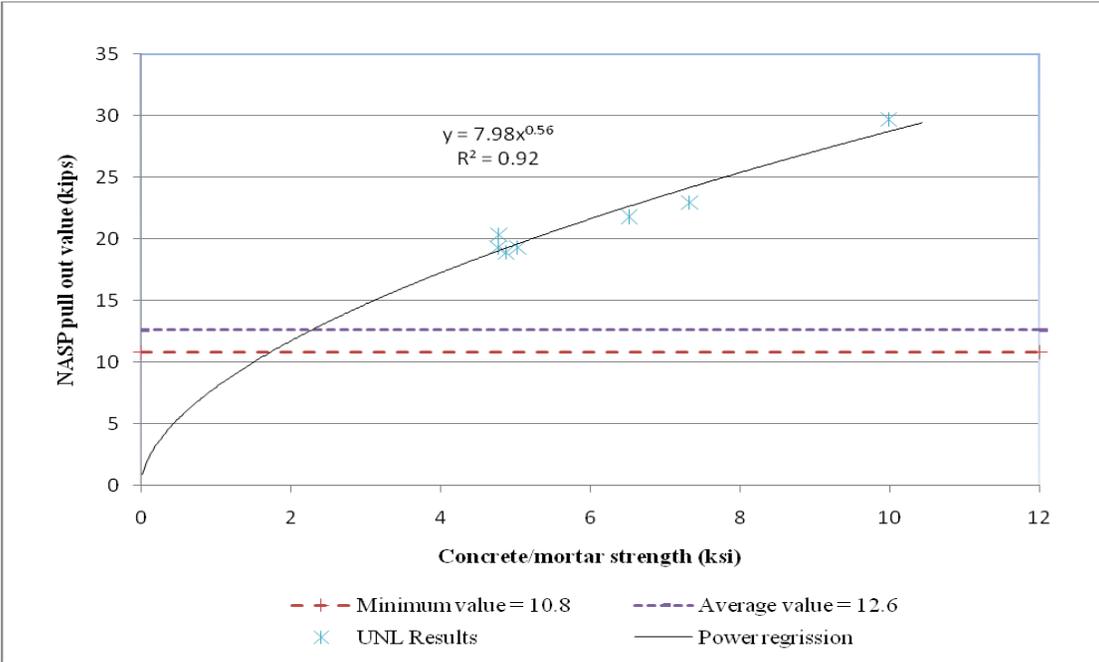
Figure 3.14: NASP bond test values for 0.6 in. diameter strands versus concrete/mortar strength

NASP bond test values for 0.7 in. diameter strands:

NASP bond test was performed on fifty-eight 0.7 in. diameter strands in mortar and concrete. The concrete used in this test had a 1-day strength varying from 4 ksi and to 10 ksi and a slump in the range of 2 to 3 in. The handling and preparation of the strands, the steel pipe, and the bond breakers were identical to the NASP bond tests conducted in sand-cement mortar. Table 3.8 shows the design of the five concrete mixtures used in this test as well as their 1-day compressive strength. Target strengths were 4, 5, 6, 8, and 10 ksi, however, actual strengths were slightly different,

Table 3.8: Concrete mixture proportions for NASP bond test specimens

Concrete Mixture Designation	Mix 1	Mix 2	Mix 3	Mix 4	Mix 5
Cement type III (lb/cy)	810	705	950	950	1050
Fly Ash, Class C (lb/cy)		378	100	100	300
Coarse Aggregate(lb/cy)	2088	1760	1700	1700	672
Fine Aggregate(lb/cy)	702	980	1150	1150	1580
Water(lb/cy)	297	260	390	330	240
Silica Fume(lb/cy)					150
HRWRA (lb/cy)	5.4	8.75	32	27	44
1-day Concrete Strength (ksi)	4.80	5.23	6.52	7.33	9.99

Table 3.9 shows the results of thirty NASP bond tests for 0.7 in. diameter strand in concrete. The concrete strengths reported in Table 3.9 were averages of three or more concrete specimens tested during the NASP test. Figure 3.15 plots the pull-out values from the NASP bond test for strands 0.7 in diameter versus the concrete strength, which results in 5 data points. Both linear and power regression formulas were developed and plotted. Figure 3.15 clearly shows that the increase in concrete strength results in a higher NASP pull-out value for strands 0.7 in diameter. Differences between average NASP test values and the predicted value using power regression formula are presented to indicate the accuracy of the developed formula. Also, the results show that the entire specimen passed the acceptance criteria presented earlier in Table 3.5.

Table 3.9: NASP bond test values for 0.7 in. diameter strands in concrete

Test	Strand diameter (in)	Mix	fc' (ksi)	N	Ave. NASP test result (kip)	S (kip)	*UNL power regression Eq.1 (kip)	Difference %
1	0.7	1	4.80	6	22.00	2.01	23.29	5.9
2	0.7	2	5.23	6	28.20	1.88	24.88	11.8
3	0.7	3	6.52	6	28.80	1.41	29.48	2.4
4	0.7	4	7.33	6	29.60	7.00	32.27	8.3
5	0.7	5	9.99	6	42.40	3.32	40.95	3.4
Average								6.4

*UNL power regression Eq.: $P(kips) = 6.96\, f_c'^{0.77} (ksi)$
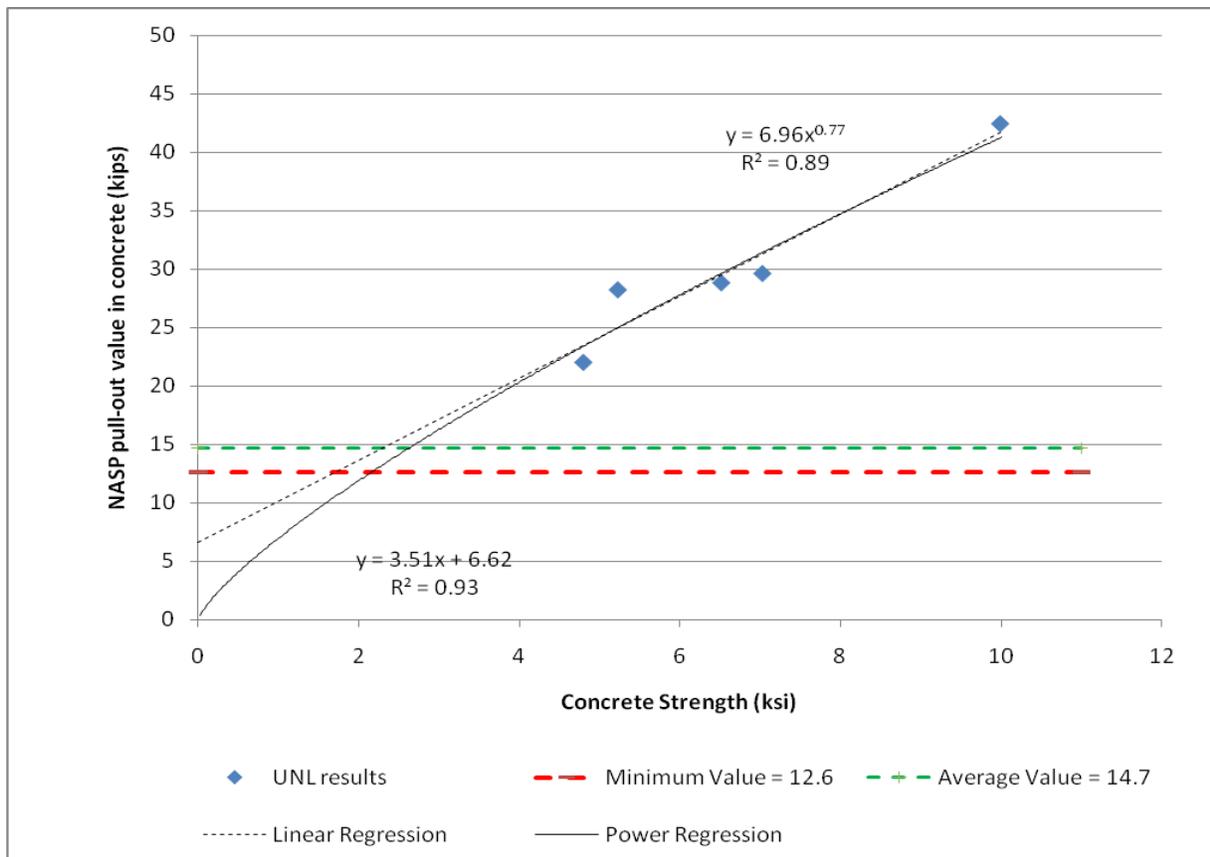
Figure 3.15: NASP bond test values for strand 0.7 in. diameter strands versus concrete strength.

The best-fit equation for 0.7 in. diameter strands is:

$$NASP(kips) = 6.96 f_c'^{0.77} (ksi)$$

Table 3.10 lists the results of twelve NASP bond tests for 0.7 in. diameter strands in mortar. These results indicate that all the specimens passed the acceptance criteria presented earlier in Table 3.5. The average difference between test values and predicted values is relatively high due to small number of tests performed.

Table 3.10: NASP bond test values for 0.7 in. diameter strands in mortar

Test	Strand diameter (in)	W/C	f_c' (ksi)	N	Ave. NASP test result (kip)	S (kip)	*UNL power regression Eq.1 (kip)	Difference %
1	0.7	0.45	4.78	4	21.25	0.55	19.03	8.5
2	0.7	0.45	4.88	4	22.56	2.45	19.06	11.2
3	0.7	0.45	5.00	4	22.30	1.85	19.24	7.2
Average								8.9

*UNL power regression Eq.: $P(kips) = 6.96 f_c'^{0.77} (ksi)$

Results of NASP bond test FOR clean and rusted strands:

In order to investigate the effect of the strand surface condition on the NASP bond test results, additional sixteen 0.7 in. diameter strands with rusted surface were tested. Figure 3.16 shows a picture of rusted and clean 0.7 in. diameter strands used in NASP bond test. Table 3.11 lists the pull-out force recorded at two different end slip values: 0.01 in. and 0.1 in. Comparing these results for rusted and clean strands indicates that rusted strands always have higher bond capacity with concrete than clean strands at end slip of 0.01 in. This is primarily due to the roughened surface of rusted strands and its effect on the coefficient of friction at the interface between the two materials. At higher end slip values, such as 0.1 in., the effect of the roughened surface on the bond capacity is significantly reduced due to the relative movement of the strand, which results in a drop in the pull-out force.

Rusted

Strand

Figure 3.16: Surface condition for 0.7 in. diameter clean and rusted strands

Table 3.11: NASP bond test values for 0.7 in. diameter clean and rusted strands

Mix #		Rusted 0.7 in. diameter strand						Clean 0.7 in. diameter strand					
			Slip 0.01 in.		Slip 0.1 in.		$\frac{NASP_{0.1\,in.}}{NASP_{0.01\,in.}}$		Slip 0.01 in.		Slip 0.1 in.		$\frac{NASP_{0.1\,in.}}{NASP_{0.01\,in.}}$
		N	Avg. (kip)	S (kip)	Avg. (kip)	S (kip)		N	Avg. (kip)	S (kip)	Avg. (kip)	S (kip)	
1	4.8	4	24.9	2.48	25.3	1.91	1.02	6	17.7	2.34	22.0	2.01	1.24
3	6.5	4	34.7	0.14	31.0	7.07	0.89	6	23.4	0.42	28.8	0.14	1.23
4	7.3	4	39.0	0.92	40.6	0.14	1.04	6	26.6	6.86	29.6	7.0	1.11
5	9.9	4	56.2	1.84	23.2	0.3	0.41	6	40.5	3.11	42.4	3.32	1.05
Average							0.84	Average					1.18
Standard Deviation							0.29	Standard Deviation					0.09

Figures 3.17a and b plot the average NASP bond test values for rusted and clean strands at end slip 0.01 in. and 0.1 in. respectively. At 0.01 in. end slip, rusted strands have approximately 40% higher NASP bond value than clean strands. However, at 0.1 in. end slip, some rusted strands had approximately the same NASP bond value of clean strands, while others had even lower NASP bond values than clean strands. It should be also noted that bond of clean and rusted strands is proportion to concrete strength at the lower end slip values.
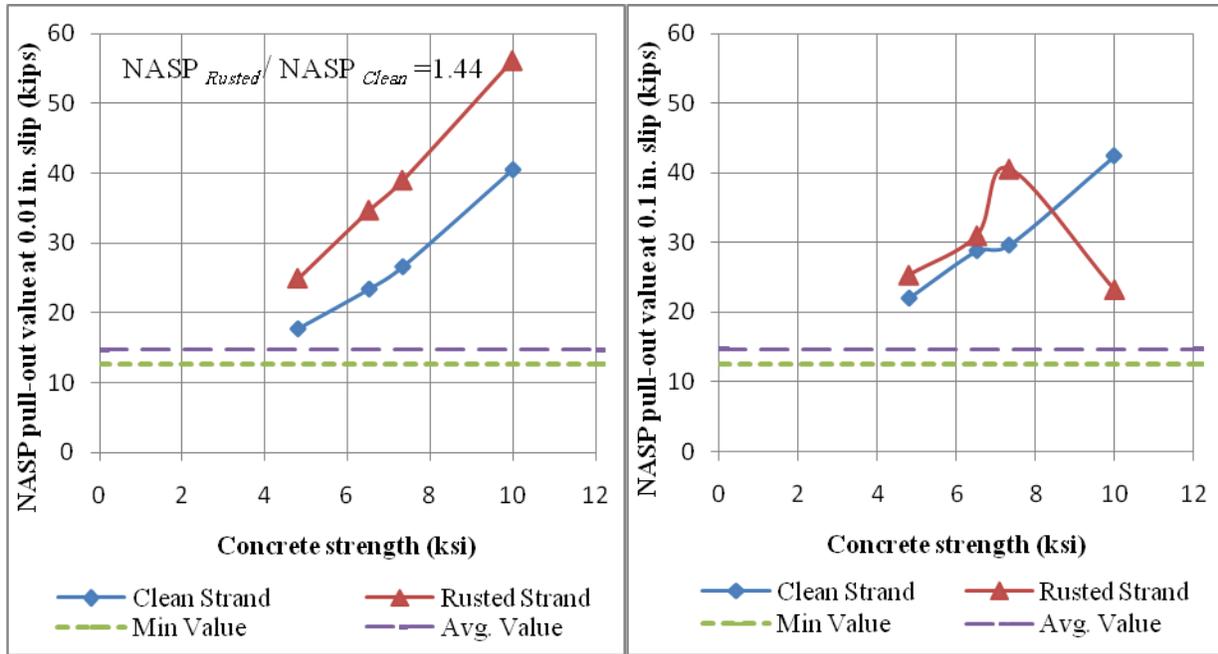
A) 0.01 in. end slip   B) 0.1 in. end slip

Figure 3.17: NASP bond test values for clean and rusted 0.7 in. diameter strands versus concrete strength

4. TESTING OF UHPC GIRDERS

4.1 Overview

The test program conducted in this study focused on evaluating the use of 0.7 in. diameter strands in conjunction with ultra-high performance concrete (UHPC) to fully utilize the benefits of 0.7 in. diameter strands. This included testing two full-scale standard bridge girders: NU900, and bridge double tee (BDT). The objectives of this testing are as follows

1. Introduce the use of 0.7 in. diameter stands at 2 in. by 2 in. end spacing

2. Determine whether current design specifications can be used for girders made of UHPC and 0.7 in. diameter strands, which fully utilize the advantages of both materials.

3. Evaluate transfer and development lengths for 0.7 in. diameter strands in UHPC girders

4. Investigate the shear capacity of UHPC girders with 0.7 in. diameter strands.

Ultra-high-performance concrete (UHPC), originally known by reactive powder concrete, is a new class of concrete that was developed in France in the mid-1990s. UHPC is a high-strength ductile material that is made of a special combination of fine sand, cement, quartz flour, silica fume, steel fibers, water, and high-range water-reducing admixture (HRWRA). The Association Francaise de Genie Civil (AFGC) in its "Interim Recommendations for Ultra High Performance Fibre-Reinforced Concretes" and the Japan Society of Civil Engineers (JSCE) in its draft of "Recommendations for Design and Construction of Ultra High Strength Fiber Reinforced Concrete Structures" define UHPC as a cementitious composite that has a compressive strength in excess of 21.7 ksi and contains steel fibers for ductile behavior (AFGC 2002; JSCE 2006). The enhanced strength and durability properties of UHPC are mainly due to optimized particle gradation, use of steel fibers, and extremely low water-powder ratio, which produces a very tightly packed mixture. Random steel fibers represent approximately 2% by volume or 6% by weight of the UHPC mixture. They are also considered the largest component of the mixture, as they are 0.5 in. in length and 0.008 in. in diameter. Steel fibers used in UHPC mixtures have a modulus of elasticity of 29,790 ksi, and a tensile strength that exceeds 290 ksi (FHWA 2006).

Despite the strength and durability characteristics of fiber-reinforced UHPC, the increase in concrete material cost represents the main impediment to its wide use in actual projects. The material cost of UHPC proprietary mixtures is over $1000 per cubic yard, including approximately $400 for steel fibers. In addition, the lengthy mixing procedure (45 minutes per batch), special placement requirements (to ensure proper consolidation and orientation of fibers), and longer curing and setting times significantly increase the production cost. Therefore, a nonproprietary UHPC made of local materials without steel fibers was developed in a parallel project and applied to the following two experiments as an economical alternative to commercial proprietary fiber-reinforced UHPC (NDOR P310, 2009). The following two sections presents the design, fabrication, and testing of two full-scale UHPC bridge girders pretensioned with 0.7 in diameter strands at 2 in. by 2 in. spacing.

4.2 UHPC NU900 Girder

The UHPC NU900 specimen was fabricated in March, 2008 by CoreSlab Structures, Omaha, and shipped to the PKI Structural Laboratory for instrumentation and testing in May, 2008. The specimen is a 40 ft long NU900 and has the cross section and reinforcement details shown in Figure 4.1. This section has adequate flexural and shear capacities required for a simply supported bridge to span 87 ft with 12 ft spacing between girder lines designed according to AASHTO LRFD. The girder is pretensioned using thirty 0.7-in.-diameter Grade 270 low-relaxation prestressing strands tensioned to $0.66f_{pu}$ due to the limited capacity of the prestressing bed. Four partially prestressed (19.6 ksi) 0.5-in.-diameter strands are placed in the top flange to control cracking at release in addition to four no. 5 Grade 60 bars used as compression reinforcement. The shear reinforcement consists of two orthogonal welded-wire reinforcements (WWRs) made of D31 at 6 in. spacing in the horizontal direction and 8 in. spacing in the vertical direction. The end zone is reinforced using four no. 6 Grade 60 bars at 2 in. spacing along the girder axis. Two 0.5-in.-thick Grade 50 steel plates are placed at the girder ends and anchored using eight 0.5-in.-diameter headed studs on each plate. The bottom flange is reinforced using two D11 WWR at 6 in. spacing and no. 3 cap bar to enclose the prestressing strands along the entire girder length in addition no. 3 at 6 in. along 3 ft from the girder ends. Figures 4.2 and 4.3 show girder reinforcement and strand spacing in the precast yard before concrete placement.
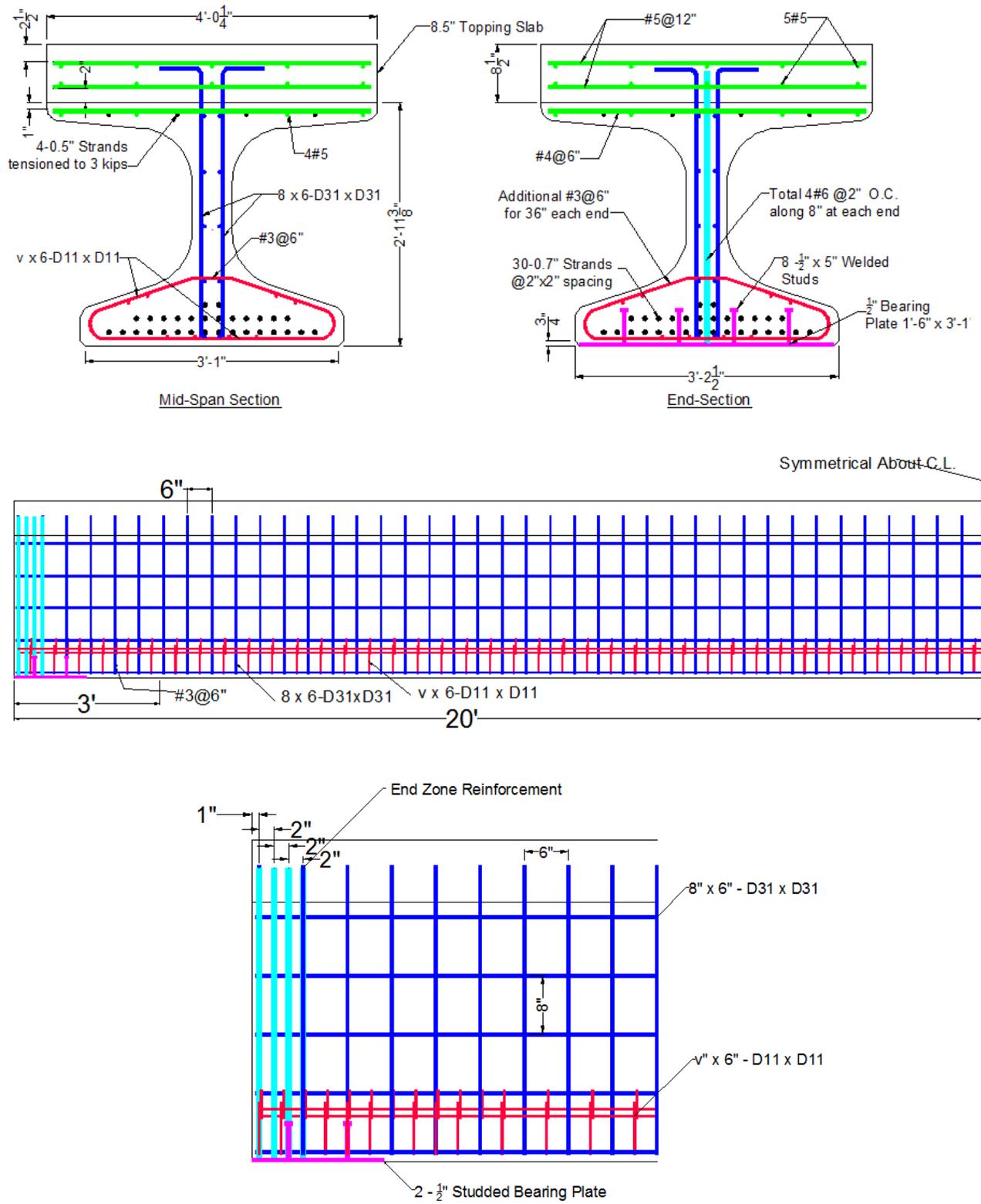
Figure 4.1: Dimensions and reinforcing details of NU900 girder specimen

Figure 4.2: Bottom flange and web reinforcement of the NU900 girder specimen

Figure 4.3: Horizontal and vertical spacing between 0.7 in. diameter strands

The girder was made of ultra-high-performance concrete (UHPC) that has a specified 1-day concrete compressive strength of 12 ksi and 28-day concrete compressive strength of 15 ksi. The girder required 6.5 yd^3 of concrete that was batched in three batches of 3 yd^3 each. The slump flow test was conducted at the plant to evaluate the self-consolidating properties of the fresh concrete. Figure 4.4 shows a 30 in. spread of the concrete immediately after batching. Upon reaching the specified release strength, strands were released using flame cut. Girder ends were inspected after release and did not show any visible cracks as indicated in Figure 4.5. This is primarily due to the significantly high concrete strength at release and the adequate end zone reinforcement as well as bottom flange confinement.

Figure 4.4: Measuring the spread diameter of UHPC used in fabricating the NU900 specimen

Figure 4.5: End zone of the NU900 girder specimen after release

To measure the transfer length of 0.7 in. diameter strands, Detachable mechanical (DEMEC) gages were placed at the two girder ends along the two sides of the bottom flange at the elevation of the centroid of prestressing strands. These gages were manufactured by Hayes Manufacturing Company in the United Kingdom and attached to the concrete surface before release using rapid set glue. The number of DEMEC gages used in each side was 19 at 4 in. spacing (102 mm), as shown in Figure 4.6 to ensure accurate readings and cover the predicted transfer length, which is 42 in. (1067 mm). DEMEC readings were taken at 1, 7, 14, 21, and 28 days using W.H. Mayes & Son caliper gage. The change in the measured distance between DEMEC gages was used to calculate the strain in the concrete at different ages.

Figure 4.6: Transfer length measurements using DEMEC gages

The transfer length can be determined using the 95% average maximum strain method (AMS) as noted in Russell and Burns (1996). After prestress release, the prestressed concrete strain is zero at the girder ends, then increases, and becomes relatively constant as the distance from the girder end increases and the strand fully transfers its force to the girder. The point where the strain becomes constant distinguishes where all of the prestressing forces are transferred to the

concrete. The transfer length can be determined by measuring the distance from the end of the girder to the point where 95% of the maximum concrete strain is measured. The strain profiles obtained from DEMEC gage readings at the two sides (1 and 2) of the two girder ends (S and N) indicated that the average transfer length of 0.7 in. diameter strands calculated using the AMS method is approximately 26 in. This value is less than the value predicted using American Concrete Institute's (ACI's) *Building Code Requirements for Structural Concrete (ACI 318-08) and Commentary (ACI 318R-08)*, which is $50d_b$, while it is significantly less than the value predicted using 2007 AASHTO LRFD specifications, which is $60d_b$. This is primarily due to the high compressive and bond strength of the UHPC used in this girder. Another observation is the change in the strain with time. This is primarily due to the shrink and creep of the prestressed concrete, which happens at higher rates at the early ages and slows down thereafter.

An 8.5 in. thick, 12 ksi concrete deck was placed over the top flange of the girder at the precast plant to simulate the composite section that has a 4 ksi deck and NU900 girder with 12 ft spacing. Figure 4.7 shows the composite girder at the precast yard. The specimen was then shipped to the PKI structural laboratory for testing. A 6 ksi concrete diaphragm was cast at each girder end as shown in Figure 4.8. Ten strands were bent and embedded in the end diaphragms, which is the common practice in I-girder bridge construction in Nebraska.

Figure 4.7: Composite concrete deck on the NU900 specimen
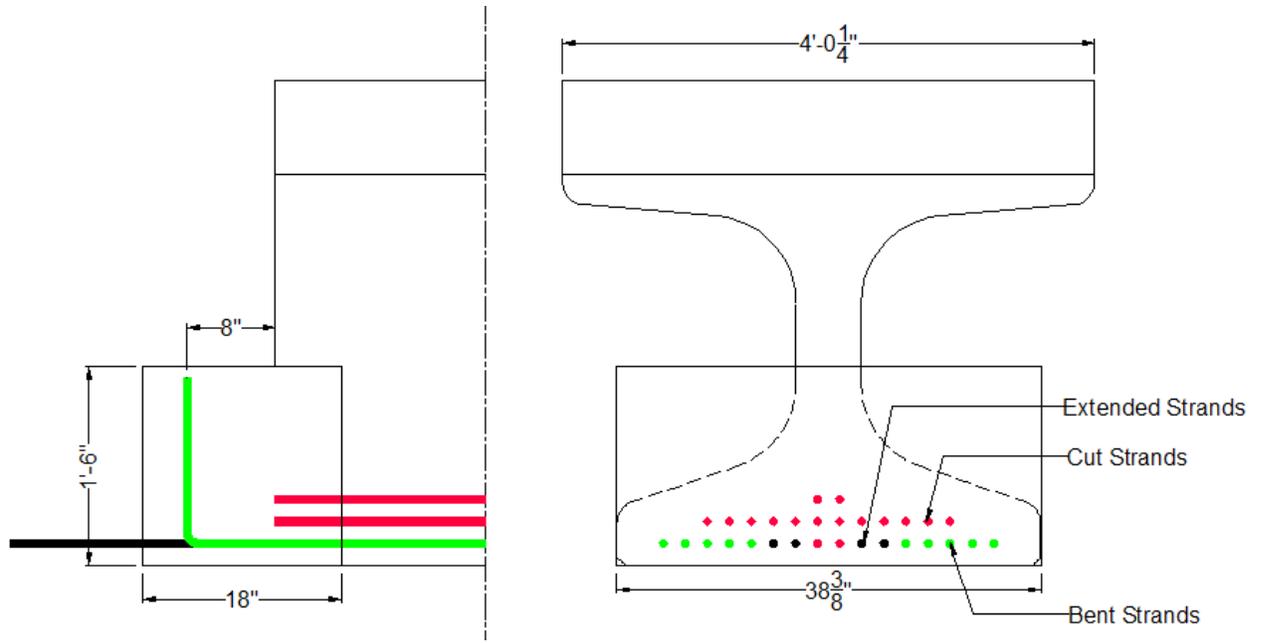
Figure 4.8: Dimensions and detailing of concrete end-diaphragms in NU900 specimen

The test setup for the NU900 girder can be found in Figure 4.10. Two Electrical Resistance Strain Gauges (ERSGs) were placed near the top and bottom flange, 3 ft toward the support from the load, to monitor the depth of the neutral axis. Two more ESRGs were placed directly under the load, offset from the centerline of the bottom flange by 6 in. These gauges were placed to allow the measurement of the maximum longitudinal strain of the bottom fiber of the girder and to help identify the first cracking. String potentiometers (ST-POTs) were used to measure the deflection of the girder directly under the load. In order to monitor strand movement during the development length tests, ST-POTs were attached to the strands such that the movement of the strands relative to the girder could be monitored. Because of a limited number of ST-POTs manual dial gauges were also used to measure end slip. These gauges were attached using insulating foam and zip ties. Figure 4.9 shows the ERSGs and SR-POTs attached to the NU900 specimen before testing.

Figure 4.9: Measuring strand end slip and surface strain in NU900 specimen

NU900 Test 1 - 15 ft From End

800 kip

15'

$1\frac{1}{2}$"

$2\frac{7}{8}$"

6"

A-A

NU900 Test 2 - 10 ft From End

800 kip

10'

North

LEGEND:

ST-POT

Dial Gauge

ERSG

$1\frac{1}{2}$"

3'

$3\frac{1}{2}$"

6"

A-A

6"

6"

$1'-7\frac{1}{4}$"

ST-POT

Section A-A
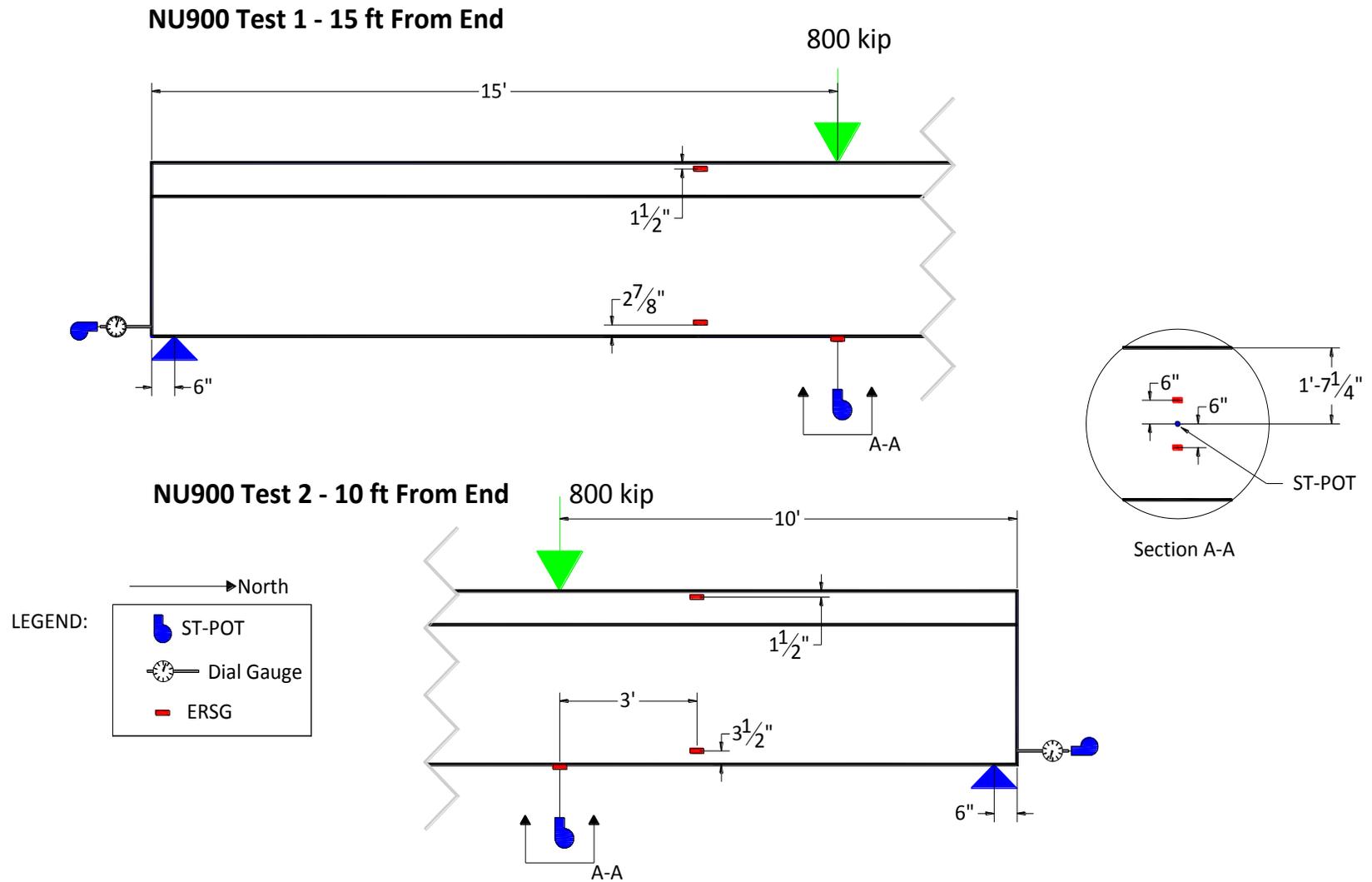
Figure 4.10: NU900 Girder Test Setups

59

To determine the ultimate capacity of the specimen more accurately, actual material properties were determined before testing. Figure 4.11 shows the compressive strength of the girder concrete versus time. Table 4.1 summarizes the results of all material testing performed on the UHPC used in specimen fabrication. Figure 4.12 also shows the actual stress-strain diagram of the 0.7 in. diameter strands used in pretensioning the girder. Table 4.2 lists the measured load at 1% strain, peak load, modulus of elasticity, and ultimate elongation for the three tested samples as well as those specified by the ASTM A416-06 and AASHTO M203-07. Actual concrete and strand properties were used in predicting the ultimate flexural capacity of the specimen.
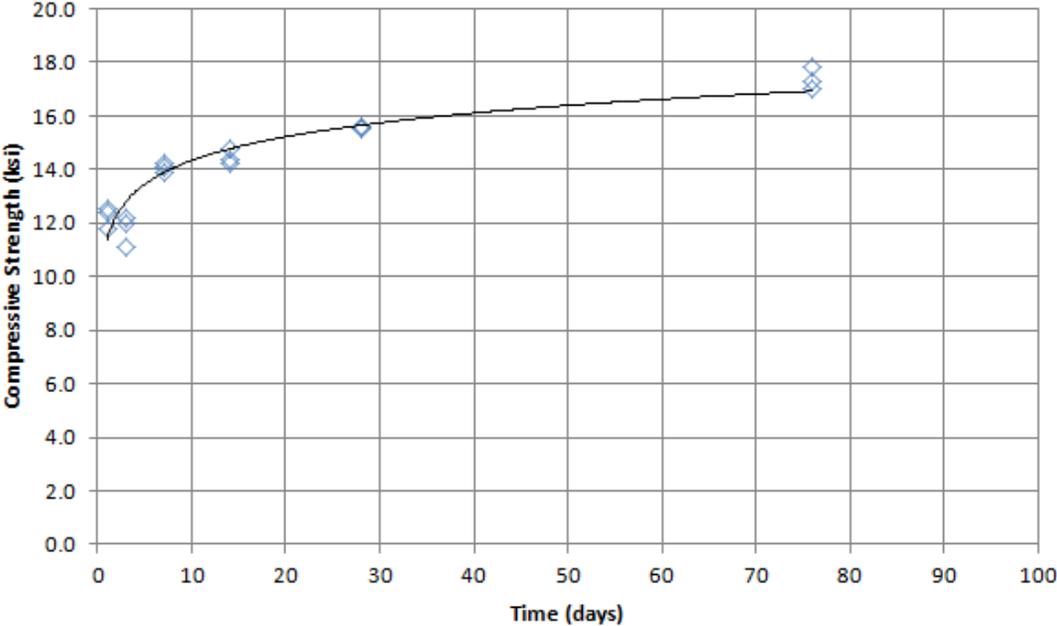
Figure 4.11: Girder concrete strength versus time

Table 4.1: Summary of UHPC material test results

	NU900 Girder
Release Compressive Strength (ksi)	12.22
28 Day Compressive Strength (ksi)	15.57
Final Compressive Strength (ksi)	17.35
28 Day MOE (ksi)	6,028
28 Day MOR (psi)	1,366
28 Day Splitting Strength (psi)	939
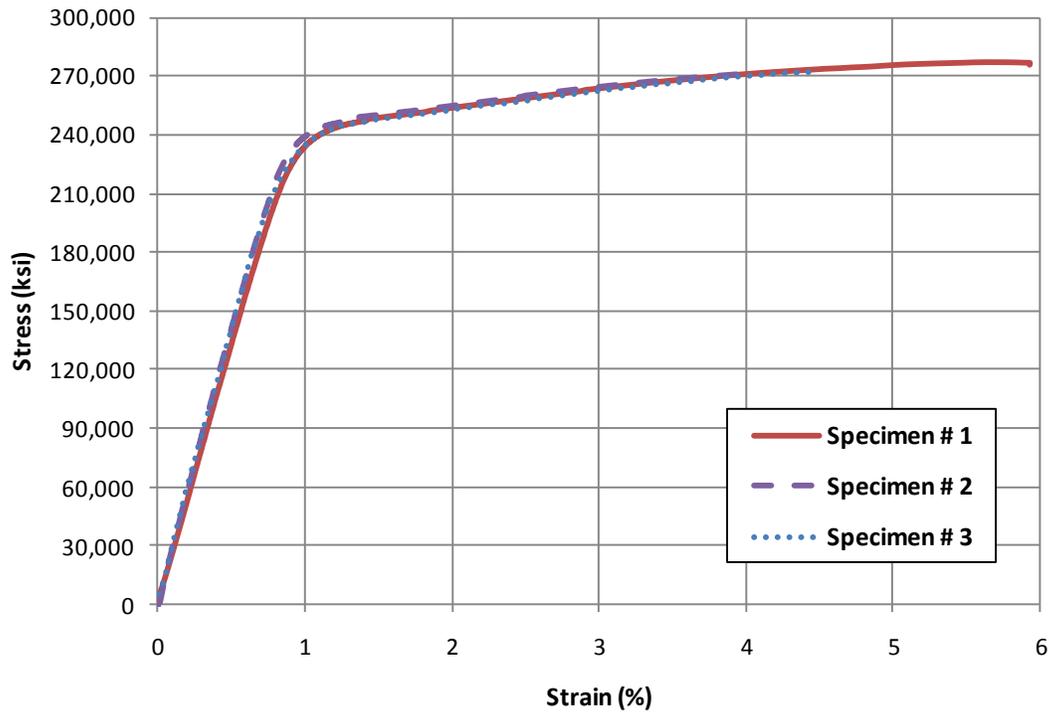
Figure 4.12: Stress-strain relationship of 0.7 in. diameter strands

Table 4.2: Results of testing three 0.7 in. diameter strand specimens

Specimen ID	Load at 1% Strain (lb)	Peak Load (lb)	Elongation (%)	MOE (ksi)
1	70,600	81,700	5.9%	27,100
2	71,200	79,800	4.0%	28,400
3	69,500	80,300	4.5%	28,500
Average	70,433	80,600	4.8%	28,000
ASTM A416-06 AASHTO M203-07	71,500	79,400	3.5%	N/A

The NU900 specimen was designed according to the AASHTO LRFD specifications to carry a point load located at 15 ft from the girder end. This is because 15 ft is the predicted development length of 0.7-in.-diameter strands according to AASHTO LRFD specifications' section 5.11.4.2.

The theoretical flexural capacity of the composite section was estimated at 7295 kip-ft, which corresponds to a point load of 779 kip including the weight of the girder. This theoretical capacity was estimated using strain compatibility and specified material properties.

The specimen was tested twice. The first test setup is shown in Figure 4.13 as the specimen was loaded at a distance of 15 ft from the end of the girder. The load was increased gradually up to the maximum capacity of the loading jack, which is 800 kips. The specimen did not fail, however, there was significant flexure and shear flexure cracking observed as shown in Figure 4.14. Cracks were observed and traced with markers at 100 kips increments up to 700 kips and labeled. Web shear cracks were first observed just before 300 kips, while flexural cracks did not begin until just before 500 kips.
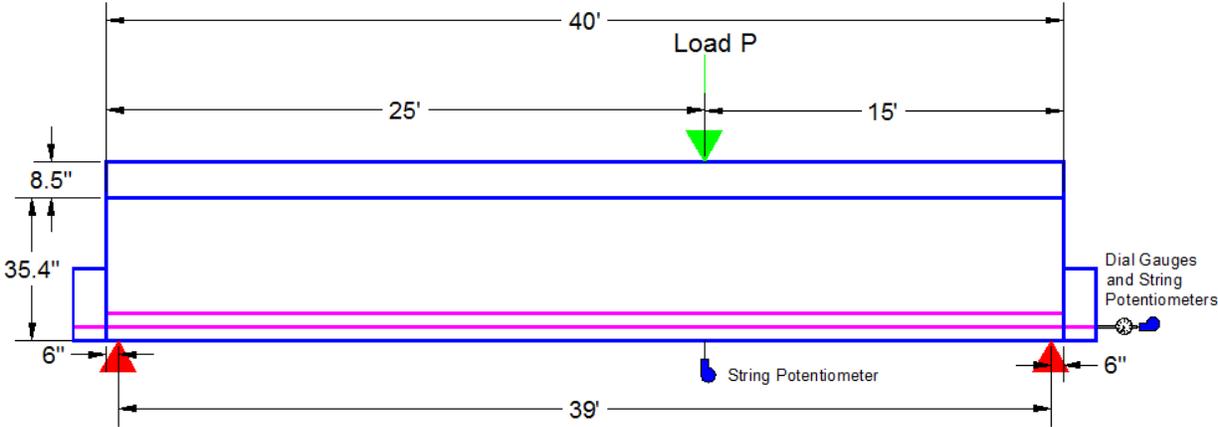
Figure 4.13: Setup of test #1 of NU900 girder specimen
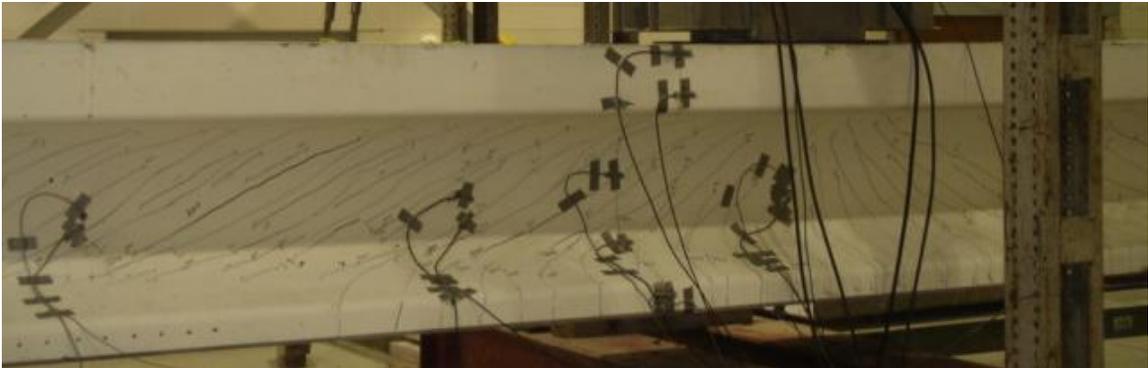
Figure 4.14: NU900 Final Crack Distribution

The load-deflection relationship of test #1 is shown in Figure 4.15. The maximum load applied was 800 kips, which corresponded to a total deflection of approximately 2.53 in. It should be noted that before unloading, the slope of the load vs. deflection curve was still relatively steep, indicating significantly more load carrying capacity. A distinctly different slope was observed near 500 kips, which corresponded to the observed cracking load. The ultimate load was not reached for the NU900 girder due to the difference in specified and actual material properties. Table 4.3 summarizes the predicted and observed capacity as well as the ultimate strand strains and stresses in the bottom row of strands. Values in table 4.3 are based on strain compatibility.
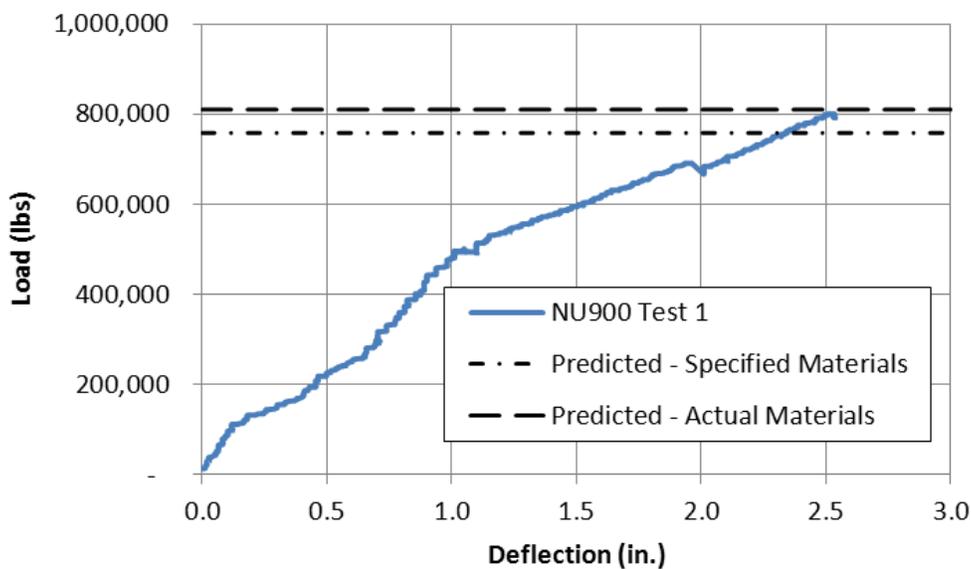
Figure 4.15: Load vs. deflection for test #1 of NU900 specimen

Table 4.3: Predicted and observed values for NU900 girder test #1

	Predicted		
	Specified Materials	Actual Materials	Observed
Total Moment Capacity (kip-ft)	7094	7567	7479
Point Load Capacity (kip)	758	810	800
Strand Strain at Ultimate (%)	1.45%	2.26%	1.91%
Strand Stress at Ultimate (ksi)	258	266	262

The bottom fiber ERSGs were used to identify the ultimate strain of the girder as well as to observe the exact cracking load and strain for the bottom fiber as shown in Figure 4.16. It should be noted that a crack was observed passing through the gauge length for both gauges; however, the crack did not pass perpendicular on either gauge, which may be the cause of the inconsistent post-cracking behavior of the ERSGs. This type of post-cracking was found to be typical of ERSG in tension regions.
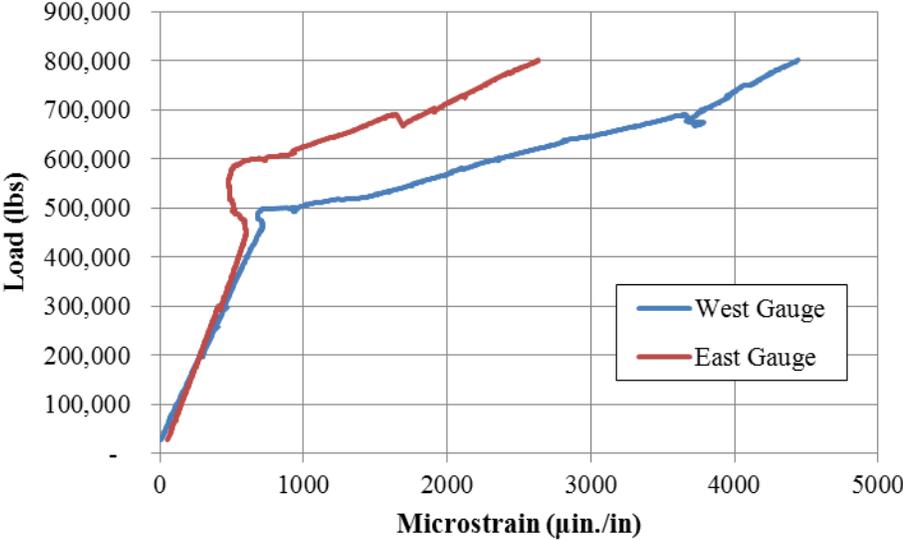
Figure 4.16: NU900 girder Test #1 bottom fiber strains

Figure 4.17 illustrates the depth of the neutral axis as the load increases using bottom and top strain gauges. It can be seen that after initial stabilization of the strains at the beginning of the plot, up to around 100 kips, the neutral axis remains at approximately the transformed un-cracked neutral axis of the composite girder. At the approximate cracking load of about 500 kips, the neutral axis re-stabilizes and gradually rises as the girder continues cracking. The graph ends at approximately the ultimate neutral axis calculated from strain compatibility. This behavior indicates that the NU UHPC does not exhibit any problems related to flexure and displays predictable, conventional behavior.
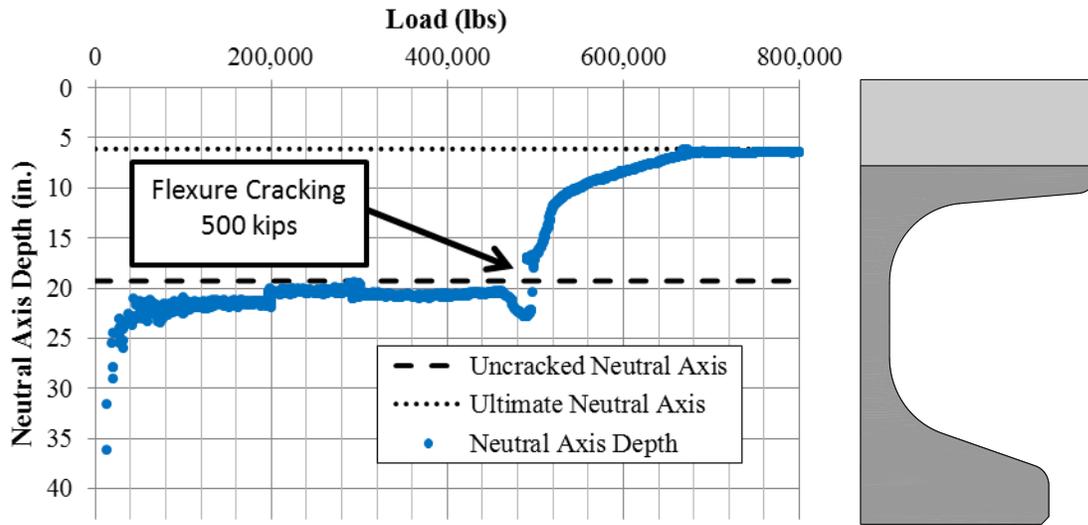
Figure 4.17: NU900 girder test #1 plot of neutral axis depth using surface mounted ERSGs

The slippage of the strands was monitored throughout the development length test with a combination of manually read dial gauges and ST-POTs. Dial gauges registered no change at any load. Figure 4.18 indicates slippage vs. load for the NU900 Test #1. The slippage gauge attached to the eastern extended strand experienced technical difficulties and was omitted from the plot. It can be seen that even though an exceptional amount of noise was registered for the ST-POT, the strand did not exceed the slippage limit of 0.01 in. needed for a bond failure.
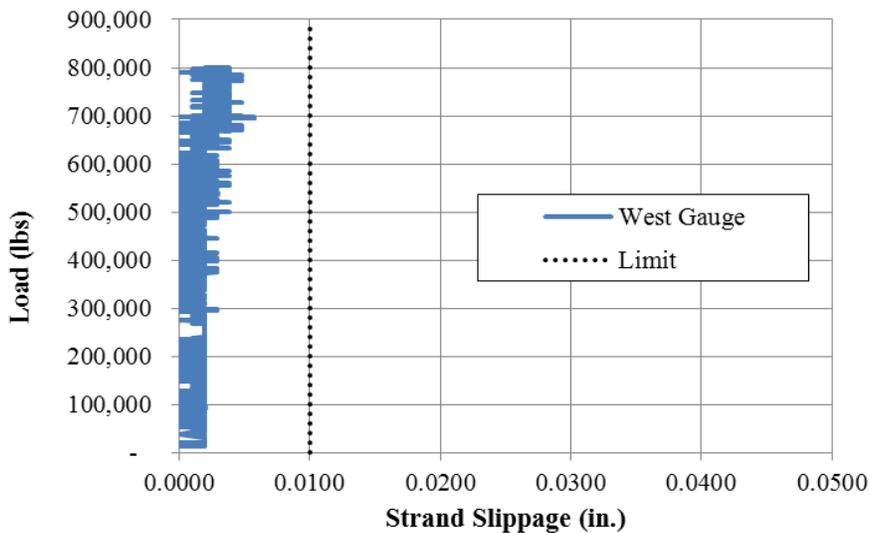
Figure 4.18:1 NU900 girder test #1: Load vs. strand slippage

The second test of the NU900 girder was performed on the opposite end of the girder, 10 ft from the support as shown in Figure 4.19. The girder was tested at this point because it was the closest the test frame could be moved toward the support, to accommodate the lifting hoops. The girder was already significantly cracked under test#1, making new cracks difficult to trace and harder to interpret. For these reasons, no new cracks were traced on the girder for the second test. Significant additional cracking occurred, but there was still no spalling. A few new shear cracks were observed shortly after 300 kips of loading. Also, shear cracking through the transfer region and the diaphragms was observed as shown in Figure 4.20, but did not seem to affect the bond of the strands. This was likely due to the heavy confining reinforcement at the end of the girder. Further flexural cracking was observed between 600 and 700 kips.
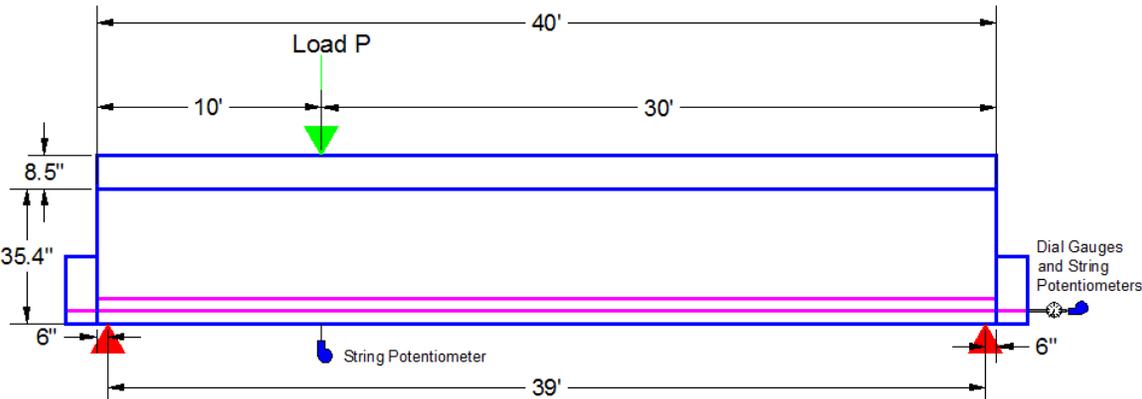
Figure 4.19: Setup of test #2 of NU900 girder specimen

Figure 4.20:2 NU900 girder test #2: Cracks propagated through transfer length

The load vs. deflection relationship for NU900 girder test #2 is shown in Figure 4.21. The maximum load placed on the girder was 800 kips, which resulted in a maximum deflection and permanent deflections of approximately 1.32 and 0.26 in., respectively, directly under the load.
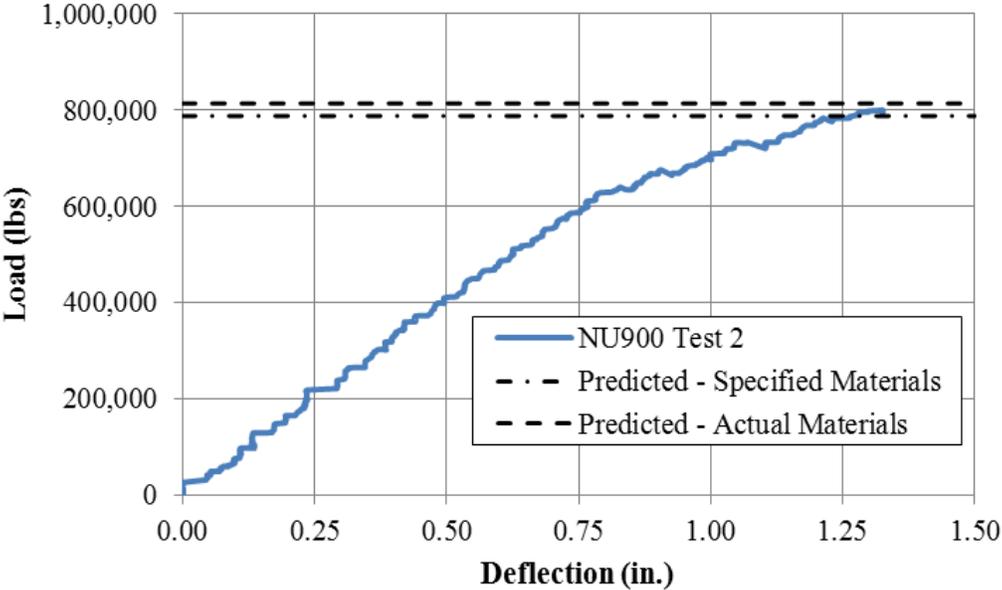
Figure 4.21: NU900 girder test #2: Load vs. deflection

Table 4.4: Predicted and observed values for NU900 girder test #1

	Predicted		Observed
	Specified	Actual	Observed
Total Moment Capacity (kip-ft)	5817	6000	5903
Point Load Capacity (kip)	788	814	800
Strand Strain at Ultimate (%)	0.76%		0.74%
Strand Stress at Ultimate (ksi)	208		204

The shape of the load vs. deflection curve shows cracking at approximately 575 kips where the graph becomes non-linear. Near the end of the plot, slope became shallower, indicating the girder was nearing failure. Bottom fiber ERSG readings are shown in Figure 4.22. Cracking load is shown to be at approximately 550 to 575 kips. The unreliability of the small gauge length ERSGs after cracking is exhibited by the West Gauge.
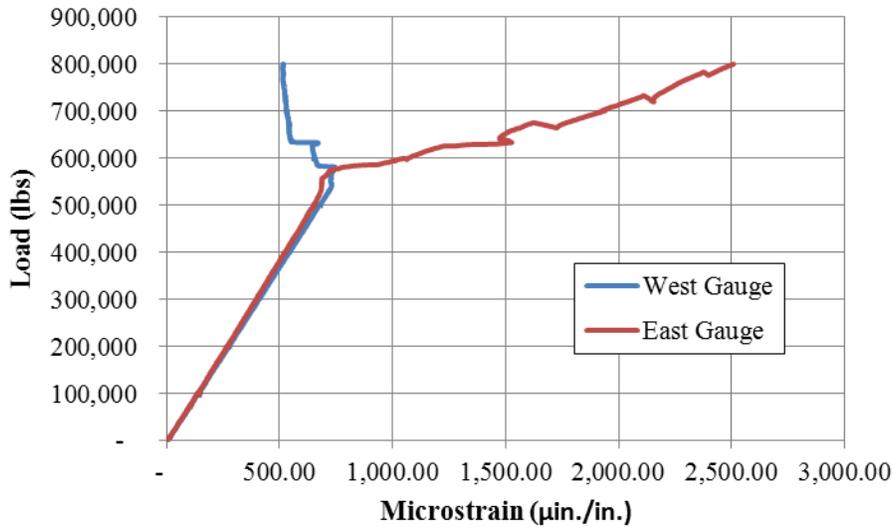
Figure 4.22: NU900 girder test #2: Bottom fiber strains

Strain readings near the top and bottom fibers of the composite section were used to construct a plot of the neutral axis depth vs. the applied load as shown in Figure 4.23. Similar to the plot from the first test, after initial stabilization, the neutral axis closely followed the transformed center of gravity of the composite section. After the cracking load and re-stabilization, the neutral axis migrated to near the ultimate neutral axis calculated by strain compatibility. The neutral axis did not achieve the predicted ultimate, indicating additional capacity.
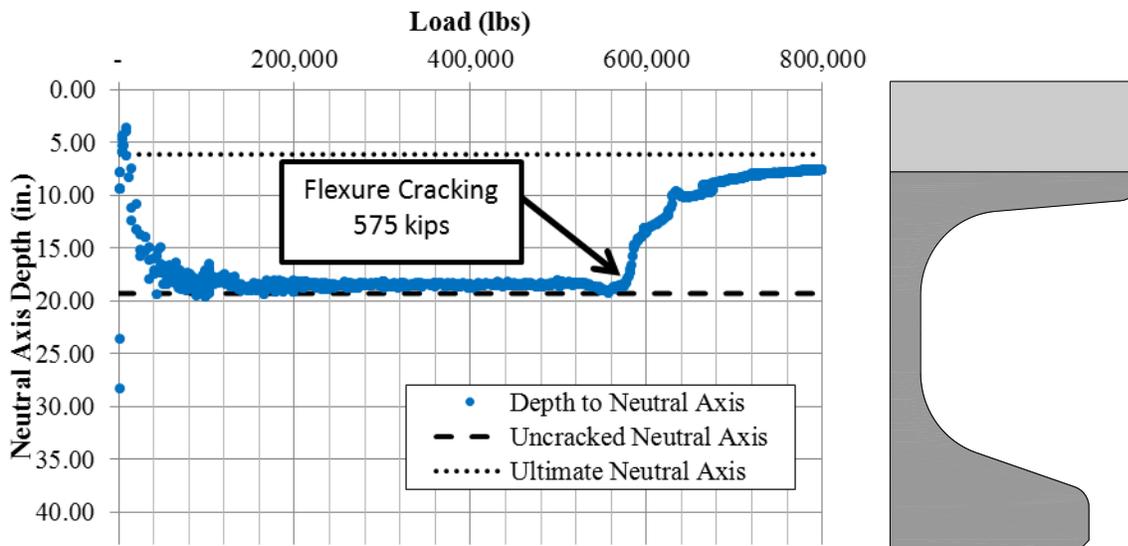
Figure 4.23: NU900 girder test #2: Plot of neutral axis depth using surface mounted ERSGs

Manual dial gauges were read at 100 kips increments and no observable slippage was noticed throughout the test. Figure 4.24 shows the slippage vs. load plot from the ST-POTs located on the free strands. Slippage of the strand was indicated by the West ST-POT, however, any slippage over the 0.01 in. limit seems to be noise from the testing equipment. This indicates that even when the specimen is loaded at 10 ft from the end of the specimen, no significant strand slippage was observed. This indicates the adequacy of the concrete strength and bottom flange confinement to fully develop 0.7 in. diameter strands even when used at 2 in. by 2 in. spacing.
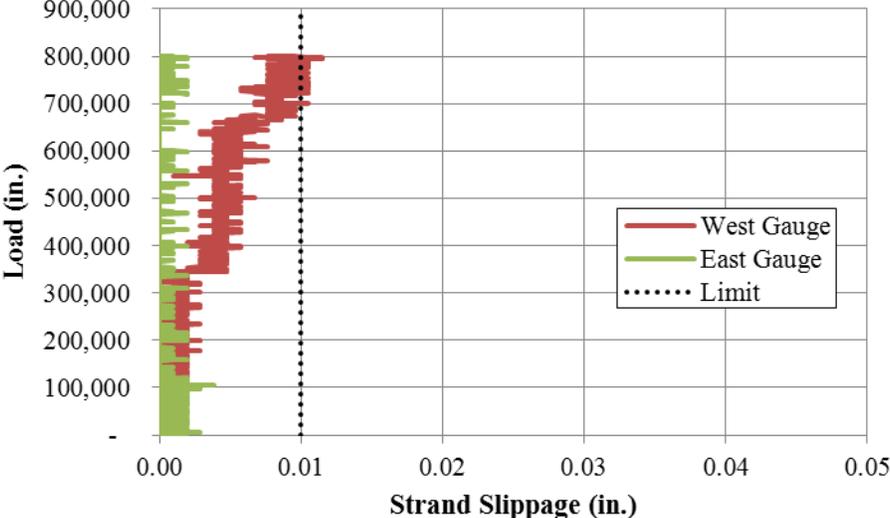
Figure 4.24: NU900 girder test #2: Load vs. strand slippage

4.3 UHPC BDT Girders

The UHPC BDT specimen was fabricated in February, 2009 by CoreSlab Structures, Omaha, and as two single tee girders to double the number of tests performed. The two halves of the DBT were shipped to the PKI Structural Laboratory for instrumentation and testing in April, 2009. Figure 4.25 shows the form available to the research team along with the proposed wood block-out pattern. The form was blocked out in order to use the concrete more efficiently and also enabled the strand centroid to match the bed centroid.
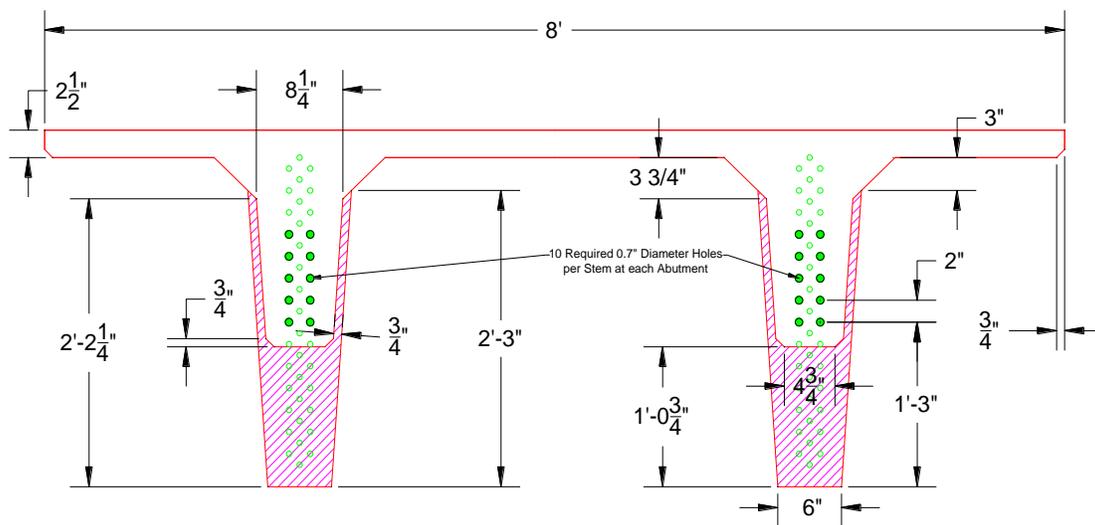
Figure 4.25: Bridge double tee form and the required block-outs (red hatch)

A 51 ft long girder was designed to resist HL-93 loading and standard bridge dead loads, with a 4 in. structurally composite deck. The girder was longitudinally reinforced with 20-0.7in Grade 270 low-relaxation prestressing strands. The precaster was not comfortable with the high levels of prestressing in the bed. Therefore, each strand was tensioned to only $0.60f_{pu}$ and oriented with the strand's centroid corresponding to the bed's centroid. The centroid of the strands at the end of the girder corresponded to the centroid of the bed. This allowed for the highest amount of prestressing to be introduced to the girder, given the limitations. The strands were then depressed at $0.4l$, symmetrically about the centerline, until each strand was touching the next, creating a fanned strand profile. The end and middle cross sections of the BDT Girder can be found in Figure 4.26.
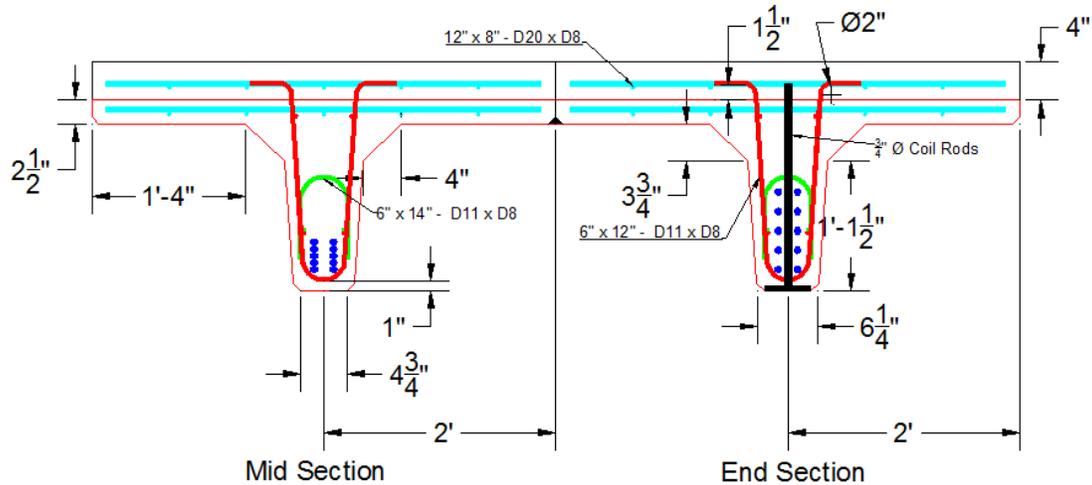
Figure 4.26: BDT Girder Cross Sections, Mid-Span Section (left) and End-Span Section (right)

Because the main purpose of the girder was to determine the anchorage and flexural behavior as well as the interaction of the still experimental components, the girder was overdesigned for shear when considering the development and midspan tests. Mild steel used in the girder was designed using Grade 80 WWR. Vertical shear reinforcement consisted of D11@6 in. connected by longitudinal D8 wires strategically located to allow for the fitting of a confinement mesh of D11@6 in., which also contained D8 longitudinal bars for stability and for the fitting of the bars into each leg. The vertical shear reinforcement was continued for the entire length of the beam; as was the confinement bars as per NDOR policy. An elevation view of the beam can be found in Figure 4.27. End zone reinforcement was designed according to Tuan et al. (2004) with three 0.75 in. headed coil rods welded to the base plate as seen in Figure 4.28. This allowed for the placement of approximately 0.44 in.^{2} of steel over a distance of h/4 and the remaining 0.88 in.^{2} of reinforcement within the remaining 3h/8. The end zone was overdesigned for bursting stress in order to ensure an undamaged test specimen. The concrete used in the BDT Girders was NU UHPC #2 used in the NU900 girder and developed in Chapter 3. The 28 day design strength of the mix was conservatively assumed to be 15 ksi, based on laboratory testing. It should be noted that the concrete strength has no effect on the ultimate flexural capacity according to strength design, due to the position of the neutral axis above the top flange.
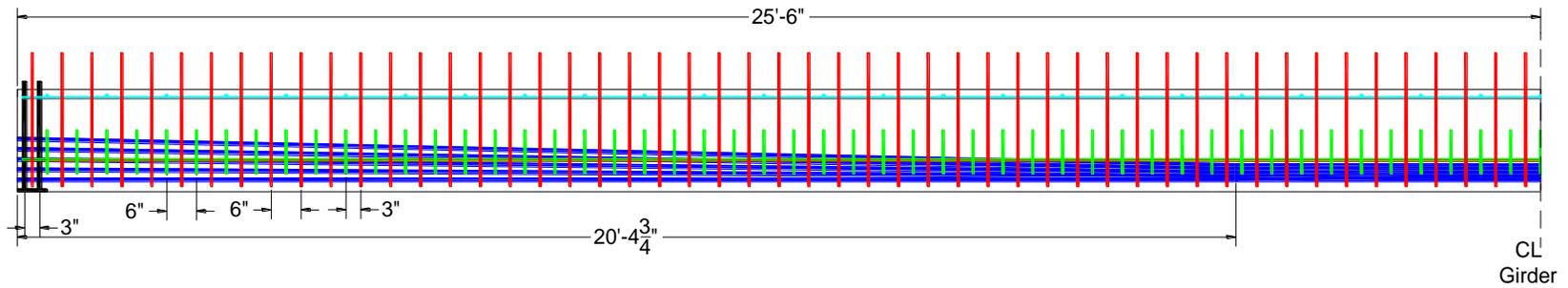
Figure 4.27: Elevation View of BDT Girder Reinforcement
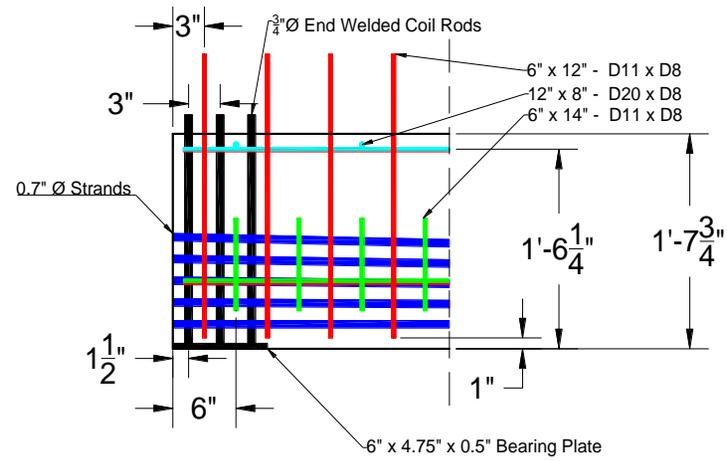
Figure 4.28 Single Stem End Zone Detail

BDT Girder Fabrication

The fabrication of the girders, due to the specially designed reinforcement, required a specific mesh placement order. First, the shear reinforcement mats (indicated in Figure 4.26) were bent and placed in the empty prestressing bed and chaired to the appropriate clearance using plastic chairs on the stems. Next, the strands were pulled out along the length of the beam using a mechanical wench and trolley setup. It is important to note one of the advantages of the double tee beds are that they are usually automated or mechanized such that strands are not pulled by workers, but by a machine, allowing for faster and safer fabrication. Following stringing of the 20 strands through the stems, each strand was chucked and threaded in the appropriate block end block holes on the end of the beds. Next, the confinement reinforcement sheets were bent and inserted into the beam, just above the strands. As stated earlier, the shape of the confinement mats were designed to fit such that the mesh need not be tied, because the longitudinal bars of the shear and confinement reinforcement touch. Next, the top flange reinforcement meshes were placed for the precast flange reinforcement. Proper clearances were maintained by discrete plastic chairs located on the flange portion of the form.

Finally, depressor rods were extended, which depressed the strands over the middle 10 ft of the beam to their prescribed positions. Strands were then tensioned to 48 kips using standard precast procedures. Researchers checked all clearances and mat offsets and found them to be at acceptable levels. Figure 4.29 shows a detailed view of one stem of the BDT Girders. Visible are each of the different mesh reinforcements, the depressor device, as well as the plywood blockout used to reduce the stem thickness. Figure 4.30 shows Prestressing Bed Features. The bed was equipped with a tarp rolling mechanism (Figure 4.30, right), which efficiently covered the bed and both girders.
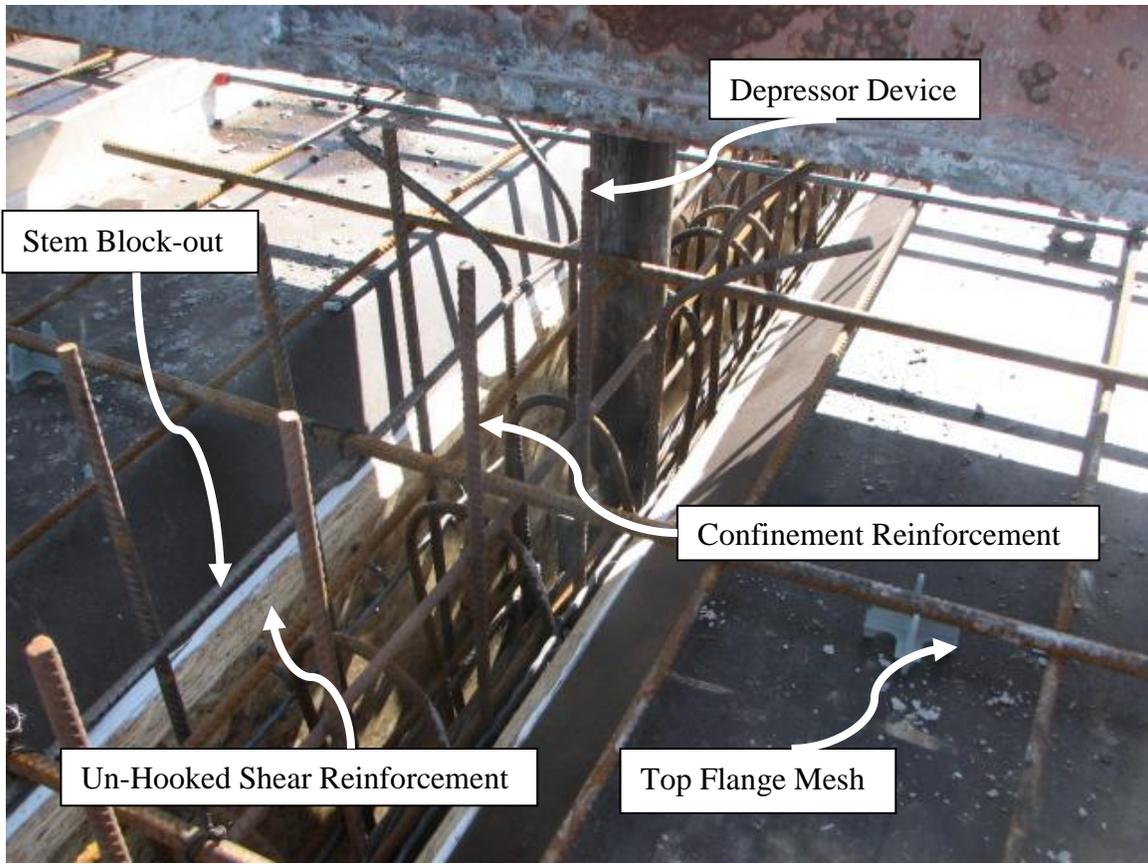
Figure 4.29: Detailed View of BDT Girder Reinforcement

Figure 4.30: Prestressing bed features: Depressor points (left) and insulating tarp (right)

Specialized mixing procedures were necessary for the successful mixing of the NU UHPC mix. Failure to follow the mixing procedure has, in the past, resulted in significant loss of flowability, strength and economy. For these reasons, the batching process was supervised by the research

team at the batching plant. The mixing procedure outlined in the mix development program above was used as well as the following specific batching program. Each BDT Girder required a minimum of 3.5 cubic yards of concrete. A total of four batches of 2.5 cubic yards each were mixed for the girders with two batches sent per truck. Flowability was checked and the first two batches were placed in a truck on "high-agitation," and immediately shipped to the site of the form, located outside. It was imperative that the mixing trucks transporting the UHPC remained at the highest level of agitation possible throughout the batching and transportation process. The concrete loses flowability rapidly after agitation/energy is no longer applied, as noted with the NU900 Girder above.

Flowability was checked at the batch plant as well as by the forms using average slump-flow diameters for both girders, which can be seen in Figure 4.31 and 4.32. After an acceptable average spread diameter of 30 in. was measured, with no segregation, a portion of the mix was dumped into a wheelbarrow for samples, and pouring of BDT Girder 1 commenced. Additional HRWR was used to maintain spread diameter after transport. No vibration was needed with the highly flowable mix. The casting and sampling process went well, and the truck was sent to the batch plant for the second mix and the process was repeated for BDT Girder 2.

Figure 4.31: Spread of BDT Girder 1

Figure 4.32: Spread of BDT Girder 2

After the pouring process was completed, all concrete samples were placed on the form next to their girders in order for the specimen to obtain the same early stage curing. The steam curing process commenced six hours after batching the concrete, according to plant procedure. Unfortunately, the curing process was interrupted by significantly below freezing temperatures and exceptionally high winds from the west that had managed to penetrate the protective insulated tarp. This was compounded by very high demand for the available steam due to high value commercial projects. Extremely low temperatures pose problems for the curing of concrete and completely eliminated the intended accelerated curing process, but likely prevented the girders from freezing. In general, this was an anomaly for the Coreslab plant. Interestingly, as demonstrated in the material properties section below, BDT Girder 2, located on the west side of the bed which took the brunt of the west wind, had the worst early curing problems, but both girders had similar strengths during testing.

Measurement of the transfer length has traditionally required DEMEC strain gauge disks to be placed at the center of gravity of the prestressing strands. This was not possible for the girders in this investigation, because the slip form employed for the BDT Girders did not come apart from the sides like a customary I-girder form. For this reason, DEMEC disks were placed along the top flanges of the girders, just outside of the protruding vertical stirrups, as shown in Figure 4.33. Each girder end had 15 DEMEC disks placed approximately 3.937 in. apart, for a total of 14 readings per end. All four girder ends were instrumented with DEMEC disks prior to release and

baseline readings were taken. The strands were released by the torch cutting method as can be seen in Figure 4.34. Unfortunately, while the girder was being released, a number of DEMEC disks were damaged by the workers cutting the strands.

Figure 4.33: DEMEC Disks Attached to Top Surface of BDT Girder

Figure 4.34: Coreslab Personnel Torch Cutting Strands (left) – Frayed Torch-Cut Strands (right)

The first strain readings were taken from the DEMEC disks in the transfer region 30 minutes following release. The DEMEC disks were again measured 14 days following release, to obtain the final DEMEC measurement. Very fine splitting cracks were observed on nearly every face of

the stems. Figure 4.35 shows typical splitting cracks, which had enhanced visibility due to excess moisture. Because of the fineness of the cracks, they were deemed of no consequence to the testing, as they were of negligible width and hardly visible. Before the deck could be placed on the BDT Girder, the holes left by the depression points needed to be filled. The mix found in 4.5 was cast into the gaps, because it was expected to reach a very high strength (above +13 ksi) in order to provide comparable stiffness to the BDT Girder concrete to reduce any effects from the non-homogeneity. The concrete mix was furnished by Coreslab as it was being used in other girder production at the time. Figure4.36 shows the filled depression point hole.

Figure 4.35: Typical Splitting Cracks at BDT Girder Anchorage Zones

Table 4.5: Concrete Mix Proportions for Concrete in Depression Points

BDT Girder Depression Point	Quantity/yd^3
3/4" Iowa Limestone (lbs)	1347
#8 Platte River Sand (lbs)	874
Class 5 Sand (lbs)	729
Type III Cement (lbs)	562
Grade 120 Blast Furnace Slag (lbs)	173
Type C Fly Ash (lbs)	130
Water (lbs)	242
WRDA (oz/yd)	43

Adva 575 (oz/yd)	95
w/cm	0.28
Target Air Content	2.50%
Slump at Batch Plant (in.)	1 - 3
Spread At Casting (in.)	25 - 29
Design Strength (ksi)	14 - 15

Figure 4.36: Filled Depressing Point Hole

The top surface of the girders could not be adequately prepared as stated above. Therefore, the tops of the BDT Girders were sand blasted in order to facilitate bond between the normal Cast-in-Place (CIP) concrete deck and the precast NU UHPC girders. The casting of the deck concrete commenced without issue, 14 days following release in order for final transfer length readings to be taken. The deck concrete was specified to be 5 ksi and was fully self-consolidating to reduce labor; the deck mix design can be found in Table 4.6. The casting and sampling of the 4 in. structural deck commenced without incident. Figure 4.37 shows the depth of the formwork and the sandblasted finish. Figure 4.38 shows the precast BDT Girders and the formwork for the CIP deck. Figure 4.39 also shows the casting of the deck and the almost finished deck.

Table 4.6 – BDT Girder Deck Concrete Mix Proportions

BDT Girder Deck	Quantity/yd^3
3/4" Nebraska Limestone (lbs)	974
Class 5 Sand (lbs)	2255
Type III Cement (lbs)	439
Type C Fly Ash (lbs)	78
Water (lbs)	207
WRDA (oz/yd)	15.51
Adva 575 (oz/yd)	15.51
AT 30 Air	1
w/cm	0.4
Target Air Content	5.00%
Slump at Batch Plant (in.)	6
Add Adv: Spread At Casting (in.)	20
Design Strength (ksi)	5

Figure 4.37: 4 in. Deep Formwork (left) – Sand Blasted Finish (right)

Figure 4.38: Unformed Precast BDT Girders (left) – BDT Girder Deck Formwork (right)

Figure 4.39: SCC Used For BDT Girder Decks (left) – BDT Girder Deck During Finishing (right)

The testing program for the BDT Girders consisted of three load tests per girder. The first test was to ensure proper development of the strands. This was accomplished by loading the girder to its ultimate predicted strength using the measured material properties at its AASHTO predicted development length. The girder was not loaded to failure because it was not desired to affect the results of the second test any more than necessary. The second test was a midspan flexure test to failure. This is an important test to determine how appropriate it is to have zero vertical clearance between the 0.7 in. diameter prestressing strands at midspan.

The third and final test on the BDT Girders was a shear test, which was designed to test both the vertical and horizontal shear capacity of the NU UHPC. In the past, issues have been raised about the ability of the NU UHPC to carry both vertical and horizontal shear. The reason for this is the lack of aggregates on the fracture surface of the concrete and the exceptionally smooth surface of the as-cast NU UHPC, respectively.

Figure 4.44 shows the schematic of the test setups for each of the load tests. Each of the three tests contained the same ERSG setup as well as the same string potentiometer ST-POT orientation, both with respect to the location of the load. Two ERSG's were located on the top of the flange (Figure 4.44, Section A-A and Figure 4.40, right) as well as on the bottom of the stem (Figure , Section B-B and Figure 4.40, left) and a pair of ERSG's, oriented to read longitudinal strains 0.5 in. above and 0.5 in. below the CIP to precast interface (Figure 4.40, bottom) were located 24 in. on either side of the load for each test.

Figure 4.40: Bottom Fiber ERSGs (right) – Top Fiber ERSG (left) –

Precast and CIP ERSGs (center)

One ST-POT was used to measure the deflection of the girder directly under the load. Another was located close to the bottom fiber to measure longitudinal tensile strains, and contained an approximate 20 in. gauge length, which can be seen in Figure 4.41. The locations of the top and bottom fiber strain measurements were intended to monitor the location of the neutral axis, which was thought to give insight into any possible issues with the flexural behavior of the NU-UHPC. Spring potentiometers (SP-POTs) were used to measure slippage of the strands on pertinent tests in order to monitor the bond quality throughout the tests. Two SP-POTs were attached to the bottom two strands on the end of the girder nearest the load to measure any strand draw-in created by inadequate bond, see in Figure 4.42.

Figure 4.41: Horizontally Mounted 20 in. Gauge Length ST-POT for Bottom Fiber Strain

Figure 4.42: SP-POTs Measuring Strand Draw-in on Bottom Strands

For the final shear test of each girder, two ST-POTs were oriented on the face of the girder directly over the locations of stirrups in order to estimate the steel's contribution to the shear capacity. Additionally, a ST-POT rosette was oriented to measure principle strains and the strain angle at the center of the shear span. Each of the ST-POTs have an approximate gauge length of 8 in. Figure 4.43 shows the ST-POTs measuring stirrup strains as well as the ST-POT rosette oriented at mid shear span. Exact locations can be found in Figure 4.44.
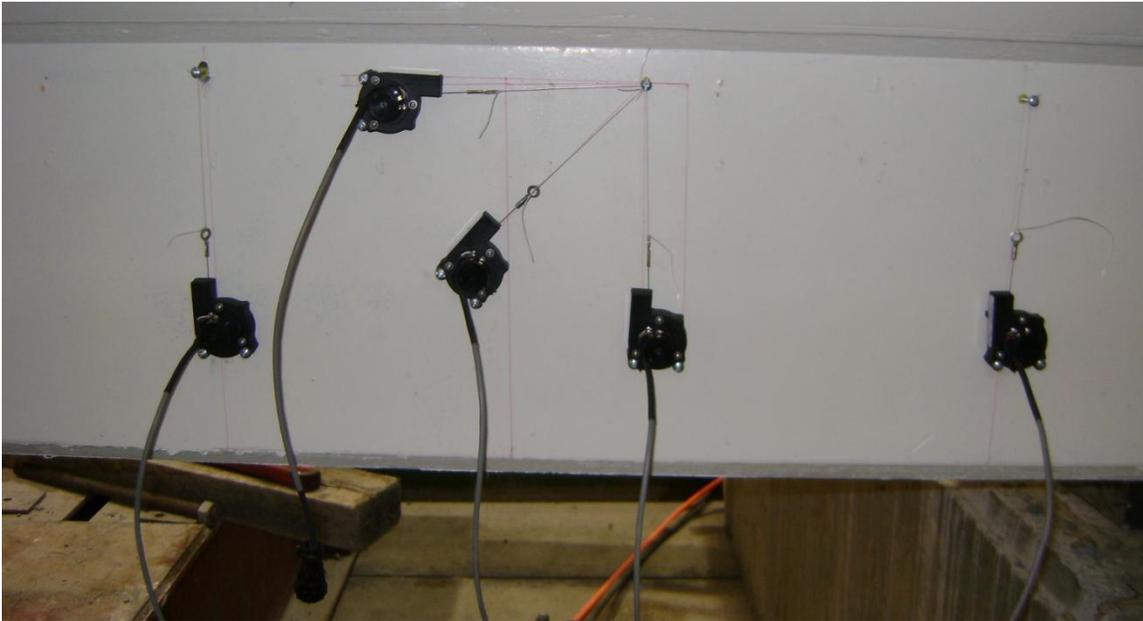
Figure 4.43: ST-POTs Measuring Stirrup Strains and ST-POT Rosette at Mid-Shear Span

BDT Test 1 - Development Length

A - A

15'

NOT TO SCALE

24" 24"

North

20"

LEGEND:
ST-POT
SP-POT
ERSG

6"

B - B

BDT Test 2 - Midspan

A - A

25' 6"

24" 24"

20"

6"

B - B

A - A

BDT Test 3 - Shear

6'

24" 24" 13" 11" 18"

6"

24"

48"

4-3/4"

1"

2-3/8"

20"

Load

1"

ST-POT

6"

6"

B - B

8" Gauge Length - Typical

Section A-A

Section B-B
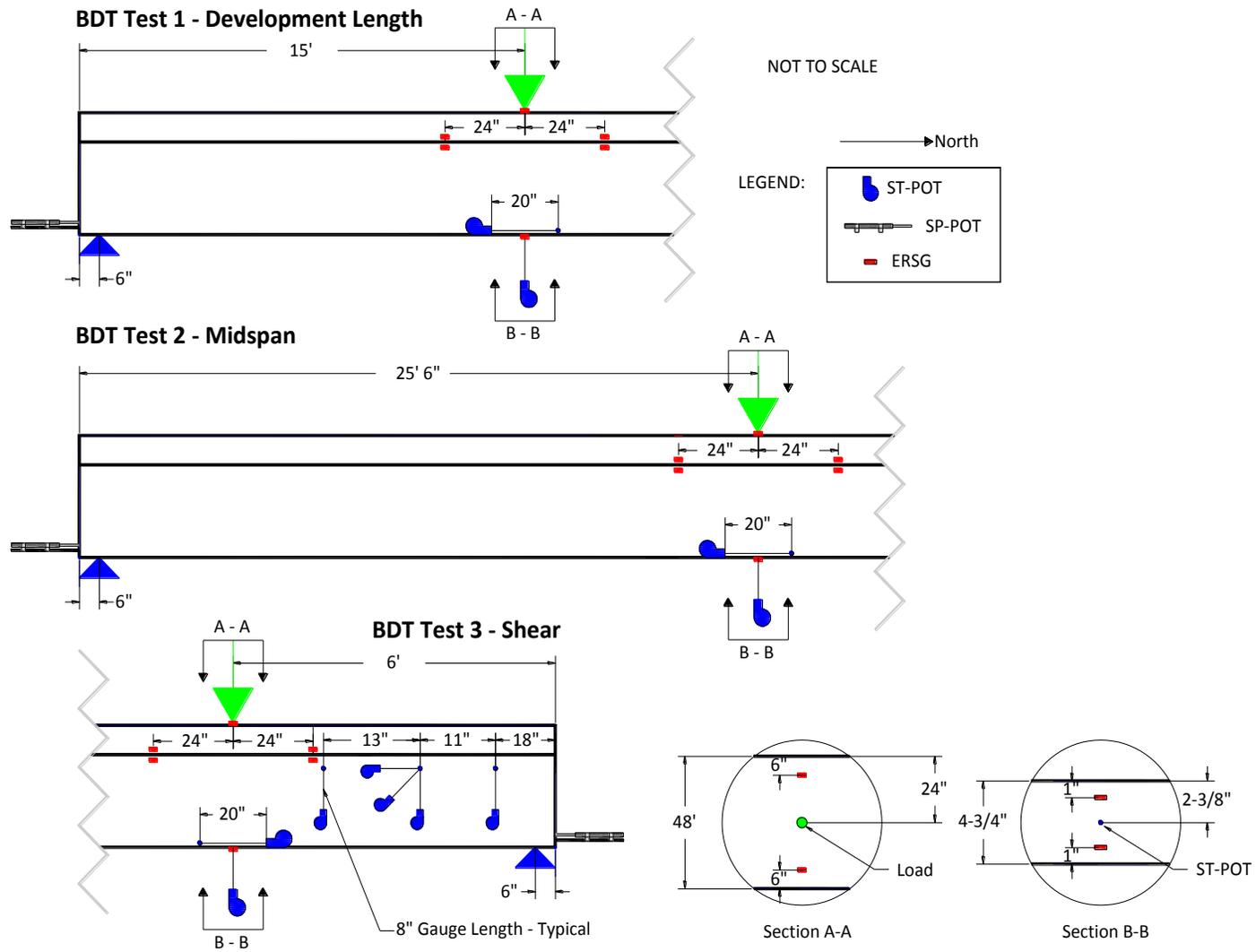
Figure 4.44: Test Instrumentation and Test Setup of BDT Girder

85

Transfer length measurements were the first tests performed on the BDT Girders. Following transfer length measurements, three full scale load tests were performed on the two BDT Girders, as outlined above in the Test Setup section. The first test was to determine if the girder could resist its calculated nominal strength at its AASHTO calculated development length. The second was to determine the midspan loading capacity. The third was to evaluate the shear performance of the NU UHPC without fibers with respect to the design code.

Transfer Length Tests

Transfer length values were recorded at release and 14 days following release. It has been well documented that the transfer length typically expands 10% to 20% over time, with the majority of the extension coming in the first 14 days (Carrol et al., 2008). Therefore, these two values were considered the initial and final transfer lengths of the beams. Results from the DEMEC strain readings were plotted versus their position along the beam along with a line indicating the 95% Average Maximum Strain (AMS) and a best fit line of the ascending/descending branch of the strain plot. Figure 4.45 through Figure 4.48 display the surface strain readings on each end of each beam and are labeled according to their as-cast orientations. DEMEC disks were damaged immediately following release of the strands.
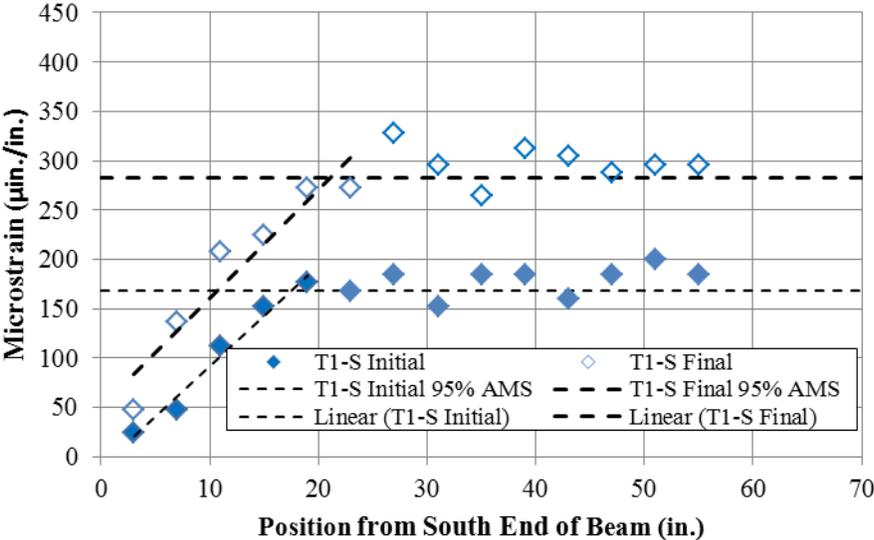
Figure 4.45: BDT Girder 1, South End, DEMEC Surface Strain Plot with Modified 95% AMS Method
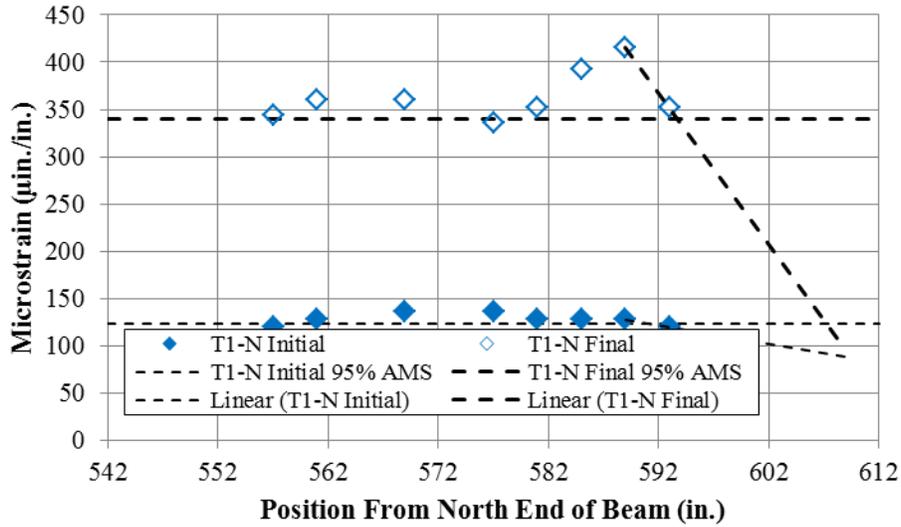
Figure 4.46: BDT Girder 1, North End, DEMEC Surface Strain Plot with Modified 95% AMS Method
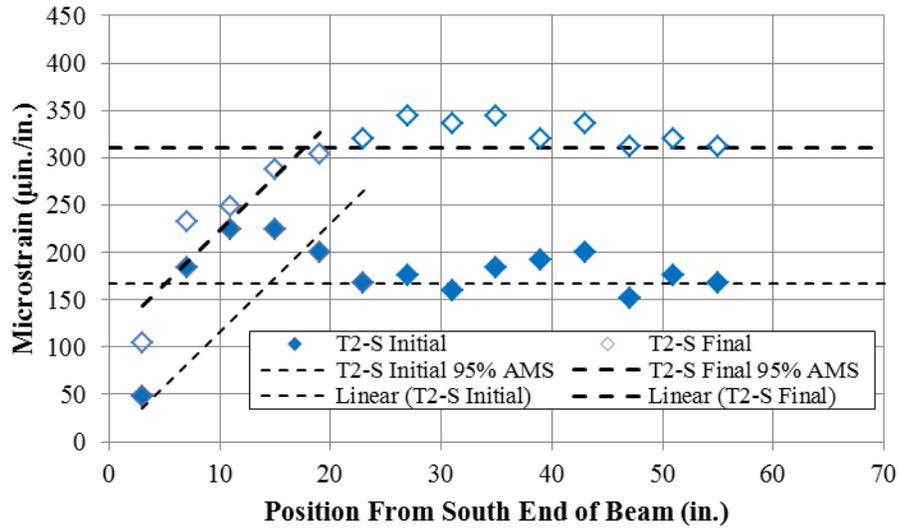
Figure 4.47: BDT Girder 2, South End, DEMEC Surface Strain Plot with Modified 95% AMS Method
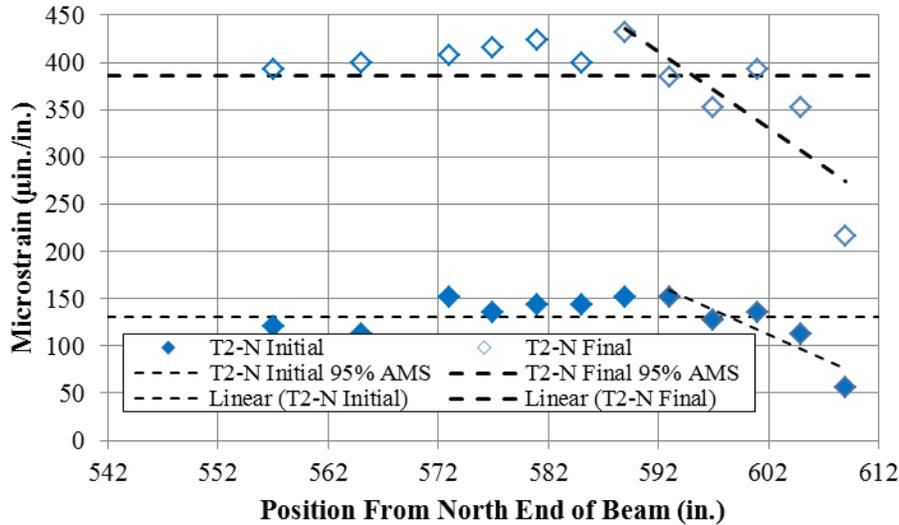
Figure 4.48: BDT Girder 2, North End, DEMEC Surface Strain Plot with Modified 95% AMS Method

The transfer length values determined from each of the four plots, with accompanying ACI and AASHTO predictions, are tabulated in Table 4.7. The transfer lengths were calculated with a modified 95% AMS method where the constant strain region of the plot is visually identified and reduced to 95%. The ascending/descending branch is also visually identified and a best fit linear curve is applied. The intersection of the 95% AMS line and the best fit curve is then calculated using the general slope intercept equation (Carrol, 2009). The author felt that this modified method introduced less variation in the transfer length determination by relying on slightly more rigorous rules for ascending branch visualization.

Table 4.7: Summary of Transfer Length Measurement Estimation

Beam End	Initial	Final	$(f_{se}/3)d_b$	ACI, $50d_b$	AASHTO,
BDT1-South End	17.5	21.1			
BDT1-North End	20.4	18.2			
BDT2-South End	14.5	17.6	33.1	35.0	42.0
BDT2-North End	13.6	16.9			
Average	**16.5**	**18.5**			

BDT Girder Development Length Tests

The progression of cracking in the development length test was the most well defined of the flexure type tests, because of their close proximity. Figure 4.49 displays the final cracking pattern of the development length test after the test frame and instrument were removed. Figure 4.50 shows the evolution of cracking as load was applied.

Figure 4.49: First Flexure Cracks 40 kips (top left), Propagation of Flexure Cracks (top right) , Web Shear Cracking to Flexural Shear Cracking, 70 kips (bottom left) , and Final Cracking Under Jack (bottom right)

Figure 4.50: BDT Girder 1, Final Cracking Pattern for Development Length Test

Figure 4.51 displays the load vs. deflection plots for the load test at the BDT Girders' AASHTO derived development length. Both girders displayed similar graphs up to the cracking load, after which the girders no longer followed the same loading path. The girders eventually regained the same slope after some initial differences post-cracking. It is unknown why this occurred, but it was deemed essentially irrelevant. It is important to remember that the girders were not taken to failure, as there were two more tests planned for each. The girders were, however, loaded to their ultimate predicted load of 96 kip. This ultimate load was predicted using the measured material properties found at the beginning of this chapter. Table 4.8 shows the predicted and observed values for the BDT Girder in the development length tests.
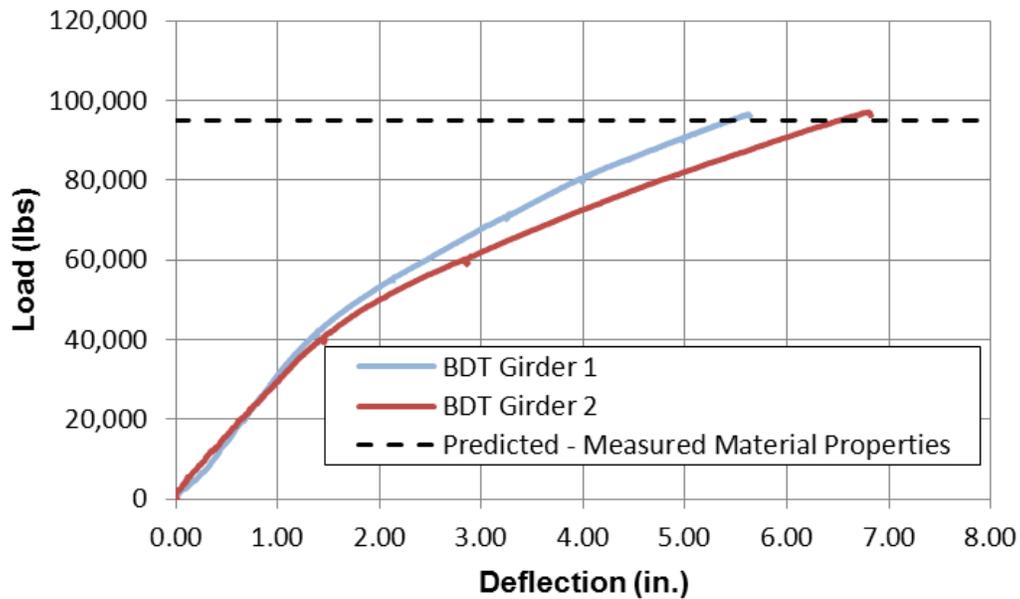
Figure 4.51: BDT Girder, Development Length Test, Load vs. Deflection

Table 4.8: Predicted and Observed Values for the BDT Girder   Development Length Tests

	Predicted		Observed	
	Specified Materials	Actual Materials	BDT Girder 1	BDT Girder 2
Total Moment Capacity (kip-ft)	1,091	1,143	1,160	1,160
Applied Load Capacity (kip)	92	95	97	97
Strand Strain at Ultimate (%)	1.63%	1.95%	-	-
Strand Stress at Ultimate (ksi)	260	263	-	-

Figure 4.52 and Figure 4.53 plot the neutral axis depth as a function of the load, as was discussed above. It can be seen from the neutral axis plots that the BDT Girders behaved as expected. BDT Girder 2 again behaved slightly differently from Girder 1; only early pre-cracking differences were noted. There again seemed to be some stabilization for both girders, pre-cracking. The pre-cracking behavior was much different, but the post-cracking behavior was similar, as the neutral axis climbed to near the predicted ultimate neutral axis. This may be attributed to poor performance of the bottom fiber ERSGs in Girder 2 or some unknown instrumentation peculiarity.
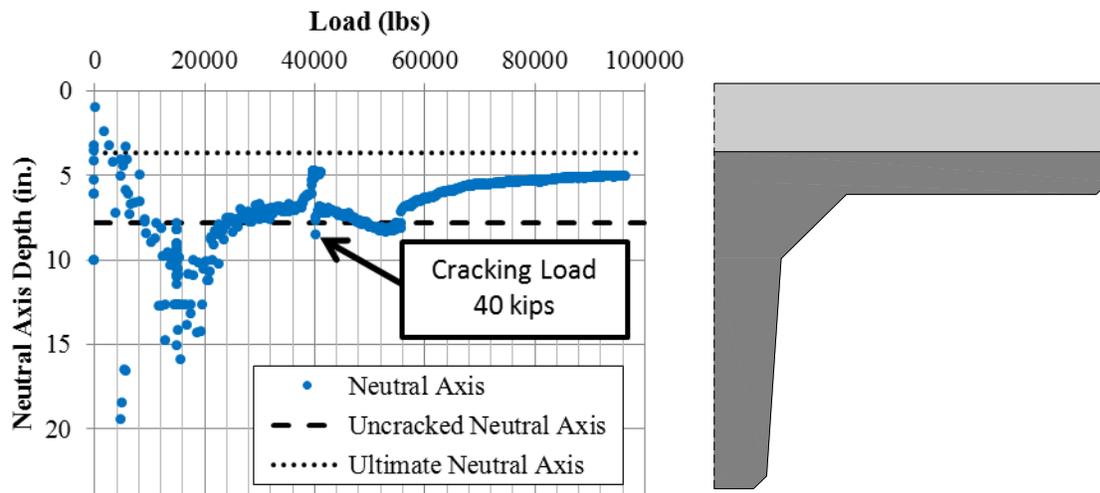
Figure 4.52: BDT Girder 1, Development Length Test, Neutral Axis Depth Plot
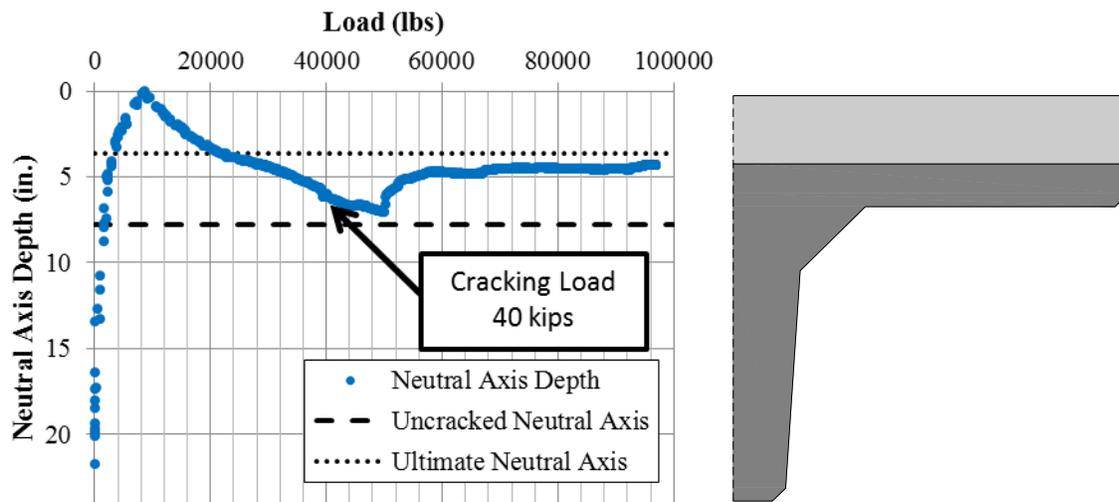
Figure 4.53: BDT Girder 2, Development Length Test, Neutral Axis Depth Plot

The strand slippages of the girders were negligible for both tests as can be seen from Figure 4.54 and Figure 4.55, which plot the load vs. strand slippage. Girder 1 displayed some migration of the West Strand inward; however, it remained under the limit for a bond failure. Girder 2's strands remain unchanged throughout the testing.
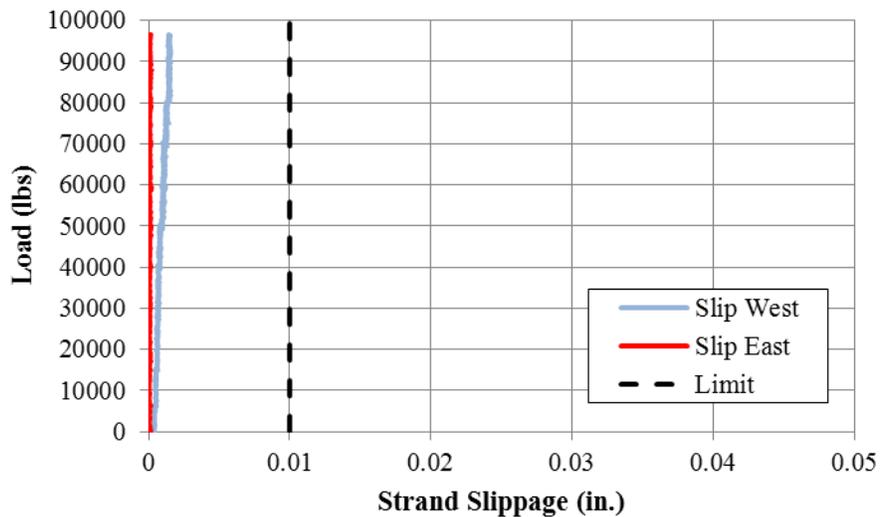
Figure 4.54: BDT Girder 1, Development Length Test, Load vs. Strand Slippage
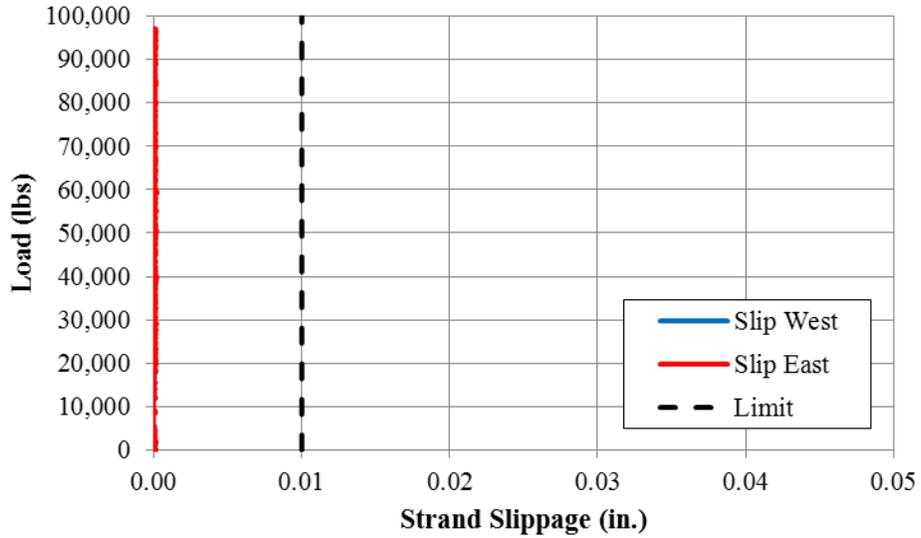
Figure 4.55: BDT Girder 2, Development Length Test, Load vs. Strand Slippage

The monitoring of the composite action of the deck showed the cross section was working according to the standard composite girder assumptions. This can be seen in Figure 4.56 and Figure 4.57 for Girders 1 and 2, respectively. There were differences in strain between clusters, but they were very small differences, which can be attributed to the difference in depth along the cross-section and the general migration of the neutral axis upward. The strains of the gauges on the North side of BDT Girder 1 indicated much higher strains than the other clusters. This seems to be an anomaly.
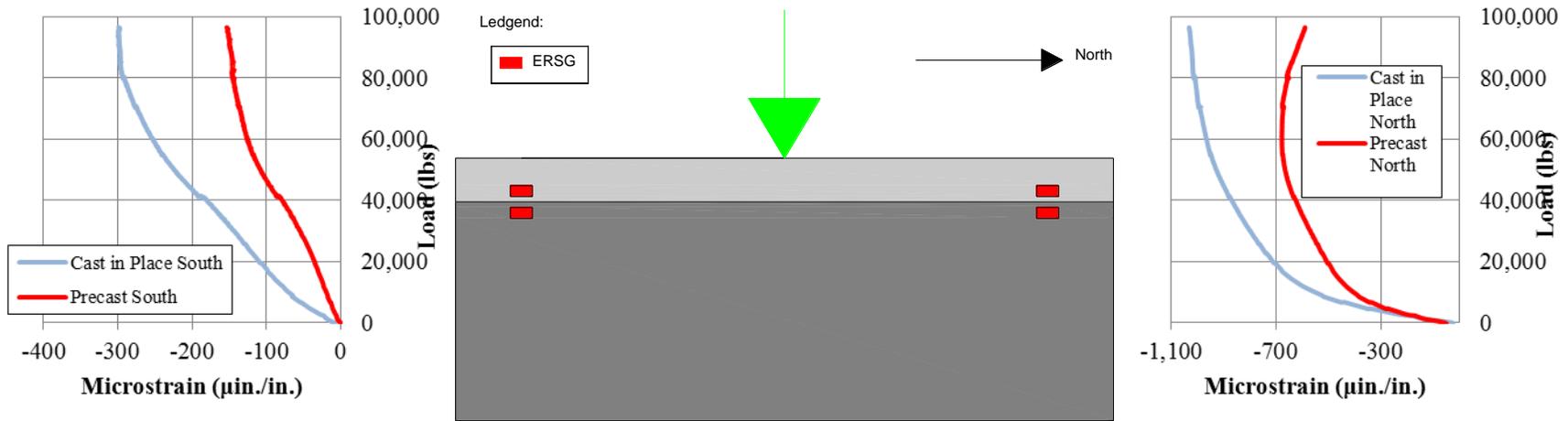
Figure 4.56: BDT Girder 1, Development Length Test, Load vs. Cast in Place and Precast Strains
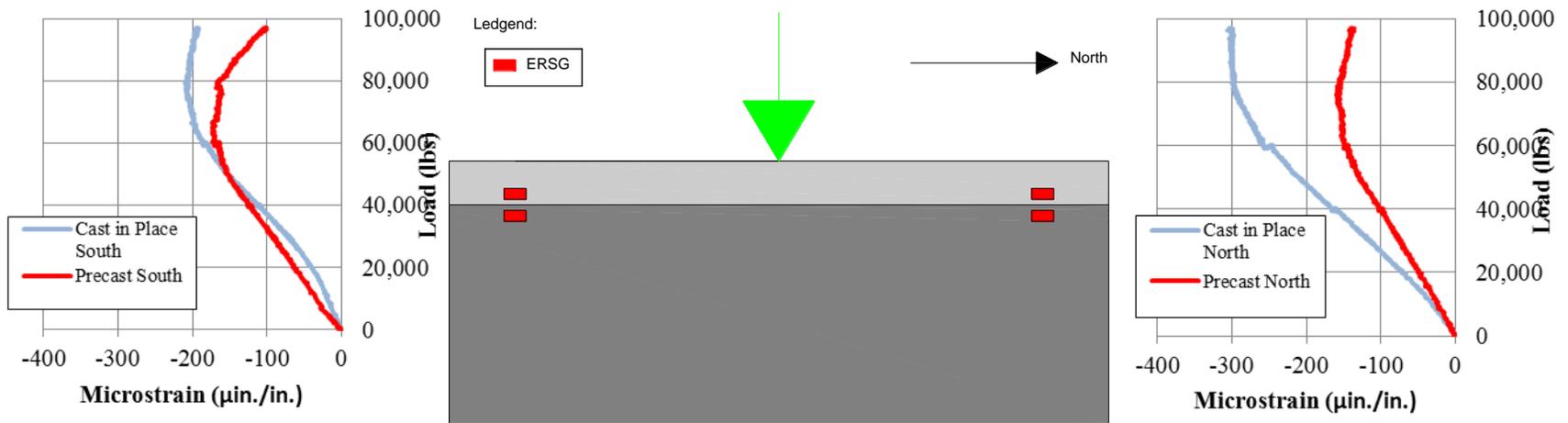
Figure 4.57: BDT Girder 2, Development Length Test, Load vs. Cast in Place and Precast Strains

It was difficult to interpret cracks for the midspan test because the girders were so damaged from the first tests. Figure 4.58 (left) shows remarking of cracks opening on the west face of the girder as cracks were marked before for BDT Girder 1. Figure 4.58 (right) shows highlighting new cracks on BDT Girder 2 east face.

Figure 4.58: Marking Re-Opening Cracks BDT Girder 1(left), and Marking New Cracks on BDT Girder 2 (right)

The maximum load applied to the girders at their mid-span was approximately 91 kips with an average maximum deflection of 11.8 in., as can be seen from the load vs. deflection diagram in Figure 4.59.
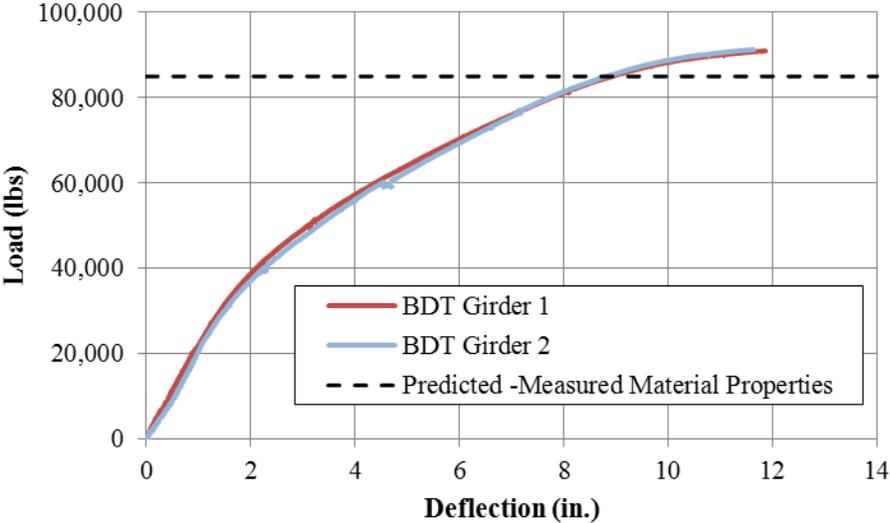
Figure 4.59: BDT Girder, Mid-span Test, Load vs. Deflection

The very large deflection of BDT Girder 2 can be observed in Figure 4.60. The observed failure mode for both BDT Girders was at first glance a classical ductile, transition failure, but upon closer inspection was accompanied by what seemed to be a delaminating of the deck, causing heavy crushing of the deck. Post-mortem photographs can be seen in Figure 4.61. Table 4.9 summarizes the predicted and observed values for BDT Girder Mid-span tests.

Figure 4.60: 11.8 in. Deflection at Failure for Mid-span Tests
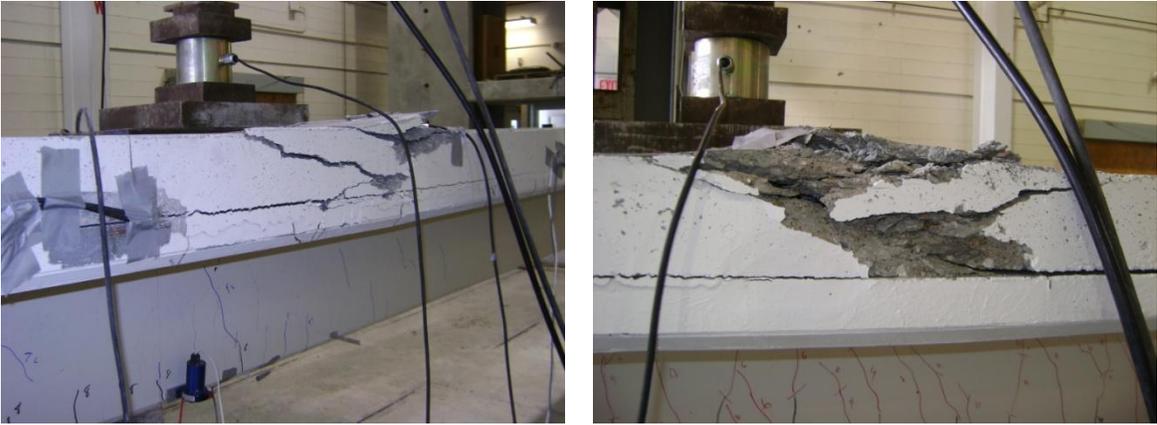
Figure 4.61: Deck Crushing and Delaminating for BDT Girder 1 (left) and BDT Girder 2 (right)

Table 4.9: Predicted and Observed Values for BDT Girder Mid-span Tests

	Predicted		Observed	
	Specified Materials	Actual Materials	BDT Girder 1	BDT Girder 2
Total Moment Capacity (kip-ft)	1,149	1,212	1,286	1,286
Applied Load Capacity (kip)	78	85	91	91
Strand Strain at Ultimate (%)	1.48%	1.80%	-	-
Strand Stress at Ultimate (ksi)	258	261	-	-

Figure 4.62 and Figure 4.63 plot the neutral axis depth vs. load for the mid-span tests. The graphs show similar patterns of stabilization near the early stages of the graph, but do not match up exactly during the pre-cracking region. The BDT Girders post-cracking response is nearly identical, with nearly exact values after the cracking load.
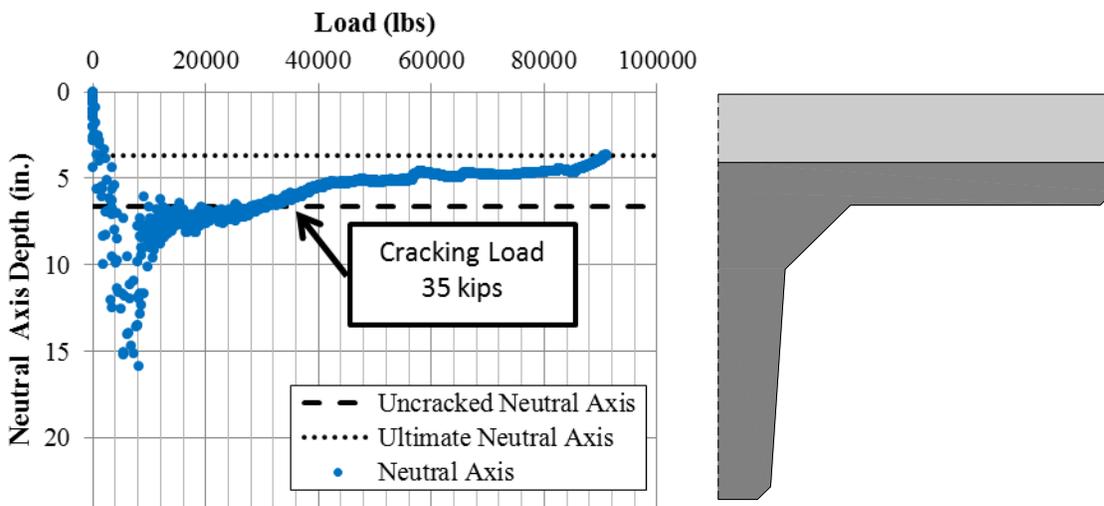
Figure 4.62: BDT Girder 1, Midspan Test, Neutral Axis Depth vs. Load
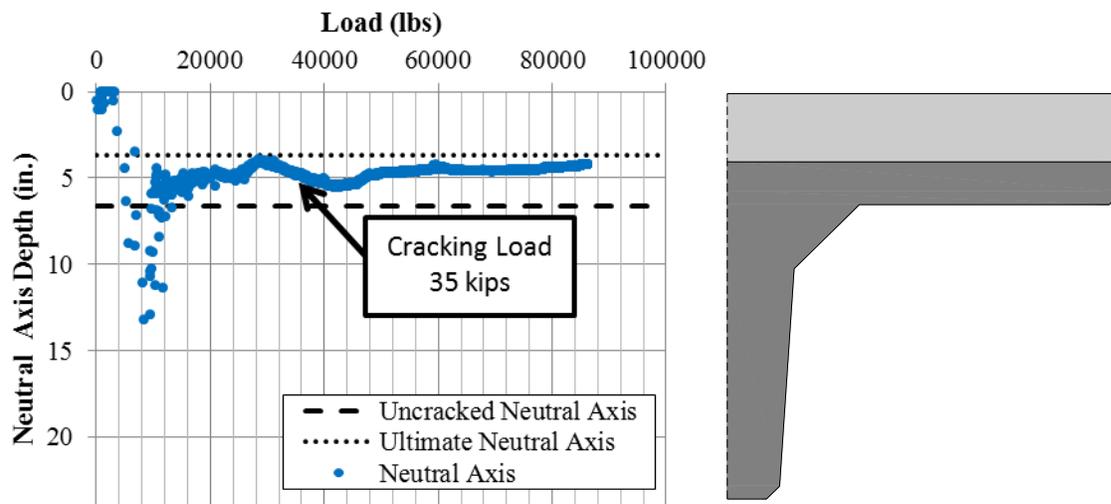
Figure 4.63: BDT Girder 2, Midspan Test, Neutral Axis Depth vs. Load

Slippage was monitored on the same end as the development length test for the midspan test. If there was to be slippage, then it would have happened on the damaged end. Figure 4.64 and Figure 4.65 present the slippage readings vs. load. BDT Girder 1 indicates a slight amount of slippage, which is still under the predefined limit for a bond failure. Interestingly though, the strand which slipped in BDT Girder 1, the bottom West Strand, was the same strand, which exhibited movement for the prior development length test. It should be noted that for BDT Girder 1, the maximum strand movement generated by the development length test (approximately 0.002 in.) and the midspan test (approximately 0.005 in.) still come in under the limit for strand slippage. What seems to be a very large slippage of the strand in BDT Girder 1, near the end of the loading cycle may be explained by the delamination of the deck from the precast girder.
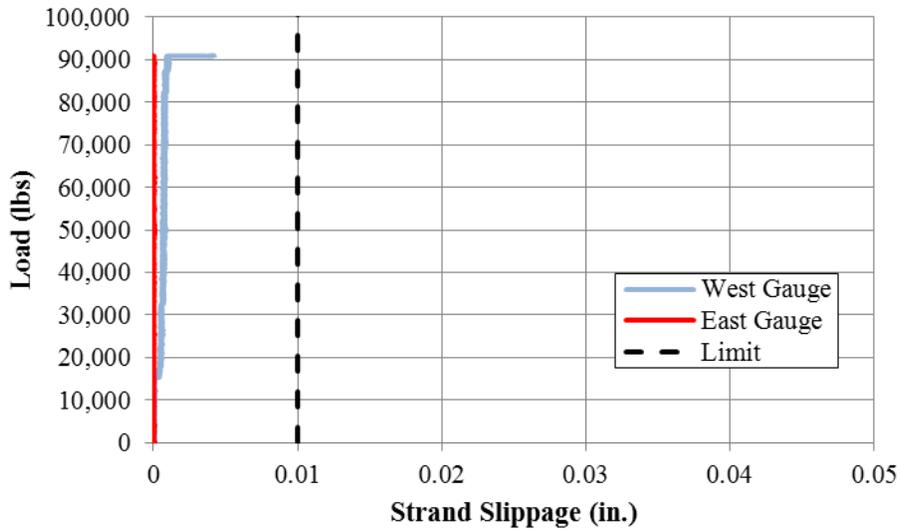
Figure 4.64: BDT Girder 1, Midspan Test, Load vs. Slippage
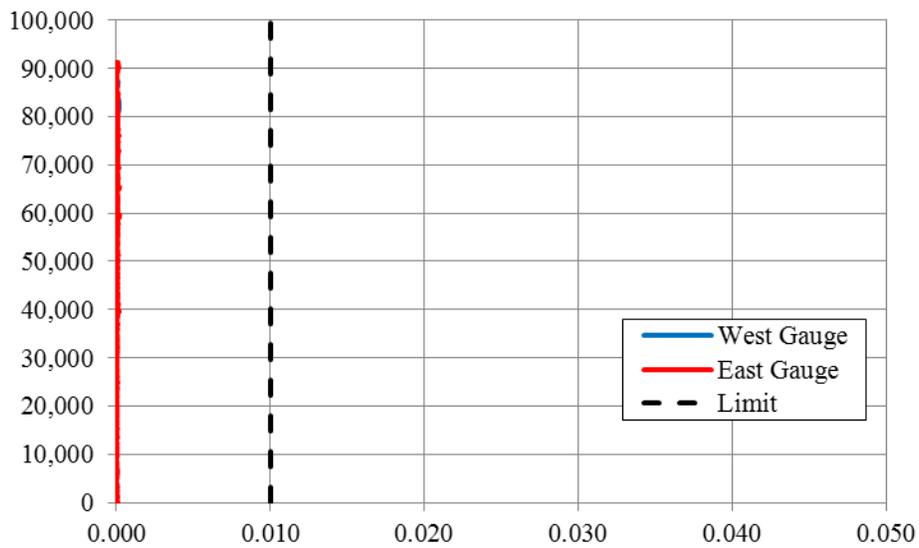
Figure 4.65: BDT Girder 2, Midspan Test, Load vs. Slippage

The delamination was monitored through the ERSGs located near the interface of the precast and cast-in-place deck. It can be seen from the plots of the ERSG output in Figures 4.66 and 4.67 that delamination occurred at the ultimate load, indicating a combined horizontal shear and flexural failure, which could not be shown by the load vs. deflection curve.
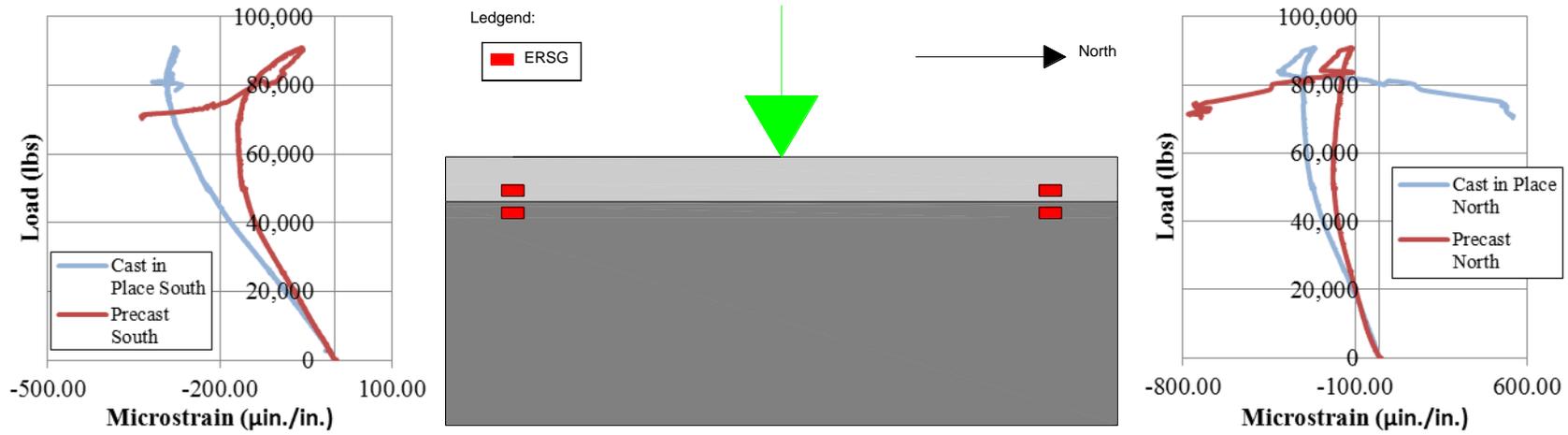
Figure 4.66: BDT Girder 1, Mid-span Test, Load vs. Cast in Place and Precast Strains
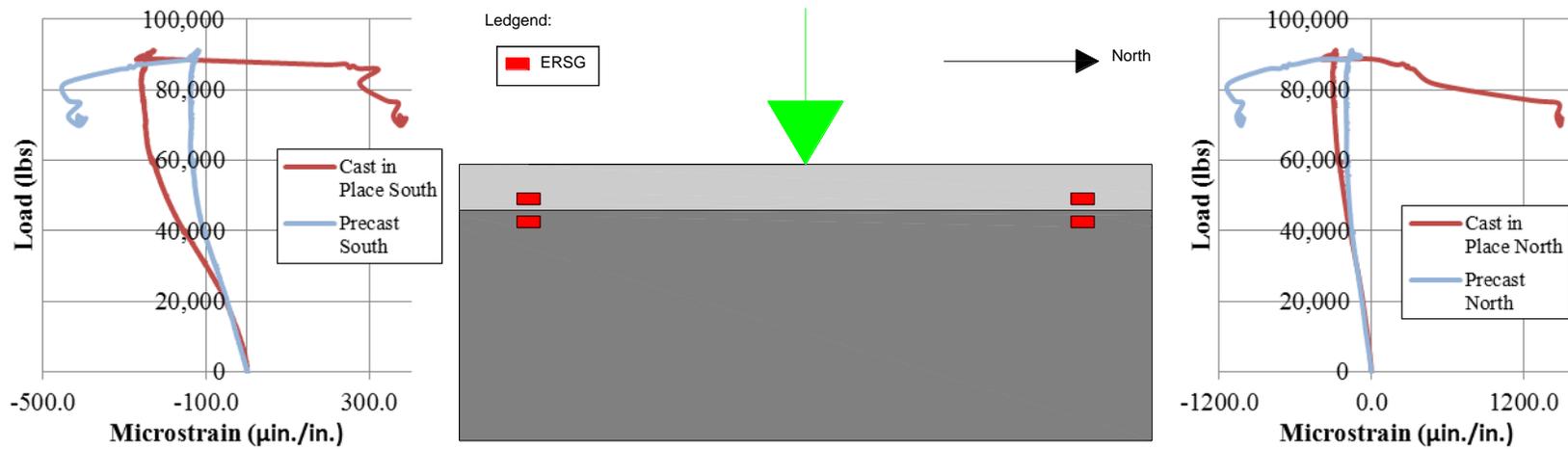
Figure 4.67: BDT Girder 2, Mid-span Test, Load vs. Cast in Place and Precast Strains

In Figure 4.66, it should be noted that the ERSGs located on the south side of the load and on the CIP deck, lost functionality upon delamination and does not exhibit the same behavior after failure as the other CIP ERSGs. All ERSGs behave normally, with respect to conventional theory, up to near the ultimate load. Gaining strain semi-linearly and then as the neutral axis begins to rise losing compressive strain gradually. If the neutral axis was to pass above the gauges, the precast ERSGs would shift from compression to tension gradually, followed by the CIP ERSGs. This is not exhibited; rather, there is an immediate shift in the gauges where the CIP ERSGs rapidly gain tension and the precast ERSGs rapidly gain compression. This shift characterizes classic non-composite behavior where the bottom fiber of the top beam shifts to tension and the top fiber of the bottom beam gains much more compression than before.

BDT Girder Shear Tests

BDT Girder 1 exhibited a combination bond/shear/flexural failure all of which was precipitated by the bond failure. Figure 4.68 shows several post-failure photographs. Heavy cracking was noticed around the anchorage zone prior to failure. Minor visible separation of the deck from the BDT Girder was noticed as well as crushing of the deck. The final cracking pattern is more indicative of a flexure failure than the intended shear failure. Inspection of the rebar showed no fracture or necking of the stirrups. Figures 4.69 and 4.70 show horizontal and vertical shear failure and shear failure surface directly under vertical stirrup ST-POT for BDT girder 2, respectively.

Figure 4.68: BDT Girder 1 Failure Details, Significant Anchorage Zone Cracks (top left), Crushing of Deck and Slight Delamination (top right), Final Crack Distribution (bottom left), and View of Exposed Reinforcement (bottom left)

Figure 4.69: BDT Girder 2, Horizontal and Vertical Shear Failure
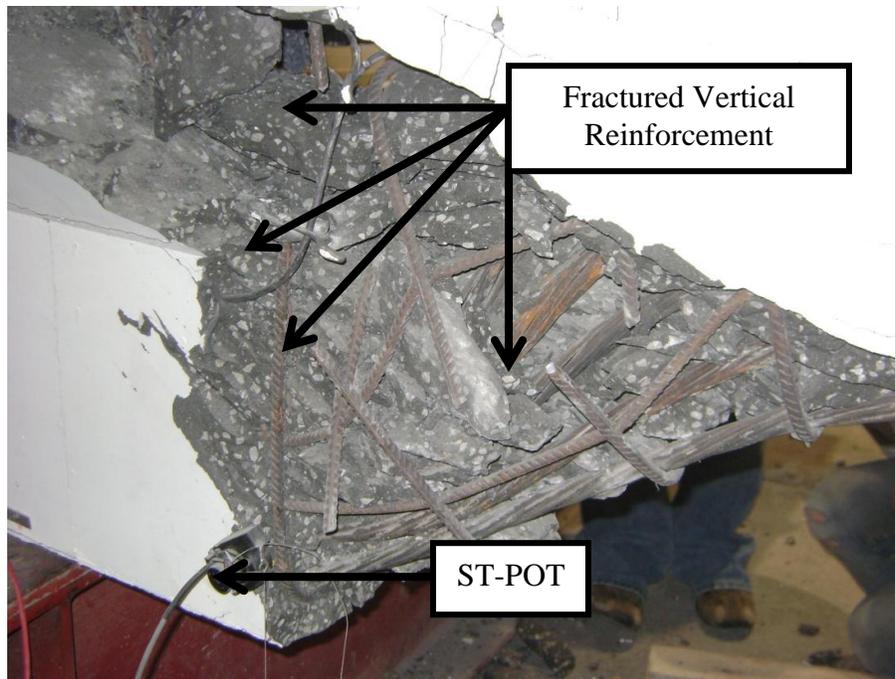
Figure 4.70: BDT Girder 2, Shear Failure Surface Directly Under Vertical Stirrup ST-POT

The load deflection curves for the two girders can be found in Figure 4.71. Both girders followed the same load path up to 185 kips, where they branched apart. Girder 1 exhibited a sudden bond failure with a maximum load of 210 kips, as discussed above. After the failure of BDT Girder 1, a diaphragm was cast around the extended strands, such as many states do, which was expected to prevent another bond failure. A bond failure was prevented; however, the addition of the diaphragm completely changed the behavior of the girder, including shear and flexural cracking patterns before displaying a shear failure at 195 kips. Table 4.10 Summarize the predicted and observed values for BDT in the shear test
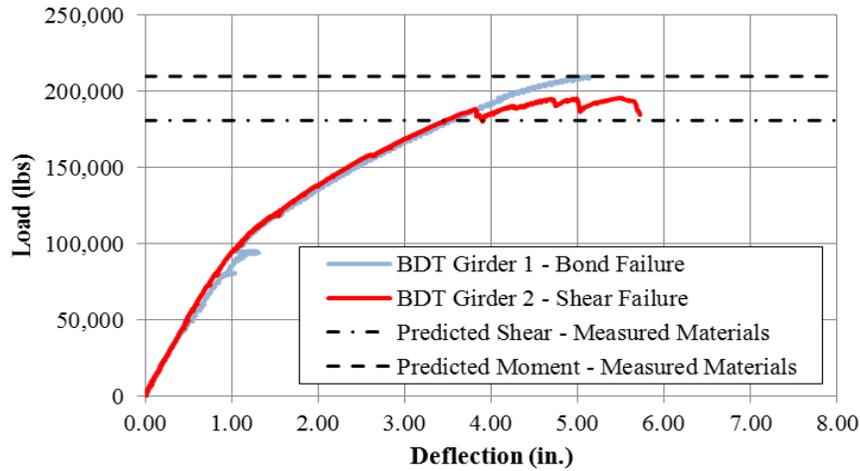
Figure 4.71: BDT Girder, Shear Test, Load vs. Deflection

Table 4.10: Predicted and Observed Values for BDT Shear Test

	Predicted		Observed	
	Specified Materials	Actual Materials	BDT Girder 1	BDT Girder 2
Total Applied Load (kip)	-	-	210	196
Applied Shear (kip)	154	170	189	176
Applied Load for Shear Failure (kip)	163	181	-	-
Applied Moment (kip-ft)	1036	1088	1,088	1017
Applied Load for Flexure Failure (kip)	200	210	-	-
Strand Strain at Ultimate (%)	1.63%	1.96%	1.96%	1.83%
Strand Stress at Ultimate (ksi)	259	263	263	260

The plots of the movement of the neutral axis with respect to load for the shear tests can be found in Figure 4.72 and Figure 4.73. The two tests show slightly different pre-cracking behavior which is mirrored by the load vs. deflection curves. They have similar stabilization behavior, and nearly identical post-cracking behavior. BDT Girder 1 appears to have a higher neutral axis at failure, which is likely due to its flexure dominated behavior.
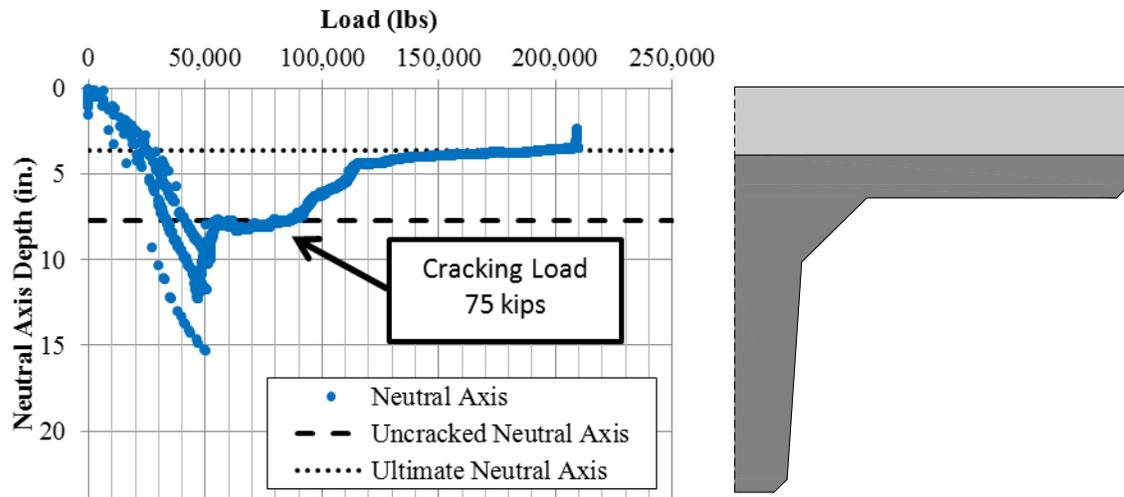
Figure 4.72: BDT Girder 1, Shear Test, Neutral Axis Depth vs. Load
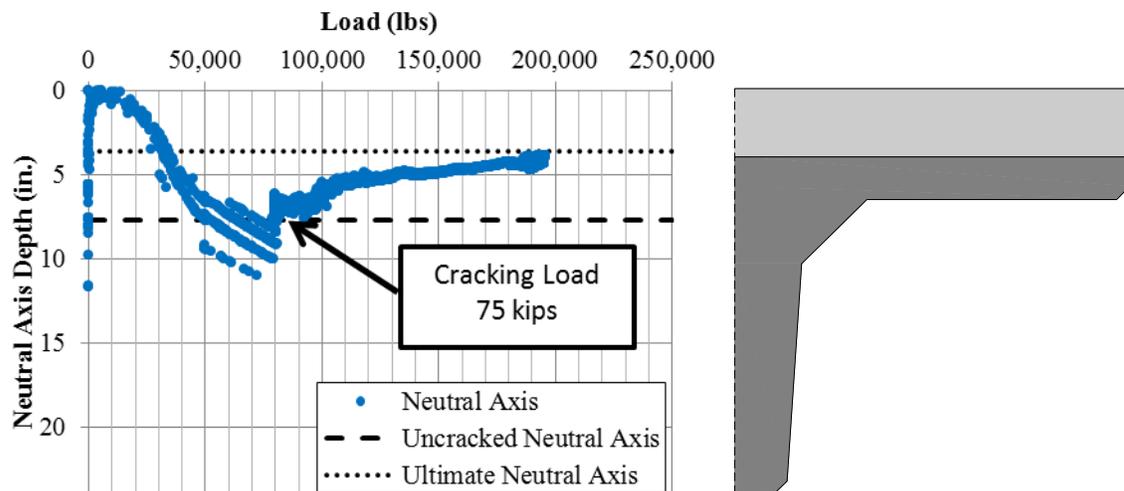
Figure 4.73: BDT Girder 2, Shear Test, Neutral Axis Depth vs. Load

Because of the use of a diaphragm for the second BDT Girder test, the strand slippage vs. load was only monitored for the first, and can be found in Figure 4.74. The east gauge began slipping first at a load of approximately 180 kips. It can be seen that both of the monitored bottom strands slipped at the failure of the girder, making it a conclusive bond failure.
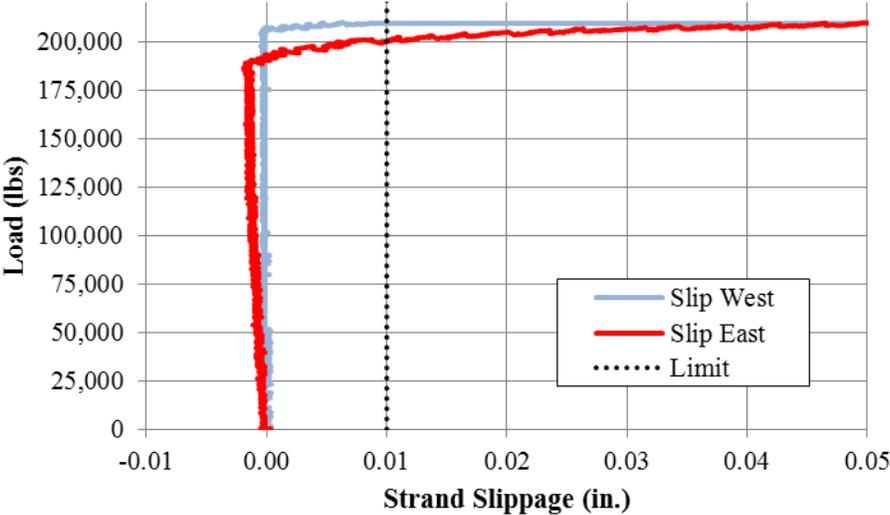
Figure 4.74: BDT Girder 1, Shear Test, Load vs. Strand Slippage

The difference in failure modes for the two girders was reflected in the horizontal shear behavior of the girder, as monitored by the ERSGs placed at the CIP to precast interface. Figure 4.75 shows the predicted behavior of BDT Girder 1's interface strain, which is similar to the development length test's lack of a horizontal shear failure. Girder 2 on the other hand, displays exactly the same type of horizontal shear failure, with the abrupt shift from composite to non-composite action, as plotted in Figure 4.76.
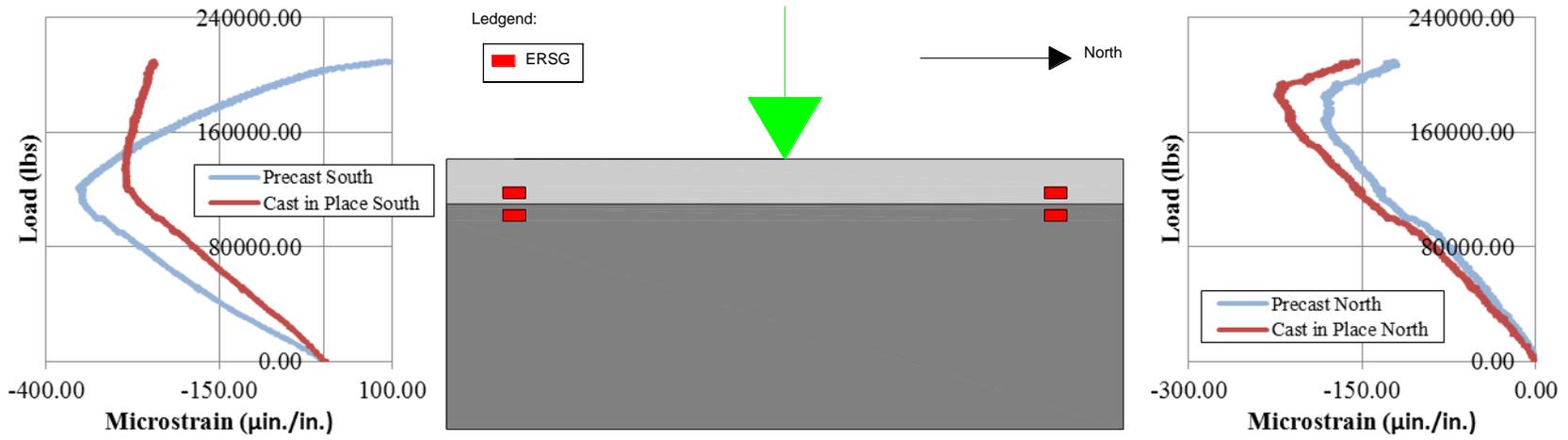
Figure 4.75: BDT Girder 1, Shear Test, Load vs. Cast in Place and Precast Strains
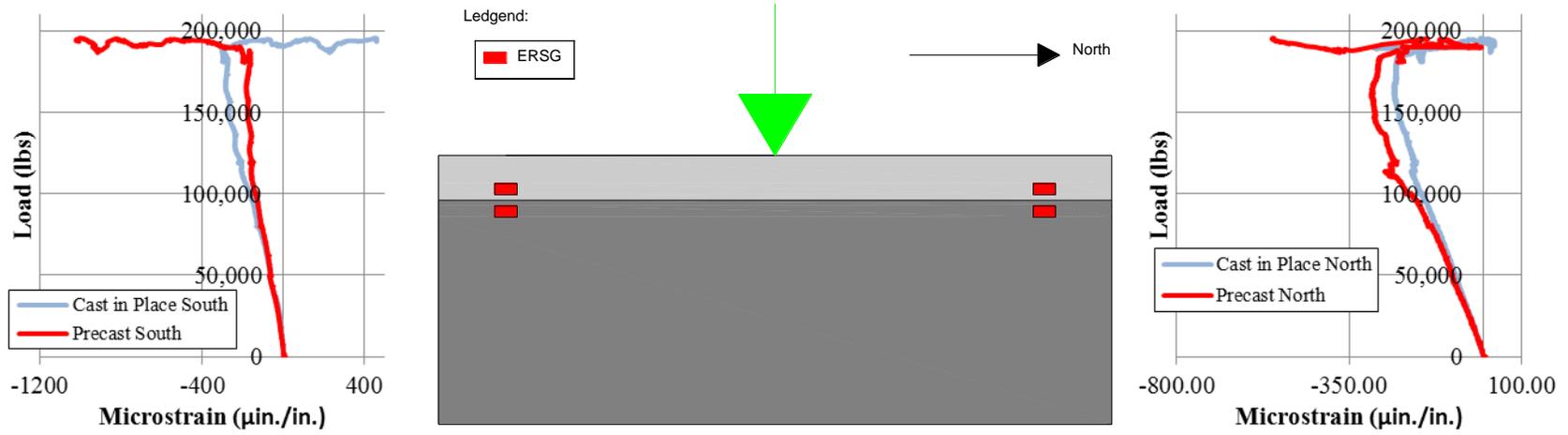
Figure 4.76: BDT Girder 2, Shear Test, Load vs. Cast in Place and Precast Strains

The failure modes of the girders were completely different, as were the cracking patterns, as discussed above. The significantly different cracking patters were echoed in the difference of the rosette readings of each girder. The strains read by the ST-POTs oriented as shown Figure 4.77 below, can be used to determine the principle stresses/strains and approximate cracking angle with a few assumptions.
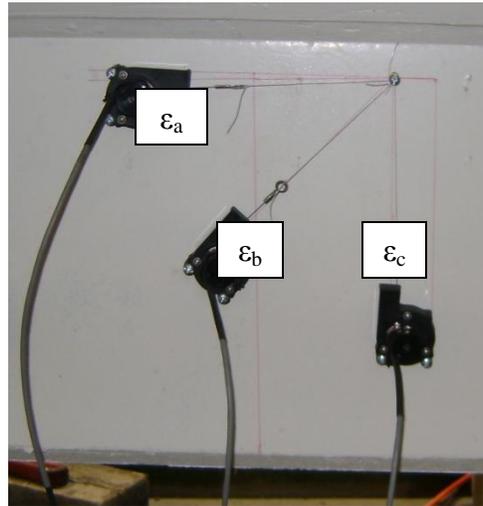
Figure 4.77: ST-POT Rosette with Nomenclature

A plane strain assumption was made for the use of a two dimensional Mohr's circle. Principle strains can be calculated directly from the known orientation of the rosette arms, as well as the data obtained from the load testing. Through the use of the following transformation equations derived from Mohr's circle, the principle strains, as well as their angles, can be calculated from the following two equations, when using the strains from the ST-POTs in Figure 4.77:

$$\varepsilon_{1,2} = \frac{\varepsilon_A + \varepsilon_C}{2} \pm \frac{1}{\sqrt{2}} \sqrt{(\varepsilon_A - \varepsilon_B)^2 + (\varepsilon_B - \varepsilon_C)^2}$$

$$\theta = \frac{1}{2} tan^{-1}(\frac{\varepsilon_A - 2\varepsilon_B + \varepsilon_C}{\varepsilon_A - \varepsilon_C})$$

If one assumes that the concrete remains linear elastic, the principle stresses may be calculated from the principle strains. These can be calculated from the following (Boresi and Schmidt, 2003):

$$\sigma_1 = \frac{E}{1 - v^2}(\varepsilon_1 + v\varepsilon_2)$$

$$\sigma_2 = \frac{E}{1 - v^2}(\varepsilon_2 + v\varepsilon_1)$$

This is not a poor assumption, as stress vs. strain graphs of the concrete indicates a high level of linearity. Principle stress and principle strain directions coincide for linear elastic materials; therefore another calculation of the principle stress angle is not required. The principle strains and compressive stresses for BDT Girder 1's rosette are presented as a function of the load in Figure 4.78 and Figure 4.79. Principle strain angle is similarly presented in Figure 4.80. Due to the relatively poor resolution of the ST-POTs, a manually implemented running average was used to clean up the principle strain angle plot. The principle strains indicate a maximum principle compressive strain of 0.0032 in./in., which corresponds to a maximum average stress through the rosette of 22.8 ksi using the above equations, as can be seen in Figure 4.78 and Figure 4.79. According to the stress vs. strain data from the concrete a compressive strain of over 0.0032 indicates the concrete has passed its peak, and is obviously no longer linear elastic. Crushing of the concrete was not observed at such a high strain but this may be due to the large gauge length and relatively intense reinforcement in that area. Stresses over 10 ksi in Figure 4.79 are invalid and are over estimations stemming from the previously mentioned linear elastic assumption. Figure 4.79 does indicate that the NU UHPC was contributing significant compressive strength to the shear resistance.
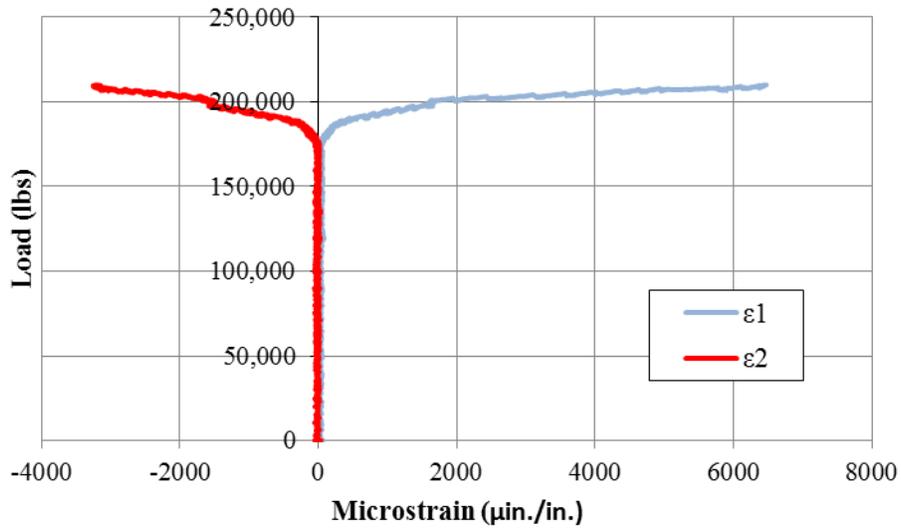
Figure 4.78: BDT Girder 1, Shear Test, Principle Strains
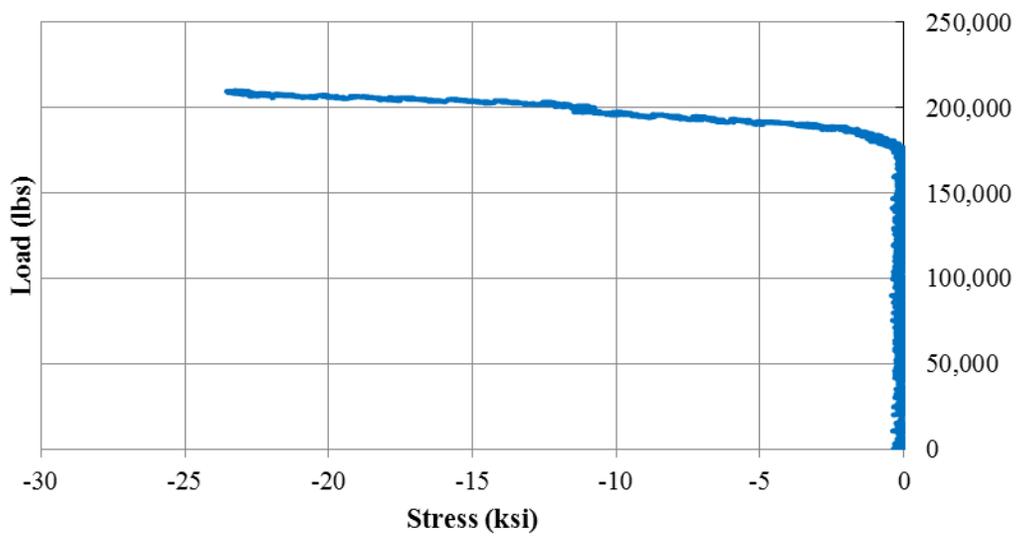
Figure 4.79: BDT Girder 1, Shear Test, Principle Compressive Stress
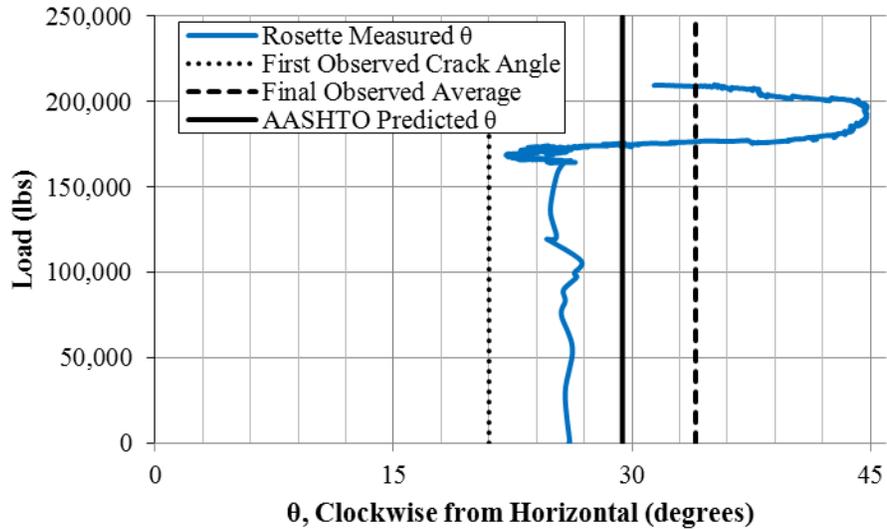
Figure 4.80: BDT Girder 1, Shear Test, Measured θ, Observed Angles and Design θ

One can see that the principle strain direction does not move much from where it first started (26o) for the majority of the loading. This is because the first crack to pass through any of the rosette legs occurred at just over 170 kips at which point the angle dropped to about 22-23o. This first crack can be seen in Figure 4.81 running through the middle leg of the rosette. Following the first crack, a number of cracks made their way through the rosette which caused the principle angle to shift and move upward and then back down. The final angle read by the gauges was approximately 32o. From Figure 4.81 a number of crack angles have been approximated. If one averages the angles, a result of 34.8o which is relatively close to the measured final angle of 32o.
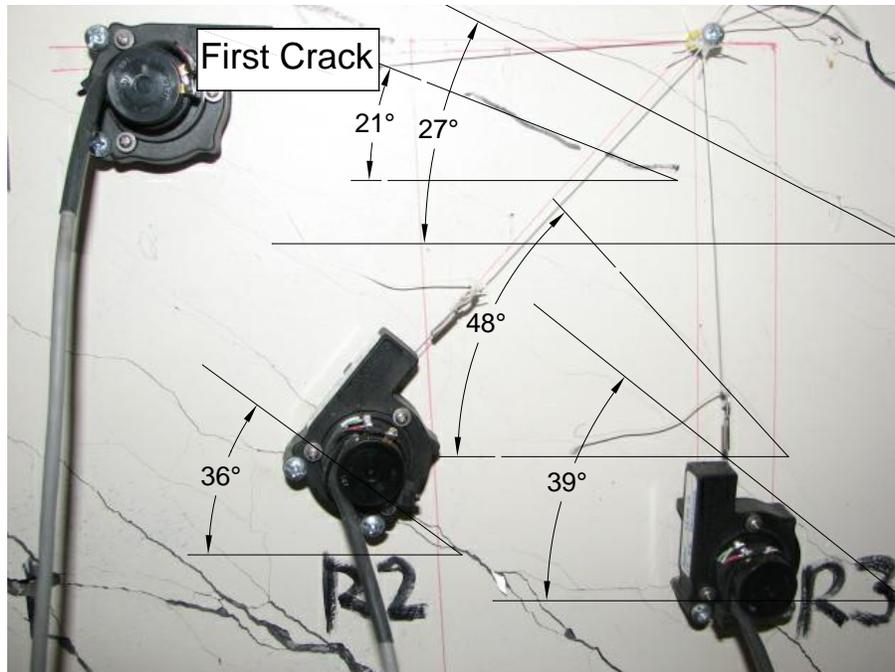
Figure 4.81: BDT Girder 1, Shear Test, Cracks through Rosette

Strains in the stirrups were measured with vertical ST-POTs. Stresses were related to these strains through the use of WWR stress vs. strain plots previously illustrated. From this information it was possible to estimate the stresses in the stirrups as the applied load increased. This plot can be seen in Figure 4.82. It seemed that the stirrups were not stressed until the girder had significantly cracked, likely because of measurement of an average strain over a relatively large distance. Strains in stirrups are known to be concentrated across cracks (Kuchma, 2008), however the large gauge length on the concrete surface did not register this.

Stirrup strains proceeded to stress at an essentially constant rate with respect to the applied load. The stirrup closest to the loading (V1) began loading first, followed by followed by the stirrup closest to the support and then the stirrup at mid span. Each stirrup's progression through the measured WWR stress vs. strain curve can be found in Figure 4.83. The stirrups all reached well over yield by the end of the test.
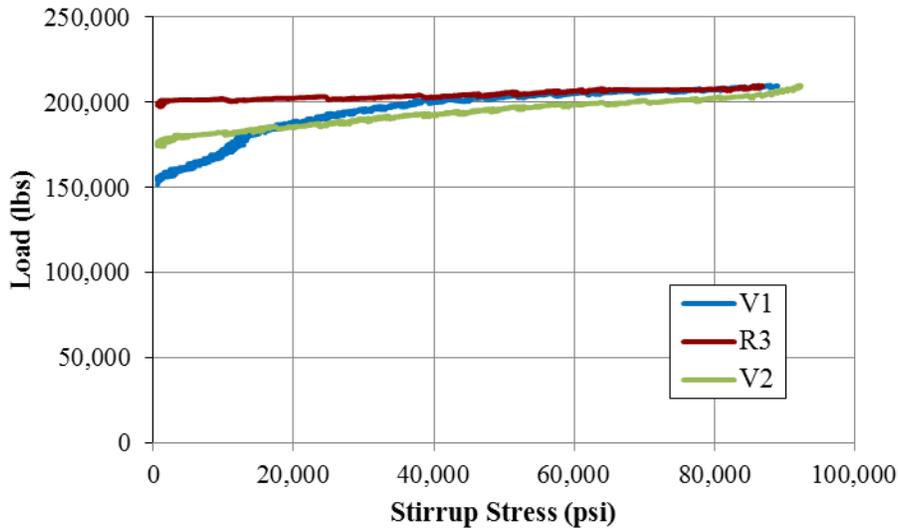
Figure 4.82: BDT Girder 1, Shear Test, Load vs. Measured Stirrup Stresses
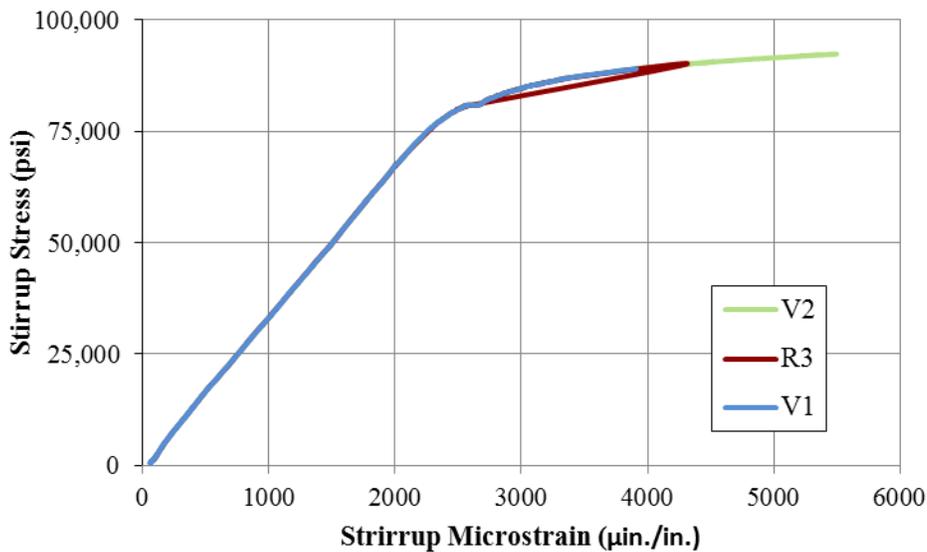
Figure 4.83: BDT Girder 1, Shear Test, Stirrup Stress vs. Microstrain Envelope

Calculation of the principle strains, stresses and angle for BDT Girder 2 used the same equations as for BDT Girder 1, the plots of which can be found in Figure through Figure 4.86. BDT Girder 2 presented many more cracks were observed on the web of the girder throughout the loading, especially through the rosette gauges. Principle strains and can be seen to suddenly increase as

more cracks propagated through the rosette in Figure 4.84. Every sudden increase indicates an additional crack or group of cracks through the rosette. These additional cracks cause redistribution of stresses in the web of the girder.

The load vs. principle compressive stress plot, in Figure 4.85, indicates a maximum compressive average stress through the rosette of 16 ksi, again this is an over estimation as the concrete does not behave linearly at the corresponding strain. After reaching the ultimate load of the girder, the principle compressive stress through the rosette abruptly drops. This abrupt drop in stress corresponds to rupture of the stirrup that is nearly directly under the vertical leg of the rosette. It should be noted that the girder seemed to have failed near the location of the rosette. The stirrup strains and compressive strains indicate, as well as the observed spalling of concrete from the stem, that this is the case. The first crack in the rosette was measured at an angle of 23° at approximately 50 kips of load as can be observed in Figure 4.87. This does not match up well with any of the semi-stable regions of Figure 4.86, but it does bisect what seems to be middle of a transition at approximately 50 kips. The average angle moves as more cracks propagate through the girder's rosette. The jumps in angle correspond to jumps in stresses and strains, as seen in Figure 4.84 and Figure 4.85. Post-mortem cracking was not measurable because of the very violent failure shown in Figure 4.70, which destroyed the girder's face. The AASHTO predicted θ at the location of the rosette was 29°. This matches up to within 1° to 2° of the measured values just before failure.
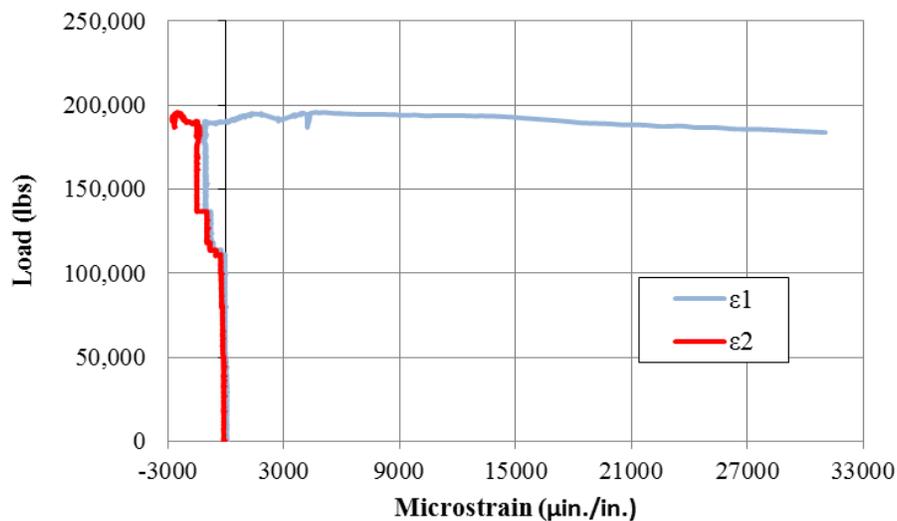

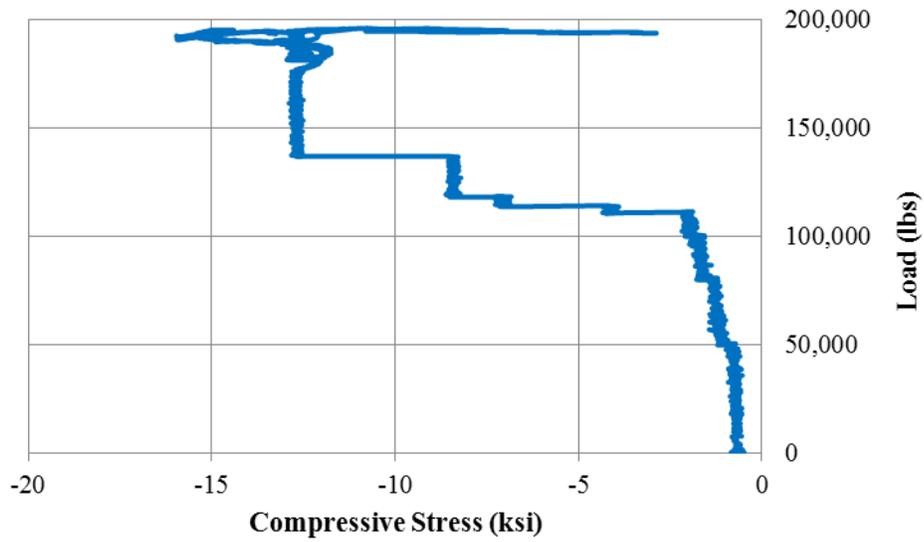Figure 4.84: BDT Girder 2, Shear Test, Load vs. Principle Strains

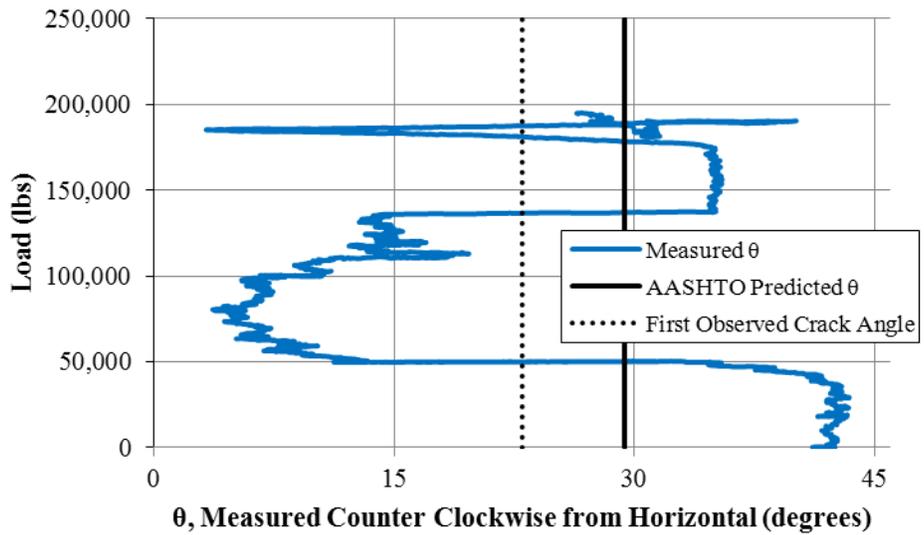Figure 4.85: BDT Girder 2, Shear Test, Load vs. Principle Compressive Stress

Figure 4.86: BDT Test 2, Shear Test, and Load vs. Measured θ, Observed Angles and Design θ
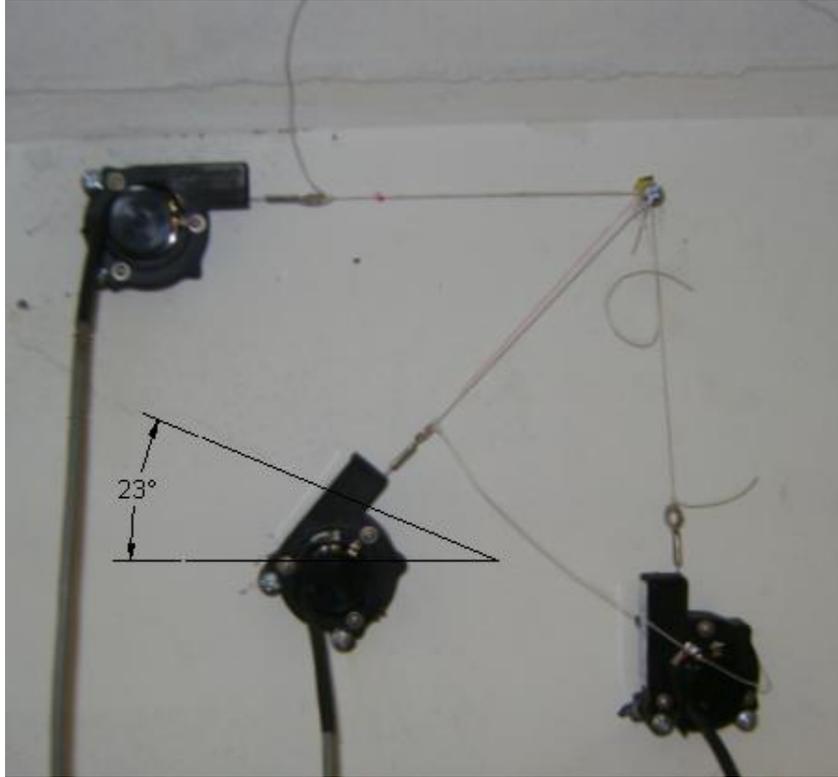
Figure 4.87: BDT Girder 2, Shear Test, First Shear Crack through Rosette

As in BDT Girder Test 1, strains in the stirrups were measured with vertical ST-POTs. Combining this data with the stress vs. strain data from the WWR stirrups, the load vs. stress diagram in Figure 4.82 was created. Even though cracking was noted before 175 kips, where the stirrups were located, the stirrups had a small amount of compressive strain. Again, the stirrup closest to the loading (V1) began loading first, followed by the stirrup closest to the support and then the stirrup at mid span. Each stirrup's progression through the measured WWR stress vs. strain curve can be found in Figure 4.89. It can be seen that the stirrup at the center of the shear span strained much more than the others, and indicated fracture just before failure.
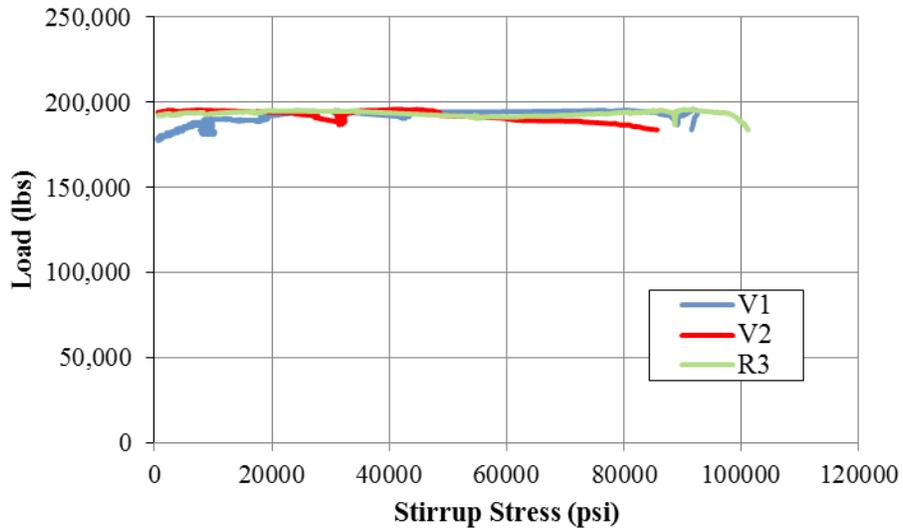
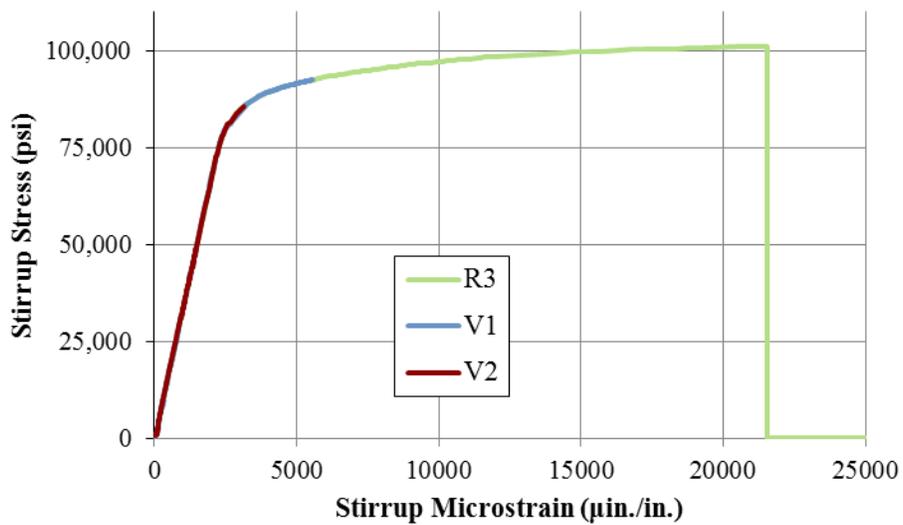Figure 4.88: BDT Girder 2, Shear Test, Load vs. Stirrup Strains

Figure 4.89: BDT Girder 2, Shear Test, Stress vs. Strain Envelope for Stirrups

118

5 TESTING OF RECTANGULAR PRISMS

5.1 Overview

The experimental investigation presented in Chapter 4 indicated that 0.7 in. diameter prestressing strands can be used at 2 in. by 2 in. spacing for UHPC girders. Additionally, measured transfer and development lengths have been determined to be within the code limits when a combination of UHPC and specified confinement reinforcement are used. This chapter presents the experimental investigation conducted to evaluate the performance of 0.7 in. diameter strands when lower concrete strengths and different levels of confinement are used. The HPC and confinement reinforcement that represent the industry practice in Nebraska are considered. This experimental investigation was conducted in three stages: 1) rectangular prisms pretensioned using one 0.7 in. diameter strands (Chapter 5); and 2) tee-shaped beams pretensioned using six 0.7 in. diameter strands (Chapter 6); and 3) full-scale NU1100 girders pretensioned using thirty four 0.7 in. diameter strands.

The literature review presented in Chapter 2 outlined a number of important studies on the effect of concrete strength on strand bond, specifically in HPC (Barnes and Burns, 1999; Kose and Burkett, 2005; Russell and Ramirez, 2008). With the combination of 0.7 in. diameter strands in HPC, the transfer and development lengths are identified and compared versus those specified by the AASHTO LRFD. Lower concrete strengths than those achieved by UHPC will be adopted to represent the current practice in the precast industry in Nebraska.

A complete spool of Grade 270 - 0.7 in. diameter strand was obtained from Producer 2 to be used in fabricating all the rectangular prism and tee girder specimens at the PKI structural laboratory. Four samples from this spool were tested to evaluate the strand mechanical properties in the same manner as outlined in Chapter 3. Table 5.1 lists the nominal minimum and experimental values of these properties for the tested strands. Figure 5.1 also plots the stress vs. strain behavior for each of the strand samples.

Table 5.1: Nominal minimum and experimental values for strands used in rectangular prisms and tee beam specimens

Strand Number	Load at 1% (lb)	Peak Load (lb)	MOE (ksi)
Nominal Minimum	*71,500*	*79,400*	*28,500*
1	69,100	80,100	28,100
2	69,500	80,100	28,092
3	69,400	79,500	26,532
4	68,300	81,000	26,389

Strand Area = 0.2952 in.^{2}
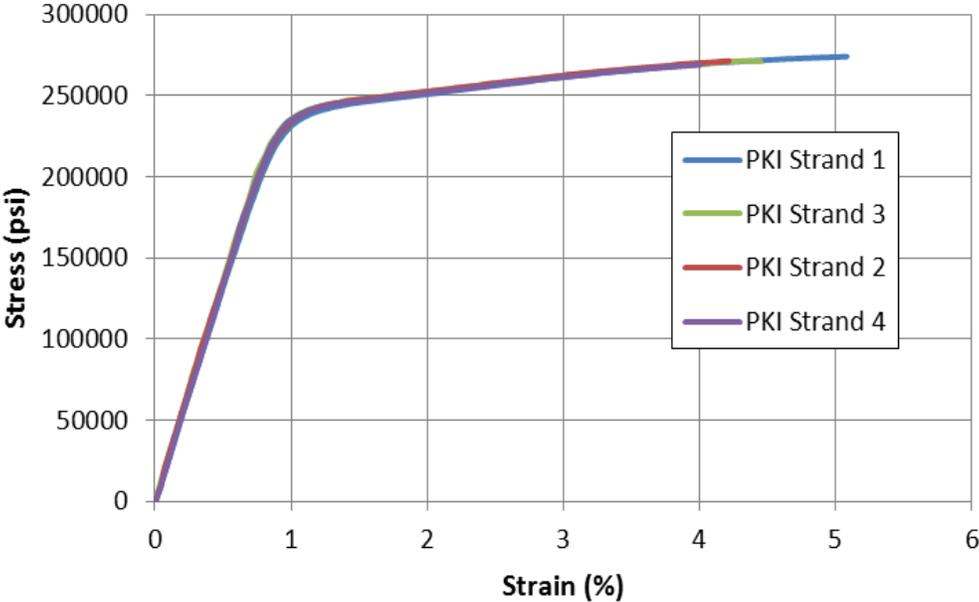
Figure 5.1: Stress vs. strain of strands used in rectangular prism and tee beam specimens

The surface quality of strands has been identified by many researchers as a significant parameter for strand bond. Figure 5.2 shows a photo of the strands pulled from the interior part of the spool. This photo indicates that the used strands had a good surface condition with minor rusty spots that are very common in the strands used for bridge girder fabrication.

Figure 5.2: Surface condition of 0.7 in. diameter strands used in test specimens

A standard self-consolidating concrete mix batched and delivered by Layman Richey Ready Mix Co. in Omaha, NE was used for all the HPC specimens presented in Chapters 5 and 6. Table 5.2 lists the constituents of this mix and their quantities for one cubic yard.

Table 5.2: High performance concrete mix design

Constituent	Quantity (lb/yd^3)
Sand Gravel	980
Screen Sand	420
1/2 Limestone	1340
Type I/II Cement	705
Class C Fly Ash	378
Pozzolith 322-N	22
Glenium 3030	140
Water	260
w/cm	0.24

5.2 Transfer Length Specimens

Four concentrically prestressed rectangular prisms were fabricated for transfer length measurements. The dimensions of the prisms were 96 in. x 7 in. x 7 in., with a single 0.7 in. diameter strand placed at the center of the prism. Each prism contained confining ties at varying spacing, as can be seen in Figure 5.3. The confining reinforcement had an outside to outside dimension of 5 in. for each leg of the square, which was bent from standard 60 ksi #3 rebar. The confining stirrups were placed at 12, 9, 6 and 3 in. on center, with the first stirrup placed at half of the inner stirrup spacing from the end. The strand was tensioned to $0.75f_{pu}$, and the specified concrete strength at release was 6 ksi to mimic the concrete strengths in Nebraska precast plants.
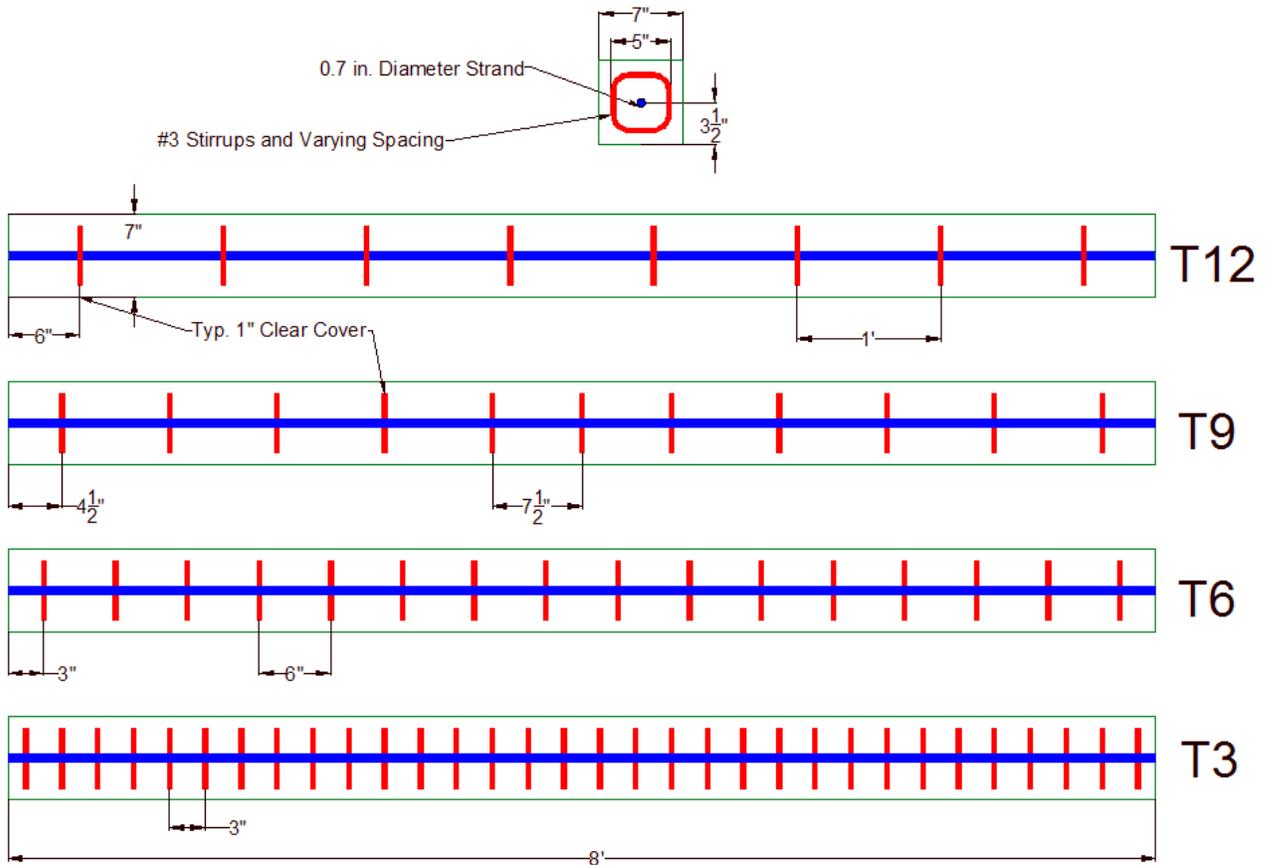
Figure 5.3: Transfer Prism Reinforcement with Specimen Nomenclature

The four rectangular prisms were fabricated at the PKI structural laboratory using the wooden forms and confinement ties shown in Figure 5.4. The strand was chucked and initially tensioned to approximately 1-2 kips to facilitate forming. Chairs were stapled to the inside of the forms on all three sides to ensure proper location and clearance of the confining reinforcement. All

reinforcement was then tied at the appropriate locations and the strand was tensioned to $0.75f_{pu}$. Ready mix self-consolidating concrete with an average spread of 25 in., shown in Figure 5.4., was used to pour the four specimens, which were cured using wet burlap. Figure 5.5 shows the layout of specimens in the prestressing bed.
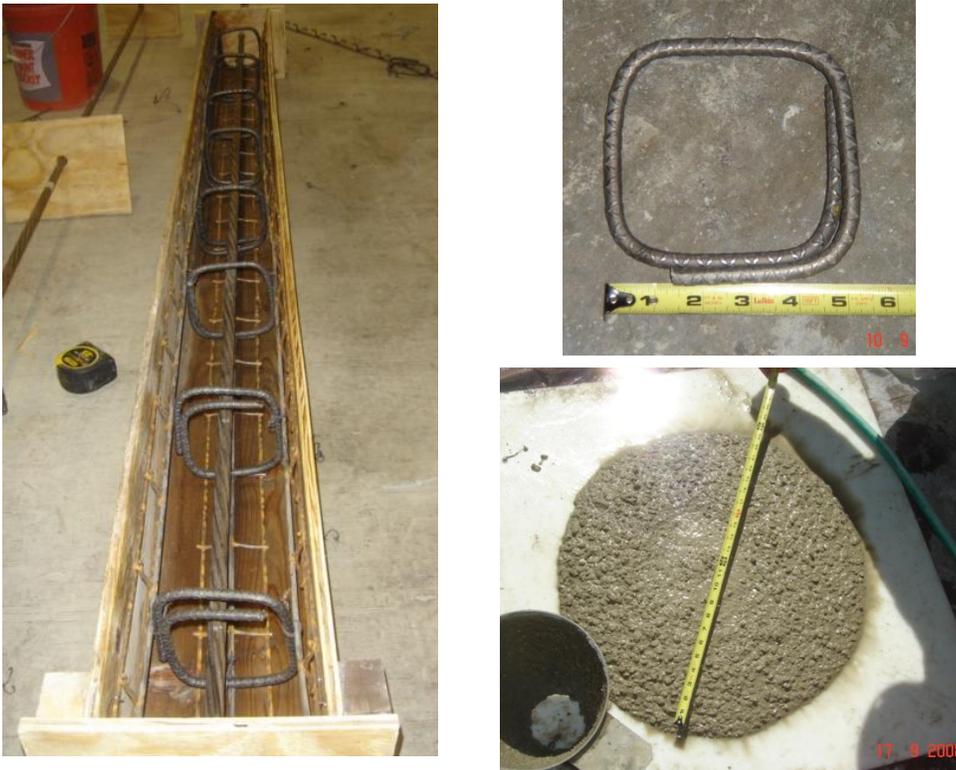

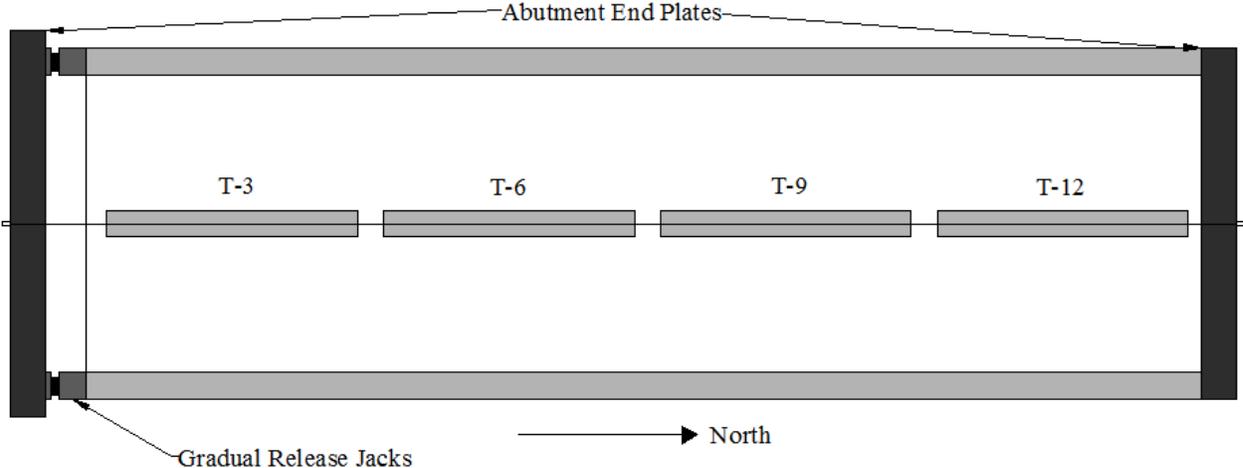Figure 5.4: Prism specimen form, reinforcement, and concrete

Figure 5.5: Layout of transfer length specimens in the prestressing bed

The four specimens were instrumented with DEMEC disks on each side (A or B), starting from each end and ending at the middle of the specimen. Disks were glued to the face of the prisms at approximately 3.937 in. centers, using the standard reference bar, starting at approximately 2 in. from each end of the prisms. Both sides of the prisms were instrumented with DEMEC disks. Figure 5.6 shows the location of DEMEC disks on the sides of the transfer length prisms. Figure 5.7 shows DEMEC disks attached to the prism specimens and DEMEC strain readings being taken. Reference readings were taken prior to strand release. Then, several readings were taken immediately after release (initial), 7 days, 14 days, and 28 days after release.
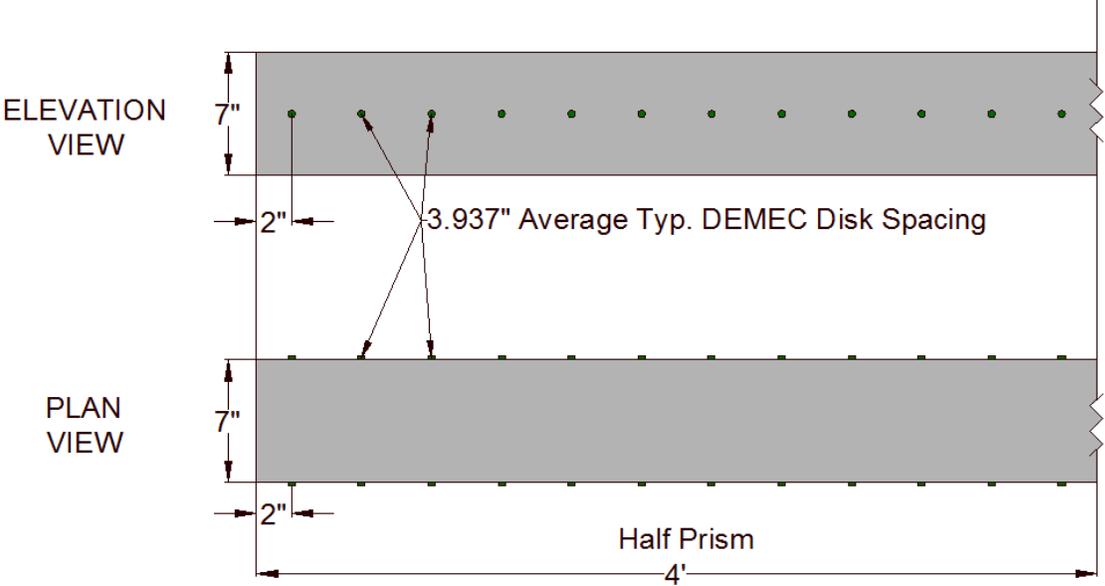

Figure 5.6: Location of DEMEC disks on prism specimens

Figure 5.7: DEMEC disks along centerline (left), and DEMEC strain readings (right)

The 95% AMS method was performed on each prism's side (A and B) and end (North and South) for a total of eight transfer regions. Figure 5.8 shows examples of surface strain plots for T9-A-S and T9-A-N regions and the 95% AMS Method used to estimate the transfer length. Figure 5.9 shows the complete strain profile for all four specimens at 1 day and 28 days after release. Table 5.3 lists all transfer length readings, calculated averages, and code predictions.
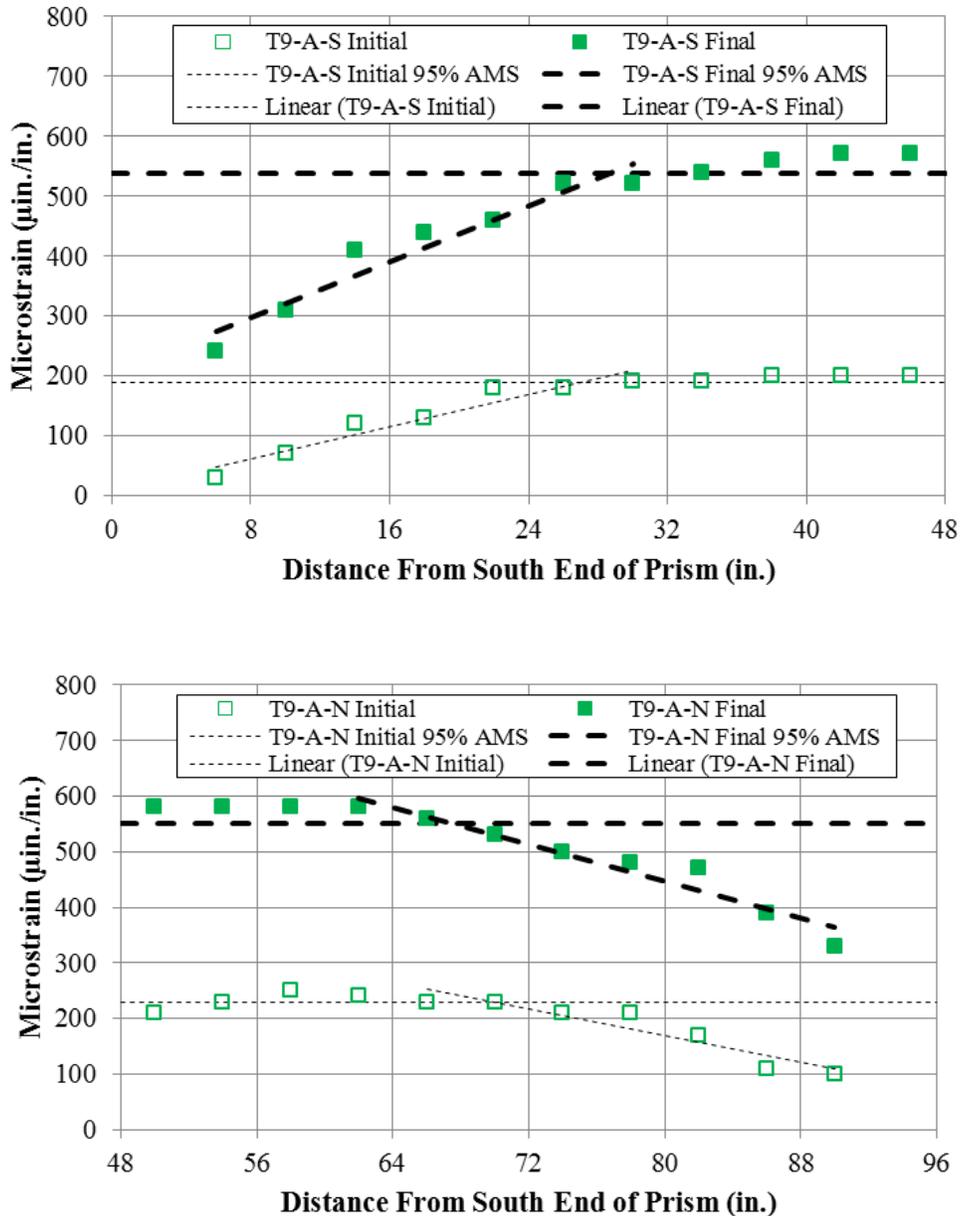

Figure 5.8: Examples for estimating transfer length using 95% AMS method in T9-A-S prism specimen (top), and T9-A-N prism specimen (bottom)
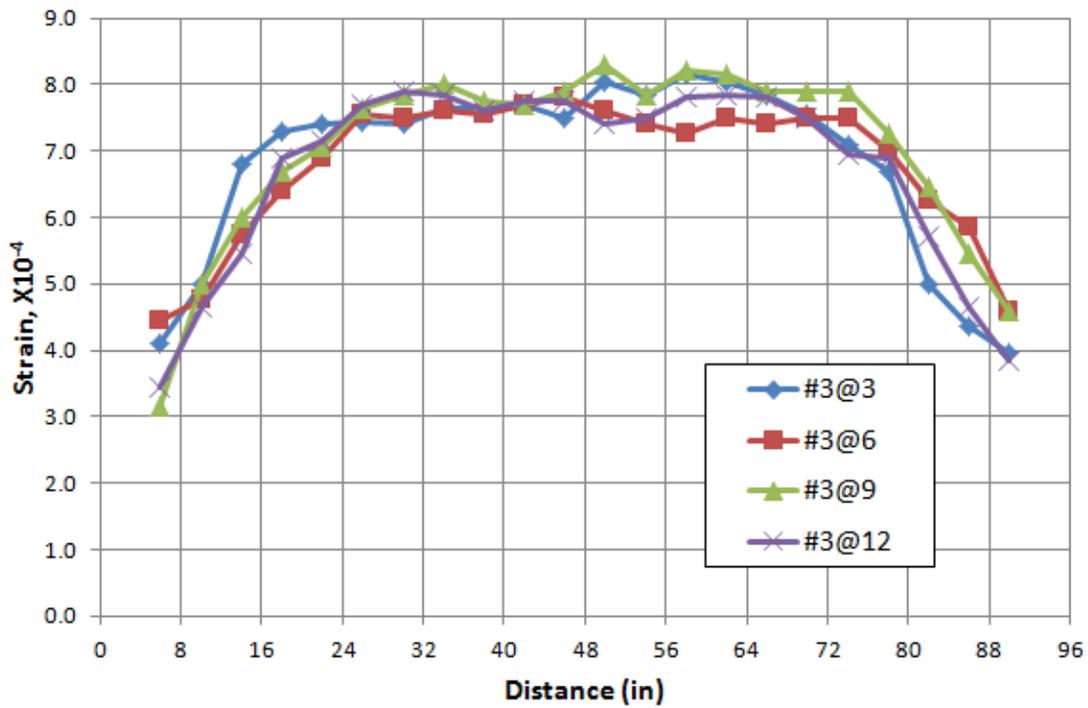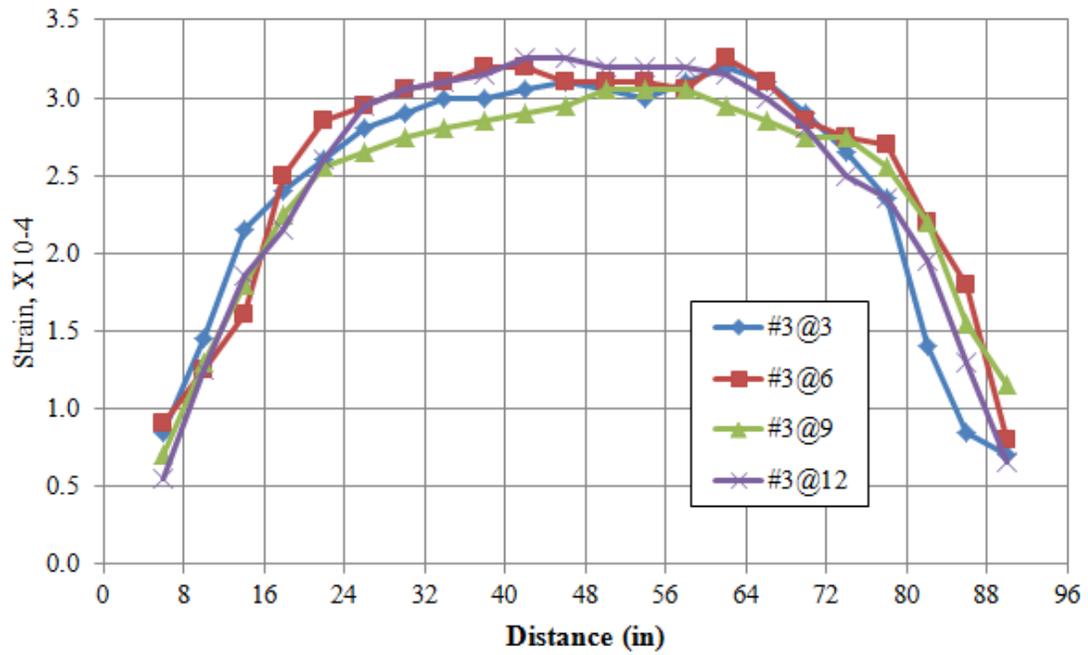
Figure 5.9: Strain profiles from 1-day and 28-day transfer length measurements for different levels of confinement

Table 5.3: Transfer length results from rectangular prism specimens

Prism Side and End	Initial 95% AMS (in.)	Final 95% AMS (in.)	Initial l_t (in.) Side Avg.	Initial l_t (in.) Overall Avg.	Final l_t (in.) Side Avg.	Final l_t (in.) Overall Avg.	ACI, 50db (in.)	AASHTO, 60db (in.)
T12-A-N	28.3	27.7	26.8		27.3			
T12-B-N	25.2	26.9		27.6		27.9		
T12-A-S	30.0	29.9	28.3		28.5			
T12-B-S	26.7	27.1						
T9-A-N	26.0	28.5	25.6		27.1			
T9-B-N	25.3	25.7		25.8		27.2		
T9-A-S	26.7	28.6	26.0		27.3			
T9-B-S	25.3	25.9					35.00	42.00
T6-A-N	26.5	26.3	24.9		24.8			
T6-B-N	23.3	23.3		25.6		26.2		
T6-A-S	25.4	26.6	26.3		27.6			
T6-B-S	27.2	28.5						
T3-A-N	26.2	28.4	27.1		27.8			
T3-B-N	27.9	27.2		27.4		28.2		
T3-A-S	27.9	29.2	27.7		28.7			
T3-B-S	27.5	28.1						

All measured transfer lengths were under both code predictions for ACI and AASHTO, indicating adequate bond performance of the 0.7 in. diameter strands in HPC. It should be noted that these transfer lengths are significantly longer than those measured in UHPC, as well as shorter than transfer lengths observed by Reiser (2007). Based on Table 5.3, it can be observed that there is a slight increase between the initial and final transfer lengths. However, the increase is not very significant, nor does it seem to have a pattern. This is likely due to the gradual release method employed and normal variation between transfer lengths. In general, significantly longer transfer lengths are found for specimen on the live end of the prestressing bed for sudden release. It would also be expected that the transfer lengths increase over time, as in the BDT Girders of the previous chapter, but a significant increase did not occur and can be attributed due to the release method. The gradual release method reduces the development of stable plastic cracking of the bond region around the strands, reducing initial transfer lengths. It also follows that there would be less stress redistribution because of fewer or less well developed plastic cracks, and therefore, less increase of the transfer length over time for the gradual release method.

Figure 5.10 plots the initial and final average transfer lengths of each side, end, and girder. It can be seen that there is no correlation between transfer length and casting position (South was the live end) or level of confinement, which is evident in Figure 5.9. This is in agreement with the conclusion of the investigation carried out on 0.5 in. and 0.6 in. strands (Russell and Burns, 1996). In this investigation, transfer length was measure experimentally on specimens with 2, 3, and 4 strands with and without confining reinforcement (#3 @ 4 in.). The conclusion was that confinement reinforcement did not contribute significantly to prestress transfer because the confinement reinforcement remains inactive until concrete cracking occurs, which is usually controlled by end zone reinforcement. Also, transfer length is mainly a function of the stiffness of the uncracked concrete section, which is hardly affected by the amount of confinement reinforcement. It should be noted that the conclusions presented above were reached by testing a single strand in rectangular prism specimens. The number of strands, spacing among strands, and shape of specimen might result in a different effect, which will be investigated in the following chapters.
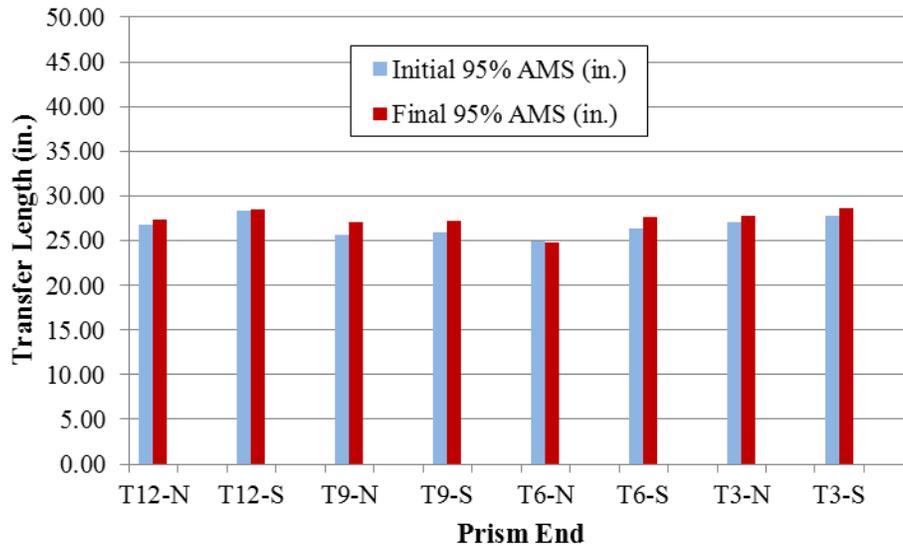
Figure 5.10: Initial and final transfer length measurement for all specimens

5.3 Pull-out Specimens

Pullout tests were performed to evaluate the bond between concrete and 0.7 in. diameter strand. Three parameters were considered in this testing: embedment length, level of confinement, and stress state of the strand. A total of thirty-nine specimens were fabricated, poured, and tested in the PKI structural laboratory: twelve 4 ft specimens, fifteen 5 ft specimens, and twelve 6 ft specimens. The specimens had the same cross section as the transfer length specimens shown in Figure 5.3. Due to the capacity limitations of the prestressing bed, the specimens were fabricated in two phases. Phase I included 21 specimens, and Phase II included 18 additional specimens Figure 5.11 shows the forms set up in the prestressing bed, while Figure 5.12 shows the test setup. This setup was designed to apply clamping force on the strand while testing to prevent strand slippage and ensure that the ultimate stress is applied. A potentiometer was attached to the strand on the other end of each specimen during testing to monitor the bond failure of the strand, which is defined as any relative movement that is greater than 0.01 inch. This value was determined based on the precision of the used potentiometer.

Figure 5.11: Forms of the pullout specimens

Figure 5.12: Pull-out test setup

Table 1 gives the pullout testing results of all thirty-nine specimens. Two types of failure were observed: strand rupture and strand slippage. Specimens that failed above the ultimate strength of 270 ksi had strand rupture, while those which failed below 270 ksi had strand slippage – except those marked with an asterisk. The rupture of those strands at a stress level below the ASTM A416-06 and AASHTO M203-07 specified 270 ksi might be attributed to stress concentration at the gripping location due to improper alignment of the inset and chuck. These specimens were still considered in the study as they resulted in stress levels very close to 270 ksi without slippage.

Table 5.4: Results of pull-out testing

Specimen No.	3 # 3 - Pre-tensioned			5 # 3 - Pre-tensioned			5 # 3 - Non-tensioned		
	4 ft	5 ft	6 ft	4 ft	5 ft	6 ft	4 ft	5 ft	6 ft
1	277	269*	278	279	278	295	249	264*	264
2	255	283	285	279	294	273	233	269	270
3	247	283	277	268*	295	286	248	255	241
4	249	280	277	278	269*	299	230	272	273
5		275			268*			269	
Average (ksi)	257	280	280	278	289	288	240	266	262
Std. Dev.	14.0	3.7	3.9	0.4	9.5	11.7	9.8	7.5	14.4

*indicates strand rupture below the ASTM A416–06 & AASHTO M203-07 standards

According to the 1996 AASHTO Standard Specifications for Highway Bridge Design Section 9.22.2, nominal reinforcement is required to enclose prestressing strands for at least a distance d from the end of the girder, where d is the depth of the girder. The specifications did not stipulate a minimum amount of confinement reinforcement. The 2007 AASHTO LRFD Specifications Section 5.10.10.2 stipulates that at least #3 deformed bars with spacing not exceeding 6 in. should be used to enclose prestressing strands. Although this statement acknowledges the need for confinement reinforcement for prestressing strands, it does not provide adequate information to quantify the effect of this reinforcement on the development length, which is not the case in the development of reinforcing bars (refer to 2007 AASHTO LRFD Section 5.11.2.1.3, and ACI 318-08 Section 12.2.3). To evaluate the effect of level of confinement on the bond between the concrete and 0.7 in. diameter strand, thirteen specimens were made using 5#3 (high confinement), Grade 60 confinement loops (i.e. stirrups) and another thirteen specimens were made using 3#3 stirrups (low confinement). Each group consisted of four 4 ft long specimens, five 5 ft long specimens, and four 6 ft long specimens. Stirrups were distributed at equal spacing. All twenty-six specimens were pre-tensioned at 59.5 kip, which is 75% of the ultimate strand strength. Figure 5.13 presents the results from the pull-out testing of the two groups of specimens. This figure indicates that the required amount of confinement to develop the 0.7 in. strand varies with the embedment length of the strand. Although 5#3 stirrups were needed for the strand to reach an ultimate strength of 270 ksi in the 4 ft long specimens, only 3#3 stirrups were needed for the same strand to reach the stress level in the 5 ft and 6 ft long specimens. Therefore,

it can be concluded that the level of confinement has a significant effect on the development of 0.7 in. strand. This effect is more pronounced on strands with a shorter embedment length than in those with a long embedment length. This conclusion will assist designers in identifying the minimum amount of confinement reinforcement required to develop 0.7 in. strand within a specific length.
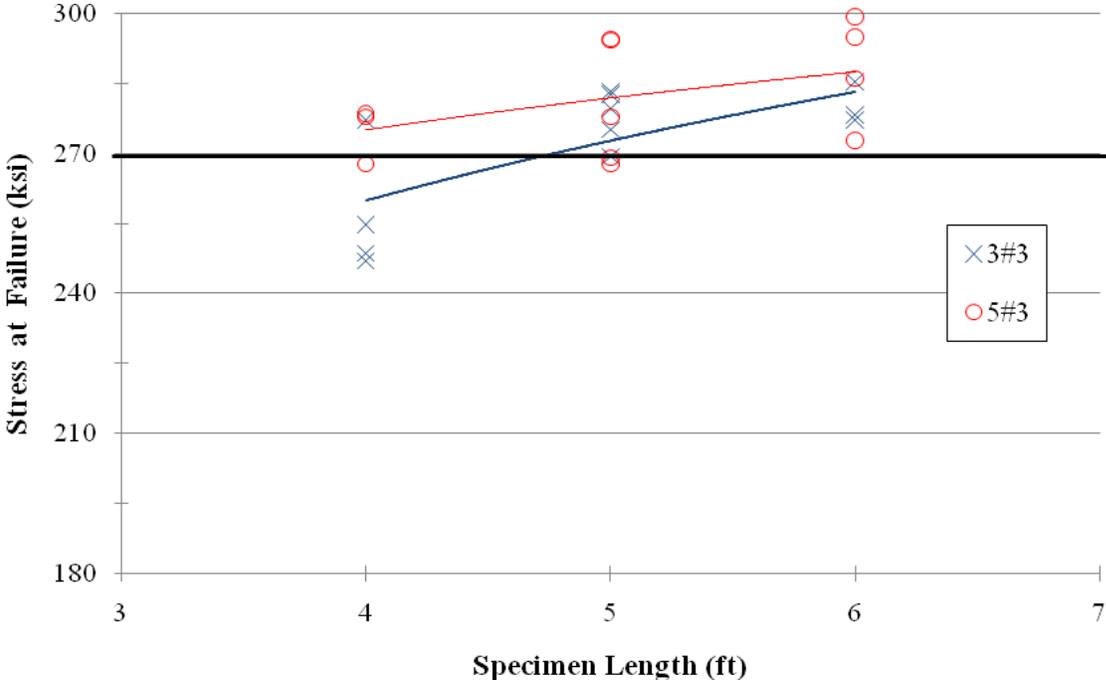

Figure 5.13: Effect of level of confinement on pull-out test results

Strand wedging, or the "Hoyer" effect, is one of the mechanisms that contribute to the transfer of prestressing force from the strand to the surrounding concrete. When the prestressing force is applied, strand elongates and its cross sectional area shrinks (Poisson's effect). At release, strands' cross sectional area at the end of the transfer length remains the same due to the applied stress, while its' original cross sectional area at the end of the members is almost restored due to the absence of stresses. This gradual change in the cross sectional area of the strand (wedge-like shape) along the transfer length results in an increased bond with concrete. Pullout tests of strand are commonly performed on non-tensioned strands for simplicity, which eliminates the contribution of strand wedging to the bond with concrete.

In this study, the effect of wedging on the development of 0.7 in. diameter strand was investigated. Thirteen specimens were tested with pre-tensioned strand, while another thirteen specimens were tested without pre-tensioned strand. Each group consisted of four 4 ft long specimens, five 5 ft long specimens, and four 6 ft long specimens that were confined with 5#3, Grade 60 stirrups. Figure 5.14 presents the pullout test results of the two groups. This figure indicates that pre-tensioning the strand results in a significant increase in the stresses at failure, and more importantly, a change in the mode of failure from gradual slippage to strand rupture. This concludes that using non-prestressed strand in pullout testing for evaluating the development length is conservative as it results in a lower bond strength and an unrealistic failure mode.
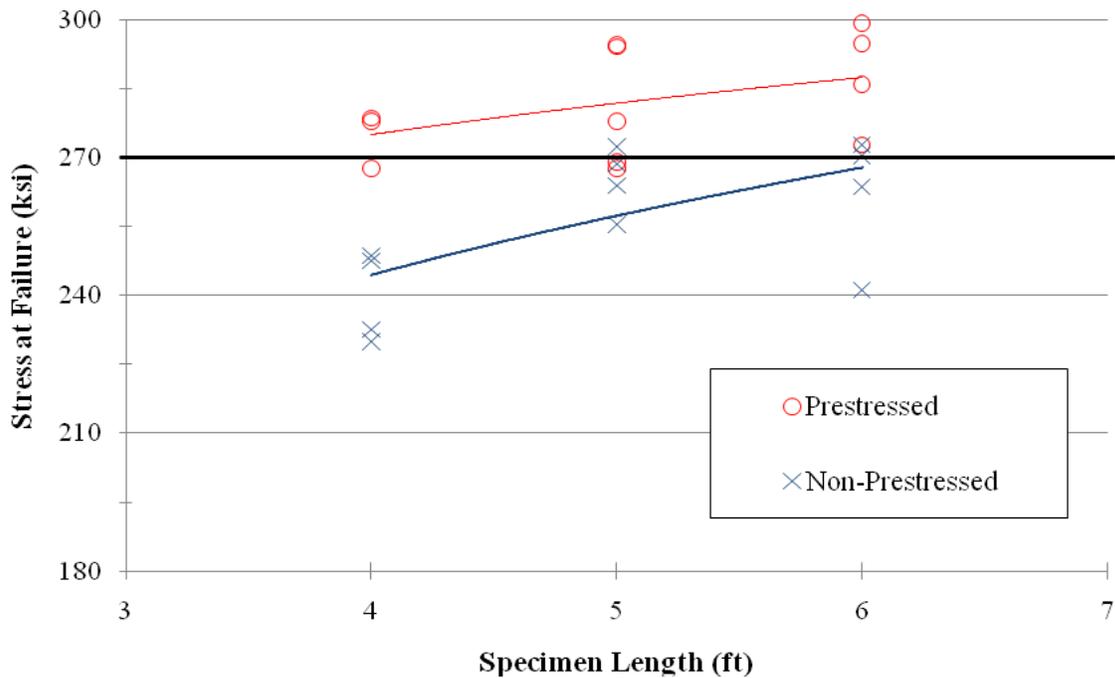
Figure 5.14: Results of prestressed and non-prestressed strand from pull-out testing

Figure 5.15 plots the results of testing all thirty-nine 0.7 in. diameter strand specimens grouped into three cases: 1) non-tensioned strands with 5#3 confinement reinforcement; 2) pre-tensioned strands with 3#3 confinement reinforcement; and 3) pre-tensioned strands with 5#3 confinement reinforcement. These three groups were designed to evaluate the effect of embedment length on

each case. Comparing case #1 versus case #3 shows the added bond strength achieved by the strand wedging that takes place at release. For all lengths, the increase is significant but not constant. This is because the embedment length itself has no impact on the wedging effect, but it has a significant impact on developing the strand up to the development length. Comparing case #2 versus case #3 shows the effect of the level of confinement on the development of 0.7 in. diameter strand. In this comparison, the embedment length has a similar effect to the amount of confinement on developing prestressing strand. Much less confinement is required to develop the strand in the 5 ft and 6 ft long specimens than that in 4 ft long specimens. This can be attributed to the increased adhesion and mechanical interlock between the strand and the concrete with the embedment length. Consequently, development length equations should take into account the amount of confinement within that length.
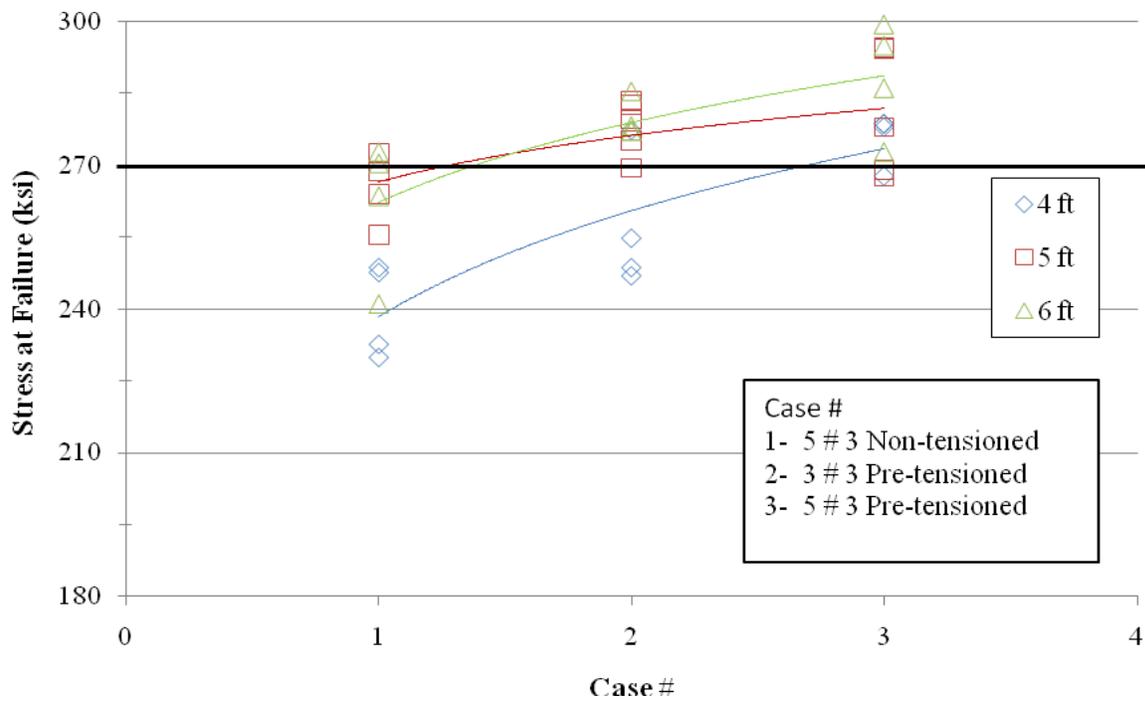
Figure 5.15: Overall results of pull-out testing

6 TESTING OF T-GIRDER SPECIMENS

6.1 Overview

The experimental investigation presented in Chapter 5 using one 0.7 in. diameter prestressing strand in HPC rectangular prisms indicated that the transfer length of 0.7 in. diameter strands is below the value predicted using AASHTO LRFD specifications and is not significantly affected by the level of confinement. This investigation also indicated that the level of confinement has significant impact of the development length of 0.7 in. diameter strands. Since the investigation was performed by pulling a single strand out of HPC rectangular prims, it could not determine whether the development length is within the AASHTO LRFD predictions, which needs to be determined through the flexural testing of prestressed girders.

In this chapter, the flexural testing carried out on eight T-girders pretensioned using six 0.7 in. diameter strands at 2 in. by 2 in. spacing is presented. Each girder is 28 ft long, which is twice the development length of 0.7 in. diameter strands calculated using AASHTO LRFD equation 5.11.4.2-1. The eight T-girders had different concrete strengths and levels of confinement to evaluate the impact of these parameters on the development length of 0.7 in. diameter strands. Four T-girders were also instrumented to measure the transfer length to confirm the conclusions made in the previous chapter. Also, two T-girders were tested in shear to evaluate the impact of having longer transfer and development length on the shear capacity of the prestressed concrete girders. All girders were fabricated and tested at the PKI structural laboratory by the research team. The properties of the concrete and prestressing strands used in these specimens are the same as those used in fabricating the rectangular prisms presented in the previous chapter.

Each T-girder was longitudinally reinforced with six 0.7 in. diameter Grade 270 low-relaxation prestressing strands tensioned $0.75f_{pu}$ and located in two rows at 2 in. x 2 in. spacing as shown in Figure 6.1. An additional four 0.6 in. diameter prestressing strands, tensioned to 2-3 kips, were used to support vertical and top flange reinforcement, in addition to reducing the required strength at release. The top flange was transversely reinforced with #3@12 in.to strengthen the flange during testing. Vertical shear reinforcement consisted of Grade 80 WWR mats of 12 in. x

8 in. – D20 x D8 and end zone reinforcement consisted of two ¾ in. diameter coil rods welded to the 0.5 in. x 6 in. x 8 in. bearing plates as shown in Figure 6.1.
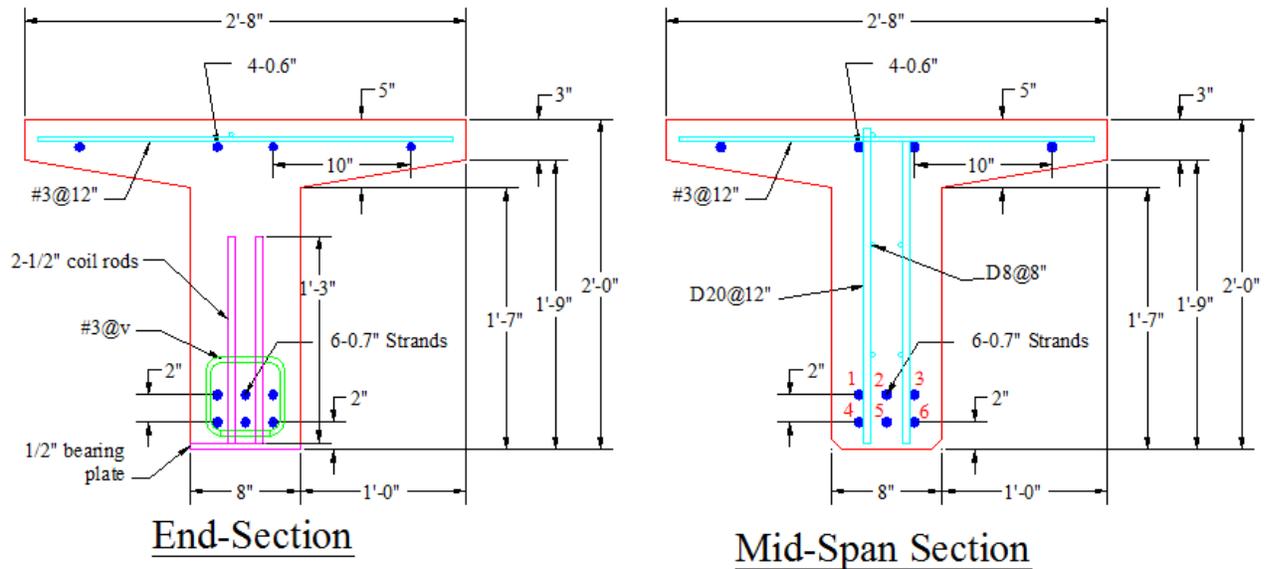

Figure 6.1: Cross sections of the T-girder specimens

To evaluate the effect of confinement reinforcement and concrete strength on the transfer length, development length, and shear capacity, No. 3, Grade 60, 5 in. x 5 in. square ties were used in all specimens at variable spacing (V) along a distance (L). Figure 6.2 shows these parameters on the side view of the specimen, while Table 6.1 lists the values of these parameters in the eight specimens. It should be noted that the AASHTO LRFD confinement reinforcement specified in Section 5.10.10.2 was used as the base confinement in all four pours for comparison purposes. Each pour include two specimens that are laid out in the prestressing bed as shown in Figure 6.3. The concrete compressive strength at the time of testing in the four pours were: A) 13,500 psi, B) 11,900 psi, C) 9,000 psi, and D) for 11,200 psi. T-girder designation was set up as follows: Girder Shape - Confinement Spacing - Confinement Distribution Distance - Concrete Strength Designation.
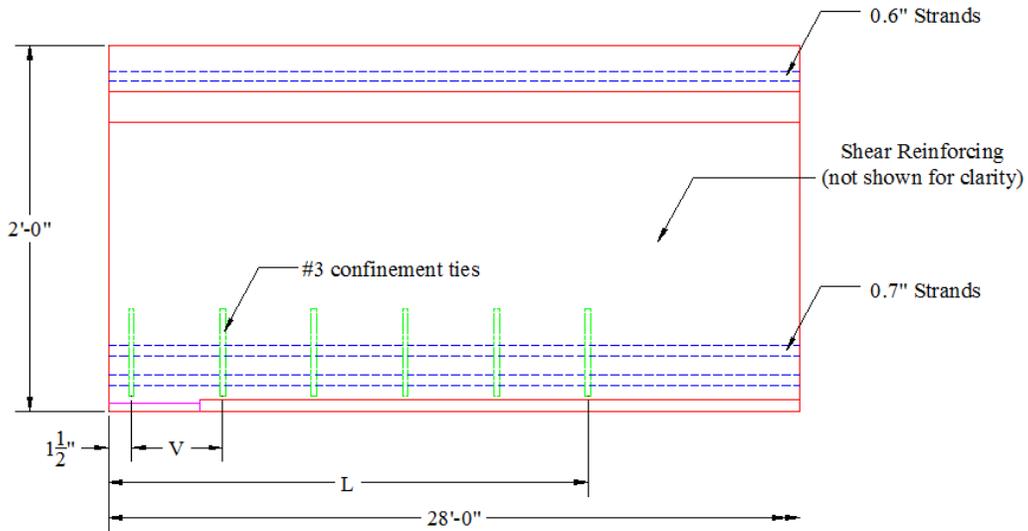
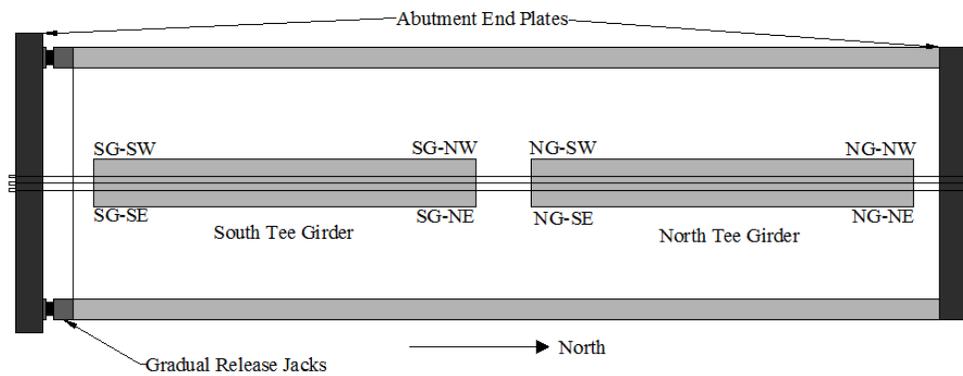Figure 6.2: Cross sections of the T-girder specimens

Figure 6.3: Layout of specimens in the prestressing bed and nomenclature of girder ends

Table 6.1: T-girder designation and parameter values

Test		Confinement			
Number	Girder Designation	Size	No. per end	Spacing-V (in)	Distribution-L (in)
1	T-6-1.5h-A	#3	6	6.0	36.0
2	T-6-0.5l-A	#3	28	6.0	168.0
3	T-6-1.5h-B	#3	6	6.0	36.0
4	T-4-1.0h-B	#3	6	4.0	24.0
5	T-6-1.5h-C	#3	6	6.0	36.0
6	T-4-1.0h-C	#3	6	4.0	24.0
7	T-12-0.5l-D	#3	14	12.0	168.0
8	T-4/6-1/1.5h-D	#3	6	4.0 / 6.0	24.0 / 36.0

The fabrication of the T-girder specimen proceeded as follows. First, plastic sheeting was placed on the floor of the prestressing bed. Next, chamfer was stapled to the bed at the appropriate spacing, immobilizing both chamfer and plastic. Then, the six 0.7 in. diameter strands were threaded through the south abutment plates, through the appropriate plywood end plates and confinement reinforcement, then finally through the north abutment plates. Each strand was chucked at both ends and tensioned to $0.75f_{pu}$ for easy tying of confinement. Following tying of the confinement, the four 0.6 in. diameter strands in the top flange were located appropriately. Vertical reinforcement was then tied to the confinement and top strand reinforcement and transverse flange reinforcement was placed, resting on the top 0.6 in. diameter strands. The foam formwork was placed under the free end of the plastic tarp, which was smoothed and stapled to the foam. The self-consolidating concrete (SCC) was then delivered by the Ready Mix truck Spread diameter was measured upon arrival and additional dosage of HRWRA was used to bring the spread to at least 22 in. Cylinder samples were taken following the adequate spread diameter and pouring of the girders commenced. Casting of the girders required no vibration and little labor due to the concrete's flowing ability. Lifting points were then inserted into the fresh concrete 2.5 ft from each end. Wet burlap curing commenced after the initial set. Figure 6.4 shows photos of the different steps of specimen fabrication.

(a) End zone reinforcement and confinement reinforcement

(b) Shear reinforcement

(c) Forming T-girder using foam blocks

(d) Slump flow test of SCC

(e) Specimen pouring, finishing, and curing

Figure 6.4: Fabrication steps of T-girder specimens.

6.2 Transfer Length Measurements

The first two T-girders in Table 6.1 were instrumented to measure the transfer length of 0.7 in. diameter strands, which resulted in a total of four transfer zones (two ends for each girder). Transfer lengths were to be determined two ways: 1) end slip measurement; and 2) surface strain measurements. End slip measurements were performed by placing a piece of masking tape on the end of each of the strands. The only exception was the bottom middle strand, because of poor access. The distance from the face of the concrete on the T-girder to the inside edge of the tape was measured immediately before and after release on three of the four girder ends as shown in Figure 6.5. One girder end was cast too close to the end of the bed, due to space limitations, which made it impossible to measure with the dial gauge. It is important to note that, in this report, these measurements are termed end slip, which is distinctly different from strand slippage due to applied load, discussed elsewhere.
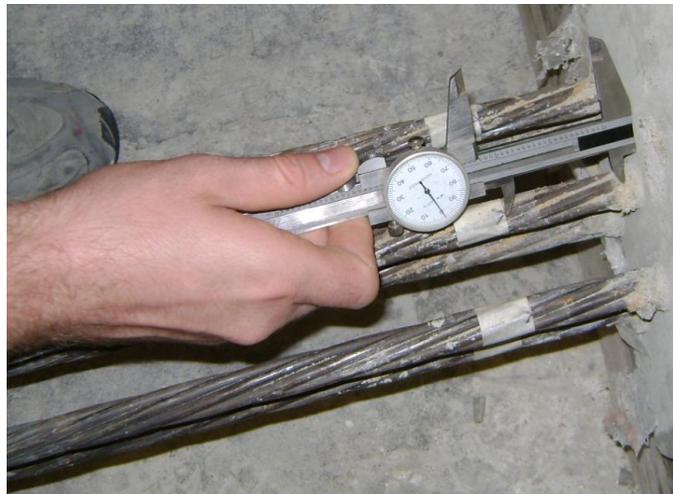
Figure 6.5: Measuring strand end slip

Concrete surface strains were also measured using DEMEC strain gauge disks attached with epoxy to the surface of the tee girders, at the level of the centroid of the prestressing strands as shown in Figure 6.6. Disks were attached starting 1 in. from the end of the girder, at a spacing of 1.969 in. for the expected maximum transfer length of $60d_b$. Subsequent DEMEC disks were attached at a spacing of 3.937 in. to ensure the transfer length was captured up to $100d_b$. Readings were taken immediately prior to release, 30 minutes following and 14 days following release in order to observe initial and final transfer length measurements as shown in Figure 6.6.
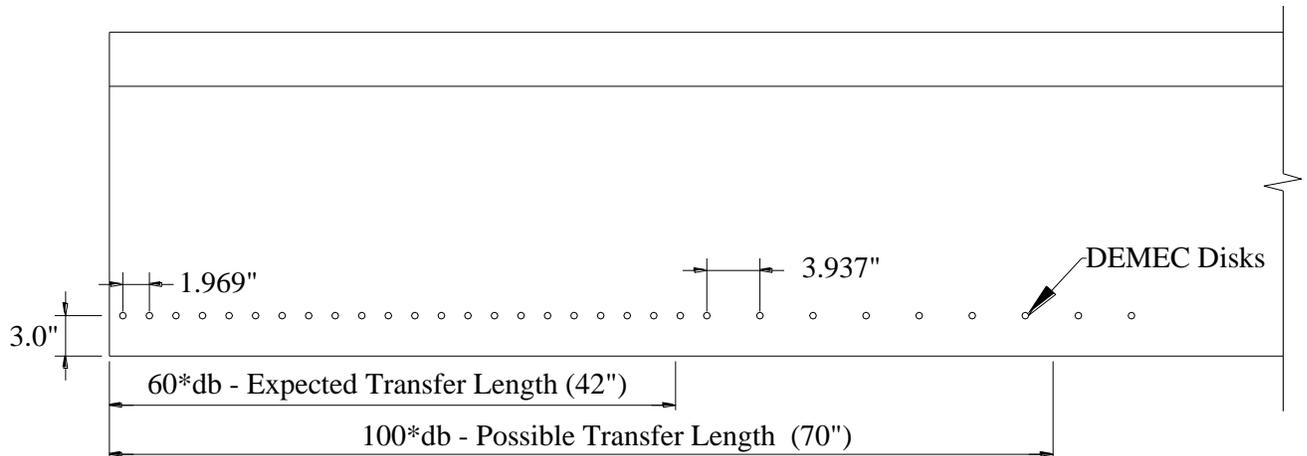
141

Figure 6.6: Measuring transfer length using surface strain method: DEMEC layout (top), Dial gauge (bottom)

The concrete compressive strength development with time is plotted in Figure 6.7. The two T-girders were released on day 6 at a compressive strength of approximately 9 ksi. This was higher than preferred by the researchers was attributed to the unexpected rapid gain of concrete strength of the mix.
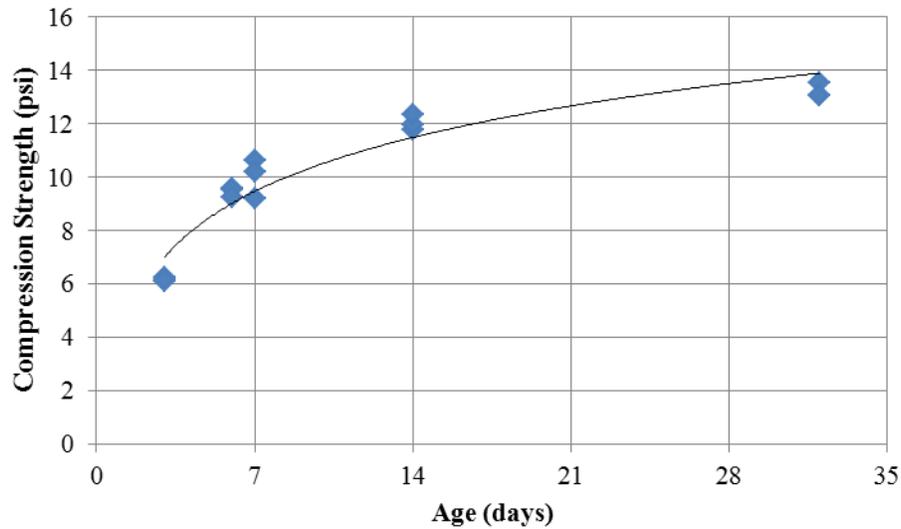
Figure 6.7: T-girder concrete compressive strength vs. age

The strands were released simultaneously with the hydraulic jacks located on the south end of the prestressing bed. Very few and fine splitting cracks were observed immediately after release and were traced with a blue marker and are shown in Figure 6.8. These cracks are not unusual and were controlled by the use of end zone reinforcement according to (Tuan, et al. 2004).

Figure 6.8: North girder end zone cracking at two sides (no visible cracks)

The transfer length of the 0.7 in. diameter strands was measured in two ways. One was typical surface strain measurements, which have been discussed previously in the report. The other was end slip measurements upon release. A theoretical relationship, discussed by Guyon (1960), can be used to estimate the transfer length from the relative movement between the strand and concrete upon release. The equation used to determine the transfer length from the end slip is shown below:

$$l_t = \frac{2E_{ps}}{f_{se} + E_{ps}\varepsilon_c} L_{es}$$

Where, E_{ps} is the MOE of the strands, L_{es} is the end slip, f_{se} is the effective prestressing, and $\in_c$ is the average surface strain of the concrete. It should be noted that the value of end slip calculated using the above equation does not include the elastic shortening of the free part of the strand, which is very small. End slip measurements are listed in Tables 6.2 to 6.4 Note that end slip measurements were not taken for the middle bottom strand, due to difficulty reaching it, as well as girder end NG-N, due to space limitations. Strand numbers are shown in Figure 6.2

Table 6.2: North girder – South end – End slip readings and calculated transfer length

NG-S Strand #	Initial (in.)	Final (in.)	Steel Shortening (in.)	End Slip (in.)	l_t (in.)
1	2.431	2.330	0.019	0.0824	21.5
2	2.436	2.329	0.019	0.0884	23.1
3	2.352	2.246	0.018	0.0880	23.0
4	2.760	2.648	0.021	0.0911	23.8
5	X	X	X	X	X
6	2.485	2.403	0.019	0.0820	21.4
			AVERAGE	0.0864	**22.6**

Table 6.3: South girder – North end – End slip readings and calculated transfer length

SG-N Strand #	Initial (in.)	Final (in.)	Steel Shortening (in.)	End Slip (in.)	l_t (in.)
1	2.440	2.340	0.019	0.0814	21.2
2	2.424	2.328	0.019	0.0775	20.1
3	2.453	2.365	0.019	0.0693	18.0
4	2.616	2.516	0.020	0.0801	20.8
5	X	X	X	X	X
6	2.676	2.602	0.020	0.0740	19.2
			AVERAGE	0.0765	**19.9**

Table 6.4: South girder – South end – Slip readings and calculated transfer length

SG-S Strand #	Initial (in.)	Final (in.)	Steel Shortening (in.)	End Slip (in.)	l_t (in.)
1	2.432	2.313	0.019	0.1004	26.1
2	2.388	2.282	0.018	0.0877	22.8
3	2.349	2.225	0.018	0.1060	27.6
4	2.357	2.245	0.018	0.0939	24.4
5	X	X	X	X	X
6	2.388	2.257	0.018	0.1310	34.1
			AVERAGE	0.1038	**27.0**

The initial and final surface strain transfer length readings for the T-girders were calculated using the Modified 95% AMS method outlined in preceding chapters. Girder ends and sides are labeled with the cardinal directions as oriented in their original position in the prestressing bed as presented in the Figure 6.3. Examples of surface strain plots with initial and final 95% AMS transfer length determination are presented in Figures 6.9 and 6.10. Table 6.5 presents a summary of transfer lengths for the T-girders, including comparison values to ACI and AASHTO predictions.
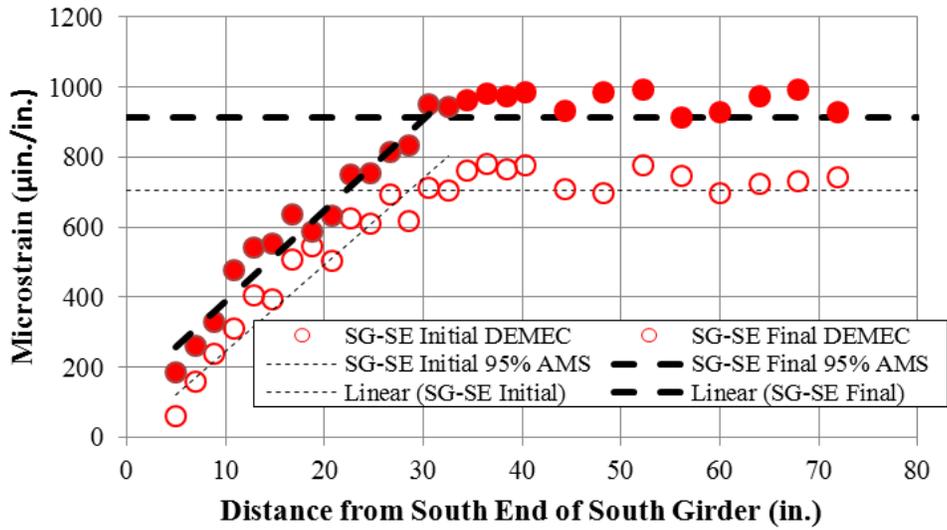
Figure 6.9: South girder–South end-Surface strain readings and initial and final transfer length
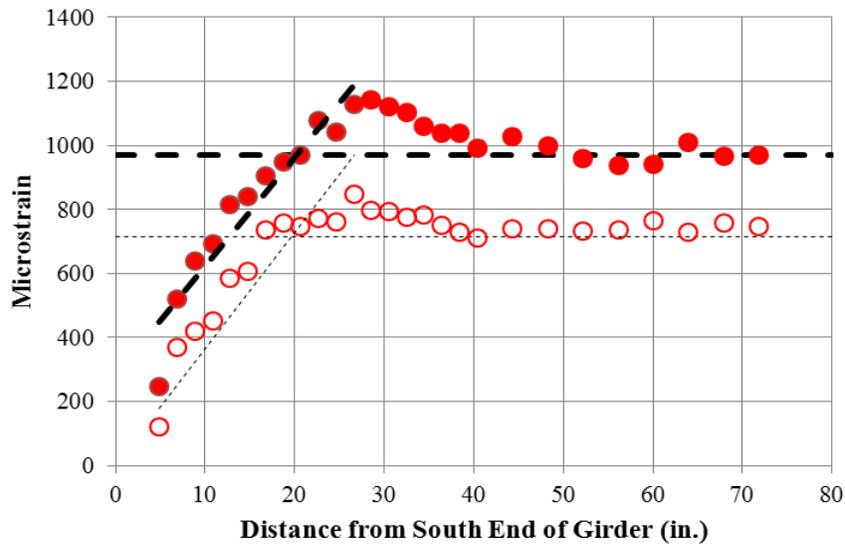
Figure 6.10: North girder–South end-Surface strain readings and initial and final transfer length

Table 6.5: T-girder transfer length using surface strain method

Beam End	End Slip lt (in.)	Initial Measurement 95% AMS Method (in.)	Final Measurement 95% AMS Method (in.)	ACI (50d_b, in.)	AASHTO (60db, in.)
NG-NW	-	21.6	22.0	35.0	42.0
NG-NE		28.4	29.1		
NG-SW	22.6	22.5	22.8		
NG-SE		19.6	20.1		
SG-NW	19.9	22.6	24.1		
SG-NE		21.9	21.5		
SG-SW	27.0	26.0	26.3		
SG-SE		28.5	30.1		

It can be seen from the transfer length data, that all transfer lengths for each side and end are estimated within the code predictions. This was expected by the researchers, based on the high concrete strength at release and the generally conservative code equations, which do not consider concrete compressive strength. A more concise plot of averaged transfer lengths for each girder end is shown in Figure 6.11. Of note, end slip measurements under-predicted surface strain measured transfer lengths for the south girder, but under-predicted for the north girder. This variability of end slip measurement has been noted by other researchers (Carrol, 2008; Marti-Vargas, 2007). However, the end slip transfer length measurements seemed to be relatively accurate.
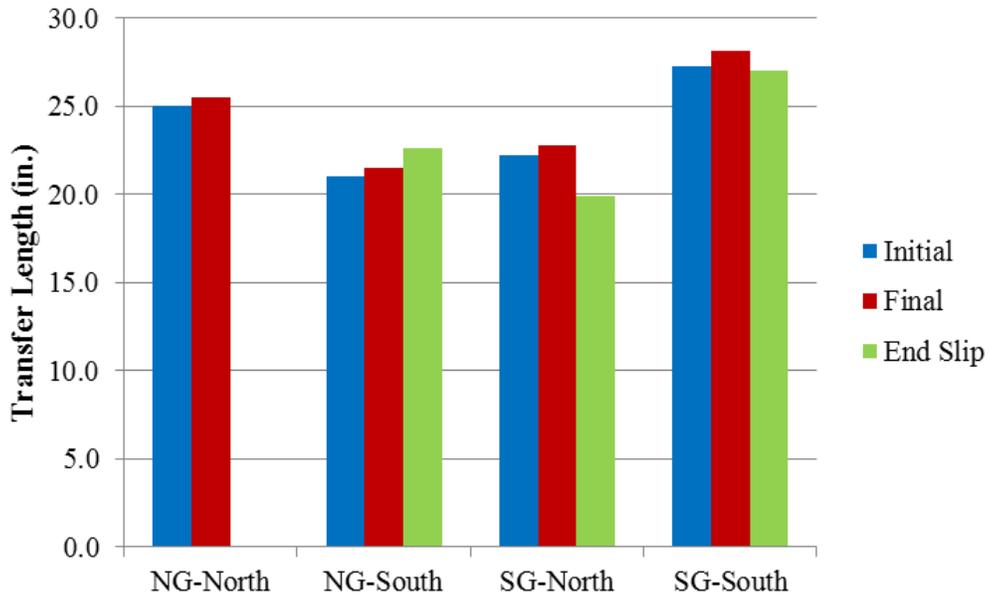
Figure 6.11: Plot of average transfer length measurement at different locations

The transfer length was measured on the next four T-girder specimens in Table 6.1 but using the surface strain method only. The initial readings taken just after release, as well as the final transfer readings, taken at fourteen days after release, were measured. A sample of the surface strain plot set up for initial and final 95% AMS transfer length determination is presented by Figure 6.12.
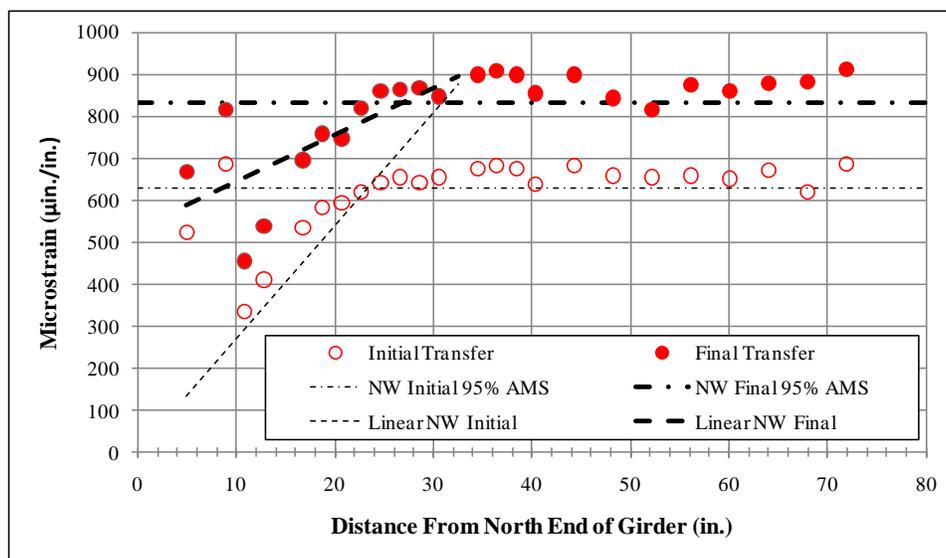

Figure 6.12: T-4-1.0h-B North end-West side-Surface strain measurements method

Table 6.6 presents the overall results from all of the six specimens. All specimens had prestress transfer at a much lower value than that predicted by AASHTO LRFD section 5.11.4.1 (42 in.). This result was expected by the researchers as the code on this subject is generally conservative, not taking into account many aspects believed to aid in reducing the length of prestress transfer from the strand to the concrete, such as concrete strength.

Table 6.6: T-girder transfer length measurement summary

Girder Designation	End-Side	Initial Measurements (in.)			Final Measurements (in.)		
		95% AMS	Girder End	Girder	95% AMS	Girder End	Girder
T-6-1.5h-A	N-W	21.6	25.0	23.0	22.0	25.5	23.5
	N-E	28.4			29.1		
	S-W	22.5	21.0		22.8	21.5	
	S-E	19.6			20.1		
T-6-0.5l-A	N-W	22.6	22.3	24.8	24.1	22.8	25.5
	N-E	21.9			21.5		
	S-W	26.0	27.3		26.3	28.2	
	S-E	28.5			30.1		
T-6-1.5h-B	N-W	24.3	22.6	20.5	25.4	16.0	20.9
	N-E	21.0			6.5		
	S-W	20.6	18.4		25.8	25.9	
	S-E	16.3			25.9		
T-4-1.0h-B	N-W	23.3	19.4	18.3	26.8	22.5	21.3
	N-E	15.5			18.1		
	S-W	18.3	17.1		21.1	20.2	
	S-E	15.9			19.3		
T-6-1.5h-C	N-W	20.8	19.3	19.1	N/A		
	N-E	17.8					
	S-W	19.8	18.9				
	S-E	18.0					
T-4-1.0h-C	N-W	25.9	19.6	18.8			
	N-E	13.2					
	S-W	20.5	18.0				
	S-E	15.5					

Figure 6.13 graphically presents the results from the transfer length testing on the T-girders. Again, it should be noted the relative proportion from actual specimen measurements to the length specified by AASHTO for design.
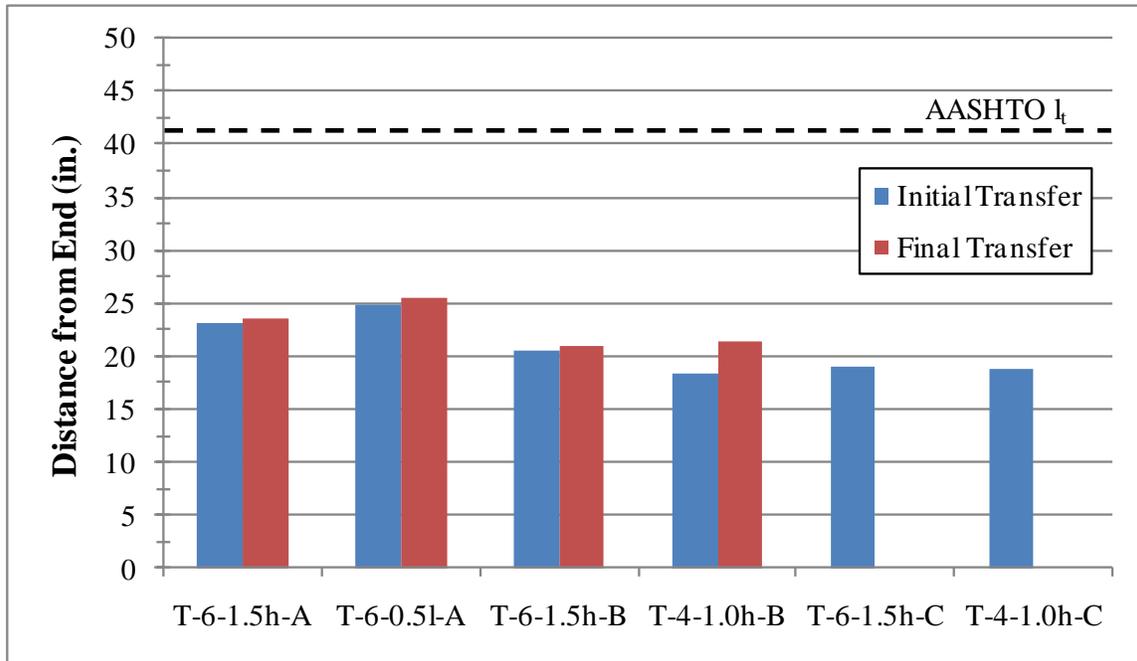
Figure 6.13: Comparing transfer length of different T-girder specimens

To compare the effect of the amount of confinement on the transfer length, results from specimens T-6-1.5h-A/B/C were compared against those of specimen T-6-0.5l-A. The results show no added benefit on prestress transfer from all the extra confinement steel, which is in agreement with the conclusions made by Russell and Burns (1996). To compare the effect of confinement reinforcement distribution, results from specimens T-6-1.5h-A/B/C were compared against those of specimen T-4-1.0h-C. Again, there was little to no effect from the distribution of the confinement reinforcement.

It should be noted that the transfer length measurements of the T-girder specimens, when compared to those of rectangular prisms, were shorter on average. This is mainly because the concrete strength at release of T-girders was significantly higher than that of rectangular prisms. Overall, the transfer length measurements for 0.7 in. diameter strands are well below the code predictions.

6.3 Development Length Testing

Development length testing was performed on the eight T-girder specimens by loading each specimen at the midspan using single point load as shown in Figure 6.14. The bottom row of strands was monitored with SP-POTs and a ST-POT as shown in Figure 6.15. Each instrument was clamped to an extended strand and connected to measure the relative movement of the strand and the girder; three SP-POTs were used for the North end, while two SP-POTs and a ST-POT were used for the South end. The instrument orientation was dictated by the instruments available. The SP-POTs reacted against a piece of aluminum attached to the face of the concrete to create a smooth surface for the arms to measure to, so the rough surface of the girder would not affect the readings. The deflection of the girder was measured directly under the load.
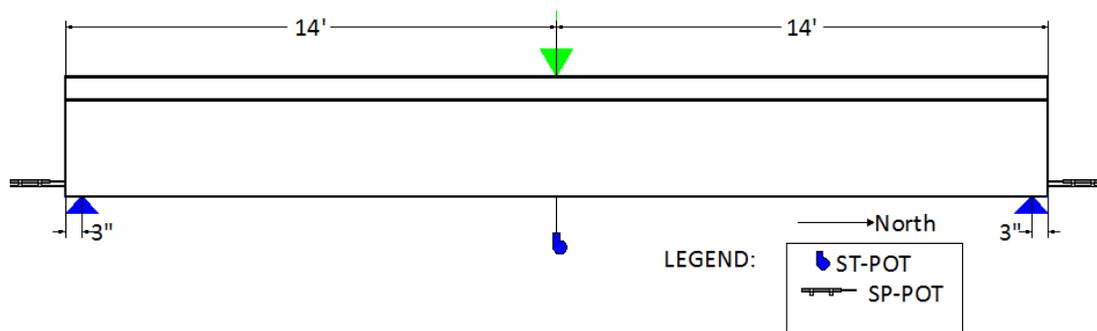
Figure 6.14: T-girder development length test setup

Figure 6.15: Bottom row of strands instrumentation using SP-POTs and ST-POTs

For the first two specimens listed in Table 6.1, development length testing was performed using one 400 kip hydraulic jack. Cracking was noticed just prior to a load of 80 kips and was marked as shown in Figure 6.16. The cracking developed as expected and was dominated by flexure shear cracking. The cracking patterns and failure modes of the North and South T-girders can be found in Figures 6.17 and 6.18, respectively. Both failures were characterized by gradual crushing of the deck until a brittle and sudden failure. The diagonal flexure shear cracks along the failure surface significantly widened, which then extended near parallel to the strands in a shear failure. The North T-girder seemed to have a slightly less violent and much more ductile failure, as evidenced by the more controlled cracking. This was likely due to the continuous confinement reinforcement in the North Tee Girder.
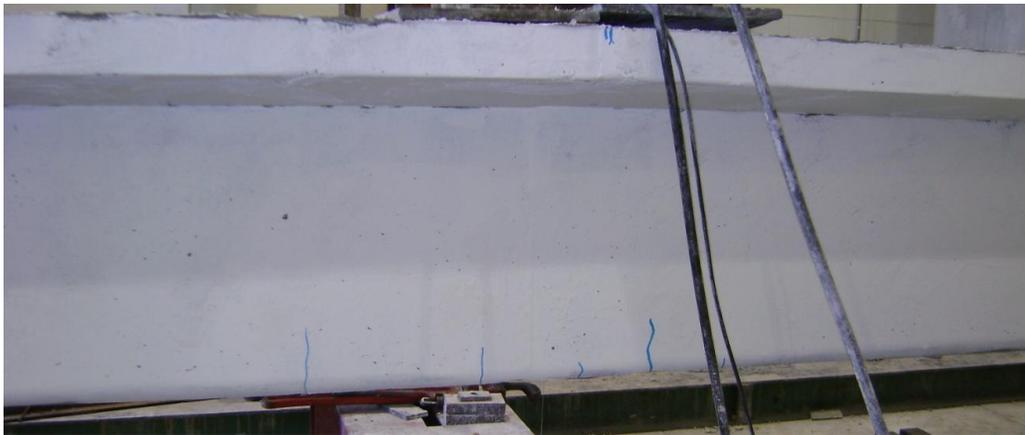
Figure 6:16: First cracking in development length testing of T-girder specimen

Figure 6.17: Failure of North T-girder specimen

Figure 6.18: Failure of South T-girder specimen
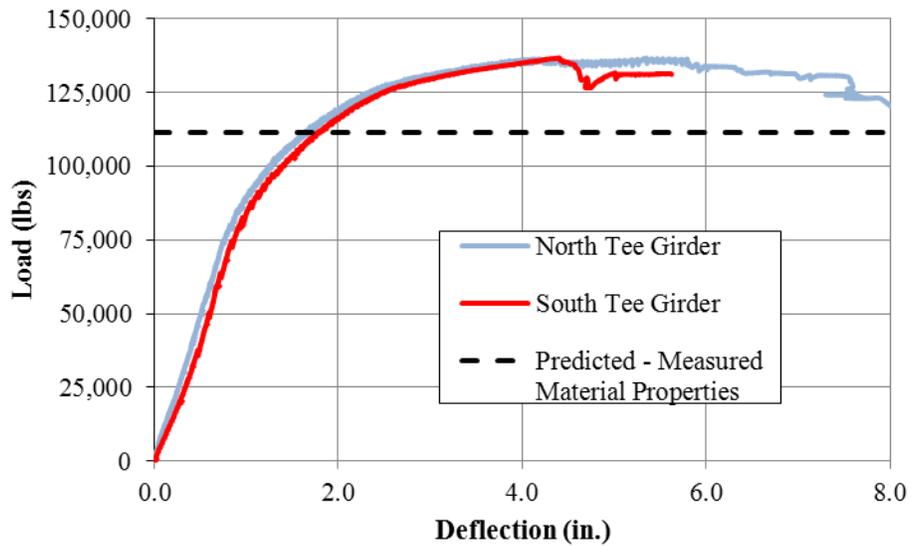
Figure 6.19: Load vs. deflection plot for the first two T-girder specimens

The load vs. deflection plot for both girders shown in Figure 6.19 indicates that both the North and the South girders exceeded predictions based on strain compatibility, which is also shown in Table 6.7. The North specimen developed significantly more deflection than the South one due to the continuous confinement reinforcement, protecting the strands, and providing the increased ductility. The continuous confinement stirrups mitigated the localized cracking near the prestressing strands close to the failure point.

Table 6.7: Predicted and observed values of development length in the first two girders

	Predicted		Observed	
	Specified Materials	Actual Materials	North Girder	South Girder
Total Moment Capacity (kip-ft)	776	798	972	972
Applied Load Capacity (kip)	108	111	137	137
Strand Strain at Ultimate (%)	2.29%	3.67%	-	-
Strand Stress at Ultimate (ksi)	266	267	-	-

The same development length testing was performed to the remaining six specimens. Table 6.8 presents the results of all eight tests, where the theoretical nominal capacity calculated using strain compatibility as well as the measured ultimate capacity are listed. These results indicate that all specimens exceeded their theoretical nominal capacities, which indicates that 0.7 in. diameter strands are fully developed in all specimens regardless of HPC strength and level of confinement.

Table 6.8: Summary of development length testing of eight T-girder specimens

Nominal Flexural Capacity [M_n]			
Girder No.	Calculated	Tested	Tested/Calculated
	(kip-ft)	(kip-ft)	(%)
T-6-1.5h-A	809	948	117.2
T-6-0.5l-A	809	948	117.2
T-6-1.5h-B	805	830	103.1
T-4-1.0h-B	805	829	103.0
T-6-1.5h-C	787	824	104.7
T-4-1.0h-C	787	879	111.7
T-12-0.5l-D	803	827	103.0
T-4/6-1/1.5h-D	803	814	101.4

Figure 6.20 provides a graphical presentation of the girders behavior while testing. The line indicating AASHTO M_n represents the required applied load, at the designated test distance which corresponds to the nominal capacity of the section incorporating the specified materials properties and with a resistance factor, φ, of 1.0. All T-girders tested met and exceeded the nominal flexural capacity for the specified materials, as well as the modified values from actual material properties.
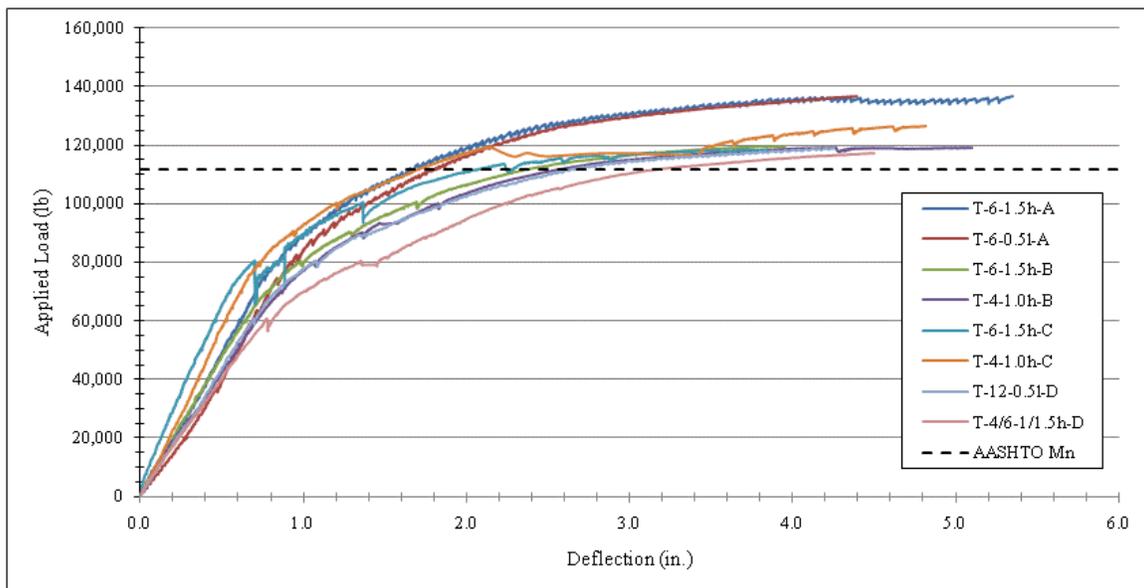

Figure 6.20: T24 Load v. Deflection Comparison

All T-girder had the same mode of failure shown earlier in Figures 6.17 and 6.18. One noticeable difference is spalling of the concrete at the bottom of the girder at mid-span. The two girders with confinement throughout the entire length, T-6-0.5l-A and T-12-0.5l-D experienced less cracking at the bottom of the web and little or no spalling of concrete upon reaching the ultimate load. It can also be seen that those two girders experienced more deflection than the other ones. This explains the added benefit of having confinement reinforcement enclosing the strands, holding the concrete, and increasing the overall ductility of the section.

While testing the T-girders, the bottom row of strands was monitored for any relative movement which would indicate a bond failure within the calculated AASHTO development length of the specimen. Figure 6.21 provides a drawing of the strand layout and designation for monitoring and reporting purposes. Figure 6.22 to 6.27 plots the data from the potentiometers during each T-girder test. The line indicating AASHTO M_n represents the required applied load at the designated test distance, which corresponds to the nominal capacity of the section incorporating the specified materials properties and with a resistance factor, φ, of 1.0. The lines at ± 0.01" represent the permitted slippage allowed by ASTM A416 to maintain the strand bond.
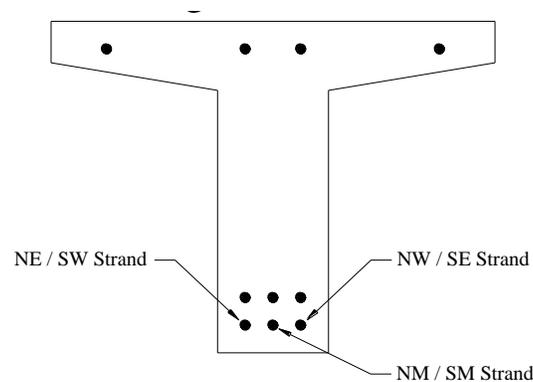
Figure 6.21: Strand designation

The lack of significant slippage in all tests indicates that the 0.7 in. diameter strands were fully developed at 2 in. by 2 in. grid spacing with an embedment length of 14 ft, in HPC T-girder specimens. Regarding the effect of amount and distribution of confinement reinforcement, the lack of strand slippage in all specimens indicates the adequacy of AASHTO LRFD minimum confinement requirements. Increasing the amount of confinement reinforcement or reducing reinforcement spacing do not increase the flexural capacity of the girder. Designing with the AASHTO specified development length and confinement reinforcement result in fully developed 0.7 in. diameter strands up to the failure load.
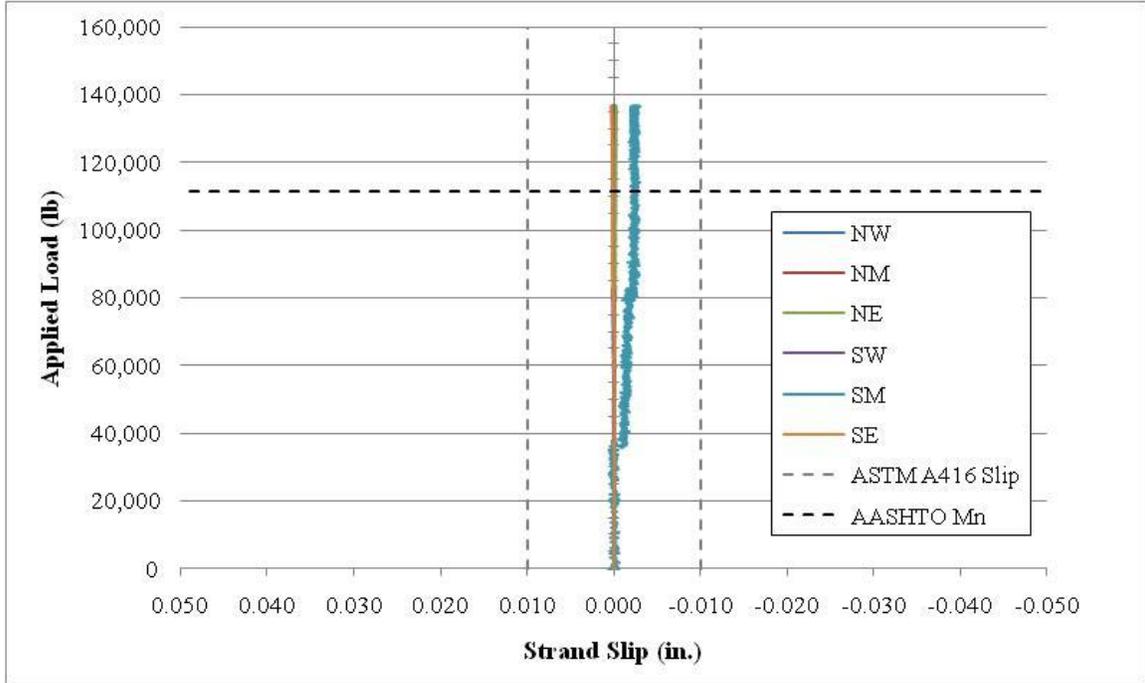
Figure 6.22: T-6-1.5h-A Development Length Test Strand Slippage
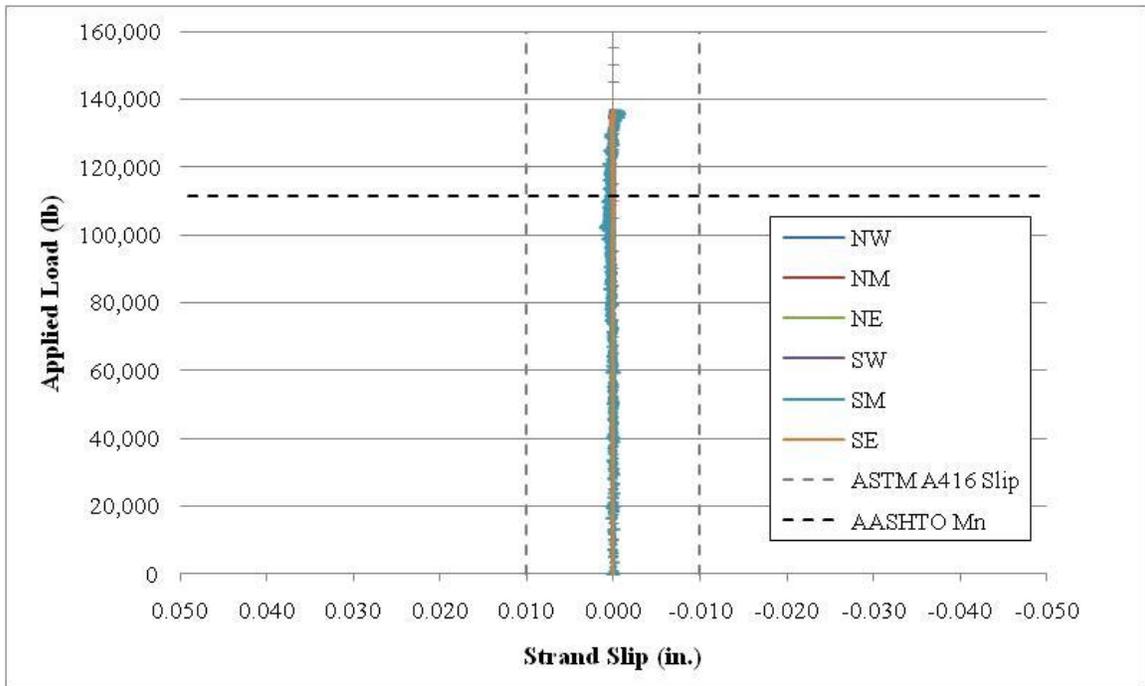

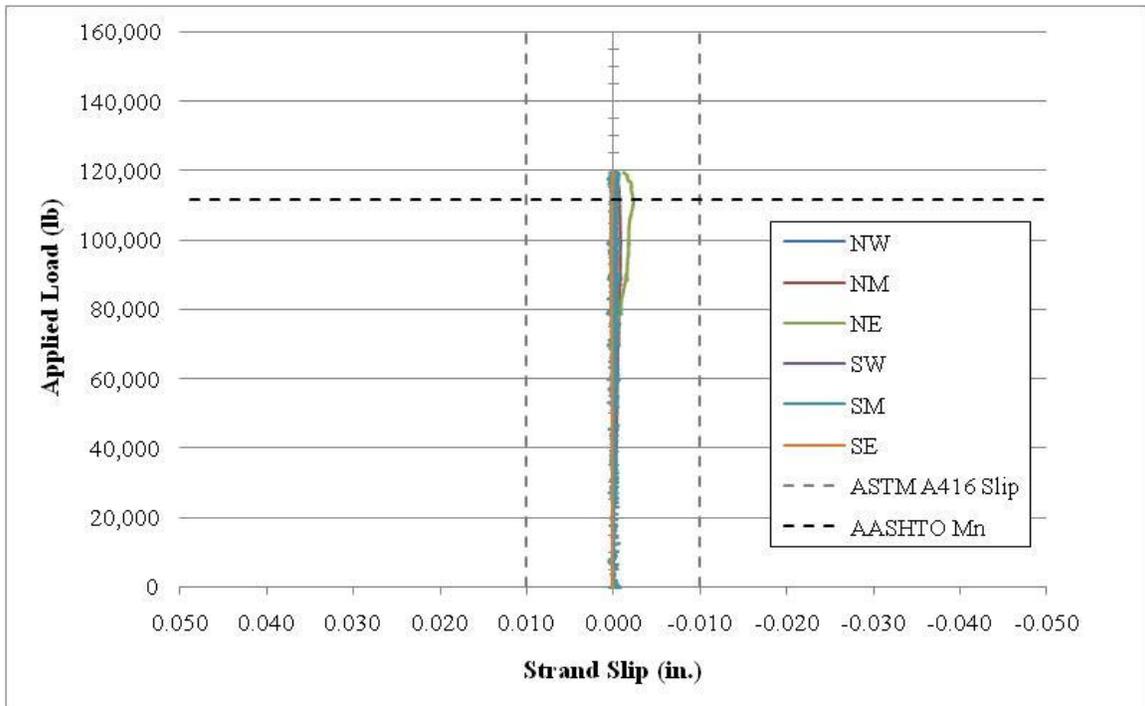Figure 6.23: T-6-0.5l-A Development Length Test Strand Slippage

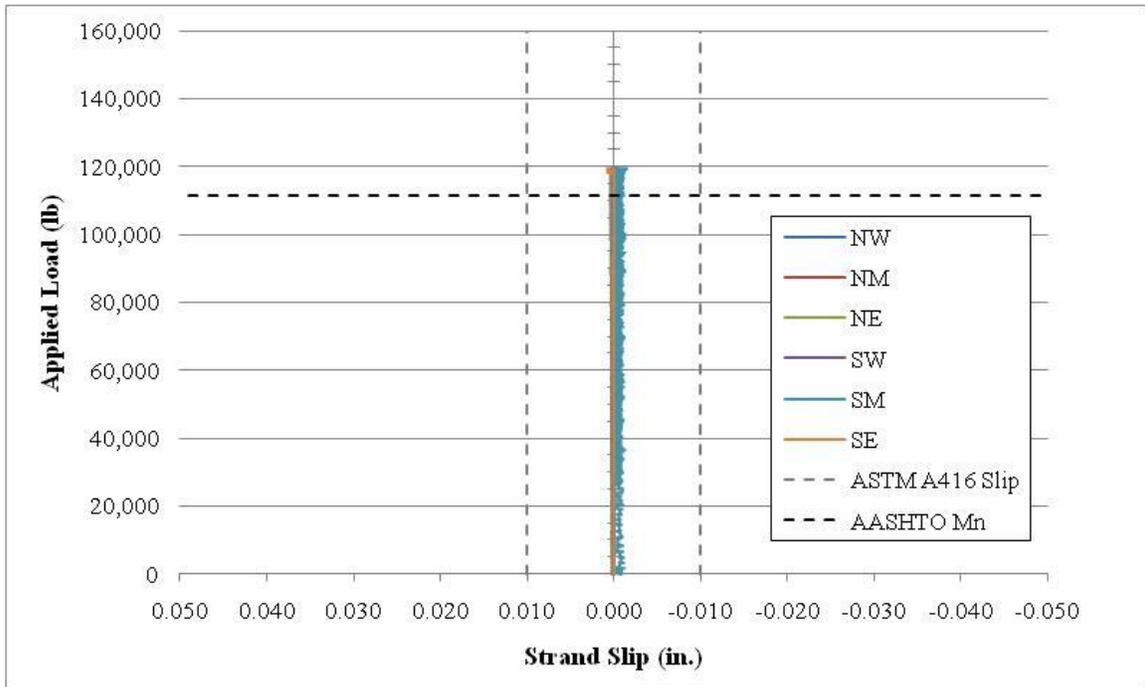Figure 6.24: T-6-1.5h-B Development Length Test Strand Slippage

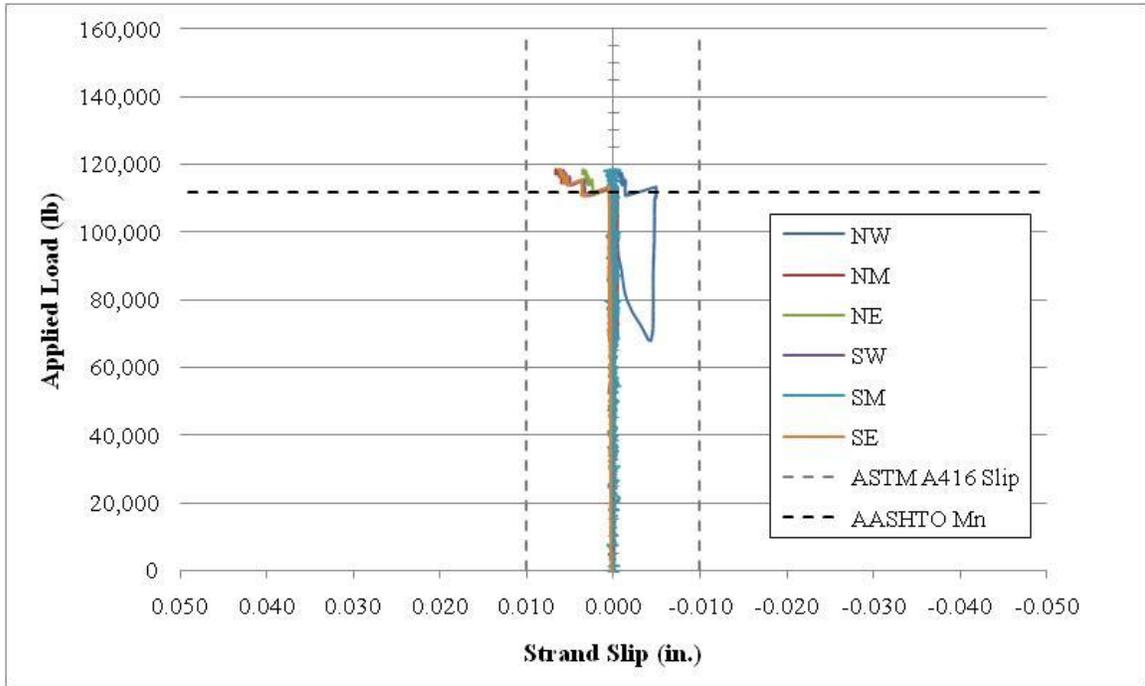Figure 6.25: T-4-1.0h-B Development Length Test Strand Slippage

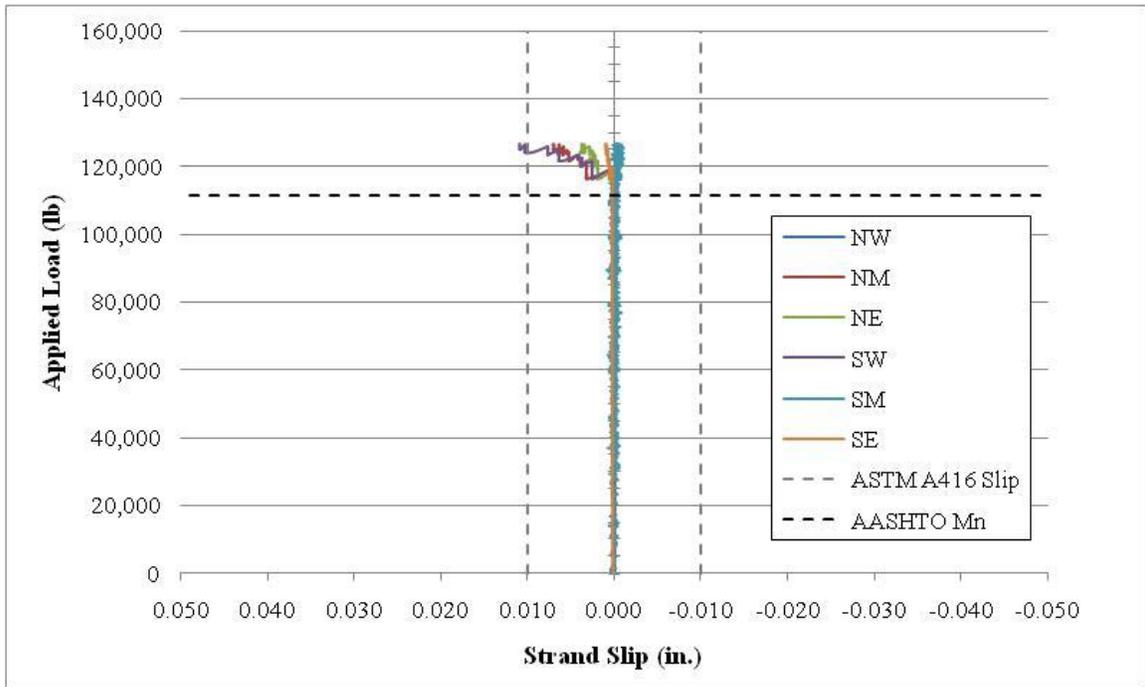Figure 6.26: T-6-1.5h-C Development Length Test Strand Slippage

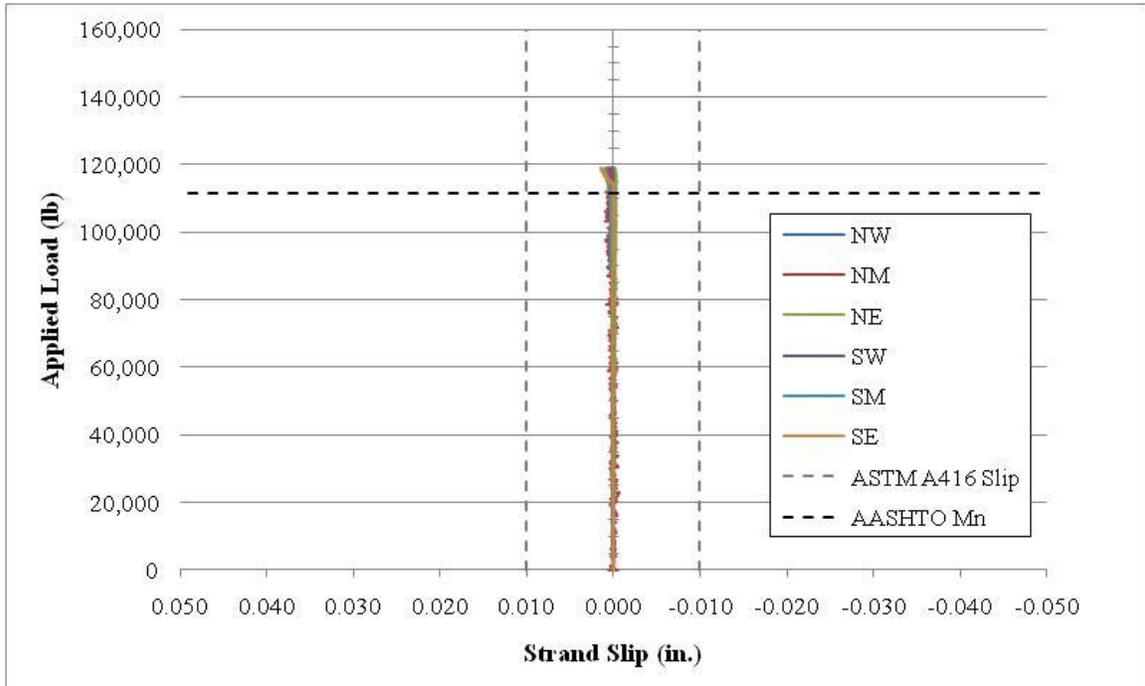Figure 6.27: T-4-1.0h-C Development Length Test Strand Slippage

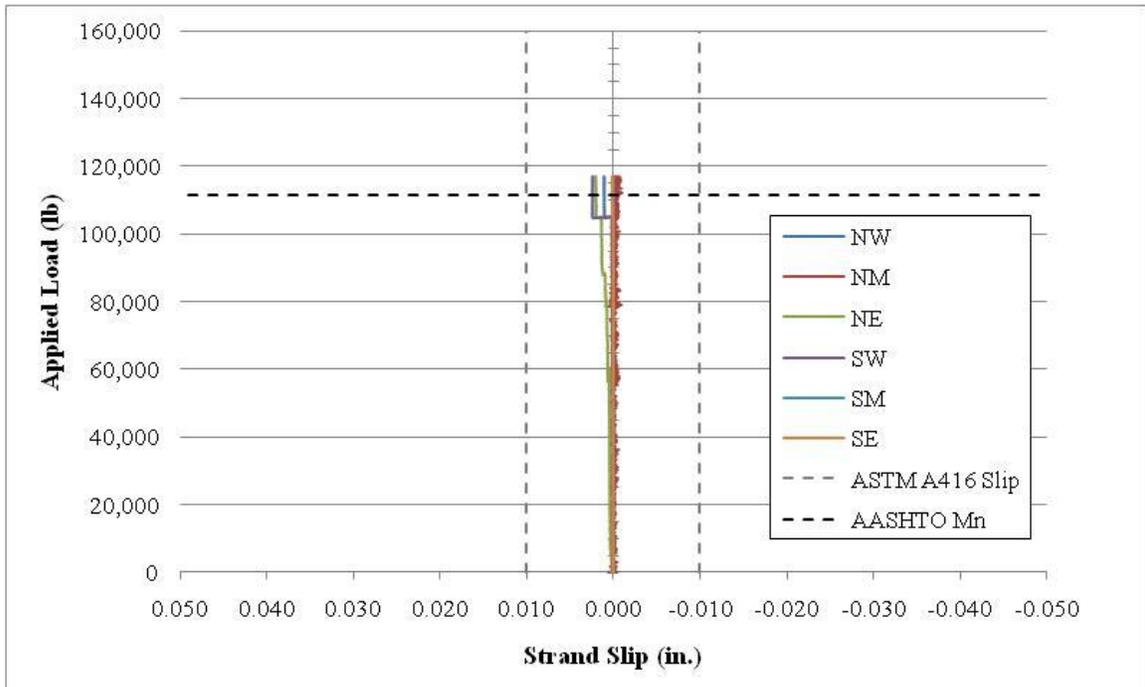Figure 6.28: T-12-0.5l-D Development Length Test Strand Slippage

Figure 6.29: T-4/6-1/1.5h-D Development Length Test Strand Slippage

6.4 Shear Capacity Testing

Four tests were performed on two of the eight T-girder specimens. The girders were loaded at a distance of 2.08h from the end support as shown in Figure 6.30. This distance, for loading, was chosen based on previous shear testing research and reporting on appropriate shear spans. (Csagoly 1991). The overall span of the girders for the shear tests was reduced to 13'-6" to perform two tests, one on each end. Also, these girders were first tested for flexure at the mid span, which resulted in a cracked zone at the mid sections. By moving the support near the mid-span of the girder, the damaged portion at the new support location would see no moment and roughly one third of the shear from the applied loading. Bottom strand slippage was monitored using three potentiometers on the tested end as shown in Figure 6.31.
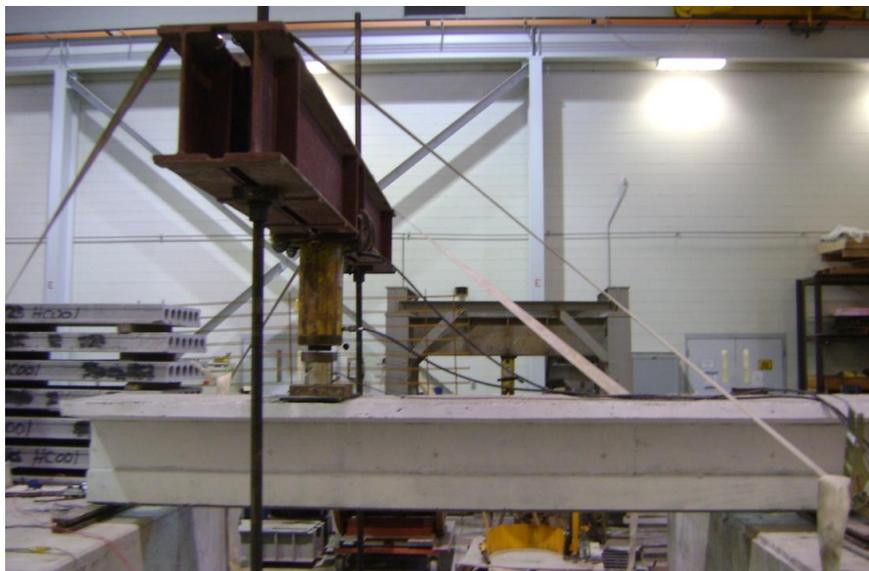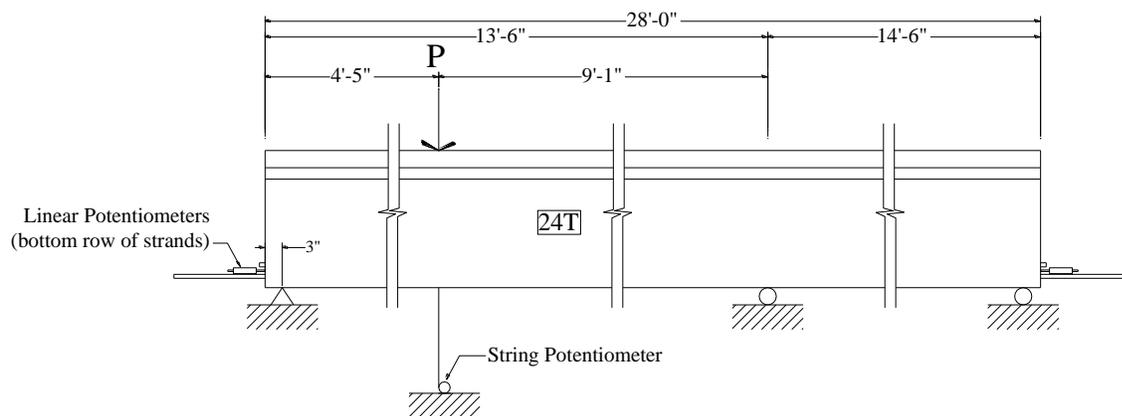

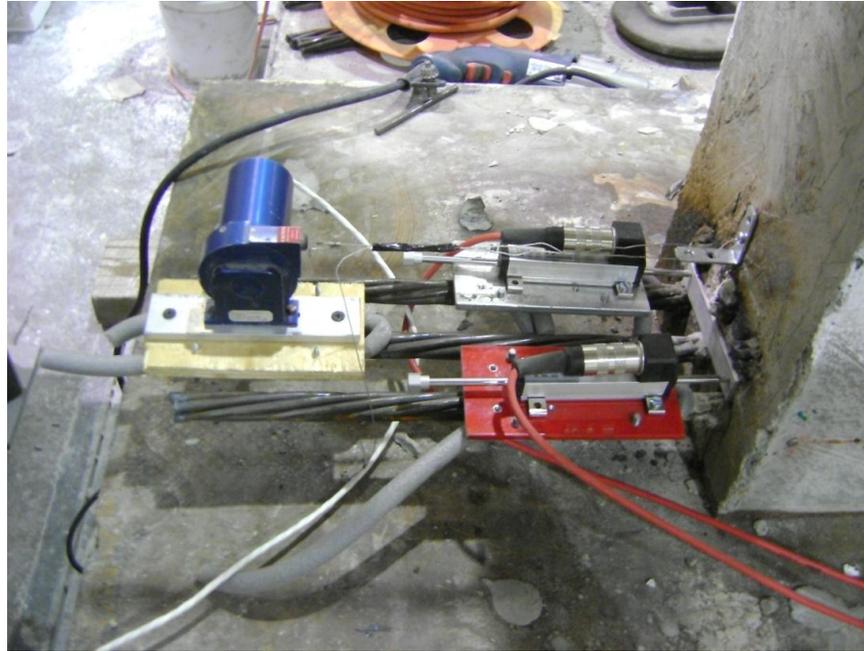Figure 6.30: T-girder vertical shear test setup

Figure 6.31: Strand instrumentation for vertical shear test

The two girders T-4/6-1/1.5h-D and T-12-0.5l-D, were tested in shear testing at both ends post their development length testing. Table 6.9 lists the test data of the four shear tests. The theoretical nominal shear capacity calculated using modified compression field theory and actual material properties as well as measured shear capacity are shown in Table 6.9. Figure 6.32 graphically presents the load-deflection relationships of the four tests. The line indicating AASHTO Vn represents the required applied load, at the designated test distance which corresponds to the nominal shear resistance of the section incorporating the actual materials properties and with a resistance factor, φ, of 1.0.

Table 6.9: Shear test results

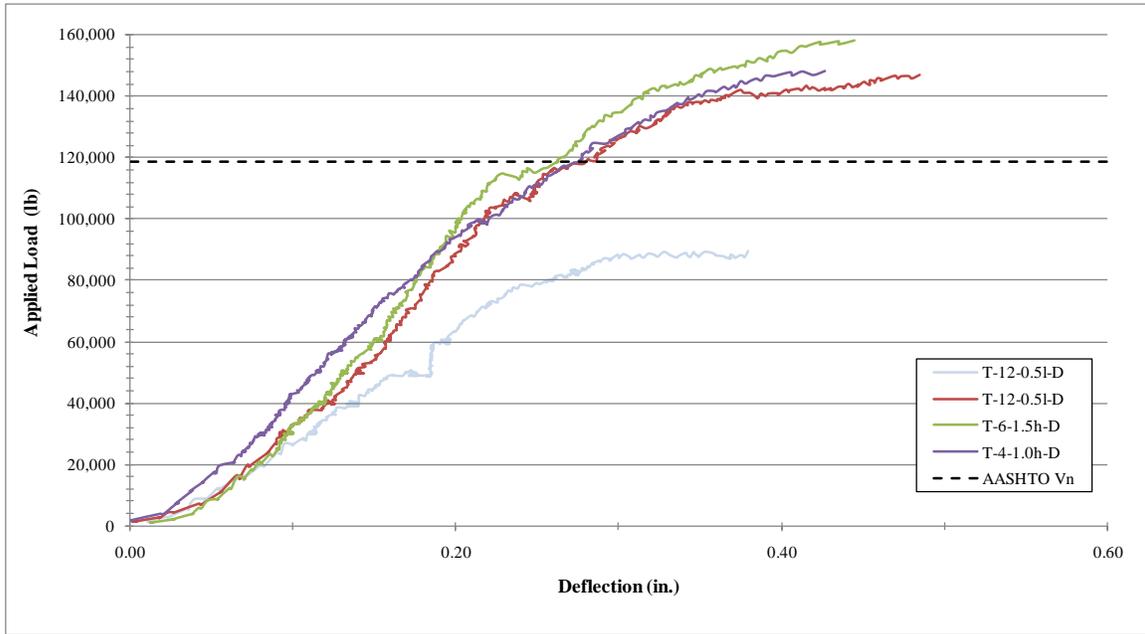| Nominal Shear Capacity [V_n]			
Girder No.	Calculated	Tested	Tested/Calculated
	(lb)	(lb)	(%)
T-6-1.5h-D	82,000	109,000	132.9
T-4-1.0h-D	82,000	102,000	124.4
T-12-0.5l-D	82,000	102,000	124.4
T-12-0.5l-D	82,000	62,000	-

Figure 6.32: Load v. deflection for all four shear tests

Figure 6.32 indicates that one result was drastically different from the other three. One end of the T-12-0.5l-D reached an actual shear capacity of 109,000 pounds, while the opposite end only obtained an ultimate capacity of 62,000 pounds. Further investigation of recorded data revealed the cause of the premature failure is the extensive cracking at the other end of the girder from development length testing, which resulted in a premature slippage of strands. For this reason, the data obtained from the low shear test will not be included in the evaluation on the shear performance of the T-girder specimens. Figure 6.33 shows the failure mode of the T-4-1.0h-D girder, which was typical for all four shear tests performed on T-girder specimens.

Figure 6.33 Shear failure mode

Figures 6.34 and 6.35 graphically present the applied load versus the average and maximum strand slippage respectively. The average slippage was calculated incorporating movement from all three bottom strands, while the maximum slippage is the greatest amount of strand movement relative to concrete during the shear testing, which took place at an outer strand in all cases.
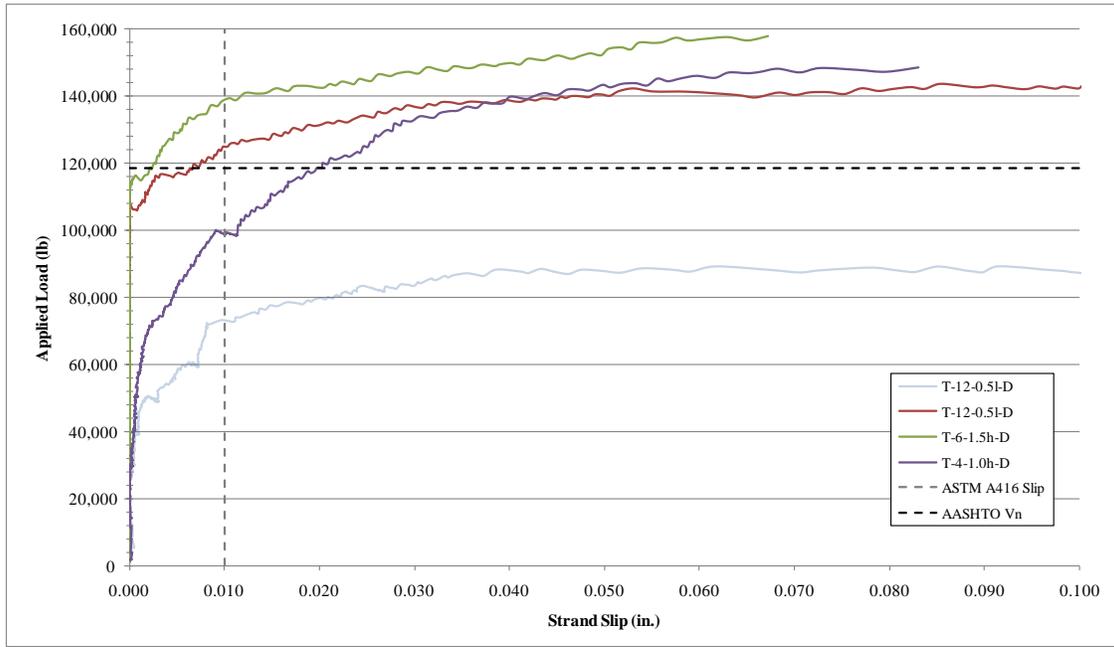

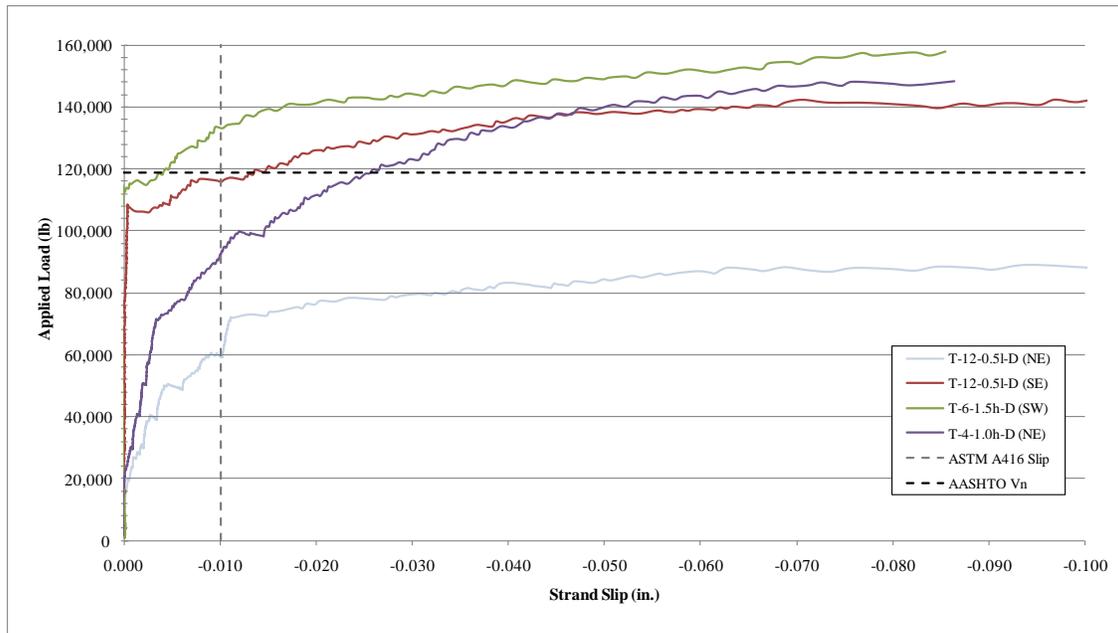Figure 6.34: Load vs. average strand slip

Figure 6.35: Load vs. maximum strand slip

In both the average strand slip case and the maximum strand slip case, the end with the confinement spaced at four inches for a distance equal to the height of the girder saw bond failure before the section reached its nominal capacity. This was not the case for either of the other two comparable cases. This may be connected to the location of the shear cracking through the transfer region of the girders' web. For the T-4-1.0h-D all of the confinement was located within the first 1.0h, twenty-four inches. The transfer length previously found on similar specimen was between twenty and twenty-five inches, and the shear cracking is clearly within the transfer region of the tested T24 girders. For this test setup, the distribution of confinement presented an effect on the bond capacity of the strands. However, even though the strands did slip on the T-4-1.0h-D section beyond the ASTM A416 limit of 0.01", the ultimate shear capacity of the section was not compromised.

In all cases, the AASHTO LRFD specified amount of confinement reinforcement, T-4/6-1/1.5h-D, and for above the minimum amount, T-12-0.5l-D, the overall capacity was shown to be around 24% above the calculated values. Something of note again with the shear test; the girder with the confinement dispersed throughout its entire length saw slightly more deflection during loading. This result was previously seen during the development length testing of the T-girders. The data seems to show that one benefit to providing confinement throughout a girders' entire length is in an increase in ductility of that member.

7 TESTING OF NU1100 GIRDERS

7.1 Overview

This chapter presents the testing of three full-scale bridge girders made of high performance concrete (HPC) and pretensioned using 0.7 in. diameter strands at 2 in. by 2 in. spacing. Since, NU I-girders are the predominant girder series used for short-medium span concrete bridges in the state of Nebraska, they were chosen for this testing. Three NU1100 were fabricated by CoreSlab Structures, Inc. (Omaha) due to the availability of the NU1100 forms to the precaster and the limitations on handling/testing of the PKI structural laboratory. Figure 7.1 shows the dimensions and section properties of NU1100 girder.

NU1100
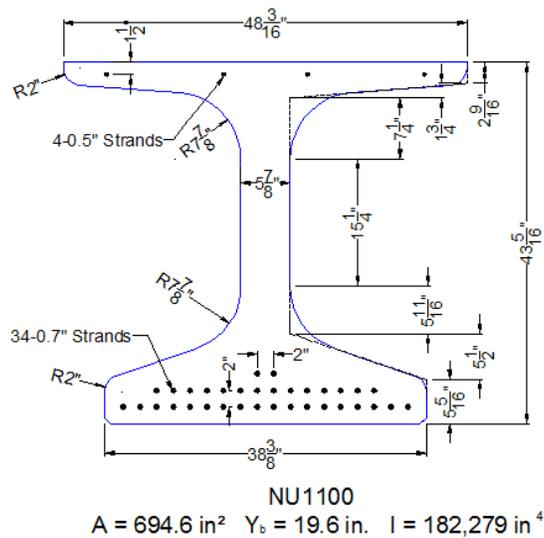A = 694.6 in² Y$_b$ = 19.6 in. I = 182,279 in⁴

Figure 7.1: Dimensions and Section Properties of NU1100

All three specimens had the same design and reinforcement detailing except for bottom flange confinement reinforcement. This is mainly to determine the required level of confinement reinforcement for 0.7 in. diameter strands to be fully developed at the AASHTO LRFD specified development length. Also, 25% of the strands were debonded from one end to evaluate the effect of debonding 0.7 in. diameter strands on the AASHTO LRFD predicted shear capacity of the girder. Each of the three specimens was tested twice: 1) a flexural test at the specified development length for 0.7 in. diameter strands (14 ft); and 2) shear test at a shear span equal to 1.75 times the girder height. Details on specimen design, fabrication and testing are discussed in the following sections.

7.2 Specimen Design and Fabrication

Specimens were designed according to AASHTO LRFD to have the flexural capacity required for constructing 120 ft long simple span bridge with 8 ft girder spacing. Such a bridge requires NU1100 girder pretensioned with thirty-four 0.7 in. diameter Grade 270 low-relaxation strands, stressed to 75% f_{pu} (59.5 kips) and distributed in three rows with eighteen in the bottom, fourteen in the middle, and two strands in the top row. Figure 7.2 shows the cross section and reinforcement details of the girders. Four 0.5 in. diameter strands were placed and fully stressed to 75% f_{pu} (30.9 kips), in the top flange of the girders to control cracking upon release of the prestress force.

For all three NU1100 specimens, one end of the girders had two groups of debonded strands as shown in Figure 7.2: 1) four strands at the bottom row were debonded up to 3.5 ft from the girder end, which is the transfer length of 0.7 in. diameter strands; and 2) four strands at the middle row were debonded up to 7 ft from the girder end, which is twice the transfer length. The girder end with debonded strands was tested for its shear capacity. This end also has ten extended strands that are bent and embedded in the end diaphragm, which is the common practice in the state of Nebraska. Each girder has a 0.5 in. by 36 in. by 18 in. bearing plate at each end with eight 0.5 in. diameter and 5 in. long steel studs welded to it. Also, four 0.75 in. diameter and 46 in. long coil rods were welded to the bearing plates and extended through the top flange into the deck to control end zone cracking. Two layers of Grade 75 welded wire mesh D20@2" were placed throughout the web with 1.125" clearance to the edge. Additional WWM reinforcing steel, Grade 75, placed in the top flange of the NU1100's consisted of D20@12" transverse and D20@6" longitudinal to reduce concrete stresses and cracking upon release.

Figure 7.3 provides the reinforcement details used by the researchers for comparing different bottom flange confinement patterns. These patterns were made up of either D4 or D11 Grade 75 mesh bent in hairpin shape, while the cap bar always consisted of a #3 Grade 60 bent bar. One detail represents the confinement specified by the 2008 NDOR BOPP, the second detail represents the confinement specified by AASHTO LRFD Section 5.10.10.2, and the third detail represents the combination of the two details.
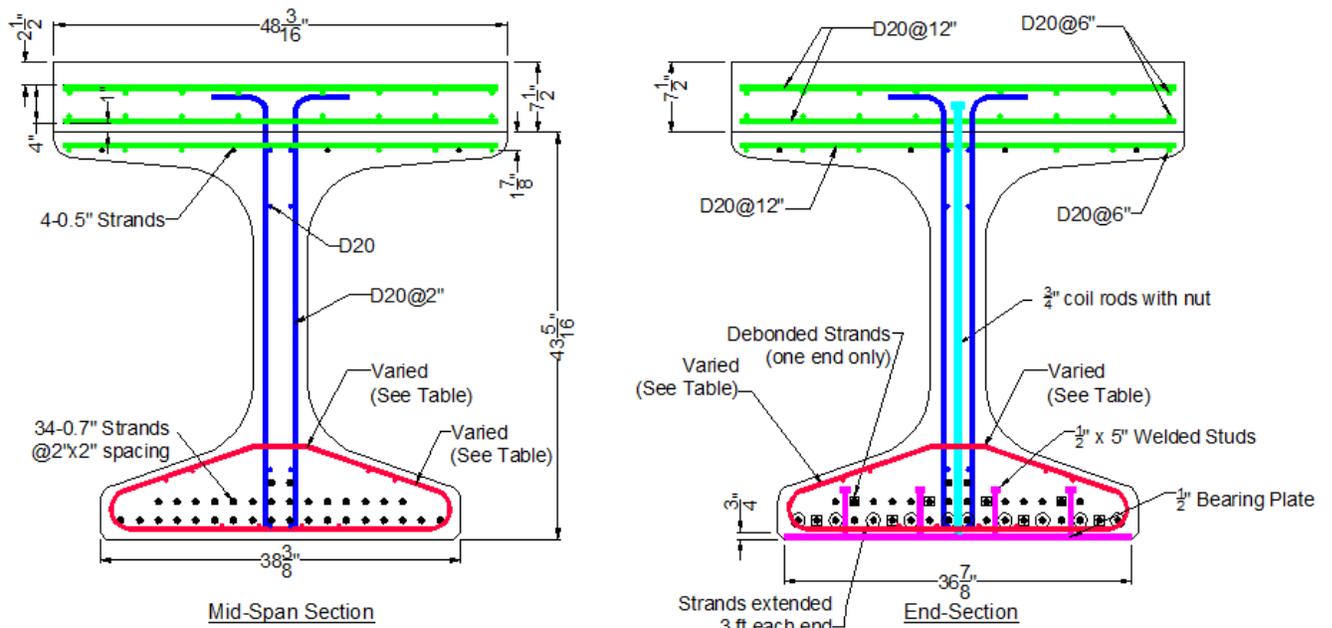
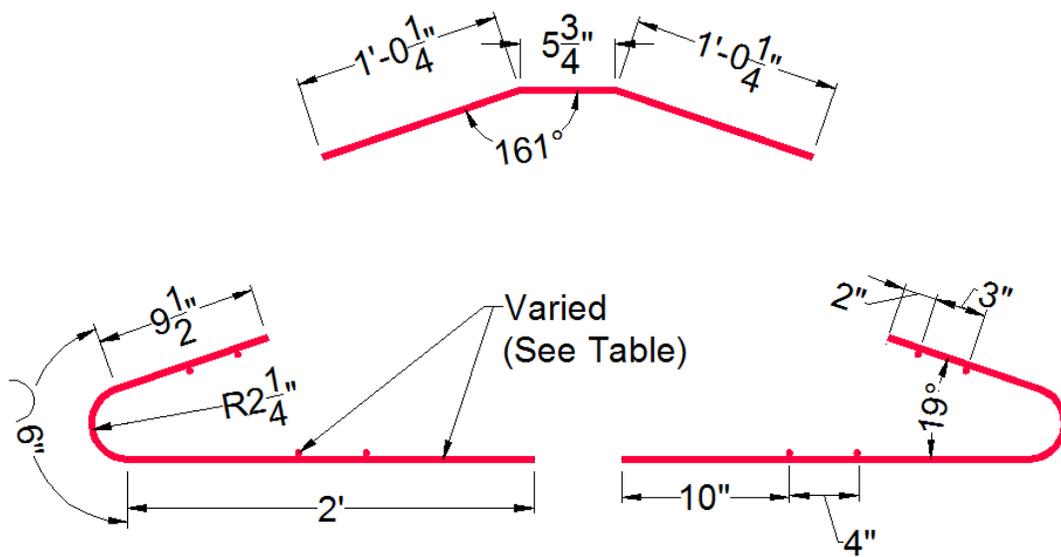Figure 7.2: Dimensions and section properties of NU1100

Figure 7.3: Detailing of confinement reinforcement

Both ends of each girder had the same confinement reinforcement detail. Table 7.1 presents the confinement reinforcement and cap bar placement specific to each girder.

Table 7.1: NU1100 confinement reinforcement details

Girder Designation	Specification	Confinement Reinforcement	
		WWM	Cap Bar
1	2008 NDOR BOPP	D4 @ 4" entire length	#3 @ 12" entire length
2	2004 AASHTO LRFD	D11 @ 6" for 72" each end	#3 @ 6" for 72" each end
3	AASHTO + NDOR	D11 @ 6" for 72" each end D4 @ 4" middle	#3 @ 6" for 72" each end #3 @ 12" middle

The concrete specified for girder design and fabrication was a SCC mix with a minimum strength at release of 8 ksi, and an f'c at twenty-eight days of 10 ksi. The design of the NU1100 specimens incorporated the addition of a concrete deck to be placed prior to any testing. The deck was designed to be 7.5" thick, the full width of the girders' top flange. The deck concrete was specified to have a final strength of 8 ksi, which was done to simulate a 7.5" deck comprised of 4 ksi concrete for a girder with eight foot spacing. Welded wire mesh was used for reinforcing the deck as two rows of D20@12" transverse and D20@6" longitudinal steel sheets were placed the length of the girder.

Three NU1100 girders topped with 7.5" of decking were fabricated at Coreslab Structures, Omaha, Nebraska. The details of the three girders were provided to the prestress company by the researchers in preparation of ordering materials and scheduling manufacture. The placement of the reinforcing steel, as well as the casting process was monitored by the research team. Figure 7.4 shows the girders after the shear and confinement reinforcement was installed, prior to placement of the side form. Figure 7.5 shows the confinement reinforcement placed for girder three, which is a combination of AASHTO requirement for the first six feet and the NDOR detail in the middle.

Figure 7.4: NU1100 shear reinforcement

Figure 7.5: NU1100 confinement reinforcement

Figure 7.6 show the pouring and finishing of the NU1100 specimens. Upon release using torch cutting, girders were removed from the precast bed, and forming for placement of the deck began. Figure 7.7 shows the deck forming and placement of the reinforcing steel. Figure 7.8 shows the placing and finishing the concrete deck on top of the NU1100 girders. Several cylinders were taken at the time of concrete placement for the girders and decking and strengths were checked at release at the plant and at the structures lab on the day of testing the each girder.

Figure 7.6: Pouring NU1100 specimens

Figure 7.7: NU1100 deck forming

Figure 7.8: NU1100 deck pouring

7.3 Flexural Testing of NU1100 Specimens

To determine the effects from confinement on the development length of 0.7 in. diameter strands in NU1100 specimens, a point load was applied to the deck at a distance of 14 ft as shown in Figures 7.9. Bearing was located 6 in. from each end resulting in an overall span of 39 ft. The loading location was chosen to satisfy current AASHTO LRFD specifications for required development length for 0.7 in. diameter strands. The applied load and corresponding vertical deflection were monitored and recorded as the load increased up to the nominal flexural capacity of the section calculated using strain compatibility. The load was stopped just above the calculated value to preserve the structural integrity of the girder for shear testing.
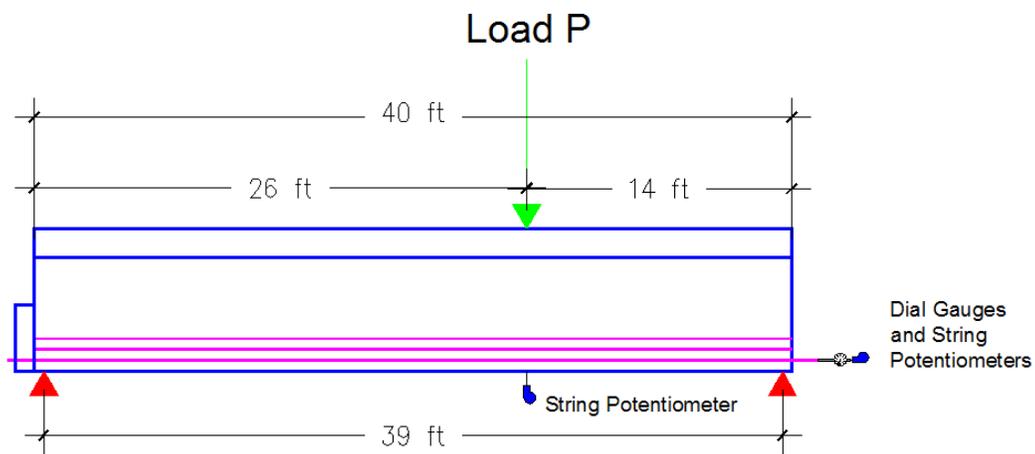

Figure 7.9: NU1100 Development length test setup

While testing, each girder was visually inspected and cracks were periodically marked to identify the failure mode. Bottom strand slippage was monitored using ten potentiometers as shown in Figure 7.10, while the two top strands were monitored via a mechanical gauge and a string potentiometer.

Figure 7.10: Strand instrumentation for development length test

Figure 7.11 plots the load-deflection relationships of the three specimens in testing the development length of 0.7 in. diameter strands. The line named nominal capacity represents M_n calculated using strain compatibility with actual material properties and a resistance factor, φ, of 1.0. Figure 7.11 indicates that the behavior of the three specimens were almost identical, which means that changing the amount and/or distribution of confinement reinforcement along the development length does not affect the flexural capacity of the girder as all the strands were fully developed. For example, girder 1 has 50% less confinement reinforcement than girder 2 over a distance equal to 1.5h, but it has more total confinement reinforcement over the development length. Testing showed that both girders had the same flexural capacity and ductility. Also, no significant impact was found on the strands bond as a result from decreasing the intensity of confinement over the initial 1.5h of the girder end.
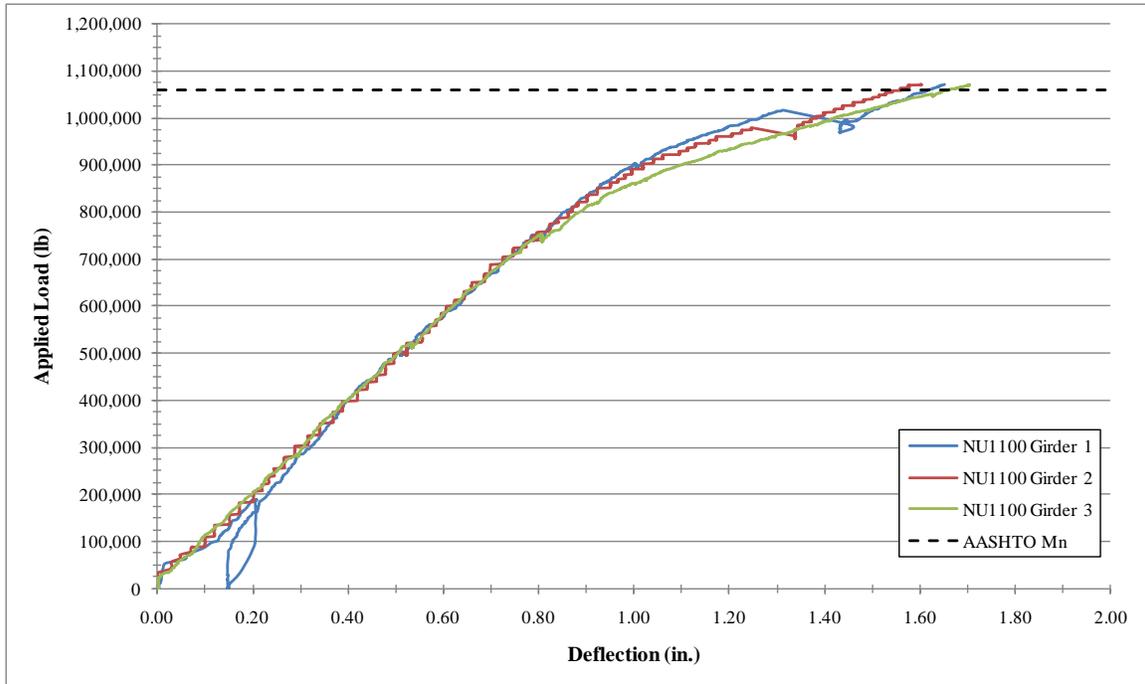
Figure 7.11: Load vs. deflection of NU1100 specimens in development length testing

Figure 7.12 shows NU1100 girder 2 after development length testing. The resulting cracks and pattern shown was typical for all three specimens. The cracks marked in black occurred before or at 500 kips, cracks marked in red occurred at a load of 750 kips, and the cracks marked in green occurred at a load of 1,070 kips.
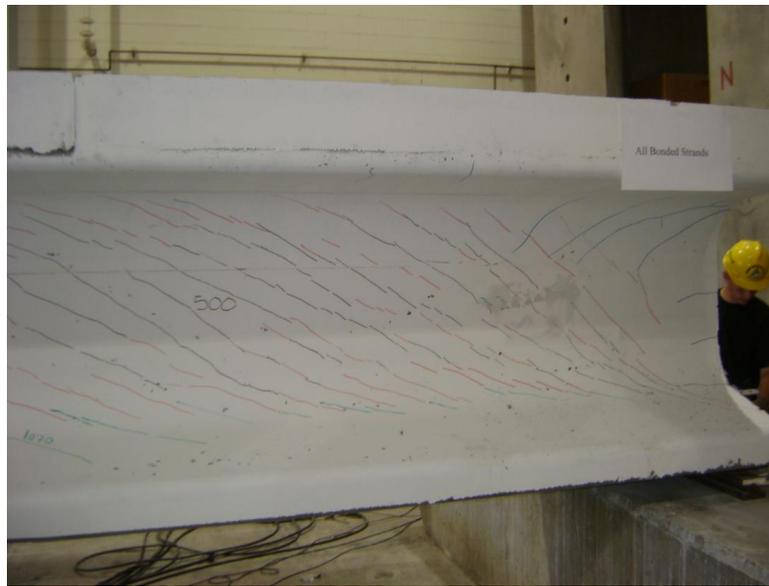

Figure 7.12: Crack pattern of NU1100 specimens after development length testing

175

While testing the NU1100 specimens in flexure, ten strands in the bottom row as well as the top two strands were monitored for any relative movement, which would indicate a bond failure within the calculated AASHTO development length of the specimen. Figure 7.13 shows strand layout and designation for monitoring and reporting purposes. Figures 7.14, 7.15, and 7.16 present the data from the potentiometers during each girders test. Again the line indicating AASHTO M_n represents the required applied load, at the designated test distance which corresponds to the nominal capacity of the section incorporating the specified materials properties and with a resistance factor, φ, of 1.0. Also the lines at -0.01"on these figures represent the permitted slippage allowed by ASTM A416 with regard to maintaining bond between the strand and the surrounding concrete. Monitoring of the two top strands during the development tests was done with both a mechanical gauge and a rotary potentiometer. In none of the three tests, for either of the top strands, was any significant slippage detected by either means of observation and documentation.
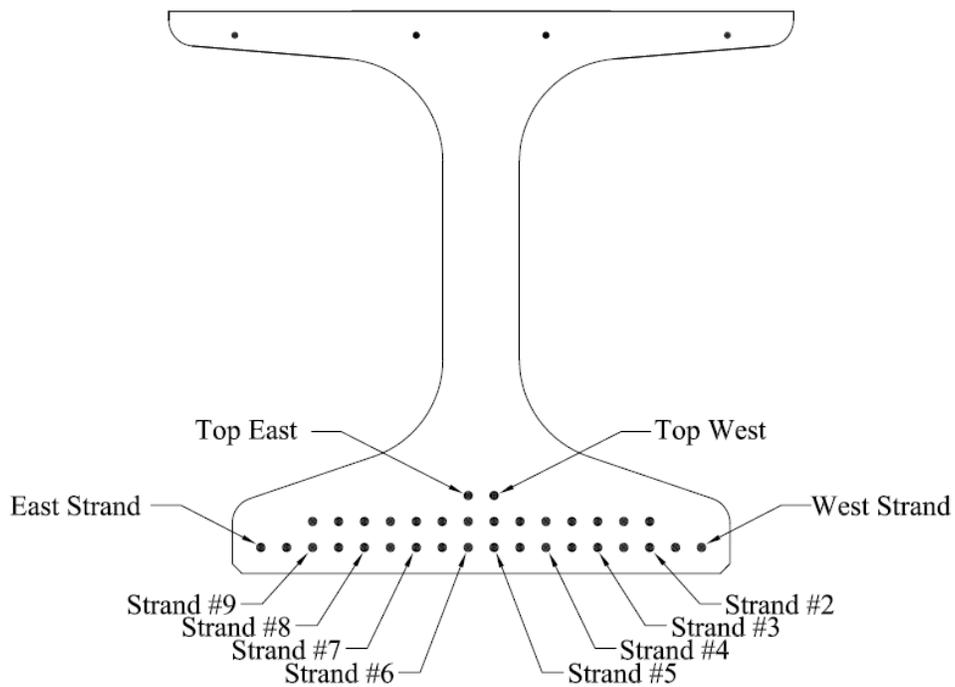

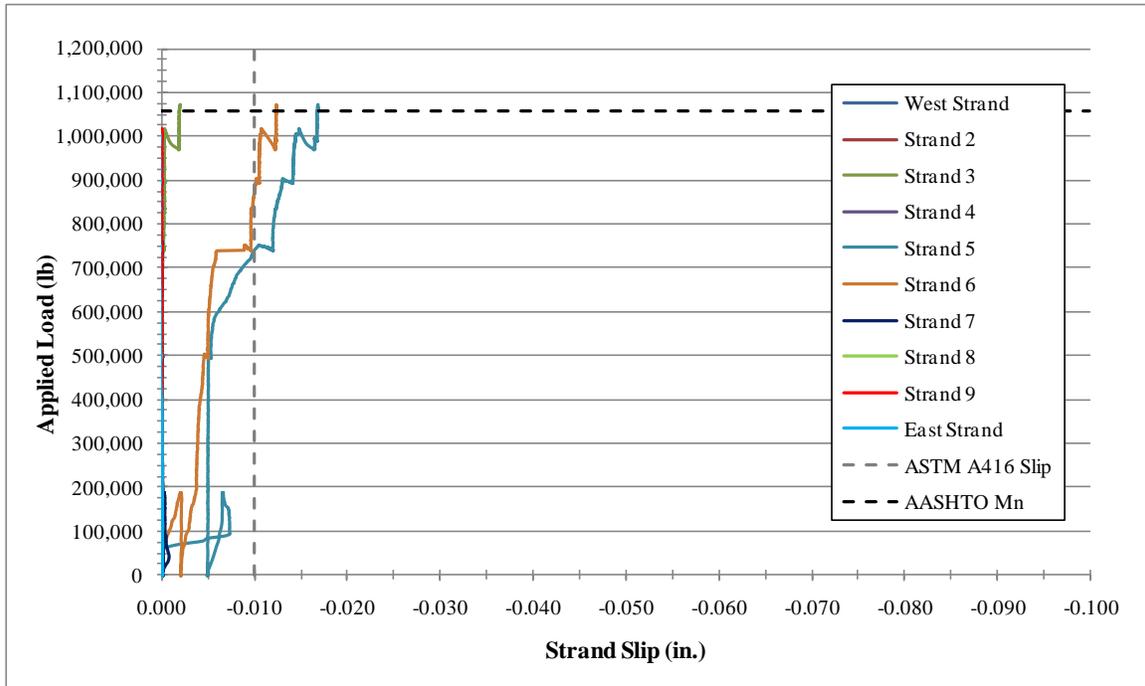
Figure 7.13: Strand designation
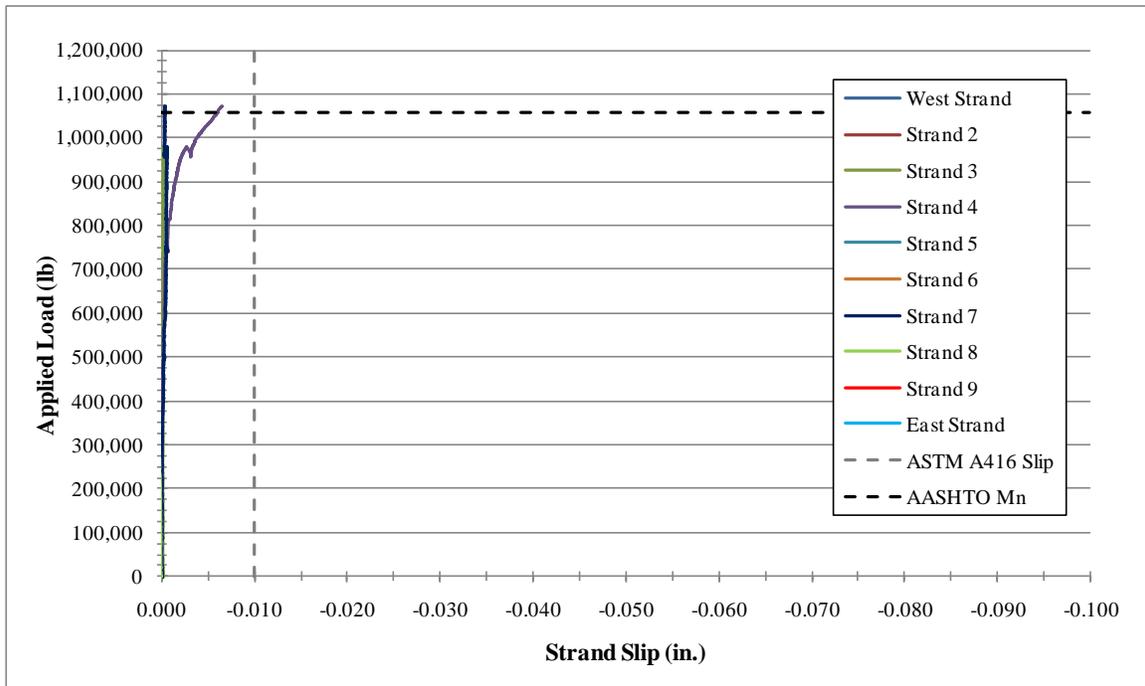
176

Figure 7.14: Strand slip in NU1100 girder 1

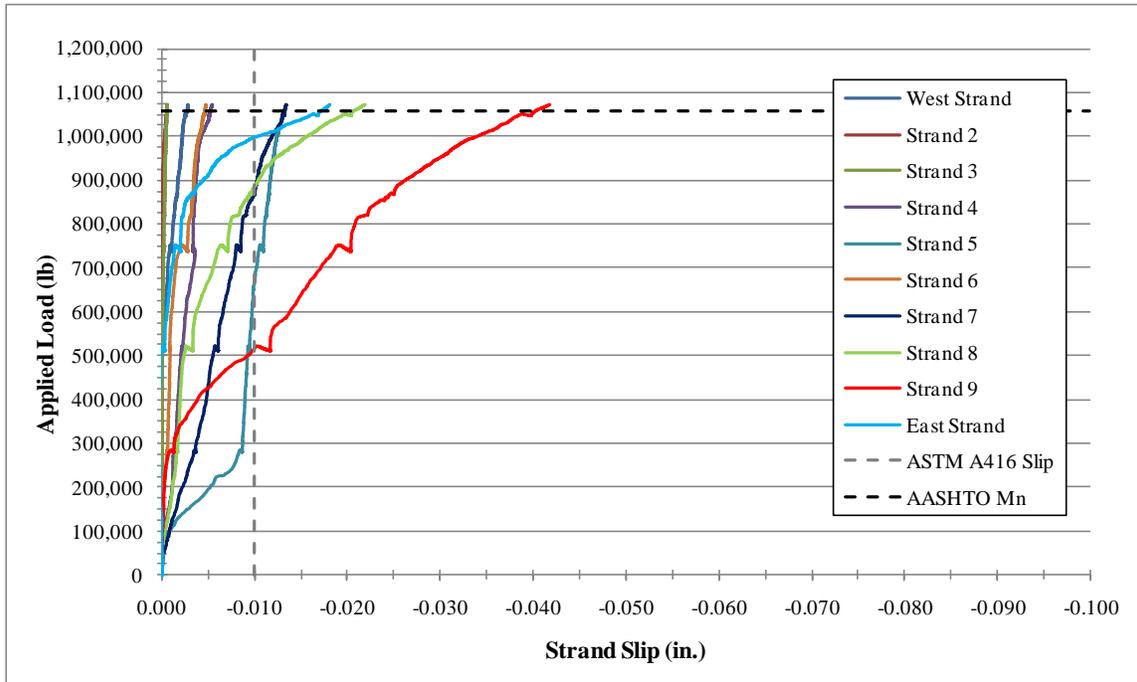Figure 7.15: Strand slip in NU1100 girder 2

Figure 7.16: Strand slip in NU1100 girder 3

The first NU1100 girder tested for development was Girder 3. Although the girder reached its nominal capacity, when the strand slippage data was analyzed it was found that half of the monitored bottom strands had enough reduction of their bond capacity to cause defined slippage. One strand in particular, Strand 9, lost bond at only around one third of its estimated capacity and had a total movement of over 0.040" during the development test. Figure 7.17 presents what was deemed the cause of the early failure for multiple strands. While testing, the bearing width at the tested end of the girder was only three inches. That condition caused a stress concentration at the bearing location, inducing cracks through the bottom flange of the girder in the transfer zone of the prestressed strands. This detail was changed prior to development tests on Girders 1 and 2 as a twelve inch by thirty inch plate was placed above the roller to increase the overall bearing area, better representing actual conditions experienced by bridge girders in the field.

178

Figure 7.17: The bearing plate used in NU1100 Girder 3 during the development length testing

Figure 7.18 plots the applied load versus the maximum strand slippage for each development length test. For girder 1, strand 5 experienced the most slippage; for girder 2, it was strand 4; and for girder 3, it was strand 9.
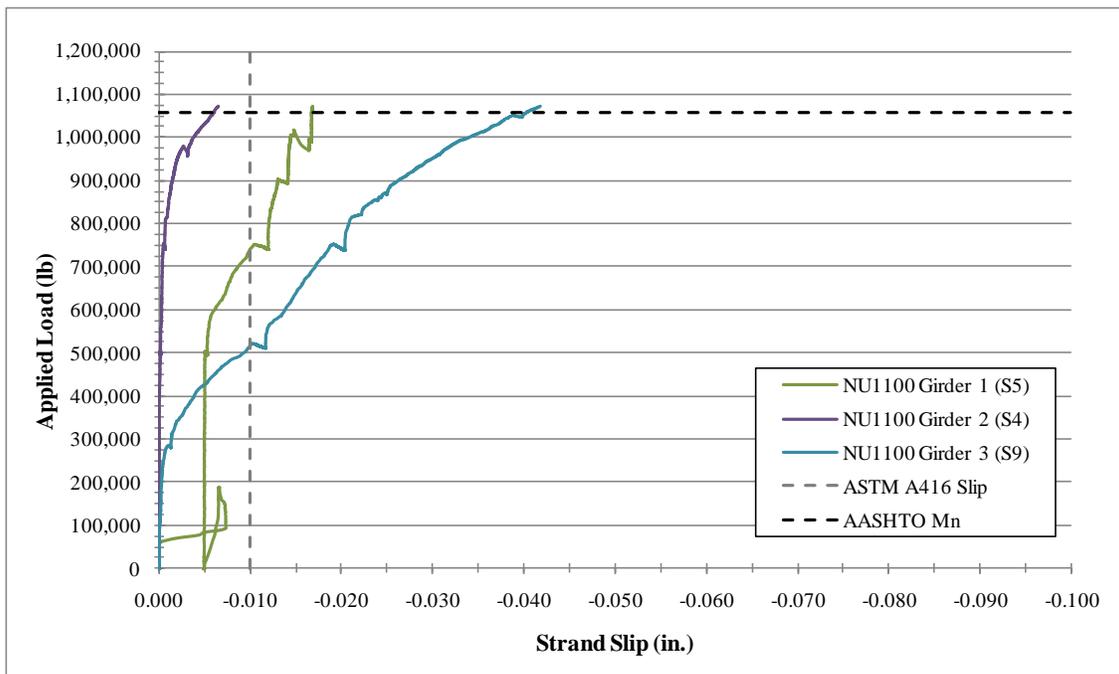

Figure 7.18: Load vs. maximum strand slip for the three NU1100 specimens

7.4 Shear Testing of NU1100 Specimens

Shear testing was performed on the other end of each of the three NU1100 girder specimens. Girders were loaded at a distance of 1.77h from the support, 8 ft from the end of the girder that has debonded strands as shown in Figure 7.19. The overall span for the test was 24 ft with each end bearing located 6 in. from the end of the girder. Figure 7.19 also shows the shear testing setup adopted in the three NU1100 girder specimens.
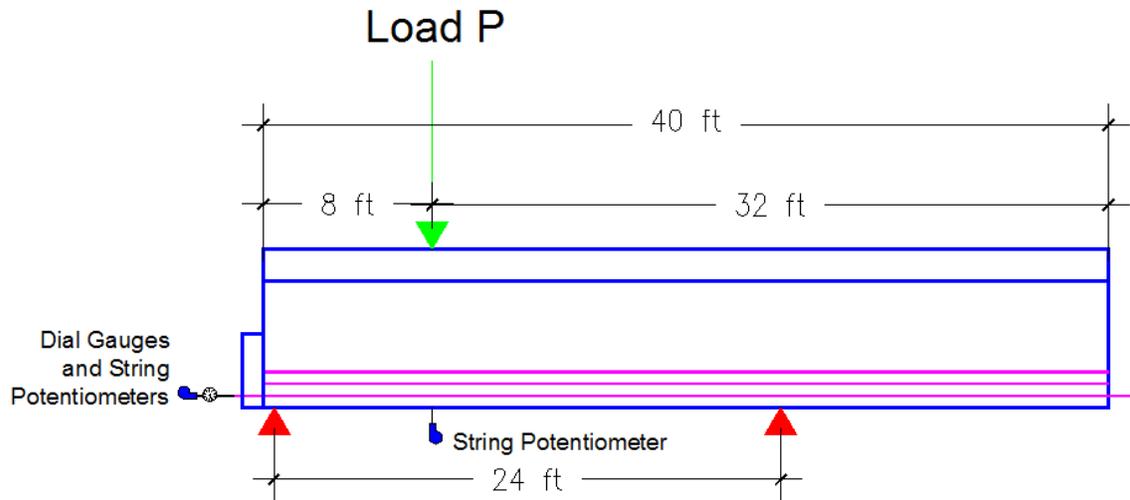

Figure 7.19: Shear test setup for NU1100 specimens

While testing, each girder was visually inspected and cracks were periodically marked to identify the failure mode. Bottom strand slippage was monitored using ten potentiometers as shown in Figure 7.20 while the two top strands were monitored via a mechanical gauge and a string potentiometer.
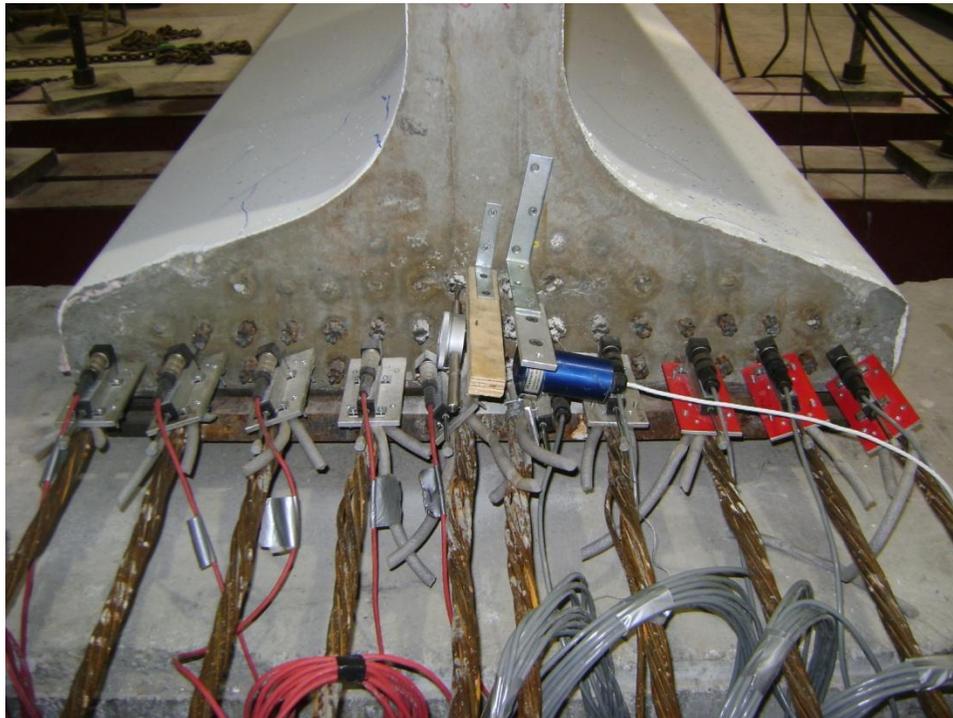
Figure 7.20: Strand instrumentation for shear testing

Figure 7.21 plots the load-deflection relationships of the three specimens tested up to failure. The dashed line represents the nominal shear capacity predicted according to AASHTO LRFD Section 5.8.3.4.2 and using actual material properties. This figure indicates that all the specimens regardless of their level and pattern of confinement had a shear capacity that is at least 16% more than the predicted value. Table 7.2 compares the theoretical and measured shear capacity of the three tested NU1100.

Figure 7.21: Load vs. deflection of NU1100 shear testing
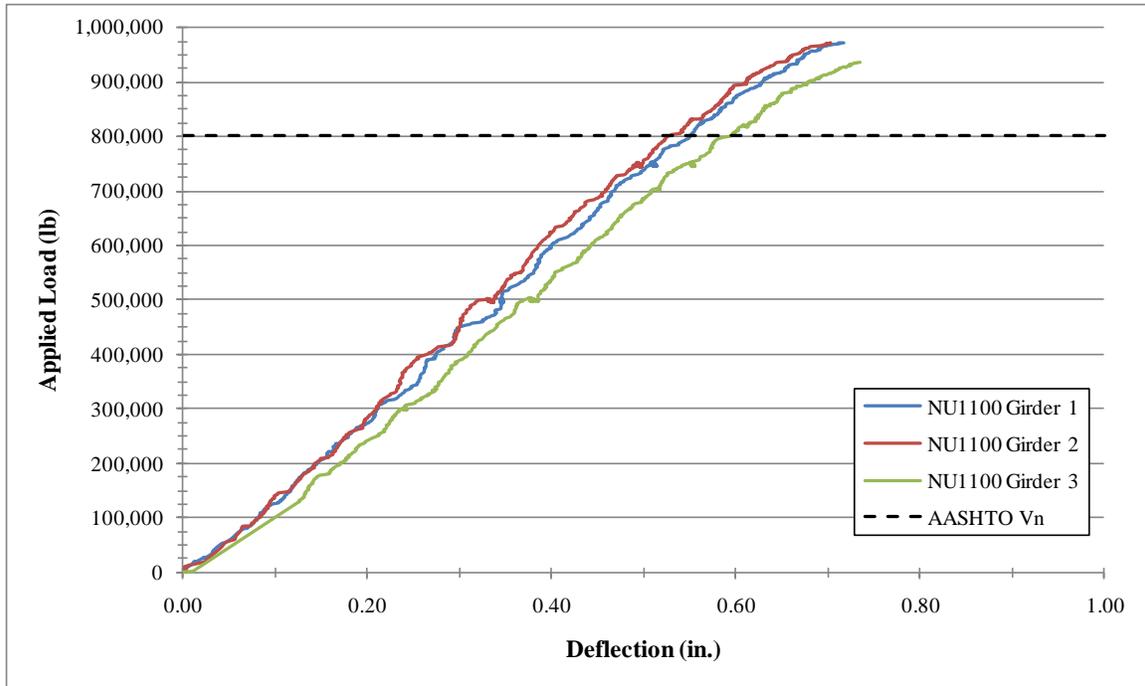
Table 7.2: Summary of shear testing results

Girder No.	Nominal Shear Capacity [V_n]		
	Calculated	Tested	Tested/Calculated
	(lb)	(lb)	(%)
1	659,000	795,000	120.6
2	659,000	796,000	120.8
3	659,000	766,000	116.2

Figure 7.22 shows an image of girder 2 after completion of the shear test. The failure mode shown was typical for all three shear tests performed at the structures lab. While testing the NU1100 girders' shear capacity, ten strands in the bottom row as well as the top two strands were monitored for any relative movement which would indicate a bond failure within the calculated AASHTO development length of the specimen. Figure 7.23 shows the strand layout and designation for monitoring and reporting purposes.
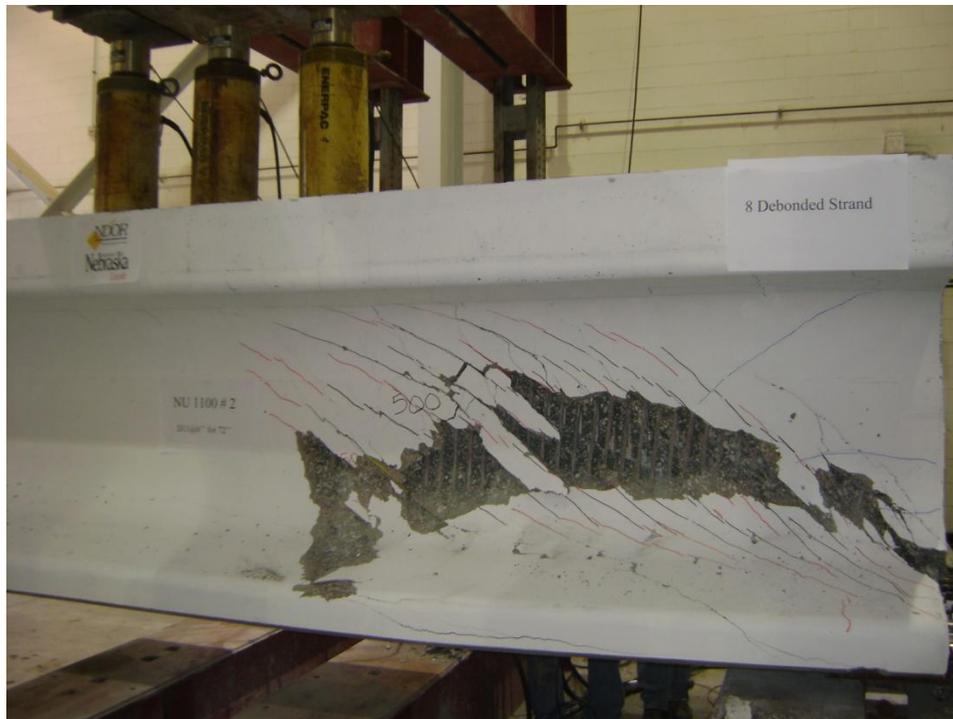
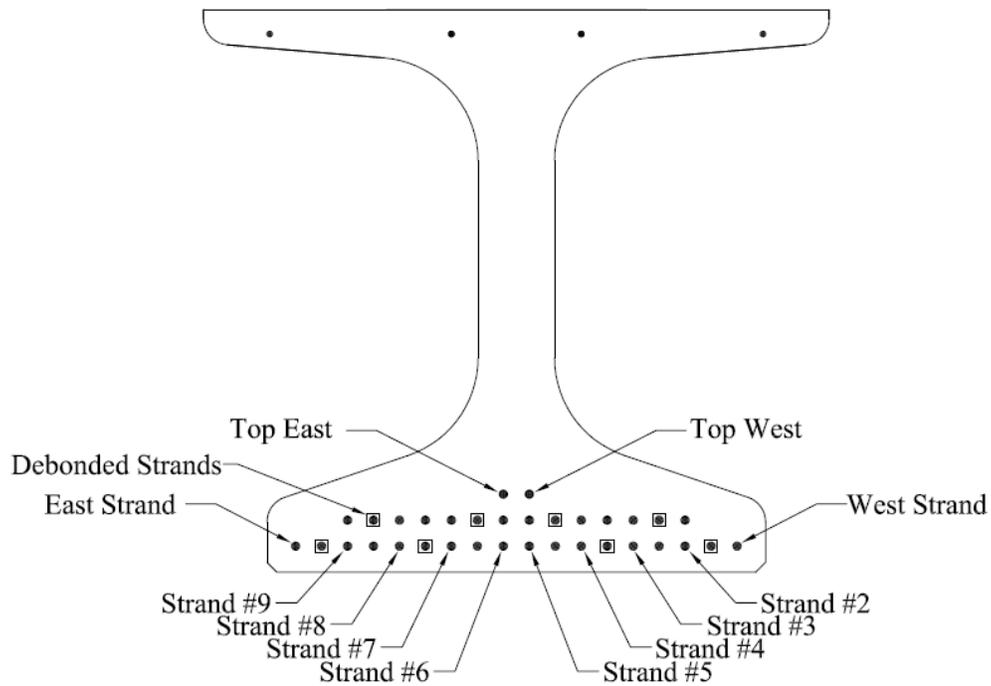Figure 7.22: Shear failure of NU1100 girder 2

Figure 7.23: Strand designation of the NU1100 shear testing

Figures 7.24, 7.25, and 7.26 present the data from the potentiometers during each girder's test. Again the line indicating AASHTO V_n represents the required applied load, at the designated test distance which corresponds to the nominal capacity of the section incorporating the actual materials properties and with a resistance factor, φ, of 1.0. Also, the lines at -0.01"on the these figures represent the permitted slippage allowed by ASTM A416 with regard to maintaining bond between the strand and the surrounding concrete. In all three NU1100 specimens, strand #4 experienced the highest slippage in all bonded strands, while none of the top strands experienced any slippage. Figure 7.24 indicates that Girder 1, with a reduced amount of confinement at the girder end, had premature slippage greater than 0.25 mm (0.01") before reaching the nominal capacity. Girder 1 also had more slipped strands than the other two specimens with higher levels of conferment. This indicates that despite exceeding the predicted nominal shear capacity in all three specimens, the level of confinement at the girder end had an impact on the bond capacity of prestressing strand under shear loading conditions.
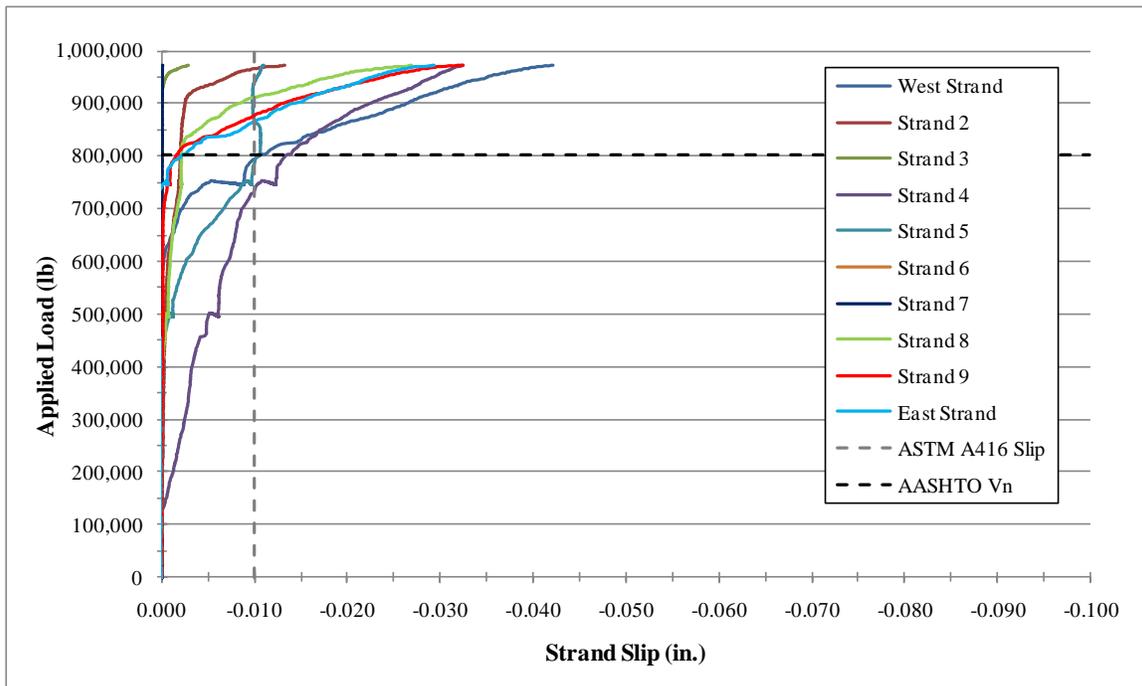
Figure 7.24: NU1100 girder 1 strand slip
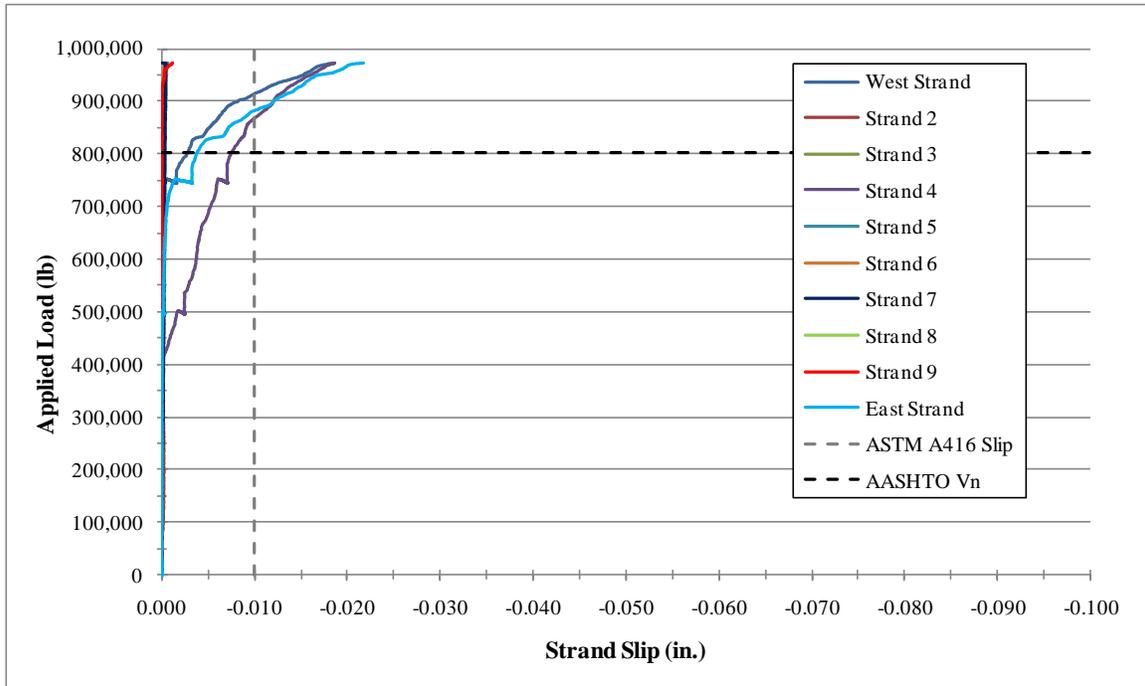
Figure 7.25: NU1100 Girder 2 strand slip
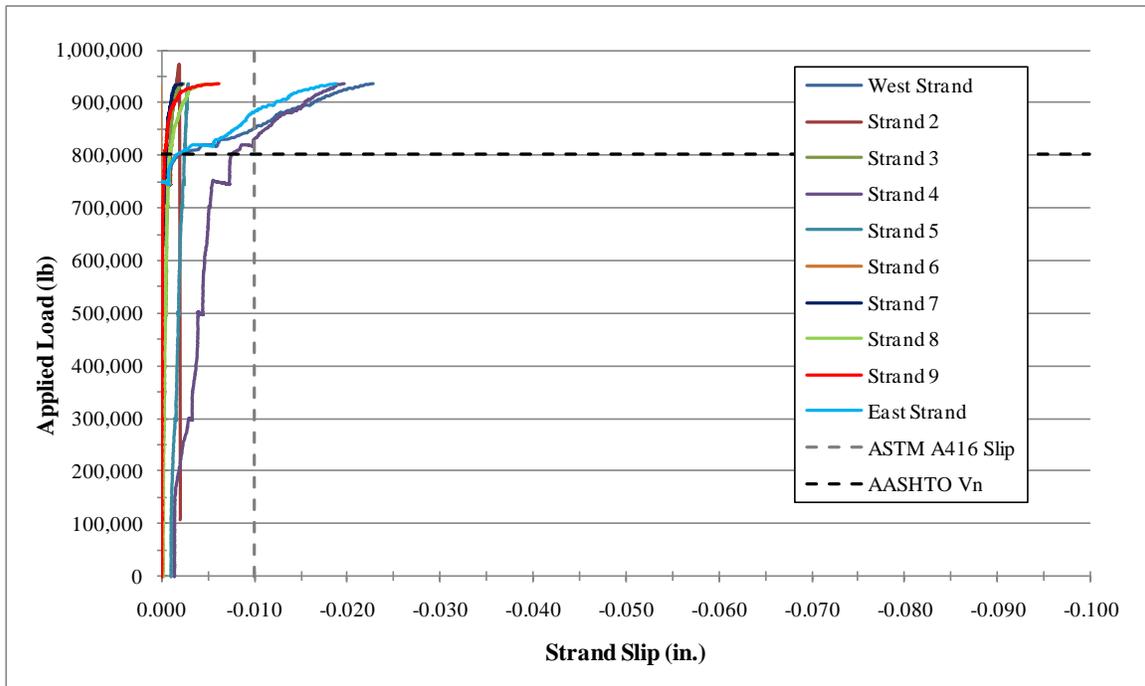
Figure 7.26: NU1100 Girder 3 strand slip

Figure 7.27 provides the applied load versus the maximum strand slippage for each shear test. The maximum strand slippage plot is of the one strand which saw the greatest amount of relative movement throughout the shear testing. For all three NU1100 girders Strand 4 experienced the most relative movement during testing but only Girder 1 had any strands which reached the ASTM defined level of slippage prior to meeting the nominal shear resistance of the section.
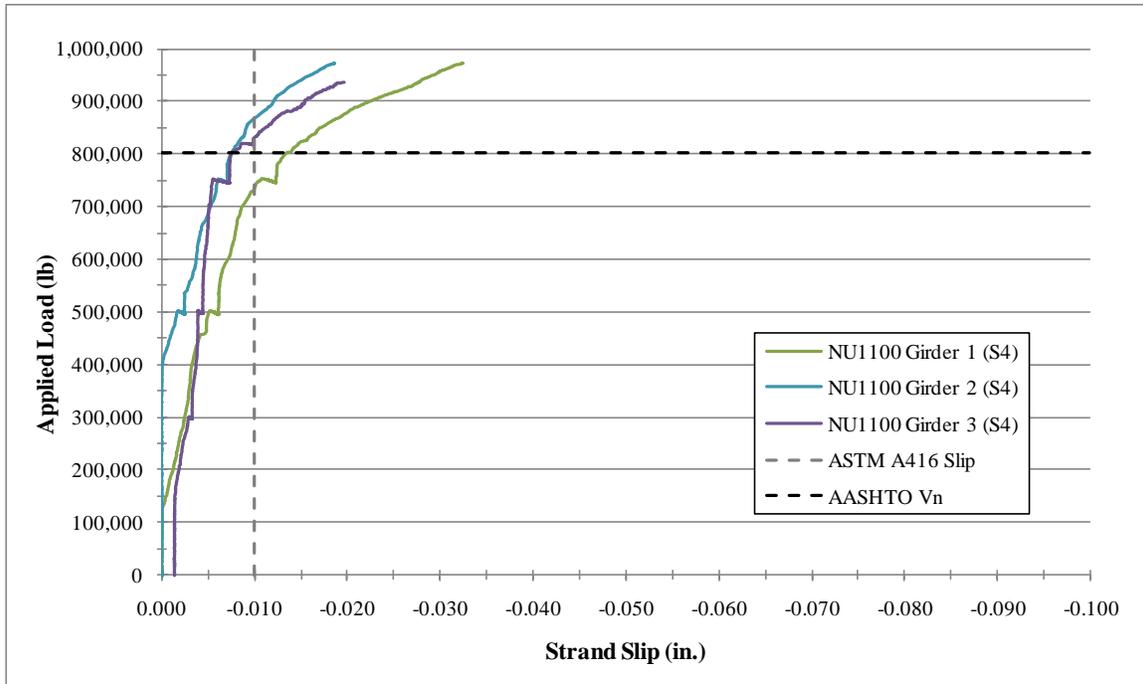
Figure 7.27: Load vs. maximum strand slip of the shear testing of NU1100 specimens

8 CONCLUCIONS AND RECOMMENDATIONS

8.1 Conclusions

This report presents the experimental investigation carried out to introduce the use of 0.7 in. diameter, Grade 270, low-relaxation strands in pretensioned concrete bridge girders. This investigation include testing strand samples for their mechanical properties, evaluating strand surface quality using NASP test method, performing transfer length measurement in several small-scale and full-scale specimens, conducting development length flexural tests on several small-scale and full-scale specimens, and evaluating the shear capacity at end sections in specimens with fully bonded and partially debonded strands. These tests were conducted on several girder sections, such as T-girder, BDT, NU900, and NU1100, as well as rectangular prism specimens. Various concrete strengths and levels of confinement were considered in this investigation. The main conclusions of this study can be categorized as follows:

a) *Mechanical Properties of 0.7 in. Diameter Strands*

The tension testing of one hundred and two 0.7 in. diameter prestressing strands obtained from two different strand producers has indicated that all the strands adequately meet the requirements of the ASTM A416-07 with the exception of the minimum yield strength requirements (90% of the specified ultimate strength). Strands obtained from one producer had average yield strength of 92.3% and standard deviation of 1.4%, while strands obtained from the other producer had average yield strength of 90.4% and standard deviation of 2.5%. Also, current strand stress-strain models, such as the PCI Design Handbook Formula, are inaccurate when applied to 0.7 in. diameter strands. The Power Formula developed in this study based on test data was found to be a more robust predictor of the behavior of the strand.

b) *Bond Testing of 0.7 in. Diameter Strands*

The experimental investigation carried out on fifty eight 0.7 in. diameter strands to evaluate its surface quality using the NASP bond test method has indicated that the NASP bond test method can be successfully applied to 0.7 in. diameter strands in both mortar and concrete. The bond of 0.7 in. diameter strands is proportional to the concrete strength and can be predicted using the following equation:

187

$$NASP(kips)=6.96 f_c^{0.77} (ksi)$$

At 0.01 in. end slip, the average NASP bond test values of rusted 0.7 in. diameter strands are approximately 40% higher than those of clean strands. However, at 0.1 in. end slip, the average NASP values of rusted strands are highly variable and can be even lower than those of clean strands.

c) Production Challenges

Challenges of using large diameter strands are mainly those associated with handling a heavier and stiffer strand. Extra caution should be considered while pulling the strand out of the spool and feeding it along the bed. Larger diameter spools are highly recommended to improve safety in strand handling. The availability of strands, chucks, and debonding sheathing is not a problem. Hold down devices for depressing 0.7 in. diameter strands are not readily available. Therefore, strand debonding or using 0.6 in. diameter strands for depressed strands is the current simple solution to this problem. Minor modifications might be needed to enlarge the bulkheads openings and increase the prestressing capacity of the jacking equipment and/or prestressing bed.

d) Transfer Length

The transfer length of 0.7 in. diameter strands is highly dependent on the concrete strength and the intensity of prestressing as it ranged from 19 in. to 29 in. These values are well below the one predicted using the AASHTO LRFD specification expression of $60d_p$, which is 42 in. Also, neither the amount nor distribution of bottom flange confinement reinforcement had a significant effect on the transfer length of 0.7 in. diameter prestressing strands at release or at 28 days after release. This is because confinement reinforcement remains inactive until concrete cracks, which does not usually occur at the time of prestress transfer. This is in agreement with conclusions made by other researcher regarding 0.5 in. and 0.6 in. diameter strands.

e) Development Length

The 0.7 in. diameter strands can be fully developed in high strength concrete (HPC) within the length predicted by the 2007 AASHTO LRFD specifications even when spaced at 2 in.

horizontally and vertically. This conclusion is provisional to the concrete strength and bottom flange confinement reinforcement adopted in this study. Based on the results of the experimental investigation presented herein, for a minimum concrete strength of 10 ksi and AASHTO LRFD specified confinement reinforcement (i.e. no. 3 at 6 in. spacing at least distance 1.5h from the girder end), 0.7 in. diameter strands can be fully developed within the AASHTO LRFD specified development length (approximately 14 ft). For a higher concrete strength (more than 15 ksi), shorter development length can be achieved. Although increased levels of confinement result in shorter development lengths for prestressing strands, the flexural capacity of prestressed girders remains the same at the AASHTO specified development length with development length factor (k) equal to 1.6 regardless of the amount and/or distribution of confinement reinforcement. It was also observed that girders with confinement reinforcement distributed along the entire length have reduced cracking and spalling of concrete, as well as improved ductility under extreme loading conditions.

f) Shear Capacity

The longer transfer and development length of 0.7 in. diameter strands than those of 0.6 in. diameter strands do not significantly affect the shear capacity of the girder at the critical shear sections (i.e. close to the support). This conclusion is also provisional to the concrete strength, number of debonded strands, and bottom flange confinement reinforcement adopted in this study. For a minimum concrete strength of 10 ksi, number and pattern of debonded strands complying with the AASHTO LRFD requirements, and bottom flange confinement at least equal to the AASHTO LRFD specified, the shear capacity can be conservatively predicted using the AASHTO LRFD shear formula. Higher levels of confinement at the girder ends improve the anchorage and prevent premature slippage of prestressing strands, however, it has negligible effect on the shear capacity of the tested girders. In all tested cases with variable confinement distribution, the ultimate shear capacity was found to be 16% - 24% greater than the AASHTO LRFD predicted nominal resistance for each section.

8.2 Recommendations

Based on the conclusions presented above, the following recommendations can be made:

- Use of power formula with the K and Q constants presented in chapter 3 to better model the stress-strain relationship of 0.7 in. diameter strands. This relationship can be used for design purposes.

- The NASP test method should be used to evaluate the surface quality of 0.7 in. diameter strands similar to 0.5 in. and 0.6 in. diameter strands. Acceptance criteria can be extrapolated by the ratio of strand diameter.

- A minimum final concrete strength of 10 ksi (at 56 days) should be used to ensure that the current AASHTO LRFD formula for transfer length and development length can be applied to 0.7 in. diameter strands spaced at 2 in. x 2 in. and tensioned up to 75% $f_{pu.}$

- Confinement reinforcement specified by AASHTO LRFD Section 5.10.10.2 should be used as a minimum reinforcement at the girder ends to provide anchorage of prestressing steel and reduce the probability of strand slippage at extreme loading conditions. Additional confinement reinforcement placed throughout the entire length of bridge can be used to improve ductility and reduce damage due over-height vehicular collision.

- Extra caution must be considered when handling 0.7 in. diameter strands due to their significantly higher weight and stiffness.

IMPLEMENTATION

By Fouad Jaber
(NDOR Bridge Division)

Large 0.7 in. diameter strands are used in cable bridges and mining applications in the US, and for post-tensioning tendons in Europe and Japan. The cross section area of each strand is 0.294 in^2, which results in 35.5% more prestressing than 0.6 in. diameter strand and 92% more prestressing than 0.5 in. diameter strand, allowing for longer spans and/or larger girder spacing. Also, for the same prestressing force, using 0.7 in. diameter strands results in fewer number of strands to jack and release, requiring fewer chucks, and produces a higher flexural capacity due to lowering the center of gravity of the strands. The Pacific Street Bridge over I-680 in Omaha, NE, is the first bridge in the world to use 0.7 in. diameter prestressing strands in the precast-pretensioned concrete girders. Due to inadequate knowledge on the behavior of 0.7 in. diameter strands and its bond with concrete at that time, strands were spaced 2 in. horizontally and 2.5 in. vertically and were tensioned at 64% of the ultimate strength, which does not fully utilize the advantages of 0.7 in. diameter strands. In addition depressing of 0.7 in. diameter strands was not attempted. Since then, several experimental investigations, presented in this report, were carried out by NDOR and UNL to evaluate the bond strength of 0.7 in. diameter strands at different levels of concrete strength and bottom flange confinement as well as using depressed 0.7 in. diameter strands. These investigations have concluded that 0.7 in. diameter strands can be tensioned up to 75% their ultimate strength and can be spaced at 2 in. horizontally by 2 in. vertically, while satisfying the transfer length and development length provisions of the 4th Edition of AASHTO LRFD specifications. The investigations have also addressed the challenges associated with handling, jacking, and depressing 0.7 in. diameter strands. Recently, the 14th Street Bridge over I-80, Lincoln, NE, was awarded federal funds under the 2010 Innovative Bridge Research and Deployment (IBRD) program to be constructed using High Performance Self-Consolidating Concrete (HPSCC) and 0.7 in. diameter strands. It should be noted that the two bridge producers in the State of Nebraska have agreed to perform necessary retooling of their facilities to accommodate the use of 0.7 in. diameter strands in this project.

REFERENCES

American Association of State Highway and Transportation Officials (AASHTO) M203. (2007). *Standard Specification for Steel Strand, Uncoated Seven-Wire for Concrete Reinforcement*. Washington, DC.

American Association of State Highway and Transportation Officials (AASHTO). (2007). *AASHTO LRFD Bridge Design Specifications,* 4th Edition with 2008 Interim Revisions. Washington, DC.

Association Francaise de Genie Civil (AFGC). (2002). *Ultra High Performance Fibre-Reinforced Concretes—Interim Recommendations*, Paris, France.

ASTM A370 (2005). *Standard Test Methods and Definitions for Mechanical Testing of Steel Products*. West Conshohocken, PA.

ASTM A416 (2006). *Standard Specification for Steel Strand, Uncoated Seven-Wire for Prestressed Concrete*. West Conshohocken, PA.

ASTM A981-07 (2007). *Standard Test Method for Evaluating Bond Strength for 15.2 mm (0.6 in.) Diameter Prestressing Steel Strand, Grade 270, Uncoated, Used in Prestressed Ground Anchors.* West Conshohocken, PA.

ASTM C109/C109M (2008*). Standard Test Method for Compressive Strength of Hydraulic Cement Mortars (Using 2-in. or [50-mm] Cube Specimens).* West Conshohocken, PA.

ASTM C1437 (2001). *Standard Test Method for Flow of Hydraulic Cement Mortar.* West Conshohocken, PA.

Barnes, R. W., Burns, N. H., and Kreger, M. E. (1999). "Development length of 0.6-inch prestressing strand in standard I-shaped pretensioned concrete beams." *Report to Federal Highway Administration*, Report No. FHWA/TX-02/1388-1, University of Texas, Austin.

Bryan J. L. (2008). "Bond and Material Properties of Grade 270 and Grade 300 Prestressing Strands" MS Thesis, Virginia Polytechnic Institute and State University, Virginia

Buckner, C. D. (1995). "A Review of Strand Development Length for Pretensioned Concrete Members," *PCI Journal*, 40(2), 84-105.

Cousins, T. E., Johnston, D. W., and Zia, P. (1990), "Transfer and development length of epoxy-coated and uncoated prestressing strands" *PCI Journal*, 35(3), 92-106.

Devalapura, R. K., and Tadros, M. K. (1992). "Stress-strain modeling of 270 ksi low-relaxation prestressing strands." PCI Journal, 37(2), 100-106.

Federal Highway Administration (FHWA) (2006). "Structural Behavior of Ultra-High Performance Concrete Prestressed I-Girders." *Publication No. FHWA-HRT-06-115*, FHWA, Washington, DC.

Guyon, Y. (1960). *Prestressed Concrete*. New York: John Wiley & Sons.

Hanson, N. W.; and Kaar, P. H. (1959). "Flexural Bond Tests of Pretensioned Prestressed Beams." *ACI Journal*, 55(7), 783-803.

Harajli, M. H., and Naaman, A. E. (1985). "Evaluation of the ultimate steel stress in partially prestressed flexural members." *PCI Journal*, 30(5), 54-81.

Hoyer, E., and E. Friedrich (1939). "Contribution to the question of bond stress in reinforced concrete elements." *Beton und Eisen 3*, March.

James, B. (2001). "Narrows Bridge, Perth, WA." *The newsletter of Engineering Heritage Australia*, The Institution of Engineers, Australia, No. 11, June.

Janney, J. R. (1954). "Nature of bond in pretensioned prestressed concrete." *ACI Journal*, 50(8), 717-736.

Japan Society of Civil Engineers (JSCE), 2006, "Recommendations for Design and Construction of Ultra High Strength Fiber Reinforced Concrete Structures," *JSCE Guideline for Concrete No. 9.* (draft)

Kaar, P.H., LaFraugh, R.W., and Mass, M.A., (1963) "Influence of Concrete Strength on Strand Transfer Length," *PCI Journal,* 8(5), 47-67.

Kose, M. M., and Burkett W. R. (2005). "Evaluation of code requirement for 0.6 in. (15 mm) prestressing strand." *ACI Structural Journal*, 3, 422-428.

Lane, S., and Rekenthaler, D. (1998). "The Ties That Bind: The 10-Year Fight for 0.6-Inch Diameter Strands", *Public Roads*, 61(5), 27-29.

Lane, S.N. (1998). "A New Development Length Equation for Pre-tensioned Strands in Bridge Beams and Piles", Report No. FHWA-RD-98-116, Federal Highway Administration, McLean, VA.

Loflin, B. (2008). "Bond and material propertied of grade 270 and grade 300 prestressing strands." Master's thesis, Virginia Tech University, Blacksburg, VA.

Loov, R. E. (1988). "General equation for the steel stress for bonded members." *PCI Journal*, 33(6), 108-137.

Martin, L.D., and Scott, L. N. (1976). "Development of Prestressing Strands in Pretensioned Members", *ACI Journal*, 73(8), 453-456.

Mattock, A. H. (1979). "Flexural strength of prestressed concrete sections by programmable calculator." *PCI Journal*, 24(1), 32-54.

Moustafa, S. (1974) "Pull-Out Strength of Strand and Lifting Loops." *Concrete Technology Associates Technical Bulletin, 74-B5*, Precast/Prestressed Concrete Institute, Chicago, IL

Nebraska Department of Roads (NDOR). (2009). "Application of Ultra-High Performance Concrete to Bridge Girders", *Report of Project Number P310*, Lincoln, NE.

Nebraska Department of Roads (NDOR) (2010) "Design Aids of NU I-Girder Bridges", *Report of Project Number P322*, Lincoln, NE.

Nebraska Department of Roads (NDOR) (2010) "Rapid Construction of Pacific Street Bridge", *Report of Project Number P587*, Lincoln, NE.

Precast/Prestressed Concrete Institute. (2004). *PCI Design Handbook (6th Ed.)*. Chicago, IL.

Preston, H. K. (1985). "Testing 7-wire strand for prestressed concrete – The state of the art." *PCI Journal*, 30(3), 134-155.

Ramirez, J., and Russell, B. (2008). "Transfer, Development, and Splice Length for Strand/Reinforcement in High-Strength Concrete", *NCHRP Report 603*.

Reiser, Nick. (2007). "Innovative Reinforced/Prestressed Concrete Bridge Superstructure Systems." MS Thesis, University of Nebraska-Lincoln, Lincoln, NE.

Peterman R. J. (2009). "A Simple Quality Assurance Test for Strand Bond." *PCI Journal*, 54(2), 143-161.

Russell, B. W., and Burns, N. H. (1996). "Measured Transfer Lengths of 0.5 and 0.6 in. Strands in Pretensioned Concrete", *PCI Journal*, 41(5), 44-65.

Russell, B. W., and Burns, N. H. (2008) "NASP Test Protocols", *Appendix I, NCHRP Report 603*.

Russell, B., W., & Burns, N., H. (1993). "Design Guidelines for Transfer, Development and Debonding of Large Diameter Seven Wire Strands in Pretensioned Concrete Girders." *Report No. FHWA/TX-93+1210-5F*. Austin: Center for Transportation Research, University of Texas at Austin.

Russell, B.W., and Brown, M.D. (2004). "Evaluation of Test Methods in Assessing Bond Quality of Prestressing Strands." *Final Report, NASP Round III Strand Bond Testing*. Oklahoma.

Russell, H. G., Volz, J. S., and Bruce, R. N. (1997). "Optimized Sections for High-Strength Concrete Bridge Girders." *Report to Federal Highway Administration (FHWA)*, FHWA-RD-95-180, August.

Schuler, G. (2009). "Producer's Experience with 10,000 psi Concrete and 0.7-in. Diameter Strands". *HPC Bridge Views*, Issue 54, June.

Shahawy, M. (2001). "A critical evaluation of the AASHTO provisions for strand development length of prestressed concrete members" *PCI Journal*, 46(4), 94-117.

Skogman, C. B., Tadros, M. K., and Grasmick, R. (1988). "Flexural strength of prestressed concrete members". *PCI Journal*, 33(5), 96-123.

Vadivelu, J., and Ma, Z. (2008) "Potential Impact of 0.7-inch Strands on Precast/Prestressed Concrete Bridge I-Girders: Spacing of Large Diameter Strands." *Proceedings of the 2008 PCI National Bridge Conference*, Orlando, FL.

Zia, P., and Mostafa, T. (1977). "Development of Prestressing Strands," PCI Journal, 22(5), 54-65.